

ESD-TR-67-357

Vol. I

**ESD RECORD COPY**

RETURN TO  
COLD LAKE RADIO PROPAGATION AND METEOROLOGICAL EXPERIMENT  
SCIENTIFIC & TECHNICAL INFORMATION DIVISION  
(ESTI), BUILDING 1211

MTR-118

Vol. I

**ESTI**

COLD LAKE RADIO PROPAGATION AND METEOROLOGICAL EXPERIMENT  
**ESD ACCESSION LIST**  
(in Three Volumes) ESTI Call No. AL 58115

Volume I

Copy No. 1 of 2 cys.

Description of a Radio-Meteorological Experiment to Measure  
Ray-Path Bending in the Troposphere with a Vertical Interferometer

AUGUST 1967

B. J. Starkey (EMI-Cossor, Ltd., Canada)

L. G. Rowlandson (The MITRE Corporation)

F/L G. A. Fatum (RCAF)

Prepared for

DEPUTY FOR SURVEILLANCE AND CONTROL SYSTEMS  
AEROSPACE INSTRUMENTATION PROGRAM OFFICE

ELECTRONIC SYSTEMS DIVISION

AIR FORCE SYSTEMS COMMAND

UNITED STATES AIR FORCE

L. G. Hanscom Field, Bedford, Massachusetts



Project 7010

Prepared by

THE MITRE CORPORATION  
Bedford, Massachusetts

Contract AF19(628)-5165

This document has been approved for public release and sale; its distribution is unlimited.

AD0659746

When US Government drawings, specifications, or other data are used for any purpose other than a definitely related government procurement operation, the government thereby incurs no responsibility nor any obligation whatsoever; and the fact that the government may have formulated, furnished, or in any way supplied the said drawings, specifications, or other data is not to be regarded by implication or otherwise, as in any manner licensing the holder or any other person or corporation, or conveying any rights or permission to manufacture, use, or sell any patented invention that may in any way be related thereto.

Do not return this copy. Retain or destroy.

ESD-TR-67-357

Vol. I

MTR-118

Vol. I

COLD LAKE RADIO PROPAGATION AND METEOROLOGICAL EXPERIMENT

(in Three Volumes)

Volume I

Description of a Radio-Meteorological Experiment to Measure  
Ray-Path Bending in the Troposphere with a Vertical Interferometer

AUGUST 1967

B. J. Starkey (EMI-Cossor, Ltd., Canada)

L. G. Rowlandson (The MITRE Corporation)

F/L G. A. Fatum (RCAF)

Prepared for

DEPUTY FOR SURVEILLANCE AND CONTROL SYSTEMS  
AEROSPACE INSTRUMENTATION PROGRAM OFFICE

ELECTRONIC SYSTEMS DIVISION

AIR FORCE SYSTEMS COMMAND

UNITED STATES AIR FORCE

L. G. Hanscom Field, Bedford, Massachusetts



Project 7010

Prepared by

THE MITRE CORPORATION

Bedford, Massachusetts

Contract AF19(628)-5165

This document has been approved for public  
release and sale; its distribution is un-  
limited.

## FOREWORD

The work reported in the three volumes of this report was supported by the Electronic Systems Division of the Air Force Systems Command, L. G. Hanscom Field, Bedford, Massachusetts, through the MITRE Corporation's Technical Objectives and Plans 7010 - Environmental Factors - under Contracts AF 19(628)-2390 and AF 19(628)-5165.

## REVIEW AND APPROVAL

This technical report has been reviewed and is approved.

*James F. Shunk*  
NOTIS R. HILL, Colonel, USAF  
Director of Aerospace Instrumentation  
Program Office

## ABSTRACT

The purpose of the experimental program described in this report was to determine the direct relationship between meteorological and radio-propagation measurements and then to evaluate the validity of radio-meteorological results for predicting the radio-propagation conditions. The experiment was carried out at the R. C. A. F. Primrose Lake Evaluation Range, Cold Lake, Alberta, Canada.

The meteorological information was derived from radio-sonde measurements and airborne microwave refractometer data. The radio experiments were based on the vertical interferometer technique, in which a single airborne transmitter (S and L Band) was used to establish an interference pattern at the ground-based receiver, due to the combination of direct and lake-surface-reflected signals.

Extreme accuracy in the measurements of the parameters involved, in particular in the interferometer experiment, was the keynote to success.

The close agreement between the effective earth's radius value obtained from the meteorological measurements and the interferometer technique indicates that this type of radio interferometer can provide meaningful and surprisingly accurate information on the radio propagation conditions. It might, in fact, provide the best method to measure integrated radio meteorological conditions when continuous monitoring is required and when the use of complex meteorological instrumentation would be impractical.

The results also indicate that the radiosonde data, if sufficient care is taken to calibrate it before launch, can give very satisfactory information about radio propagation conditions. Aircraft refractometer measurements, of course, provide a great deal more fine structure than the radiosonde. However, unless this data can be related to the horizontal and temporal variations prevalent, it may lead to a misunderstanding about the effective propagation conditions.

## ACKNOWLEDGEMENT

The Cold Lake Radio Propagation and Meteorological Experiment was sponsored by the "Joint USAF/RCAF ECCM Evaluation Group."

The participating members in the experiments were designated "The Multipath Propagation Panel" of the above, larger Joint Group. The authors wish to acknowledge the cooperation and coordination provided through the Joint International Group and presently represented by the Canadian and United States cochairmen:

Wing Commander I. Gillean  
Director of Electronic Warfare  
Canadian Forces Headquarters  
Ottawa, Ontario

Mr. R. Creamer  
Electronic System Program Analyst  
416M/418L  
Electronic Systems Division  
Bedford, Massachusetts

Financial support was obtained from:

AFHQ-63/70, T & DI-RCAF  
AF19(628)-5165 - USAF

The Cold Lake Radio Propagation and Meteorological Experiment is reported in three volumes:

- Vol. I - Description of a Radio-Meteorological Experiment to Measure Ray-Path Bending in the Troposphere with a Vertical Interferometer
- Vol. II - Determination of Radio Propagation Conditions from Interferometer and Lake Surface Measurements
- Vol. III - Description of the Vertical Reflection Interferometer and the Measurement Accuracy

## TABLE OF CONTENTS

		<u>Page</u>
LIST OF ILLUSTRATIONS		ix
LIST OF TABLES		x
SECTION I      GENERAL DESCRIPTION	1	
INTRODUCTION	1	
BACKGROUND	4	
SIMPLE PRINCIPLES	6	
EARLY EXPERIMENTS	16	
COLD LAKE EXPERIMENT	20	
SECTION II     METEOROLOGICAL MEASUREMENTS	27	
DESCRIPTION OF MEASUREMENT		
TECHNIQUE	27	
SELECTION OF MEANINGFUL PROFILES		
FOR RAY-TRACING ANALYSIS	37	
SECTION III    RADIO PROPAGATION	45	
INTRODUCTION	45	
Ground Receiving Equipment	45	
Transmitter	48	
PLER RANGE AND ALTITUDE SERVICES	49	
Data Reduction	50	
Computation of Effective Earth's Radii	53	
Factors Affecting Accuracy of		
Experimental Results	57	
SECTION IV    EXPERIMENTAL DATA	60	
INTRODUCTION	60	
Mission 102    17 Sep 64    0952-1435	61	
Mission 103    21 Sep 64    1130-1521	70	
Mission 104    22 Sep 64    0422-0917	80	
Mission 105    23 Sep 64    1145-1506	90	
Mission 106    24 Sep 64    0927-1402	99	
Mission 107    28 Sep 64    1602-2002	113	
Mission 108    30 Sep 64    1254-1653	121	
Mission 109    1 Oct 64    1606-1941	130	
Mission 110    5 Oct 64    0402-0753	137	
Mission 111    6 Oct 64    0403-0805	147	
Mission 112    7 Oct 64    0402-0813	157	

TABLE OF CONTENTS (CONT.)

		<u>Page</u>
SECTION IV	EXPERIMENTAL DATA (CONT.)	
	Mission 113 8 Oct 64 0400-0800	165
	Mission 114 8 Oct 64 1556-1952	173
SECTION V	SUMMARY AND CONCLUSIONS	181
	SIGNAL AMPLITUDE CHARACTERISTICS	181
	REFRACTIVITY PROFILES	185
	EFFECTIVE EARTH RADIUS CALCULATIONS	186
	CONCLUSIONS	194
APPENDIX I	THE "EFFECTIVE EARTH RADIUS" CONCEPT	197
APPENDIX II	INTERFEROMETER ERROR ANALYSIS	204
REFERENCES		211
DISTRIBUTION LIST		213

## LIST OF ILLUSTRATIONS

<u>Figure Number</u>		<u>Page</u>
1	Radio Refractivity vs Height - Standard Atmosphere	7
2	Refraction of Radio Signal in Standard Atmosphere	8
3	Effective Earth's Radius Concept	8
4	Vertical Interferometer Straight Ray Geometry	12
5	Vertical Interferometer Interference Pattern	14
6	Map of Cold Lake Area	21
7	Terrain Profile from Peter Pond Lake to Cold Lake	23
8	Typical Aircraft Flight Plan for Measurement of Radio Refractivity	29
9	Comparison of Refractometer and Radiosonde Index Profiles	31
10	Ray-Tracing Geometry	33
11	Temporal Variation of Refractivity Over Cold Lake	38
12	Spatial Variability of Refractivity Data Near Surface of Cold Lake - Surface Wind 13 MPH from South	39
13	Spatial Variability of Refractivity Data Near Surface of Cold Lake - Surface Wind 6 MPH from North	40
14	Spatial Variability of Refractivity Data Near Surface of Cold Lake - Surface Wind 5 MPH from Southeast	41
15	Spatial Variability of Refractivity Data Near Surface of Cold Lake - Surface Wind 15 MPH from West	42
16	Block Diagram of Ground Receiving and Recording System (In Van)	46
17	Contours of Maximum Expected Errors for Various Combinations of Experimental Parameters	59

## LIST OF ILLUSTRATIONS (CONT.)

<u>Figure Number</u>		<u>Page</u>
18	Effective Earth Radius Difference (n. m.) Between Ray-Tracing and Interfero- meter Results vs Range	187
19	Variation in Elevation Angle Error $\Delta \epsilon$ (mr) for 100 n. m. Variation in $A_e$ vs Transmitter Range	189
20	Elevation Error Angle Difference and Transmitter Height Difference Between Ray-Tracing and Interferometer Results vs Range	191
21	Flat Earth Reflection Geometry	197
22	Geometry of Flat Earth Approximation	199
23	Geometry of Flat Earth Approximation (II)	205

## LIST OF TABLES

<u>Table Number</u>		<u>Page</u>
I	List of Missions Completed	25
II	Calculation of Refraction Effects	32
III	Comparison of Refraction Variables for Two Profiles	34
IV	Sample Computer Printout of Monitor Van Data	51
V	Effective Earth's Radius vs Range	52
VI	Sample Computer Printout of $A_e$ vs Range for Minima	54
VII	Summary of Signal Characteristics	182
VIII	Summary of Interferometer $A_e$ Values	192
II-1	Interferometer Accuracy for $A_e$ Determination	209

## SECTION I

### GENERAL DESCRIPTION

#### INTRODUCTION

Radar technology has advanced to a state where the atmosphere itself is imposing the limiting restriction on accuracy. Equipments to correct for errors caused by atmospheric refraction are now an integral part of many tracking and height-finder radar systems.

To make meaningful evaluations of proposed or existing correction techniques, it is necessary to have instruments that measure real-time variations of the index of refraction. It is equally important to determine the effect of index variations on system accuracy, which implies an analytical capability such as a ray-tracing program.

Refractive index up to high altitudes can be measured by ascents of meteorological balloons with radiosondes (the oldest technique), or by refractometers carried by aircraft or helicopters. Radiosonde measurements, which have a slow response to changes in the parameters concerned, are based on sampling at relatively large altitude intervals. Therefore, it is normally considered that the radiosonde measurements give only rather crude information, without any details concerning the fluctuations of the refractive index with height. These details can be provided by refractometer measurements.

Whatever the results of these types of meteorological measurements, their significance in applications to radio propagation problems can be assessed only by a direct comparison between the meteorological measurements and radio propagation results. Although very large quantities of radio meteorological measurements are now available, surprisingly little information can be found concerning the detailed quantitative correlation of these data with radio propagation experiments.

The purpose of the experimental program described in this report was to determine the direct relationship between meteorological and radio propagation measurements in a way which would help in evaluating the validity of radio-meteorological results for predicting the radio propagation conditions.

The parameters which can be measured in radio experiments, involving a radio transmitter and receiver at two ends of a radio path, are the signal amplitude, relative phase and the angle of arrival at the receiver, and the elevation angle at the transmitter. In general, it is not possible to determine the exact path of the radio wave between the terminal points, even though this path could be determined from a detailed knowledge of the refractive index structure over the path. This means that any comparison between the radio and meteorological results must be based only on the comparison of the angle of arrival and the

relative phase of the received signal with the same parameters derived from meteorological measurements.

These parameters, and, in particular, the elevation angle, can be measured directly by the use of high-resolution radar systems. However, the radar techniques required could be rather expensive and also restrictive in the choice of area considered favorable for this type of measurement, and in the flexibility of available frequencies.

The vertical interferometer technique can also lead indirectly to the determination of the required parameters. This method, in turn, can be greatly simplified by carrying out measurements over a perfectly reflecting surface such as smooth water, in which case, a single transmitter is sufficient to establish an interference pattern at the receiver due to the combination of the direct and lake-surface-reflected signals. This technique is simple, flexible, and as will be seen later, provides sufficient accuracy to correlate small changes in the angle of arrival with equally small changes in meteorological conditions.

The comparison of elevation angles carried out over a fixed-length path would not lead to any deep insight into the effects of the meteorological structure of the atmosphere in two dimensions, that is, for a wide range of possible elevation angles. This leads to a requirement for an experiment in which the transmitter-receiver spacing

could be varied rapidly enough to avoid excessive temporal variations in the meteorological conditions. An aircraft-mounted terminal is a logical solution here.

## BACKGROUND

The Directorate of Electronic Warfare (DEW) at Canadian Forces Headquarters, Ottawa, developed a mobile microwave receiver system to evaluate signal characteristics transmitted from aircraft. The equipment could record the received signal strength versus time for several microwave frequency bands and planes of polarization. An RCAF North Star aircraft was available to provide a source of microwave transmissions. This equipment, including a digital data logging and processing system and also an accurate distance measuring equipment, comprised the necessary transmitter and receiver for a vertical interferometer experiment.

During the early part of 1962, The MITRE Corporation obtained the use of a C131B USAF aircraft for tropospheric investigations. The aircraft was fitted with a microwave refractometer, various probes, recorders and associated test equipment to measure tropospheric refraction parameters. A digital logging system was also included to make possible the acquisition and processing of large quantities of data.

The computer facilities at MITRE permitted the development of an extremely accurate ray-tracing analysis. This accuracy was essential to measure the effect of index of refraction variations in the atmosphere on microwave transmissions and to compare experimental and analytical results.

The final important requirement was a location for tests where a reflecting interferometer experiment could be conducted. Accuracy was the keynote to a successful experiment. The position of the signal aircraft would have to be known precisely with respect to the microwave receiving site. The reflection point corresponding to the heights and distances of the signal aircraft would have to remain within the boundaries of a smooth water area. Support facilities for participating aircraft and subsidiary meteorological measurements were required. After a thorough search for an appropriate location, the RCAF-Primrose Lake Evaluation Range (PLER) at Cold Lake, Alberta, Canada, was selected. One of the advantages of this facility was the availability of a number of photo-theodolites for accurate range and elevation measurements on the participating aircraft.

This choice and also the final specifications for the instrumentation required was made after several preliminary trials were carried out at a number of various locations in Canada and the U. S. Some of these trials have been described in Refs. [1] and [2].

A successful outcome for a joint, international experiment of this magnitude required a high degree of cooperation between the organizations involved. Fortunately an instrument for establishing this cooperation was available under the terms of reference of the Joint USAF-RCAF ECCM Evaluation Group. This organization had been formed to evaluate and recommend common equipment and techniques for ADC, North American Air Defense. The DEW-MITRE groups participating in the interferometer tests were designated "The Multipath Propagation Panel" of the larger joint group.

#### SIMPLE PRINCIPLES

The index of radio refraction,  $n$ , determines the velocity of propagation of an electromagnetic signal. At most, the magnitude of this index varies by a few hundred parts in a million within the troposphere. It is therefore convenient to define an index of radio refractivity,  $N$ , which represents the variational part of the index of refraction, where,

$$N = (n-1) \cdot 10^6 \quad (1)$$

As shown in the literature [3] not only is the velocity of propagation inversely proportional to  $n$ , but the direction of propagation bends towards the region of increasing index. For an atmosphere without any variation of the index  $n$ , (or, refractivity  $N$ ), an electromagnetic signal

travels in a straight line and with a velocity equal to  $c/n$ , where  $c$  is the velocity in vacuum. A simplified model of the troposphere assumes that  $N$ , the radio refractivity, decreases linearly with height as shown in Figure 1. For the so-called "standard atmosphere," the magnitude of the refractivity gradient is about  $-1.2 \text{ N units per 100-foot change in altitude}$ . An electromagnetic signal in this constant  $N$ -gradient atmosphere will be continuously bent towards the region of increased refractivity, that is, downwards and at a constant rate. This results in the signal following an arc of a circle as shown in Figure 2. It has been shown (Ref [4]) that from the point of view of radio signal propagation

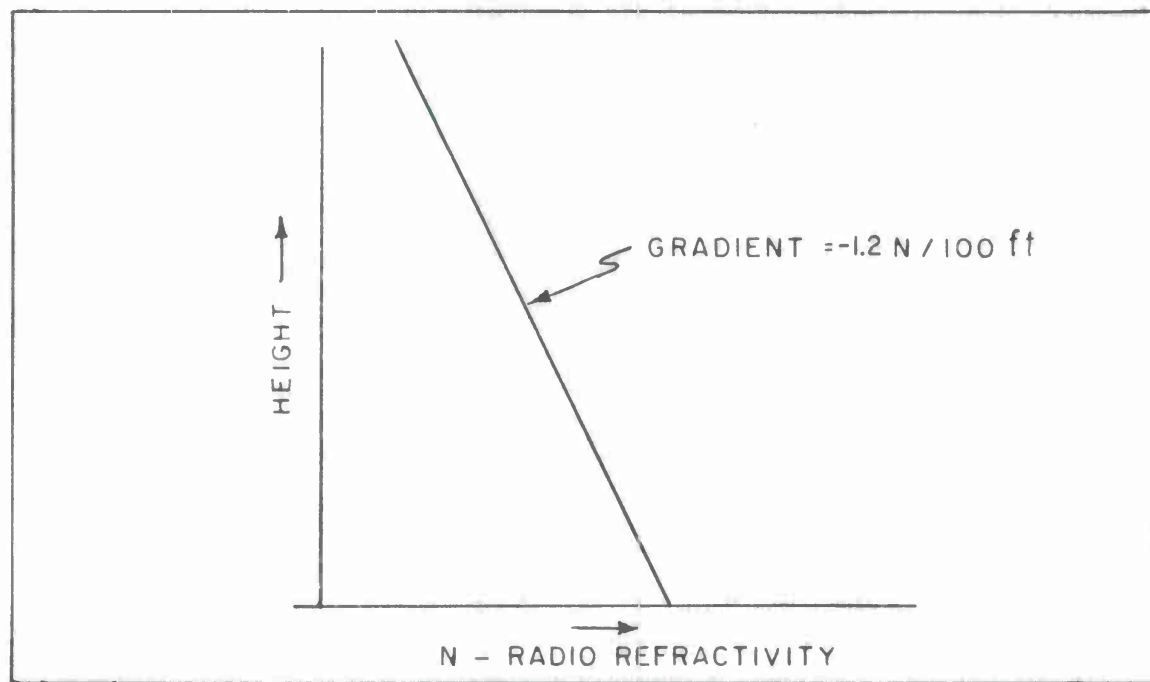


Figure 1. Radio Refractivity vs Height - Standard Atmosphere

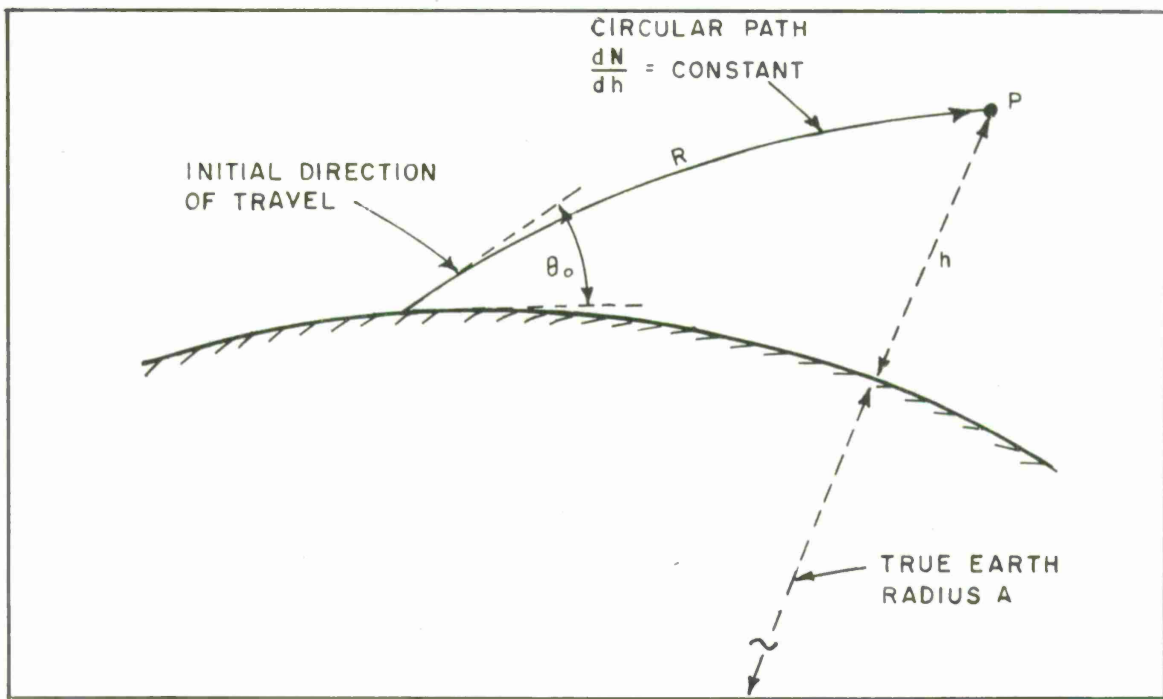


Figure 2. Refraction of Radio Signal in Standard Atmosphere

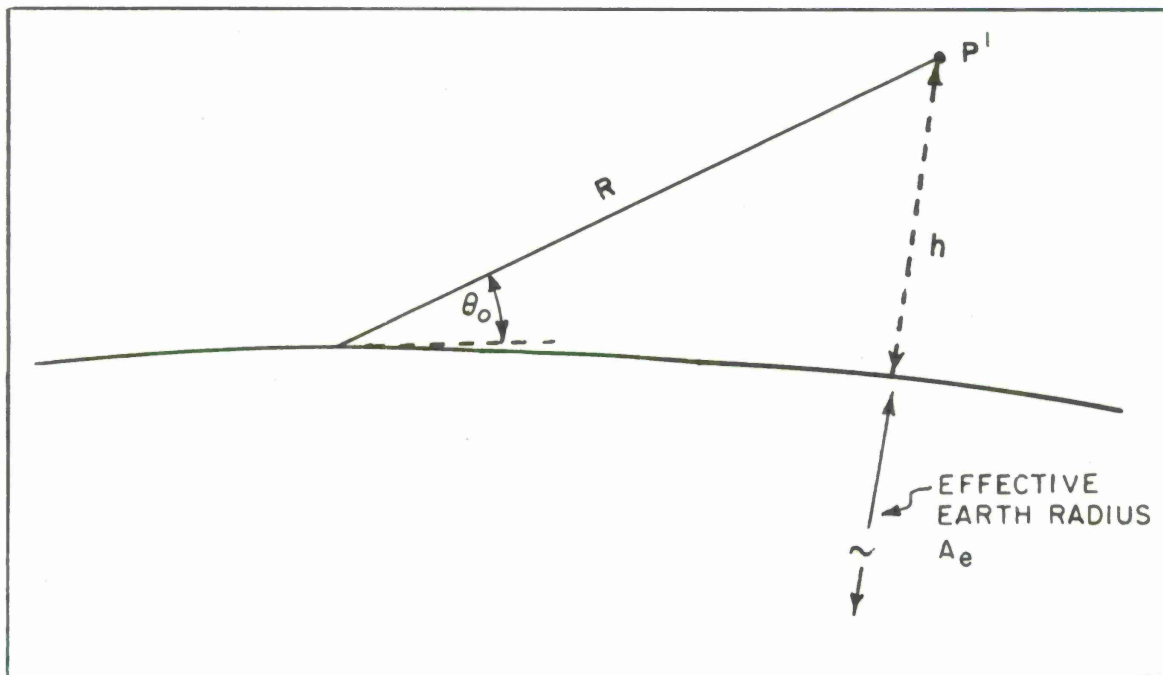


Figure 3. Effective Earth's Radius Concept

the configuration of Figure 2 is fully equivalent to that of Figure 3, in which the signal path is a straight line, but the earth's radius has been increased by a factor  $k$ . This radius, called the effective earth's radius,  $A_e$ , is then given by (Ref. [5]),

$$A_e = k \cdot A \quad (2)$$

where

$A$  = the true earth's radius,

and

$$k \simeq \frac{n_0}{n_0 + A \cdot \frac{dn}{dh}} \quad (3)$$

where  $n_0$  is a representative value for the surface index, but is essentially unity, and  $\frac{dn}{dh}$  equals the refractive index gradient, and is negative in the standard atmosphere.

This transformation is very convenient from the point of view of both physical interpretation and mathematical analysis. Ref [4] shows that this transformation preserves the basic parameters important in radio propagation considerations, that is, terminal heights, path lengths, and the initial elevation angles.

Under conditions when the radio refractive index,  $n$ , decreases with height (e. g., for the standard atmosphere),  $dn/dh$  is negative to give  $A_e > A$ . Obviously, as the magnitude of  $dn/dh$  increases, the

magnitude of  $A_e$ , or correspondingly, the  $k$  factor, increases. The standard gradient of  $-1.2 \text{ N}/100 \text{ feet}$ , discussed previously, gives a  $k$  value of about  $4/3$ . This condition is commonly referred to as a "4/3 earth" where the effective earth radius,  $A_e$ , is  $4/3$  larger than the real earth radius,  $A$ .

The vertical gradient of radio refractivity,  $dn/dh$ , normally varies with height and to a lesser extent in the horizontal direction over the earth's surface. Obviously, under such conditions the effective radius concept is no longer applicable because the signal path cannot be reduced to a straight line. However, because of the convenience provided by this concept, it would still be possible to generalize the effective earth's radius approach by defining an "equivalent effective earth's radius." This equivalent radius would provide the same initial elevation angle as the real ray for a given range and height. This concept is discussed in more detail in Section III. In fact, this equivalent  $A_e$  can be derived from the interferometer patterns as measured in radio propagation experiments. The true significance of this generalized effective earth's radius cannot be established without experimental confrontation of meteorological and radio propagation results, and, in fact, one of the objectives of the experiments described in this report was to determine the applicability of this concept for the interpretation of radio meteorological conditions.

Intuitively, this equivalent effective earth's radius corresponds to a mean value of the refractivity profile over the signal path in question. Knowing the refractivity profile representative for a given radio signal path, it is possible, by ray tracing, to calculate in detail the shape of the radio ray starting at a given initial elevation angle at the receiver and terminating at a given height corresponding to the radio signal transmitter height. The computation carried out for a number of elevation angles leads to a corresponding number of ranges, determining the position of the transmitter. As mentioned before, the initial elevation angle, range, and transmitter height determine an equivalent effective earth's radius. In other words, there is one radius ( $A_e$ ) for an arc of a circle which will pass through the transmitter and receiver heights and also satisfy the correct value of initial elevation angle and range to the transmitter. This type of analysis therefore generates the values of  $A_e$  for different ranges, applicable for given geometrical conditions. These values then can be directly compared with the  $A_e$  values derived from radio propagation measurements using the vertical interferometer technique.

In the reflection interferometer technique the signal from the transmitter arrives at the receiving antenna via two paths (Figure 4), i.e., by the "direct ray" ( $S_1$ ) and by the "ground reflected ray" ( $S_2$ ).

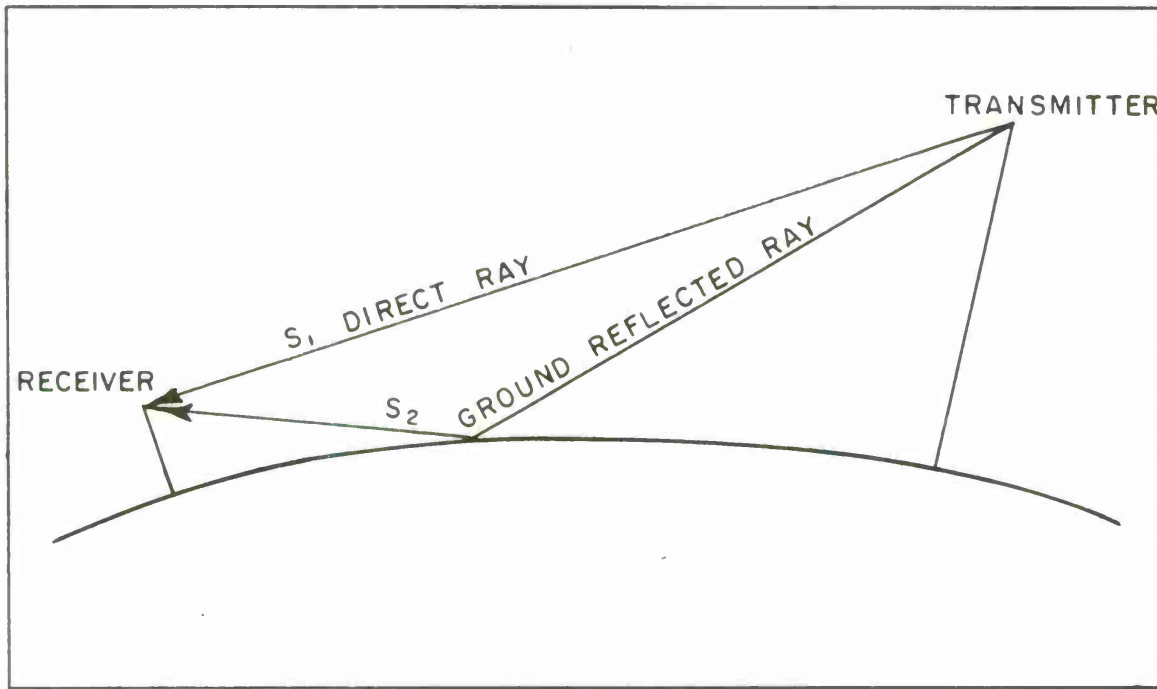


Figure 4. Vertical Interferometer Straight Ray Geometry

$S_1$  and  $S_2$  combine vectorially according to their phase differences and also their relative amplitudes.

The phase difference between the two signals is a function of the path length difference of the two rays in terms of wavelengths ( $\lambda$ ) of the transmission frequency and also of the phase change in the ground reflected ray due to the characteristics of the reflecting medium. For water and shallow angles of incidence the phase change on reflection is very close to 180 degrees for both vertical and horizontal polarizations. Therefore, the two signals will be out of phase and will tend to cancel

for path length differences which are integral multiples of the transmission wavelength.

Assuming that the power received from  $S_1$  is  $P$ , then the power received from  $S_2$  will be  $\rho P$ , where  $\rho$  is the ground reflection coefficient. Therefore, when  $S_1$  and  $S_2$  are in phase, the resultant received power will be

$$P_r = (1 + \rho) P \quad (4)$$

and when  $S_1$  and  $S_2$  are 180 degrees out of phase

$$P_r = (1 - \rho) P \quad (5)$$

As the signal aircraft flies a radial track at a constant altitude towards the receiver, the path length differences gradually increase through  $(1, 2, 3, \dots, n) \lambda$  producing an interference pattern as illustrated in Figure 5.

For a perfectly reflecting surface, the reflection coefficient  $\rho = 1$ ; therefore, the maxima of the interference pattern will have an

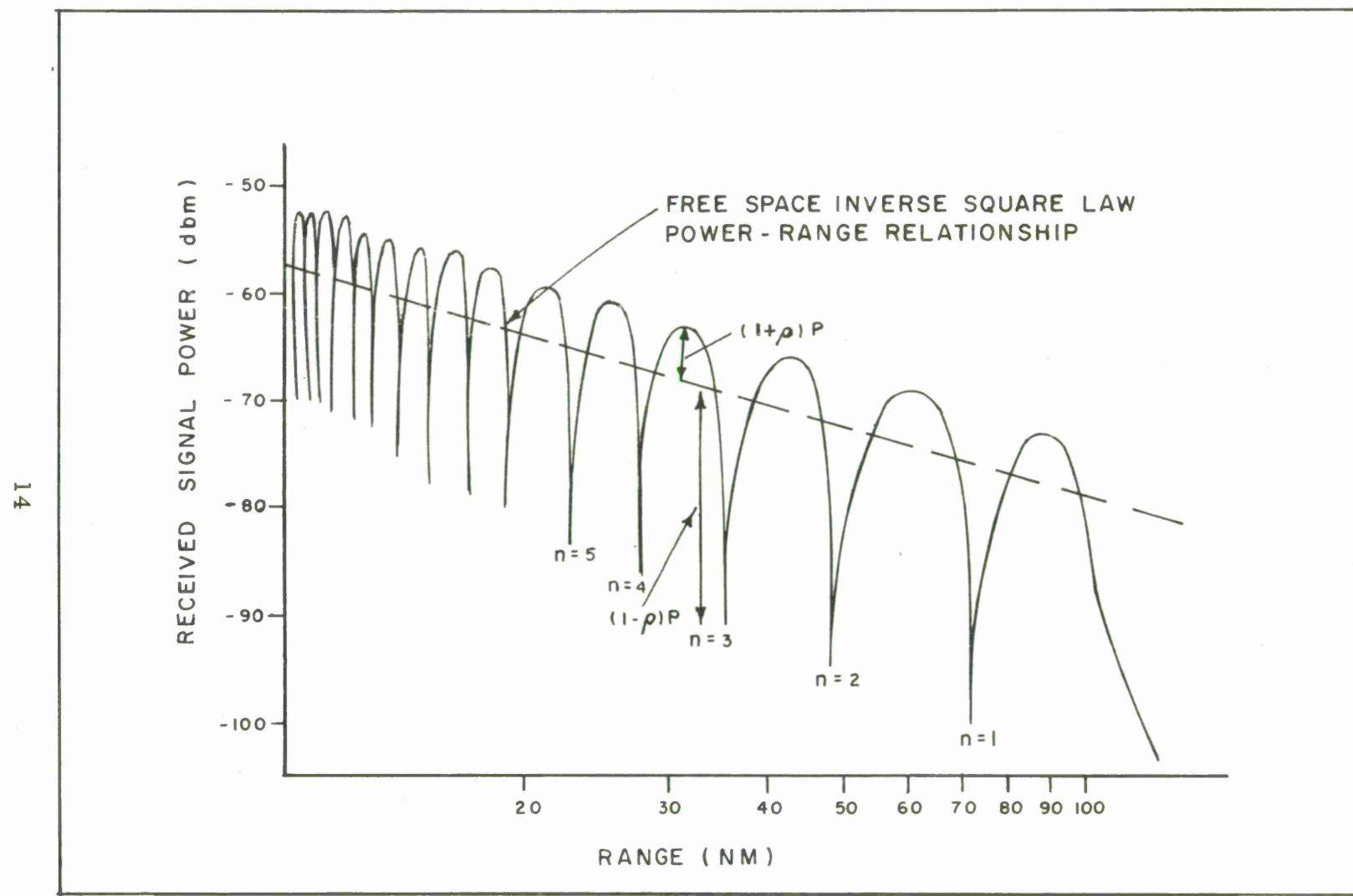


Figure 5. Vertical Interferometer Interference Pattern

amplitude of 2P or 3 db above the free space inverse square law power-range relationship. Conversely the minima of the interference pattern are deep and clearly defined.

As shown in Appendix I, for a straight ray geometry and a spherical earth, there is a direct relationship between the positions of the interference pattern minima and the earth radius. In the case of a constant refractive index gradient atmosphere, the real earth's radius,  $A$ , has to be replaced by the effective earth's radius,  $A_e$ , the significance of which was explained in the previous section.

If the refractivity profile is not linear, the derivation of the  $A_e$  values from the positions of the interference pattern minima can, of course, be carried out as in the case of a linear refractivity profile. Now, however, the results will not be constant for individual minima; i.e., the  $A_e$  values will no longer be constant and independent of range between the receiver and transmitter terminals. The meteorological significance of the  $A_e$  values so derived was discussed in the previous section.

One of the objectives of the experiment described here was to determine the positions of the interference minima, corresponding to a given flight configuration, accurately enough to obtain meaningful

calculations of the  $A_e$  values and, correspondingly, the angles of arrival of the radio signals.

## EARLY EXPERIMENTS

Radio propagation experiments have been carried out over the past several decades. A review of these past programs shows that many radio-meteorological experiments were designed to investigate the effects of anomalous propagation in radio signal characteristics. Meteorological measurement support was provided to determine the general propagation conditions, that is, the prevalence or apparent absence of surface or elevated ducts, but without a great amount of consideration being given to the spatial or temporal variation of the fine structure of radio refractivity. Of course, in many cases it was sufficient to establish that anomalous propagation was present and to determine the effects on radio propagation in a general way. The Cardigan Bay<sup>[6]</sup> and Canterbury Plains<sup>[7]</sup> experiments provided close correlation between the meteorological conditions and their general effect on radio signal propagation. The results provided increased understanding of the effects of anomalous propagation and large-scale meteorological conditions on radio signal propagation. Similarly, early experiments by the Radiation Laboratory of MIT, <sup>[8]</sup> and the later work on propagation in the Trade Wind and evaporation ducts, <sup>[9, 10]</sup> showed a high degree of correlation between

signal level and multipath effects as the height and intensity of these super refraction conditions varied. The reports available describing earlier work are extensive and the above references were selected only to show examples of earlier work. The reader should refer to the recent NBS-CRPL book on "Radio Meteorology" for extensive references. [11]

In the past decade, considerably more effort has gone into experiments to provide information on the angle of arrival and range errors introduced by refraction effects, even to include errors produced by the ionosphere. The use of a vertical reflection interferometer to measure these parameters was recently (1961) investigated by Smythe Research Associates. [12]

In an attempt to reduce the requirement for direct, real-time and -place refraction measurements, a considerable effort has gone into the development of models of the atmosphere. The refractivity profiles of these models are based on the average behavior of the atmosphere derived from statistical analysis of many years of radiosonde data. The Central Radio Propagation Laboratory (NBS) has contributed a great deal of information in this area. [11] Analysis shows that the models may be better predicted by including surface and initial gradient information at a particular location. Certainly the earlier investigations of the

Lincoln Laboratory<sup>[13]</sup> and more recently the Electromagnetic Research Corporation,<sup>[14]</sup> as well as other published reports,<sup>[15]</sup> show that the model behavior depends upon the geographical location and its associated meteorological conditions. To summarize, it has generally been found that models which are not tailored to suit local conditions are ineffective where very high accuracy is required. In particular, combined analysis of the effect of small scale atmospheric irregularities with radar or interferometer tracking errors shows that the model atmosphere approach is not very applicable. Although a combination of radiosonde and aircraft measurements could lead to improved accuracies, this latter approach is very time-consuming and unwieldy.

One might say that in earlier experiments the correlations between meteorological and radio propagation characteristics were not sufficiently detailed or accurate and that conclusions reached were of a very general nature. Certainly trends and associated effects were evident, but the results were insufficiently accurate to establish the possibility of predictions using actual measurable parameters. In the Cold Lake experiment the main effort concentrated on the possibility of drawing detailed conclusions about the accuracy of predicting the radio signal propagation characteristics from meteorological measurements; conversely, it was expected that the results would reveal information

about the possibility of using the radio interferometer technique independently to define an effective refraction condition as a function of the initial elevation angle and the range and height of the ray. In fact, a compilation of these effective radii for known positions of the signal source presented a challenging question as to whether or not an effective refractivity profile could be derived which would define the overall propagation conditions or at least reveal the degree of nonstandard behavior in the atmosphere.

Obviously, to obtain a high degree of correlation between the separate methods of analysis used in the experiment, the radio refractivity had to be measured as accurately as possible. Surface, radiosonde, and airborne refractometer measurements were all combined to determine the refractivity profile and its temporal and spatial variations. The details of these measurements and their interpretations are discussed in Section II. From previous calibrations of aircraft measurements against surface, tower and radiosonde data, it was found that the radio refractivity could be determined in clear air, using the airborne refractometer, to an absolute accuracy of  $\pm 2$  N units and with a relative accuracy of about  $\pm 0.5$  N units. Therefore, a great deal of fine structure could be measured both in the vertical and horizontal variations of the radio refractivity. As will be discussed later, this abundance of fine structure can sometimes be more hindrance than help.

The object in specifying the design of the reflection interferometer experiment was to achieve accuracies in the order of  $\pm 200$  nautical miles or better in the  $A_e$  determinations. To accomplish this sort of accuracy meant that individual parameters had to be measured with considerable precision. The following accuracies were obtained: The receiving antenna height, relative to the reflecting surface was surveyed to within  $\pm 0.05$  ft; the height of the transmitter, relative to the reflecting surface, was found to be  $\pm .25$  feet throughout the range of the flight path; the wavelength of the frequencies used could be measured to better than  $\pm 0.001$  ft; and the determination of the position of the interference minima was carried out to within  $\pm 100$  ft. The methods used to measure the various parameters are described in Section III with a more detailed analysis in Volume III of this report (MTR-118).

#### COLD LAKE EXPERIMENT

A map of the Cold Lake area is shown in Figure 6. The RCAF station at Cold Lake provided the necessary support facilities for the aircraft and participating crews. The ground receiver was located on a 40-foot cliff on the south shore of Cold Lake providing an 11-mile stretch of open water for the reflecting surface. The flight path of the signal source aircraft (360 degrees magnetic) was chosen so that the aircraft overflew Cold Lake, Primrose Lake, Vermette Lake and

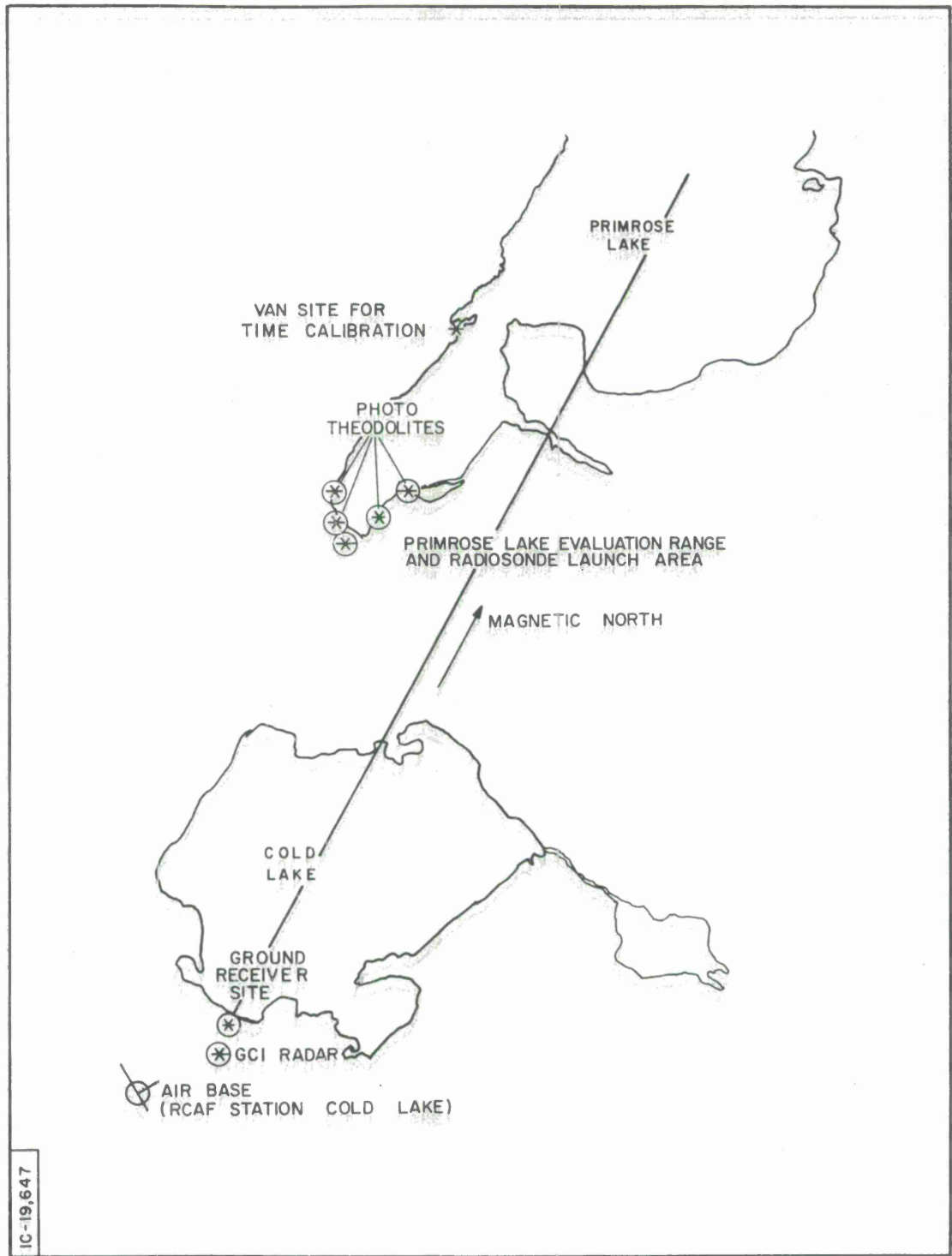


Figure 6. Map of Cold Lake

Peter Pond Lake. The terrain profile along the track is shown in Figure 7. The hills on the north shore of Cold Lake reduced the horizon range somewhat but otherwise had little effect on the interferometer experiment.

The Primrose Lake Evaluation Range (PLER) exercised close control of the participating aircraft through the use of M33C radars. Phototheodolites sited around the panhandle of Primrose Lake were used to give positional data on the signal source aircraft while it was within range, and served to check the accuracy of range measurements using a radar co-located with the receiver. Theodolite data was also required to calibrate a radar altimeter in the signal aircraft. Meteorological support was supplied by PLER in the form of radiosonde releases from within the range area and psychrometric measurements on the surface of Cold Lake.

Additional meteorological support was obtained from the RCAF station at Cold Lake for use in calibrating the meteorological aircraft sensors during preflight and postflight operations.

The 42nd Radar Squadron, located about three miles south of the receiving site, provided control and surveillance for the aircraft when outside of the range of PLER. Positional fixes on the meteorological aircraft were also available from the radar squadron data center.

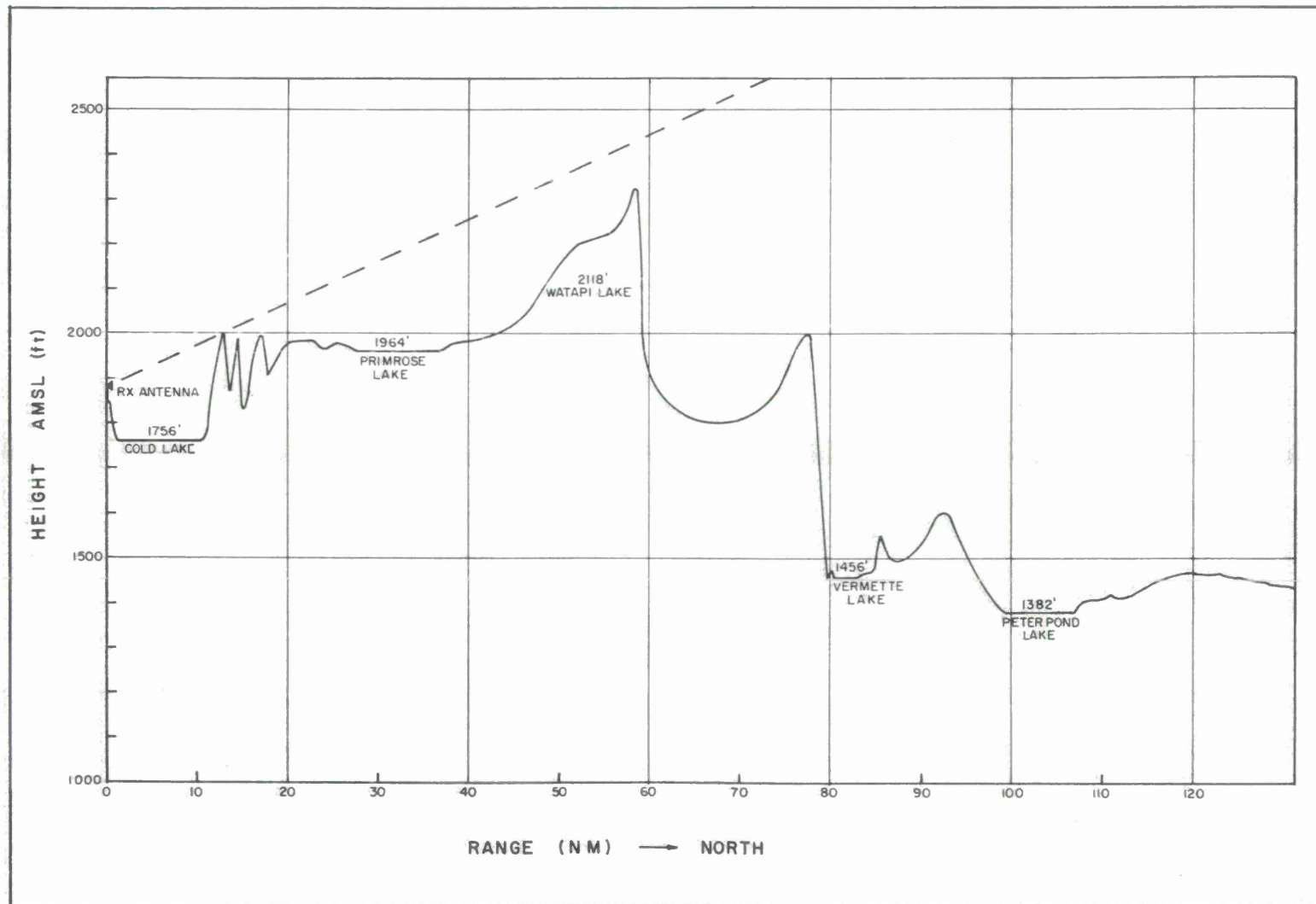


Figure 7. Terrain Profile from Peter Pond Lake to Cold Lake

The radio signal aircraft missions normally included three sets of outbound and inbound flights (legs); each leg covering a single frequency, polarization, and nominal altitude. Individual legs of one mission could differ in any of these parameters. Efforts were made to ensure that the flights would cover various periods of the day; e. g., sunrise, mid day, sunset, and nighttime. Table I outlines the details of the missions, including the type of meteorological measurements which were available for each.

Table I

## List of Missions Completed

DATE	MISSION	INTERFEROMETER MEASUREMENTS			METEOROLOGICAL MEASUREMENTS					COLD LAKE SURFACE MEASUREMENTS
		LEGS OUT/IN	FREQ BAND/POL	TX HEIGHT (FT)	LOCAL TIME (MST)	REFRACTOMETER PROFILE	RADIOSONDE TIME	PROFILE	LAUNCH TIME	
17 Sep 64	102	1/2	S/V	8600	0952-1102	102-1	0942-1122	102	0949	Data taken
		3/4	S/H	8600	1127-1236	102-2	1142-1314	102	1207	
		5/6	L/H	8600	1327-1435	102-3	1204-1344	102	1409	
21 Sep 64	103	1/2	S/H	8600	1130-1240	103-1	1032-1214	103	1100	Data taken
		3/4	S/H	8600	1252-1403	103-2	1032-1214	103	1259	
		5/6	S/H	8600	1412-1521	103-3	1219-1359	103	1507	
22 Sep 64	104	1/2	S/H	7000	0422-0530	Not available		104	0415	No surface data
		3/4	S/H	7000	0537-0649	Not available		104	0616	
		5/6	S/H	7000	0657-0917	Not available		104	0850	
23 Sep 64	105	1/2	S/H	8600	1145-1254	Not available		105	0933	No surface data
		3/4	S/H	8600	1301-1413	Not available		105	1145	
		5/6	S/H	4300	1423-1506	Not available		105	1420	
24 Sep 64	106	1/2	S/H	4300	0927-1015	106-1	1201-1355	106	1016	Data taken
		3/4	S/V	4300	1029-1117			106	1207	
		5	S/V	7000	1143-1203			106	1350	
		7/8	S/H	7000	1303-1402					
28 Sep 64	107	1/2	S/H	7000	1602-1721	107-1	1609-1805	107	1613	Data taken
		3/4	S/H	7000	1728-1839			107	1759	
		5/6	S/H	7000	1852-2002			107	1934	
30 Sep 64	108	1/2	L/H	4300	1254-1400	108-1	1318-1509	108	1324	Data taken
		3/4	L/H	7000	1422-1535			108	1507	
		5/6	L/H	7000	1543-1653					

25

(Continued on page 26.)

Table I (Cont.)

DATE	MISSION	INTERFEROMETER MEASUREMENTS			METEOROLOGICAL MEASUREMENTS					COLD LAKE SURFACE MEASUREMENTS
		LEGS OUT/IN	FREQ BAND/POL	TX HEIGHT (FT)	LOCAL TIME (MST)	REFRACTOMETER	RADIOSONDE	PROFILE	TIME	
1 Oct 64	109	1/2	L/H	4300	1606-1702	109-1	1611-1730	109	1608	Data taken
		3/4	L/H	7000	1710-1821	109-3	1747-1920	109	1744	
		5/6	L/H	7000	1831-1941			109	1913	
5 Oct 64	110	1/2	S/H	7000	0402-0511	Not available		110	1413	No surface data
		3/4	L/H	7000	0524-0634			110	0628	
		5/6	L/H	7000	0642-0753			110	0818	
6 Oct 64	111	1/2	S/H	7000	0403-0514	111-1	0406-0602	111	0415	Data taken
		3/4	L/H	7000	0531-0644	111-3	0611-0735	111	0611	
		5/6	L/H	7000	0652-0805	111-4	0611-0735	111	0739	
7 Oct 64	112	1/2	S/H	7000	0402-0518	112-1	0428-0551	112	0400	Data taken
		3/4	L/H	7000	0535-0652	112-2	0726 spiral	112	0500	
		5/6	L/H	7000	0700-0813			112	0730	
8 Oct 64	113	1/2	L/H	8600	0400-0512	113-1	0402-0526	113	0413	Data taken
		3/4	L/H	8600	0519-0639	113-3	0540-0700	113	0558	
		5/6	L/H	8600	0646-0800	113-5	0720 spiral	113	0825	
8 Oct 64	114	1/2	L/H	8600	1556-1710	114-1	1558-1720	114	1559	Data taken
		3/4	L/H	8600	1716-1831	114-2	1735-1859	114	1737	
		5/6	L/H	8600	1836-1952	114-3	1913 spiral	114	1917	

## SECTION II

### METEOROLOGICAL MEASUREMENTS

#### DESCRIPTION OF MEASUREMENT TECHNIQUE

The radio refractivity structure had to be accurately determined along the direction of the received radio signals. This was necessary, not only to interpret the effect of atmospheric variations on radio signal propagation, but to achieve accurate ray-tracing calculations for comparison with results obtained independently using the interferometer.

The magnitude of the radio refractivity is given by

$$N = \frac{77.6}{T} \left[ p + \frac{4810 e}{T} \right] \quad (6)$$

where  $T$  is the air temperature ( $^{\circ}$ K),  $p$  is the air pressure (millibars), and  $e$  is the water vapor pressure (millibars).

The air temperature and pressure remain reasonably constant at any given altitude, unless the area is in contact with a weather front. In general, for essentially clear flight conditions at Cold Lake, the presence of fronts in the test area can be dismissed. Therefore, any large changes in both the vertical and horizontal variations of the radio refractivity were due to the local variability of water vapor. In addition,

the modifications which normally result from advection, wind speed and direction, solar radiation, air temperature, and surface water temperature also contribute to the concentration of water vapor over such large lakes as Cold Lake and Primrose Lake. Therefore, it was expected that the radio refractivity would be variable both in space and time due to these surface conditions, terrain, and local meteorology.

To monitor these variations, aircraft measurements of the radio refractivity were made along the direction of travel of the radio signals and at sufficient heights to cover all possible paths within the radio signal horizon. A typical flight plan is shown in Figure 8, where it is noted that both vertical and horizontal soundings were obtained. This pattern was repeated twice during each mission, which would then show any significant temporal effects. The rapid point-to-point transitions during the horizontal legs was purposely planned to monitor spatial variations over the test area.

The Crain refractometer used in the meteorological aircraft measures the changes in the index of refraction of the air passing through a microwave cavity. [16, 17] To obtain correct values of the index change, it was necessary to eliminate errors in the measurements caused by thermal expansion of the cavity and ram air pressure. These errors, and the methods used to remove them, are fully discussed in Volume II

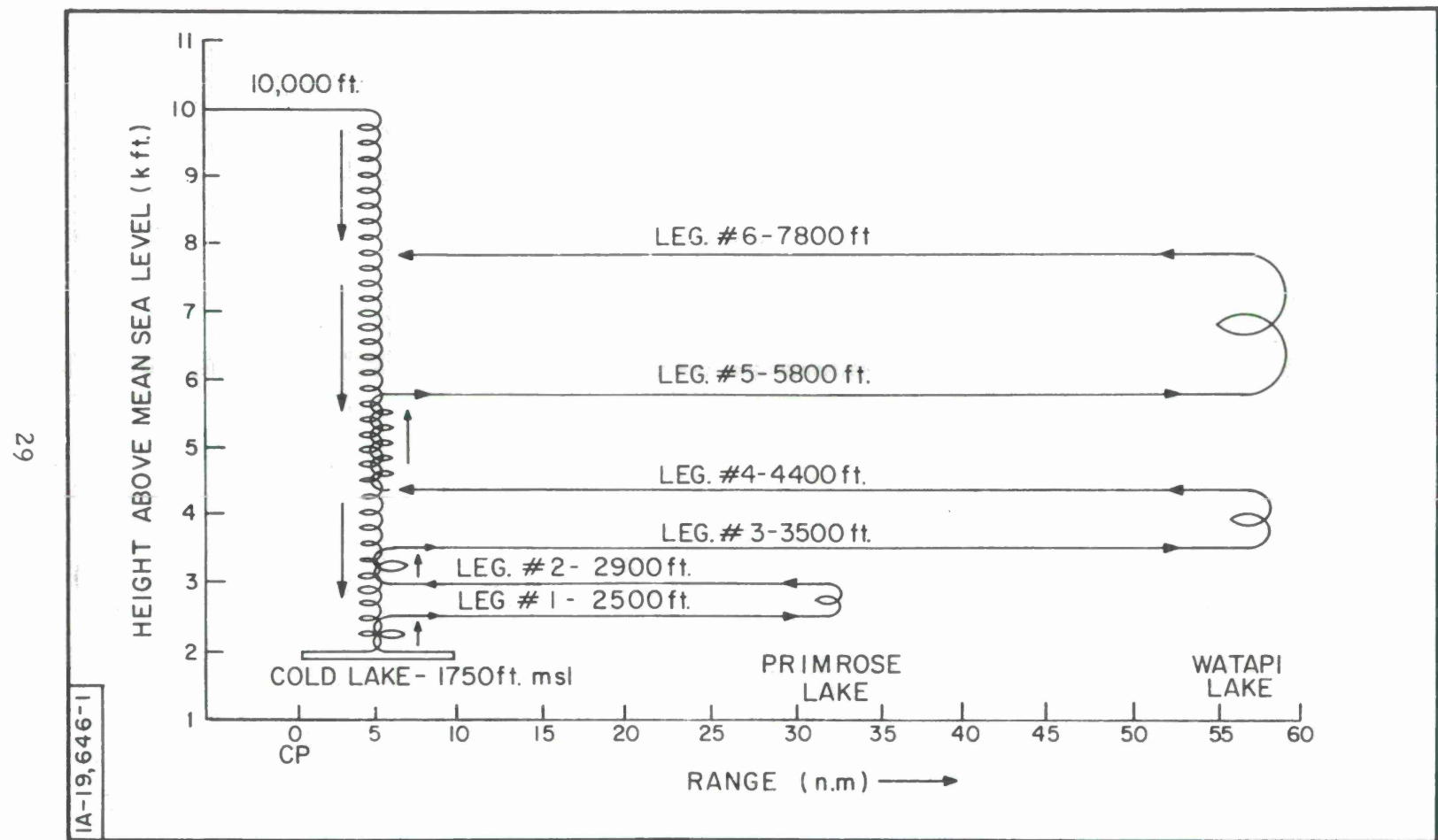


Figure 8. Typical Aircraft Flight Plan for Measurement of Radio Refractivity

of this report. A sensitive air pressure instrument and a radar altimeter provided independent measures of aircraft height. Of course, the radar data was useful only over the lake areas. The height accuracy attainable was about  $\pm 25$  feet which permitted small changes in refractivity to be observed within small height intervals. Details of the aircraft equipment and data recording and processing facilities are discussed in Volume II.

An example of a vertical refractivity profile, together with a radiosonde profile, is shown in Figure 9. The sensitivity of the refractometer is obviously much greater than the radiosonde. However, as will be apparent later on, this abundance of fine structure can lead to some reservations on the unrestricted use of this data to represent the effective propagation conditions. For example, a ray tracing analysis was carried out using these two profiles. As shown in Table II the ray was launched at an initial elevation angle  $\theta_0$ , of 18 mr, and at a height of 60.4 feet. The ray was first traced using the aircraft refractivity profile to heights from 8750 to 8950 feet above the reference surface of Cold Lake. At these heights the tracing was stopped and the characteristics of the ray path were determined. Figure 10 defines the parameters presented in the table, namely, the electrical path length  $R$ , the range error ( $R-R_0$ ), the total bending  $\tau$ , and the elevation angle error  $\epsilon$ .

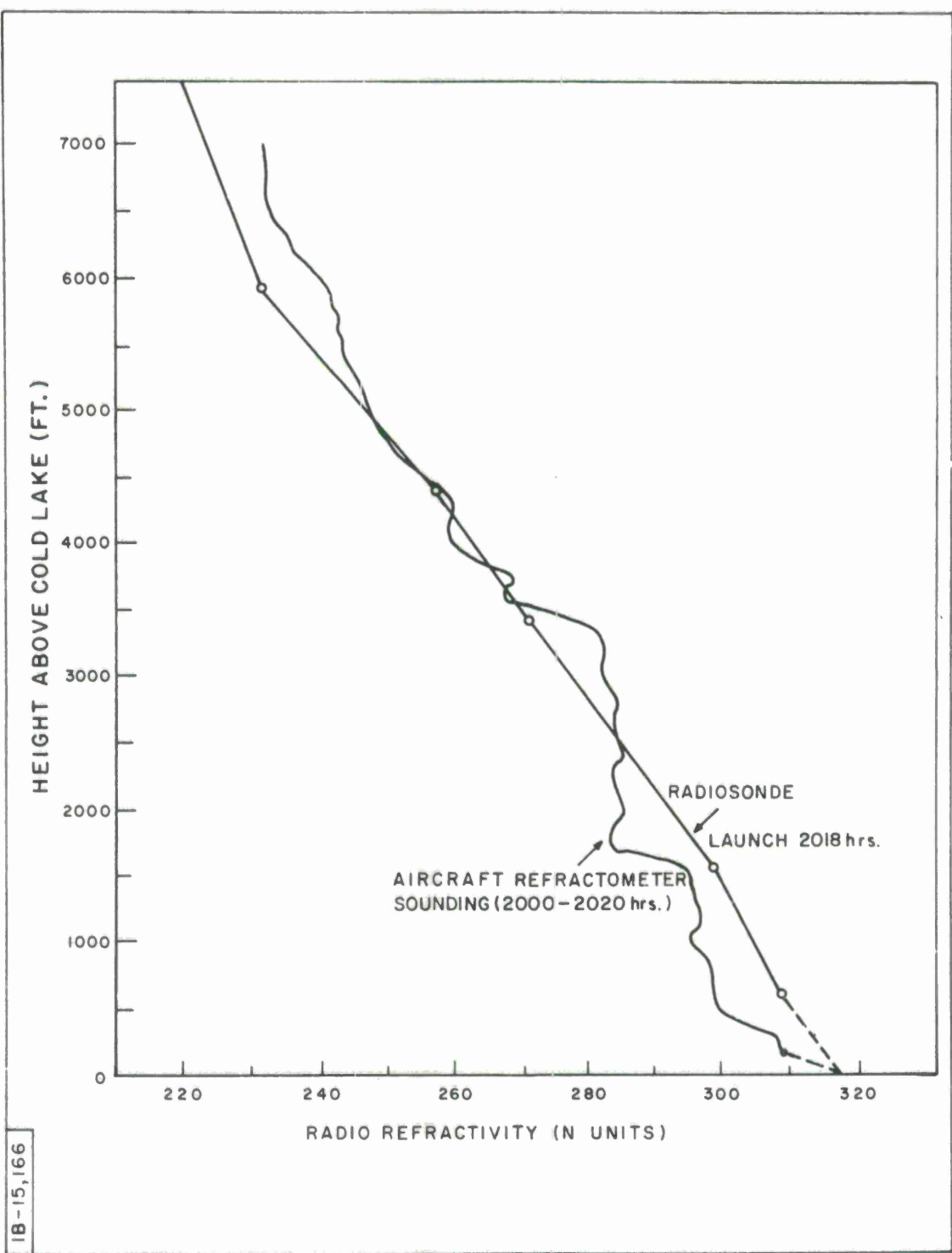


Figure 9. Comparison of Refractometer and Radiosonde Index Profiles

Table II

## Calculation of Refraction Effects

<u><math>h_2</math></u>	<u>Range R(mm)</u>	<u>Range Error (R-R<sub>0</sub>) ft.</u>	<u>Total Bending <math>\tau</math>(mr)</u>	<u>Elevation Angle Error <math>\epsilon</math>(mr)</u>	<u>k</u>	<u>Effective Earth's Radius <math>A_e</math>(nm)</u>
8750.0	58.135	98.84984	3.8869643	1.8508379	1.282458	4406.11
8800.0	58.400	99.21361	3.9110985	1.8601380	1.282619	4406.69
8850.0	58.665	99.57561	3.9351915	1.8694472	1.282783	4407.27
8950.0	58.	100.29431	3.9832550	1.8880917	1.283120	4408.47

32

n(h) = Profile I (A/C Sounding Primrose 2000-2020 hours)

 $h_1$  = 60.4 ft. $\theta_0$  = 18.0 mr $h_2$  = Nominal A/C Pressure Altitude, 8850 ft. (Cold Lake)

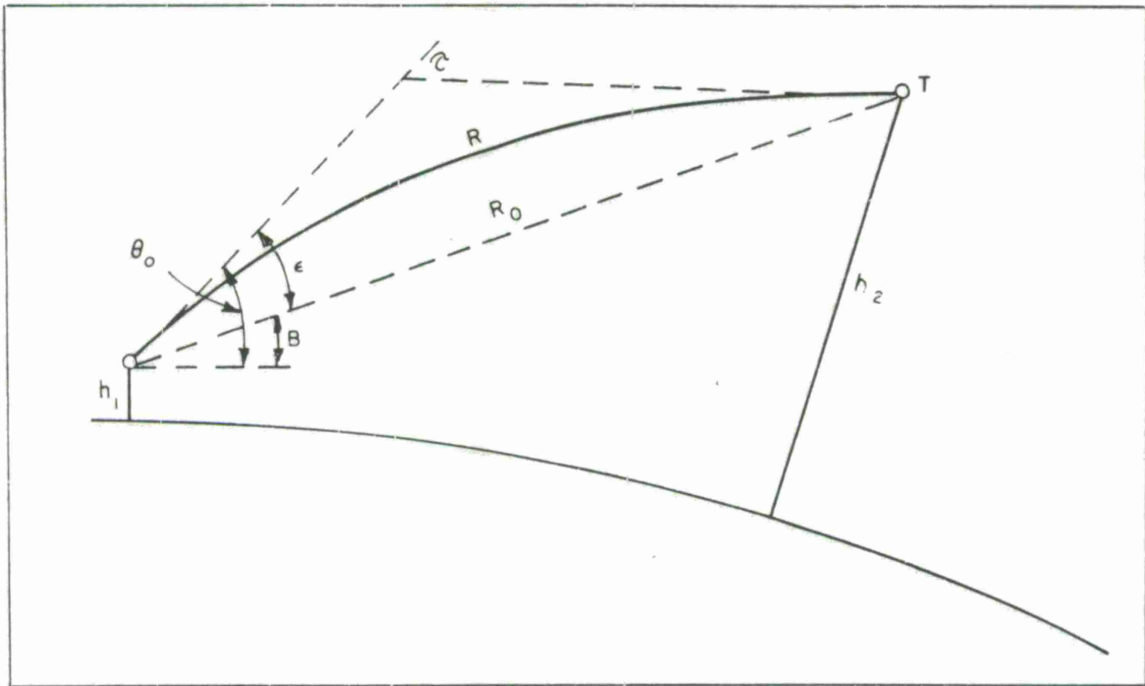


Figure 10. Ray-Tracing Geometry

The quantities  $k$  and  $A_e$  were described in previous sections. Table III shows the difference between the sets of data using the aircraft profile first and then the radiosonde profile. With respect to accuracy requirements placed on the Cold Lake test (i.e., less than 200 n.m. standard error between interferometer and ray-tracing calculations of  $A_e$ ), it is significant to note that the differences in the determinations of  $A_e$  are about 170,000 feet or about 30 n.m. This is an acceptable error for the initial elevation angle of 18 mr and demonstrates that the radiosonde profile provides a good average representation of the propagation

Table III  
Comparison of Refraction Variables for Two Profiles

$h_2$	Range Difference (nm)	Range Error Difference ft.	$\tau$ Difference	$\epsilon$ Difference	k Difference	(kft) $A_e$ Difference
8750.0	-3.194377	1.510333	-0.424719	-0.296876	-0.056308	177.816468
8800.0	-3.208281	1.519930	-0.412768	-0.297425	-0.056154	174.597458
8850.0	-3.221475	1.529104	-0.400832	-0.297911	-0.055990	171.164189
8900.0	-3.233967	1.537854	-0.388911	-0.298333	-0.055816	167.524125
8950.0	-3.245766	1.546181	-0.377005	-0.298695	-0.055633	163.684481

Profile I = A/C Sounding - Primrose 2000-2020 hours

Profile II = Radiosonde Sounding - Primrose 2000-2020 hours

$h_1$  = 60.4 ft

$\theta_0$  = 18.0 mr

$h_2$  = Nominal A/C Pressure Altitude, 8850 ft (Cold Lake)

All differences are aircraft profile results minus radiosonde profile results.

conditions. Of course, at lower elevation angles, the differences between profiles become more apparent, a subject which is dealt with at considerable length below.

The radiosonde profiles were obtained three times during each five-hour test period. The launch site was advantageously located along the direction of the radio signal path and about 25 nm from the receiver site (see Figure 6). Before each launch, the sensors were brought to equilibrium with the local air mass, and their readings were checked against psychrometric measurements at the same point. The care taken before launch paid excellent dividends in the quality and, as will be shown, the usefulness of the radiosonde data in the ray-tracing results. At the launch site, surface measurements were made of the wind speed and direction, pressure, and sky conditions. This information was extremely useful for correlation with the Cold Lake surface measurements which are discussed below. Volume II contains all the particulars of the surface and radiosonde data recorded for each launch.

Surface measurements were made from a boat located near the center of Cold Lake and along the direction of the radio path. Since this surface is the reflector in the interferometer experiment, it was considered essential to monitor the radio refractivity characteristics in the event that the reflected ray should be trapped by a surface layer,

or the signal pattern disturbed by periods of large-scale wave motion. Psychrometric measurements, as well as wind speed and direction, were obtained at an approximate height of 8 feet above the mean lake surface. Surface water temperature measurements were also made to determine the magnitude of the saturated value of radio refractivity, that is, where the vapor pressure  $e$  is at saturation for a water temperature  $T$ . These surface data were also valuable to check the aircraft calibration which was performed by having the aircraft fly at extremely low levels (less than 50 feet) over the boat, then later checking the aircraft measurements against the psychrometric surface measurements.

Since the radiosonde launch height was several hundred feet higher than the level of Cold Lake, the surface measurements provided a value of radio refractivity which was used to extrapolate the radiosonde profile down to the Cold Lake level. The readings above the surface and at the water level were also intended to reveal information about the stability of the local air mass and the N deficit from which one might weigh conditions, suitable or otherwise, for the formation of stratified super-refractive layers. The details of this inquiry have been reserved for discussion in Volume II. It is sufficient to state here that the predictions based on this approach are confounded by the extreme variability of prevailing conditions. Cold Lake is relatively small and surface

propagation conditions respond to the effects of the wind speed and direction and local meteorological conditions and apparently much less to micrometeorological effects at the lake surface.

#### SELECTION OF MEANINGFUL PROFILES FOR RAY-TRACING ANALYSIS

The radiosonde profiles were chosen for the final ray-tracing analysis but not independently of the aircraft measurements. In fact, as will be shown later, the aircraft profiles may very often provide results in agreement with those obtained by the interferometer. However, in the overall analysis the radiosonde representation of the propagation conditions is very well correlated with the observations obtained using the interferometer. The importance of the aircraft measurements cannot be underestimated because, as Figures 11 through 15 show, the presence of temporal variations are clearly evident in the aircraft measurements as well as the intensity, stratification, and abundance of small elevated layers. Examination of the radio signal reveals details, such as greater than free-space loss with range, and a "staircase" pattern of signal drop-offs, that would be virtually impossible to explain without a knowledge of the refractivity fine-structure.

As an example of the use of aircraft information, Figure 11 shows three refractivity profiles over Cold Lake taken at intervals of

about two hours. These measurements show that significant refractivity variations were present, indicating that the propagation conditions in the test area were changing rapidly with time. The variations near the surface are relatively large, which could cause large deviations in the interferometer calculations of  $A_e$ .

The aircraft refractometer measurements near the surface of Cold Lake generally indicated larger refractivity gradients than could be derived from the radiosonde data when both lower readings were extrapolated to the measured surface values. The spatial variability of refractivity data near the surface is illustrated in Figures 12 through

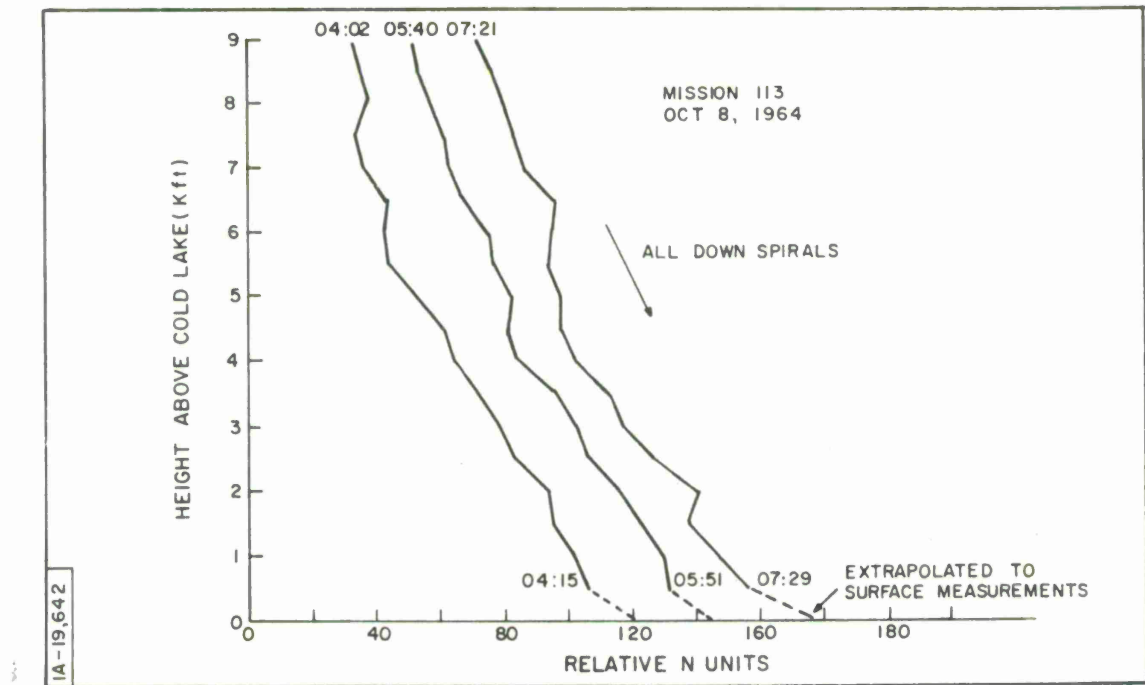


Figure 11. Temporal Variation of Refractivity Over Cold Lake

IA - 19, 638

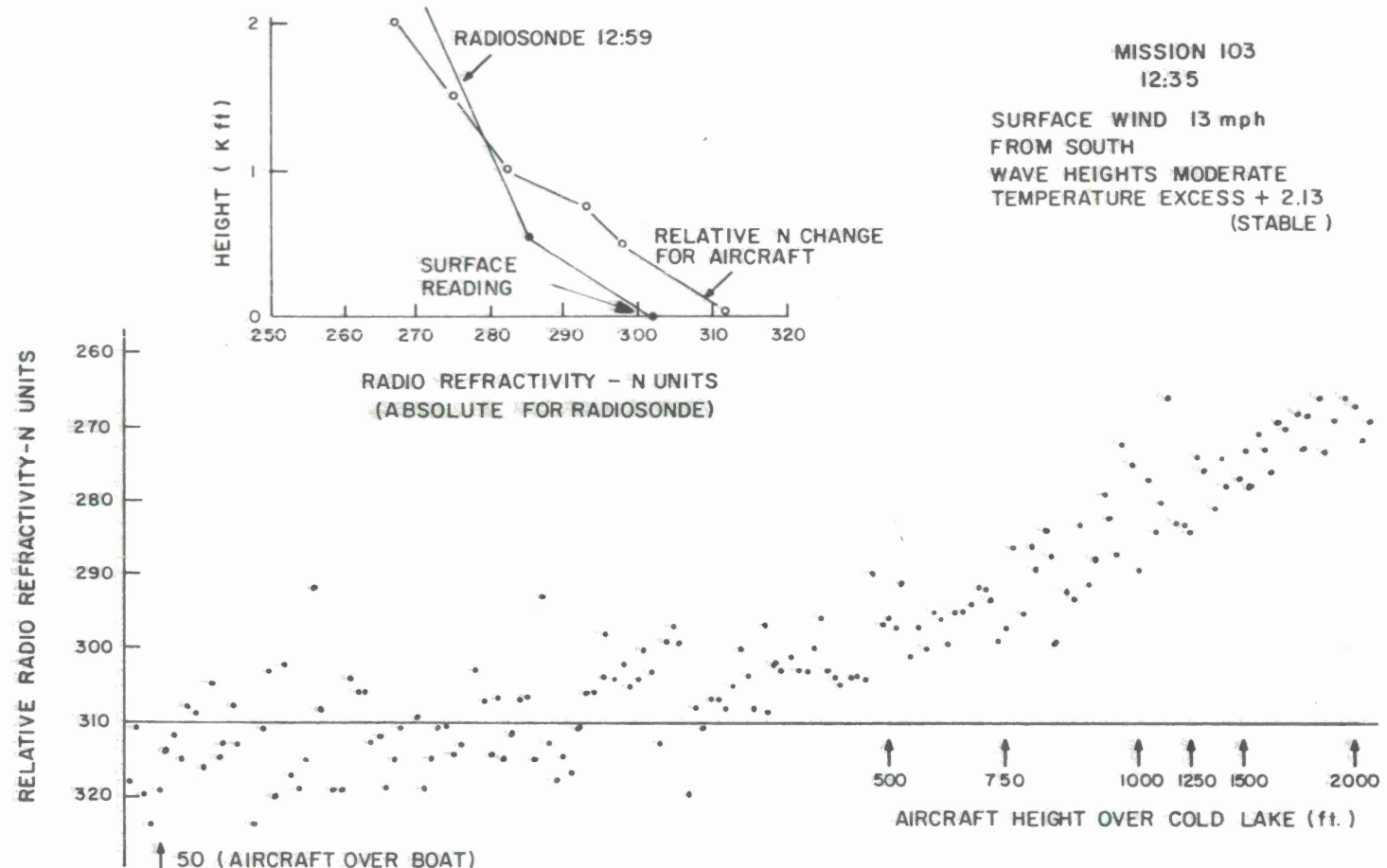


Figure 12. Spatial Variability of Refractivity Data Near Surface of Cold Lake - Surface Wind 13 MPH from South

1A-19,640

MISSION 107  
16:23

SURFACE WIND 6 mph  
FROM NORTH  
WAVE HEIGHTS MODERATE  
TEMPERATURE EXCESS  
- 5.54° (UNSTABLE)

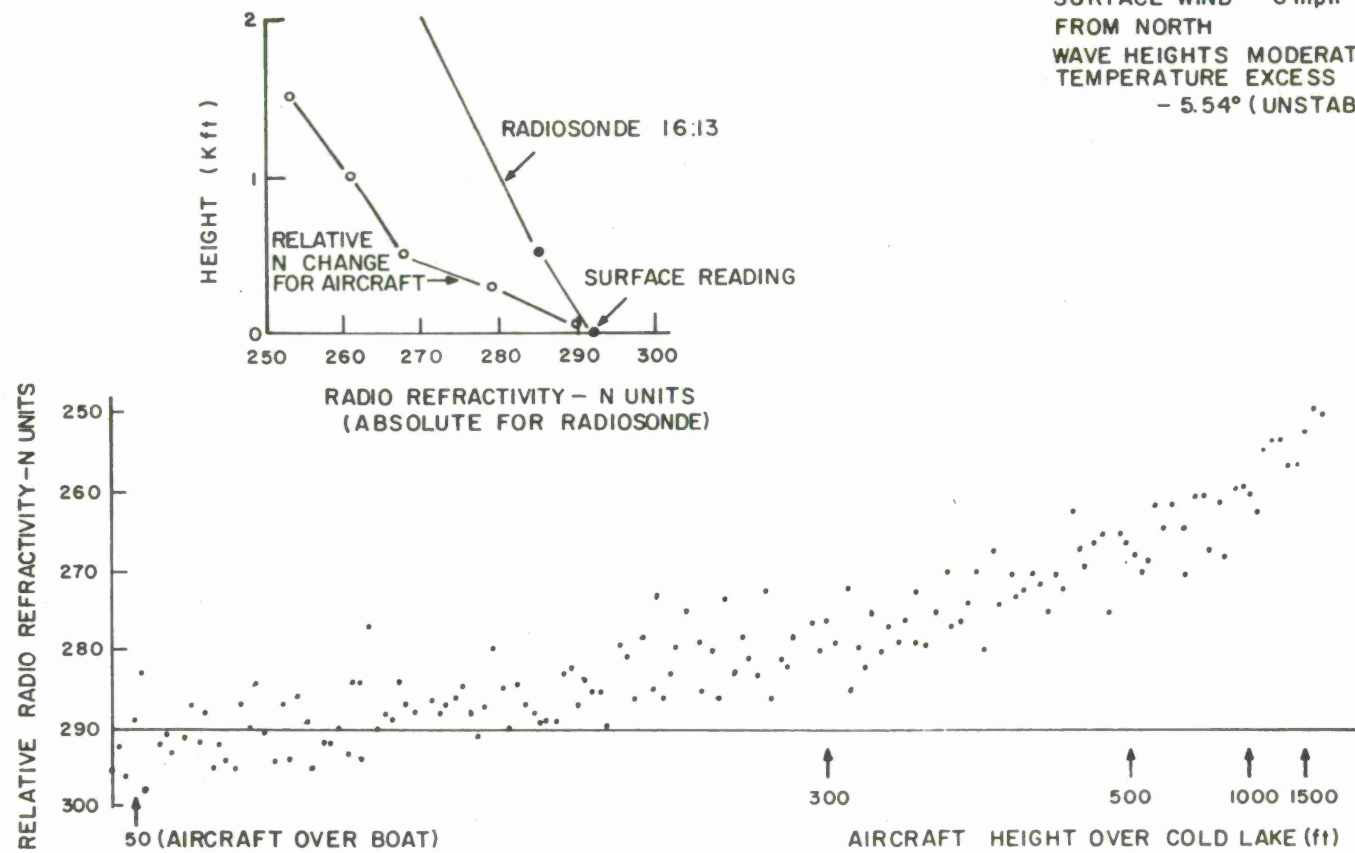


Figure 13. Spatial Variability of Refractivity Data Near Surface of Cold Lake - Surface Wind 6 MPH from North

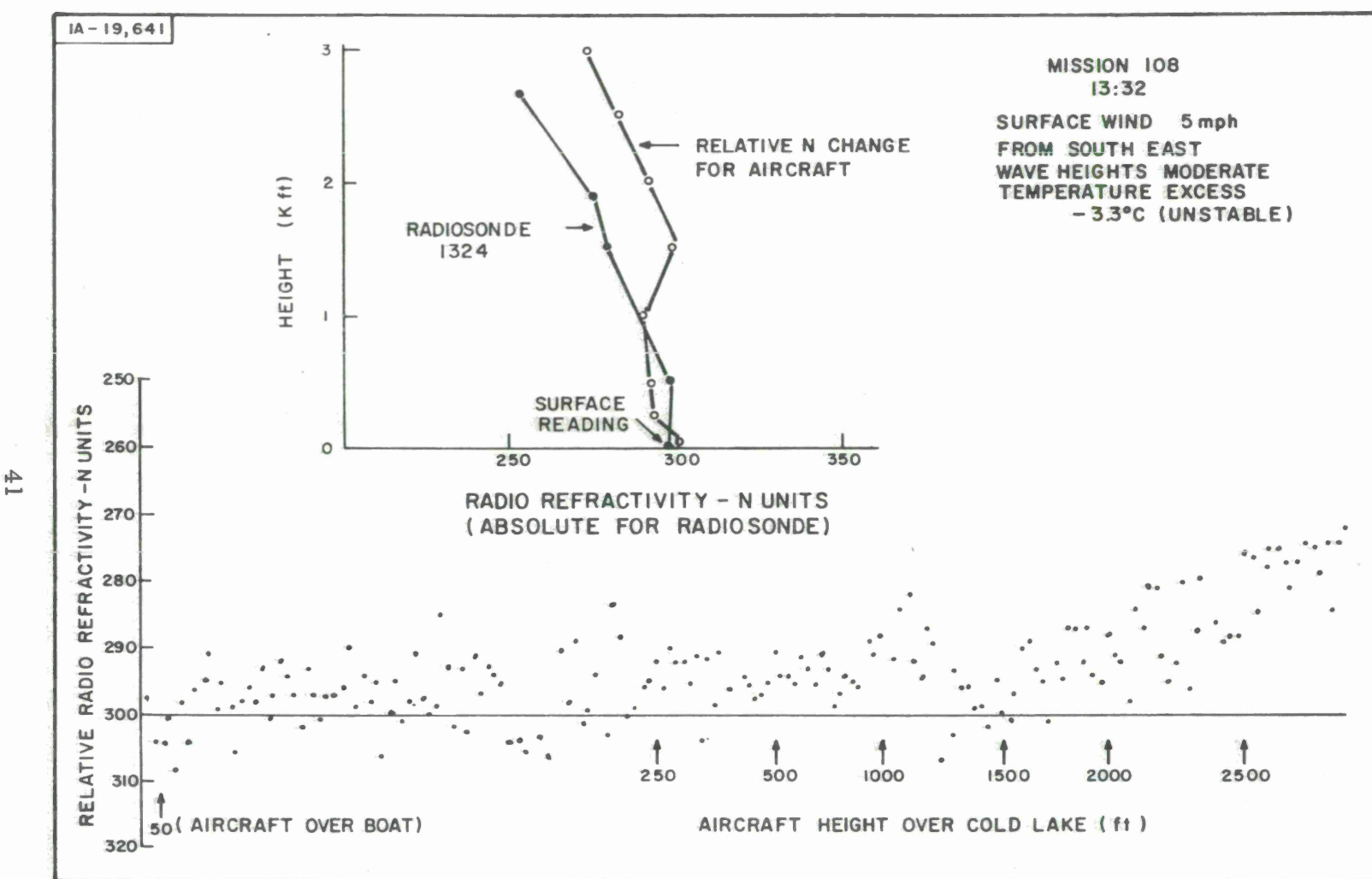


Figure 14. Spatial Variability of Refractivity Data Near Surface of Cold Lake - Surface Wind 5 MPH from Southeast

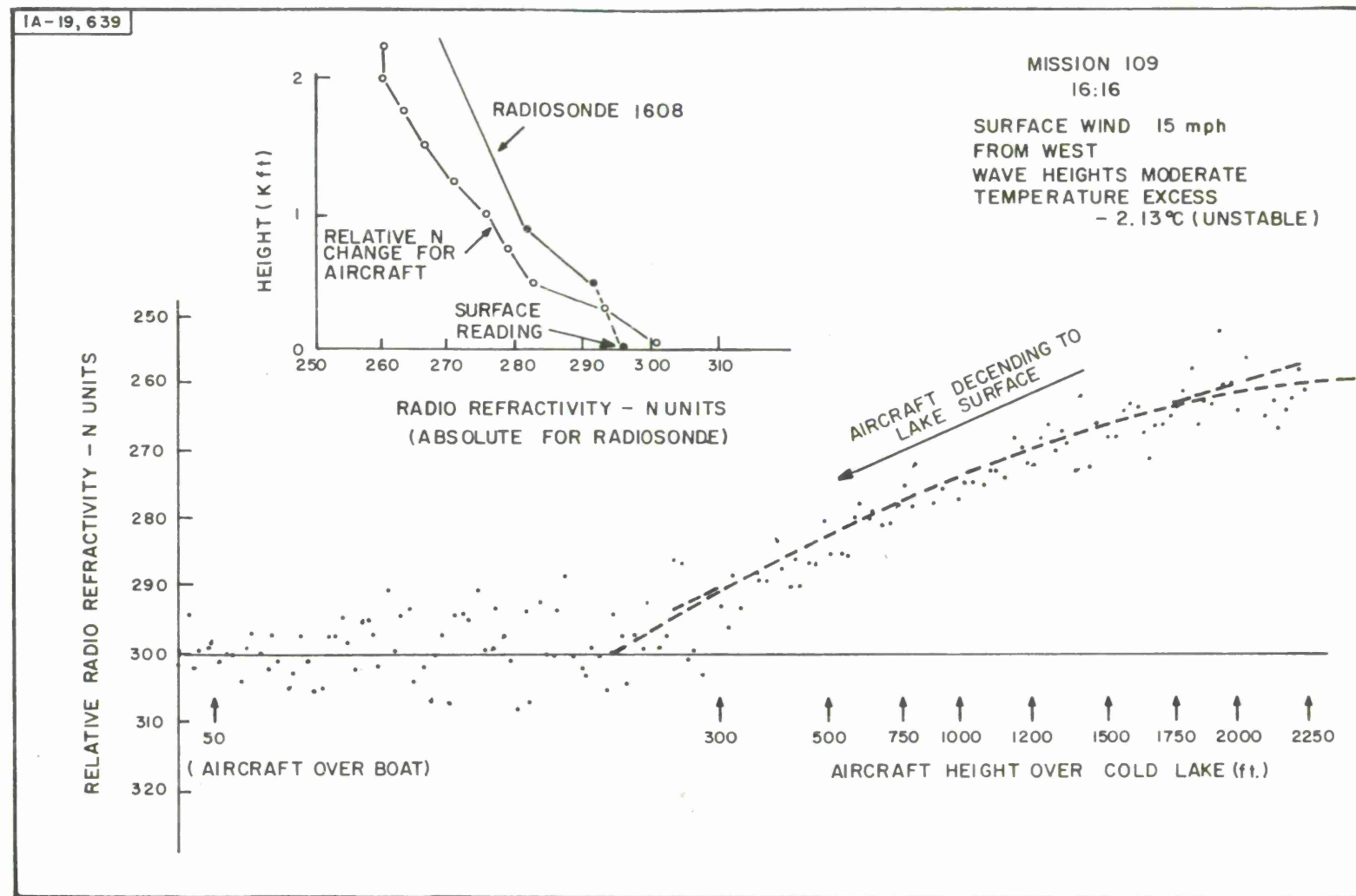


Figure 15. Spatial Variability of Refractivity Data Near Surface of Cold Lake - Surface Wind 15 MPH from West

15. These show how the measured relative refractivity varies as the aircraft makes a descending radial pass from approximately 2000 foot altitude to 50 foot altitude over the boat on the surface of Cold Lake. The inserted plot on each graph gives an estimation of apparent profiles for both aircraft and radiosonde (extrapolated) data. The refractivity values show wider variations as the aircraft approaches the surface. The increasing variability could be caused either by an increase in the horizontal refractivity inhomogeneity or by some other mechanism, such as the presence of microscopic liquid water droplets in the medium. It is known that the presence of physical material in the refractometer cavity increases its resonance frequency as does a normal reduction in the refractivity of the ventilating medium. Therefore, the "droplet" theory might provide an explanation for both the biases apparent in the low-level refractivity profiles and for the large fluctuations. In any case it will be seen later that the low-level aircraft data is nearly always inconsistent with the extrapolated radiosonde profile and the interferometer results.

In summary, it may be stated that radiosonde data was used to great advantage in the ray-tracing analysis. However, these profiles were tested against aircraft measurements to substantiate their mean-value representation of the refractive conditions at the higher levels. At the lower levels the aircraft measurements were used mainly to

provide qualitative information about the refractivity behavior between the lowest levels of radiosonde data and the Cold Lake surface measurements. The ray-tracing profiles will be shown in the later sections in conjunction with the comparison of results. Comments are noted with respect to these profiles vis-a-vis the characteristics of aircraft information.

## SECTION III

### RADIO PROPAGATION

#### INTRODUCTION

This section gives a general description of the instrumentation and techniques utilized in the radio propagation experiment. Further detailed information is included in Volume III of the report, which also includes a description of the techniques for computing the effective earth's radii.

#### Ground Receiving Equipment

The ground receiving equipment used in the trials consisted of the Canadian-built electronic countermeasures field strength monitor van, which was developed primarily to evaluate the signal characteristics of airborne ECM transmitters. A simplified block diagram of the installation is shown in Figure 16.

Standard gain horn antennas were used on both S- and L-bands with a beamwidth of about 30 degrees (half-power points) in both the vertical and horizontal planes. With this beamwidth, the signal source aircraft could remain within the beam without altering the azimuth or elevation of the antennas, for transmitter ranges from 100 down to 10 nautical miles from the receiver and for aircraft altitudes under 10,000 feet.

94

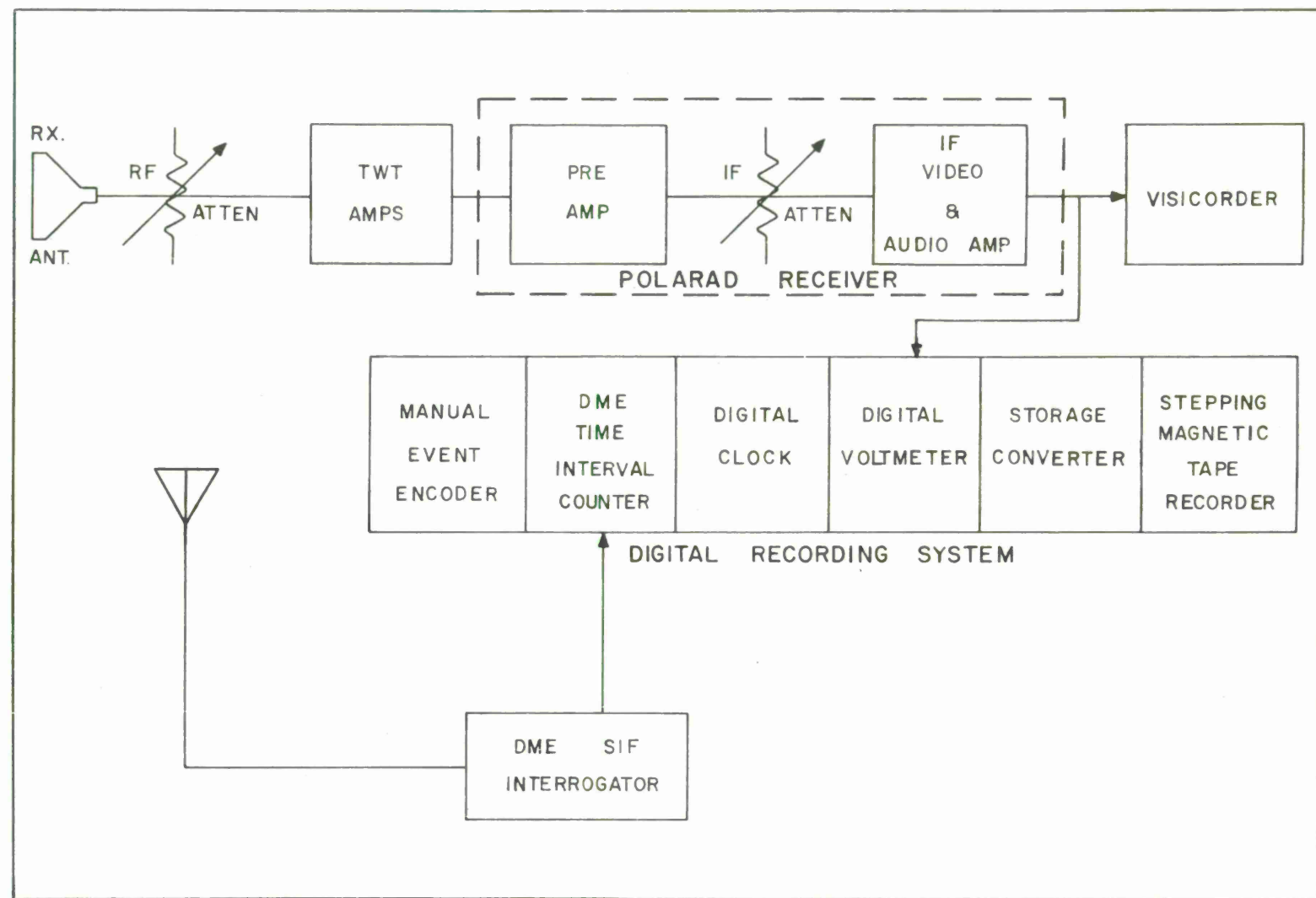


Figure 16. Block Diagram of Ground Receiving and Recording System (In Van)

Cascaded, broadband travelling wave tube (TWT) amplifiers were used to drive a Polarad receiver (bandwidth 6 MHz). The output amplitude of the receiver was recorded by an oscillograph paper chart recorder (Honeywell Visicorder). The output was also digitized at a sampling rate of once per second. Radio frequency attenuators were used ahead of the TWT's to prevent saturation of the system in the presence of strong signals. The receiver was operated with the AGC off to permit the recording of fast fluctuations in the received signal. Manually adjustable attenuators were used between the preamplifier and the IF amplifiers to keep the amplitude of the received signal "on-scale" on the receiver output meter. Read-out of the RF and IF attenuator positions was fed automatically to both the analog and digital recorders.

To provide a continuous, accurate measurement of the range between the airborne transmitter and the receiver, a standard IFF/SIF interrogator was modified to interrogate the SIF transponder in the aircraft at the once-per-second sampling rate, and, simultaneously, to start a time interval counter. When the reply from the aircraft was received and decoded, the counter was stopped. The digitized time interval (radar range) was recorded in the digital recording system. The distance measuring equipment (DME) was calibrated during the Cold Lake Experiment and was found to provide an accuracy of  $\pm$  85 feet at ranges within line of sight.

A digital clock provided the synchronizing triggers for the automatic recording system. The triggers were also supplied to one galvanometer in the visicorder. Central time, binary-identified, one-second pulses, which were transmitted on VHF by PLER to synchronize phototheodolite operations, were also received in the van and applied to another galvanometer in the visicorder. It was possible, therefore, to accurately correlate the events recorded by PLER with the events recorded in the monitor van. The overall timing accuracy was found to be about  $\pm 0.1$  seconds, thereby contributing a  $\pm 25$ -foot error in the DME range to the transmitter.

#### Transmitter

The signal-source aircraft was an RCAF North Star from the Central Experimental and Proving Establishment (CEPE) at Uplands, Ottawa. Wide-band (about 30 MHz), noise-modulated transmitters were used on L- and S-bands with nominal powers of 800 and 400 watts respectively. The majority of the trials were carried out using horizontal polarization; however, a few were run on S-band using vertical polarization. The antennae on both L- and S-bands were nominally omnidirectional.

The aircraft flew a constant pressure altimeter course with the nominal height established by radar altimeter readings over Cold

Lake at the beginning of each mission. The SCR718 radar altimeter readings were thereafter recorded at 20-second intervals as the aircraft overflew the several large lakes along the track. From these measurements, true altitude data was obtained which could be referred to the Cold Lake reflection surface level. These readings provided the majority of the data used to determine the aircraft height. The reading accuracy of this altimeter was about  $\pm$  50 feet; however, it was discovered later, by comparison with the phototheodolite results, that the readings were consistently high by about 75 feet and they were corrected accordingly.

#### PLER RANGE AND ALTITUDE SERVICES

The PLER phototheodolites, located 25 miles from the ground receiver, were used to track the signal source aircraft and to record positional information at 10-second intervals during the period that the aircraft was within their optical range. The PLER M33C tracking radars, with associated plotboards, were used to slave the phototheodolites and to produce plots of the position of the signal-source aircraft. Correlation of events was achieved by recording tone transmissions, central time, phototheodolite synchronizing pulses, and radar plotboard minute event marks, on oscilloscope recorders.

The height information on the North Star as reduced from the phototheodolite data (accuracy  $\pm$  10 feet at short range) was used to calibrate or correct the radar altimeter data mentioned above.

#### Data Reduction

A program was written for the IBM 7094 computer to reduce the output tapes from the monitor van digital recording system. The computer printouts were then used to plot the graphs of signal amplitude (calibrated as dbm at the input to the TWT amplifier) vs. range (n. m.) between the receiver and transmitter. A sample printout is shown in Table IV. The remainder of the printouts, which are quite extensive and of no general interest, are stored at MITRE.

The visicorder records were used to obtain the best possible accuracy in determining the ranges of interference pattern minima. The exact times at which the minima occurred were noted. The computer printouts of DME range vs. time were then plotted in the region of the observed fade. The exact range of the fade was then interpolated from the smoothed plot. The values thus obtained were used to calculate the effective earth's radii ( $A_e$ ) as described in the following section. The  $A_e$  values vs. the ranges at which minima occurred are presented in an appendix to Volume III. A sample of this information is shown in Table V. The first set of ranges of minima (fades) were obtained from the visicorder analysis. These values were later checked against the computer

Table IV. Sample Computer Printout of Monitor Van Data

AIRCRAFT HEADING AND ALTITUDE	CENTRAL TIME IN SECONDS	PLER RANGE R <sub>1</sub> (ft)	DME RANGE R <sub>2</sub> (ft)	R <sub>1</sub> -R <sub>2</sub> (ft)	AIRCRAFT HEADING AND ALTITUDE	CENTRAL TIME IN SECONDS	PLER RANGE R <sub>1</sub> (ft)	DME RANGE R <sub>2</sub> (ft)	R <sub>1</sub> -R <sub>2</sub> (ft)
Radial Outbound 8600 ft AGL APX-25 Normal	564.82	8702	8691	11	Radial Inbound 8600 ft AGL APX-25 Low	2897.00	161860	161690	170
	574.82	9494	9450	44		3013.33	118680	118545	135
	584.82	11207	11114	93		3084.90	92146	92058	88
	594.82	13503	13411	92		3157.84	65229	65140	89
	604.82	16116	15944	172		3262.13	27455	27337	118
	614.82	18930	18828	102		3272.13	23968	23890	78
	624.82	21861	21687	174		3282.13	20547	20413	134
	634.82	24867	24793	74		3292.13	17255	17119	136
	644.82	27939	27816	123		3303.13	14194	14077	117
	732.83	55864	55786	78		3312.13	11513	11379	135
	809.30	80748	80666	82		3322.13	9610	9478	132
Radial Inbound 8600 ft AGL APX-25 Normal	881.24	104090	104011	79		3997.25	43652	43544	108
	953.02	127310	127236	74		4007.25	42614	42500	114
	1305.72	155650	155538	112	Orthogonal 8600 ft AGL APX-25 Normal	4017.25	42444	42365	79
	1408.29	117460	117271	189		4361.10	43163	43065	98
	1480.12	90946	90842	104		4371.10	43337	43257	80
	1552.32	64463	64371	92		4381.10	43885	43758	127
	1641.67	32066	31967	99		4391.10	44777	44650	127
	1651.67	28522	28395	127		4782.55	44208	44100	108
	1661.67	25030	24931	93		4797.55	43221	43114	107
	1671.67	21576	21496	80		5207.30	44498	44392	106
	1681.67	18277	18166	111		5222.30	45330	45209	121
	1691.67	15155	15076	79		5977.20	44260	44146	114
Radial Outbound 8600 ft AGL APX-25 Low	1701.67	12378	12254	124		5987.20	43893	43763	130
	1711.67	10253	10175	78		5997.20	43690	43606	84
	1721.67	9203	9150	53	Orthogonal 100 ft AGL APX-25 Normal	6007.20	43712	43616	96
	2133.78	9078	9054	24		6335.27	43922	43867	55
	2143.78	10539	10470	69		6345.27	43688	43557	131
	2153.78	12716	12584	132		6365.27	43861	43768	93
	2163.78	15294	15169	125		6678.80	44163	44048	115
	2173.78	18115	17981	134		6688.80	43720	43606	114
	2183.78	21045	20931	114		6698.80	43564	43458	106
	2193.78	24077	23958	119		6708.80	43688	43557	131
	2203.78	27177	27066	111		6965.53	43817	43704	113
	2213.78	30321	30173	148		6975.53	43544	43458	86
	2285.87	53567	53454	113		6995.53	43988	43875	113
	2358.40	77197	77048	149					
	2430.16	100787	100698	89					
	2502.40	124170	124075	95					

Table V. Effective Earth's Radius vs Range

MISSION	102												DATE	17 Sep 64			TIME	0952-1102												BAND	S			POLAR	Vert.	$\lambda$	.2948 ft.		
LEG	1 OUTBOUND												h <sub>1</sub>	58.90			ft.	h <sub>2</sub>	8600			ft.																	
FADE NO.	20	19	18	17	16	15	14	13	12	11	10	9	8	7	6	5	4	3	2	1																			
TIME	09	57:35	57:55	58:15	58:38	59:02	59:28	59:58	00:31	01:10	01:52	02:40	03:37	04:42	05:56	07:18	08:47	10:30	12:25	14:52	17:37																		
D.M.E. ( $\mu$ sec.)	327.78	343.96	359.98	378.66	398.30	419.59	443.80	470.42	501.22	536.06	572.72	618.19	671.11	727.56	803.16	873.62	947.10	1038.77	1155.47	1286.25																			
RANGE OF FADE (NM)	1	26.536	27.845	29.141	30.653	32.242	33.964	35.923	38.077	40.569	43.307	46.354	50.023	54.314	58.881	64.998	70.699	76.644	84.061	93.503	104.08																		
RADAR ALT. (ft. A.C.L.)	←	←	←	←	←	←	←	←	←	←	←	8600	→	→	→	→	→	→	→	→	→	→	8575	→	→	→	→	→	→	→	→								
EFFECTIVE A EARTHS B RADIUS (NM) C	4000	4440	4625	4475	4525	4450	4050	4325	4275	4280	4320	4325	4170	4300	4425	4575	4575	4650	4725	4550	4475	4550	4575																

LEG 2 INBOUND

52

FADE NO.	20	19	18	17	16	15	14	13	12	11	10	9	8	7	6	5	4	3	2	1									
TIME	10	51:37	51:13	50:45	50:14	49:46	49:08	48:31	47:46	47:01	46:02	45:09	43:58																
D.M.E. ( $\mu$ sec.)	326.46	341.95	358.98	377.95	395.41	419.30	442.00	470.01	498.61	533.94	569.16	613.73					NO	DME	AVAILABLE										
RANGE OF FADE (NM)	1	26.426	27.682	29.060	30.595	32.008	33.941	35.777	38.044	40.358	43.216	46.066	49.672																
RADAR ALT. (ft. A.C.L.)	8600	→	→	→	→	→	→	→	→	→	→	→	→	→	→	→	→	→	→	→	→	→	→	→	→	→	→	→	
EFFECTIVE A EARTHS B RADIUS (NM) C	3740	4100	4200	4250	4400	4050	4030	4300	4150	4250	4150	4250	4090	4150	4250														

METEOROLOGICAL RESULTS

PROFILE NO. 1 TIME 0952-1122 AIRCRAFT - 102-1

PROFILE NO. 2 TIME 1142-1314

AIRCRAFT 102-2

RANGE	17	21	25	30	35	43	56	71	93	108	13	17	23	29	49	68	83	94	103								
EFFECTIVE EARTHS RADIUS	1	4491	4536	4585	4667	4782	4989	5422	6164	7703	9068	5158	5159	5161	5163	5180	5212	5260	5322	5397							

REMARKS:- Radar Altimeter corrections for Effective Earths Radii A, B and C are 0, -50, and -100 ft

printout values, and, where they differed by more than 0.03 n. m., the computed range was entered in the second line. In some instances, normally at long ranges, it was difficult to determine the precise position of the fade. In these cases, the first value recorded was the mid-position of the fade as determined from the analog records, while the other two values were computed from minimum amplitudes in the region of the fade as taken from the computer printout.

The A, B, and C lines of  $A_e$  values were computed for the transmitter height obtained from the radar altimeter data, referenced to Cold Lake and corrected by the amounts indicated under "Remarks" at the bottom of the table. The spread in the values of  $A_e$  is therefore indicative of a corresponding experimental error in the transmitter height determinations.

#### Computation of Effective Earth's Radii

The relationship between the  $A_e$  values, the height of the transmitter and receiving terminals, and the range for the interference pattern minima were computed for a spherical earth geometry as described in Appendix I. The results have been tabulated for several values of the parameters involved. A sample of the tabulation is shown in Table VI. These tables were used to determine the  $A_e$  values in any given experimental situation. The computations also included the range of the reflecting

Table VI

Sample Computer Printout of  $A_e$  vs Range (n.m.) for Minima

Tide = 0.0   H1 = 59.95    $\lambda$  = 0.7125   H2 = 4225.0

A	EFF	3300.0	3500.0	3700.0	3900.0	4100.0	4300.0	4500.0	4700.0	4900.0	5100.0	5300.0	5500.0	5700.0	5900.0
<b>N (Order of Fade)</b>															
1      51.48    52.56    53.59    54.58    55.53    56.43    57.30    58.14    58.95    59.72    60.47    61.20    61.90    62.58															
2      39.26    39.83    40.36    40.86    41.33    41.77    42.19    42.58    42.96    43.32    43.66    43.98    44.29    44.59															
3      30.99    31.29    31.58    31.84    32.08    32.31    32.52    32.72    32.91    33.08    33.25    33.41    33.55    33.69															
4      25.25    25.43    25.59    25.74    25.87    26.00    26.12    26.22    26.32    26.42    26.51    26.59    26.67    26.74															
5      21.16    21.26    21.36    21.45    21.53    21.60    21.67    21.74    21.80    21.85    21.90    21.95    22.00    22.04															
6      18.13    18.20    18.26    18.31    18.37    18.41    18.46    18.50    18.53    18.57    18.60    18.63    18.66    18.68															
7      15.82    15.86    15.91    15.94    15.98    16.01    16.04    16.07    16.09    16.11    16.13    16.15    16.17    16.19															
8      14.01    14.04    14.07    14.10    14.12    14.14    14.16    14.18    14.20    14.22    14.23    14.24    14.26    14.27															
9      12.56    12.58    12.61    12.62    12.64    12.66    12.67    12.69    12.70    12.71    12.72    12.73    12.74    12.75															
10     11.38    11.39    11.41    11.42    11.44    11.45    11.46    11.47    11.48    11.49    11.49    11.50    11.51    11.51															
11     10.39    10.40    10.42    10.43    10.44    10.45    10.45    10.46    10.47    10.48    10.48    10.49    10.49    10.49															
12     9.56    9.57    9.58    9.59    9.60    9.60    9.61    9.62    9.62    9.63    9.63    9.63    9.64    9.64															
13     8.85    8.86    8.87    8.87    8.88    8.88    8.89    8.89    8.90    8.90    8.91    8.91    8.91															
14     8.24    8.24    8.25    8.25    8.26    8.26    8.27    8.27    8.28    8.28    8.28    8.28    8.29    8.29															
15     7.70    7.71    7.71    7.72    7.72    7.72    7.73    7.73    7.73    7.74    7.74    7.74    7.74															
16     7.23    7.24    7.24    7.24    7.25    7.25    7.25    7.25    7.26    7.26    7.26    7.26    7.27    7.27															
17     6.81    6.82    6.82    6.82    6.83    6.83    6.83    6.83    6.84    6.84    6.84    6.84    6.84    6.84															

(Continued on page 55.)

Table VI (Cont.)

	Tide = 0.0		H1 = 59.95		$\lambda$ = 0.7125		H2 = 4225.0							
A EFF	3300.0	3500.0	3700.0	3900.0	4100.0	4300.0	4500.0	4700.0	4900.0	5100.0	5300.0	5500.0	5700.0	5900.0
N (Order of Fade)														
18	6.44	6.45	6.45	6.45	6.45	6.46	6.46	6.46	6.46	6.46	6.46	6.47	6.47	6.47
19	6.11	6.11	6.11	6.12	6.12	6.12	6.12	6.12	6.13	6.13	6.13	6.13	6.13	6.13
20	5.81	5.81	5.81	5.81	5.82	5.82	5.82	5.82	5.82	5.82	5.83	5.83	5.83	5.83
21	5.54	5.54	5.54	5.54	5.54	5.54	5.55	5.55	5.55	5.55	5.55	5.55	5.55	5.55
22	5.29	5.29	5.29	5.29	5.29	5.29	5.30	5.30	5.30	5.30	5.30	5.30	5.30	5.30
23	5.06	5.06	5.06	5.06	5.06	5.07	5.07	5.07	5.07	5.07	5.07	5.07	5.07	5.07
24	4.85	4.85	4.85	4.85	4.86	4.86	4.86	4.86	4.86	4.86	4.86	4.86	4.86	4.86
25	4.66	4.66	4.66	4.66	4.66	4.66	4.66	4.67	4.67	4.67	4.67	4.67	4.67	4.67

point from the receiving terminal and the elevation angle of the lake-reflected ray. These data could be used to resolve doubts in marginal situations when the reflecting points might fall dangerously close to the far shore of Cold Lake or when the signal path appeared too close to the hilltops on the radio horizon.

Special precautions had to be taken to achieve the required accuracy for various parameters; these included the receiving antenna height, the transmitter aircraft altitudes, the aircraft range at any given time, the signal frequency, and an accurately defined central time system.

The receiving antenna heights were obtained by means of a repeated survey between a graduated rod fixed to the Cold Lake dock and the physical center of the receiving antennas. A separate measurement was obtained for each frequency band and polarization. The water level on the graduated rod was recorded periodically throughout the trials to provide a correction for possible changes in the lake level. The accuracy of these measurements was about  $\pm$  0.05 feet.

The received radio frequency could be measured to within 0.25 MHz by means of FXR wavemeters. However, to allow for slight drifts during missions, and from one mission to the next, accuracy limits of  $\pm$  5 MHz were assumed at L-band and  $\pm$  10 MHz at S-band

( $\pm 0.001$  foot in  $\lambda$ ). Checks were made prior to each leg of a mission to ensure that the frequency remained within these limits.

The methods used to determine aircraft range and altitude were discussed above in previous sections and are explained in detail in Volume III. The accuracy of the positions of minima was found to be better than  $\pm 100$  feet and the height accuracy better than  $\pm 25$  feet.

#### Factors Affecting the Accuracy of Experimental Results

The use of the effective earth's radius concept to interpret propagation conditions depends in the first place on the accuracy of the experimental results. The magnitude of the errors involved are calculated in Appendix II using the approximate equations which are derived in Appendix I. It should be noted that the equations shown in Appendix I were derived on the assumption that a phase shift of 180 degrees occurs on reflection. In the case of the real reflecting surface (Cold Lake), an error in the phase shift might be introduced by the forward scatter component of the signal due to ripples and waves. The magnitude of this error is somewhat difficult to determine because of the lack of precise data concerning the scatter effect.

Separate effects due to maximum errors in the measurement of the individual parameters, as well as the combined effect of errors in all parameters, are tabulated in Appendix II for each of the flight

configurations used throughout the trials. Figure 17 shows the contour of maximum expected errors for the various combinations of experimental parameters used in the trials.

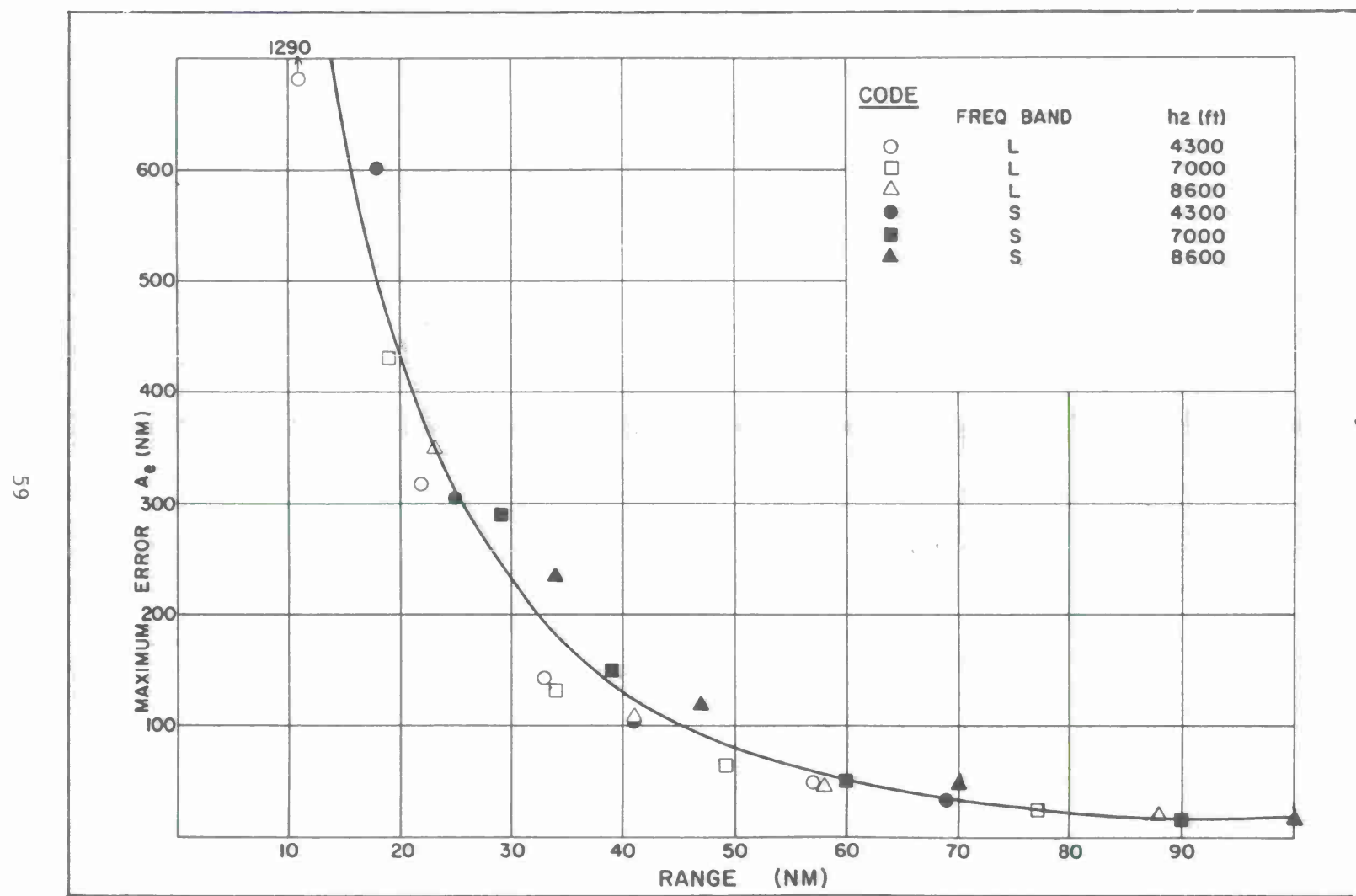


Figure 17. Contour of Maximum Expected Errors for Various Combinations of Experimental Parameters

## SECTION IV

### EXPERIMENTAL DATA

#### INTRODUCTION

All the results obtained from the experiment are summarized graphically and grouped according to each particular mission. Within each mission the results are generally broken down into time periods equivalent to two legs of interferometer data except when there was some advantage in discussing the whole mission. The results show:

- ( a) received radio signal amplitudes versus range,  
where the inverse square law decrease with range  
is shown by the solid line and the experimental  
envelope by the dashed line,
- (b) meteorological refractivity profiles,
- (c) effective earth's radii computed from the interferometer  
measurements, as well as the independent radii calcula-  
tions using the ray-tracing analysis.

The graphical data for each mission is followed by summarizing comments which point out salient features of the results relating to meteorological conditions and the general agreement of experimental data.

MISSION 102 - Spanning Noontime  
Time: 0952-1102, 17 September 1964  
Legs 1, 2

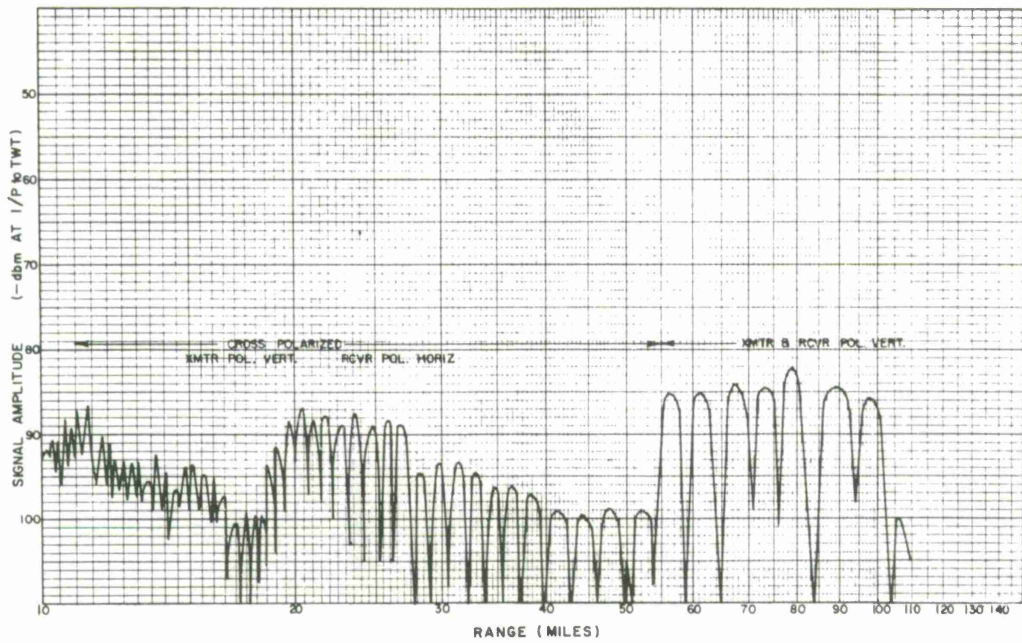
Amplitude vs. Range Graphs - Leg 1

The transmitter and receiver were cross-polarized at ranges below 50 n. m., which explains the nonstandard amplitude behavior.

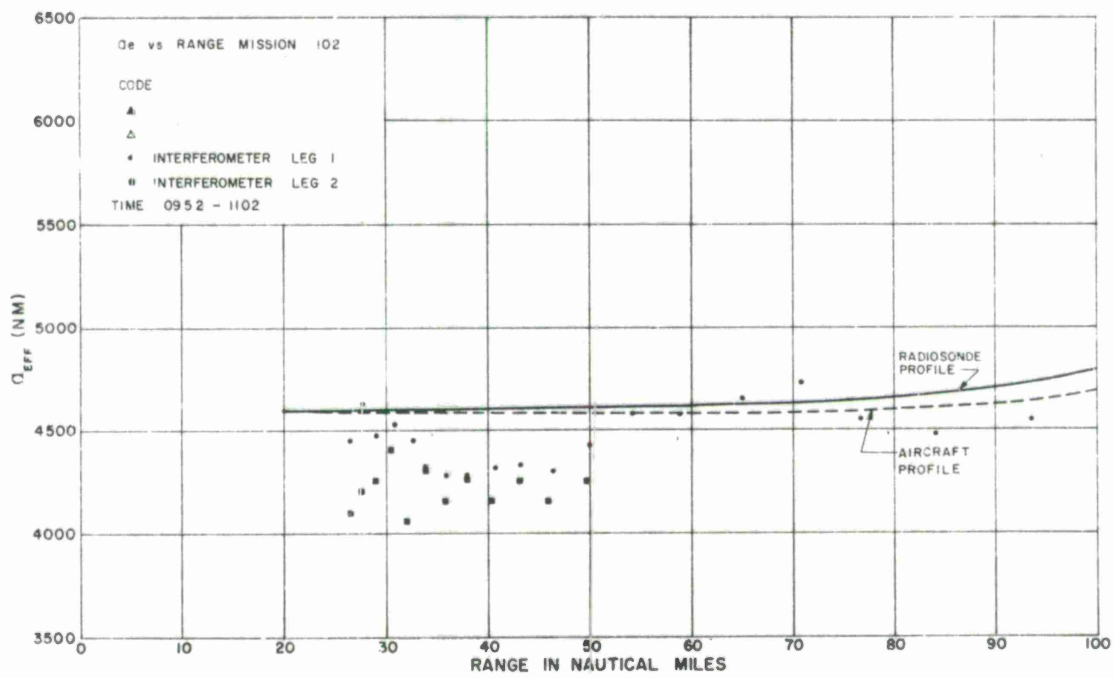
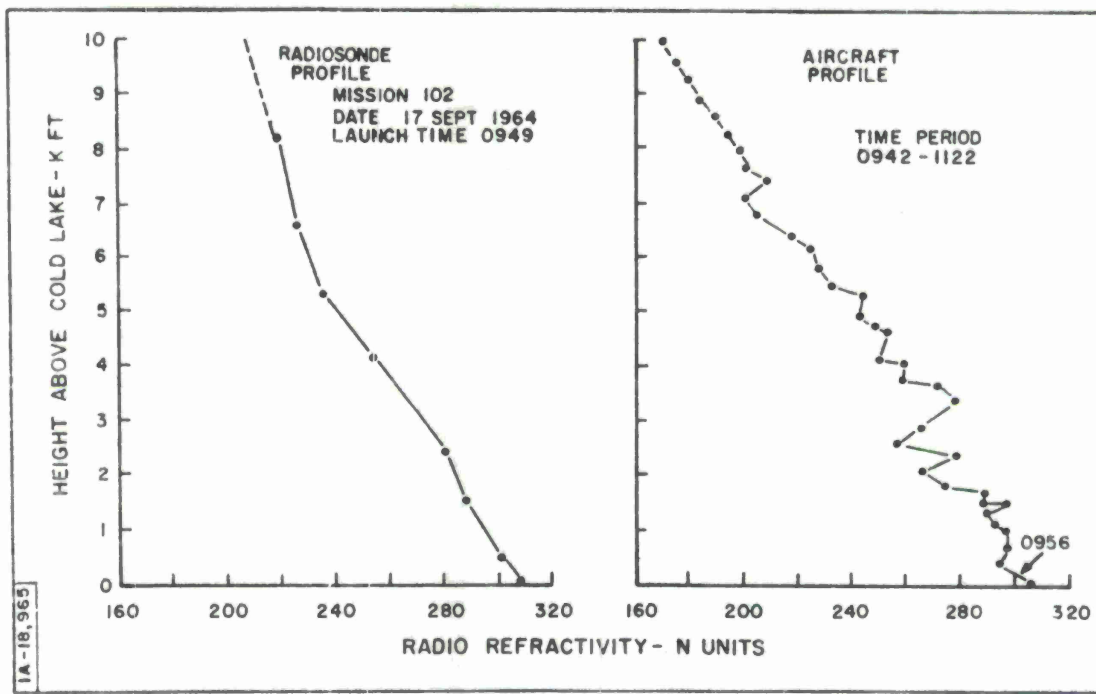
Effective Earth's Radii

The  $A_e$  calculations determined from the ray-tracing technique show that the radiosonde and aircraft profile are in good agreement with the interferometer values. The difference between  $A_e$  values calculated using the radiosonde and interferometer data is equivalent to an elevation error angle difference of 0.575 milliradians at 90 n.m. and about 0.15 milliradians between 55 and 75 n.m. At reduced ranges the error increases significantly as the radar (DME) range error becomes proportionately larger with respect to the actual range.

SIGNAL AMPLITUDE V/S RANGE  
MISSION 102 LEG 1 DATE 17 SEP 64 TIME 0952-1020  
BAND S FREQUENCY 3336 Mc/s POLARIZATION NOTE  $\lambda$  2947 ft  $h_1$  58.90 ft  $h_2$  8600 ft



No data for leg 2



Mission 102 (Continued)

Time: 1127-1236, 17 September 1964

Legs 3, 4

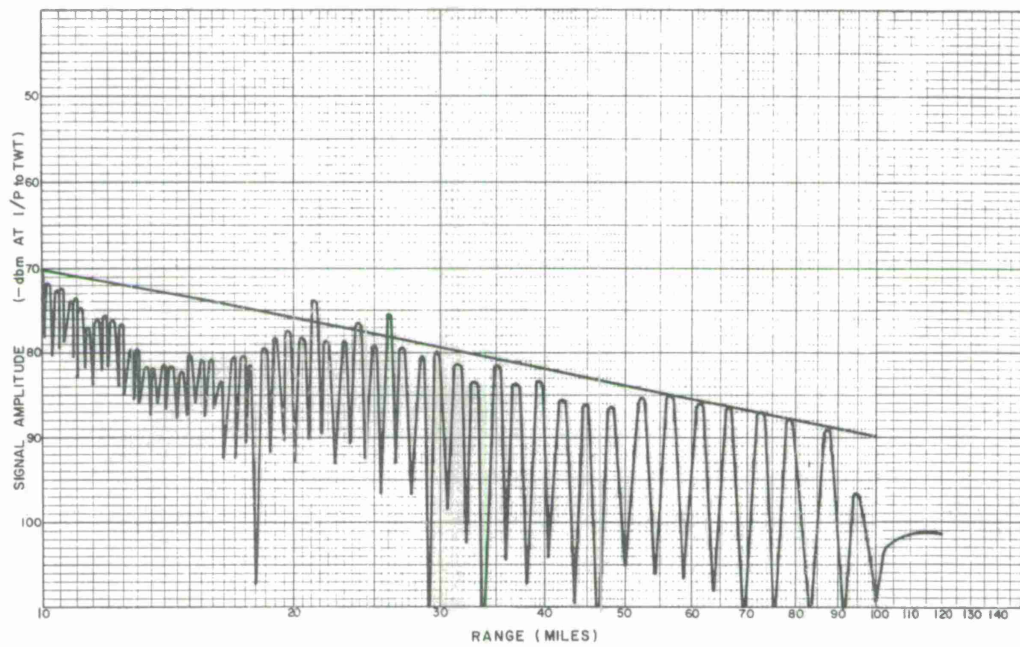
A comparison of the  $A_e$  plots indicates that the radiosonde profile provides much closer agreement with the interferometer data than does the aircraft data. The large difference between aircraft and radiosonde results is due to the excessive gradient represented by aircraft measurements near the surface. Possible explanations for this gradient were presented in a previous section.

Time: 1327-1435, 17 September 1964

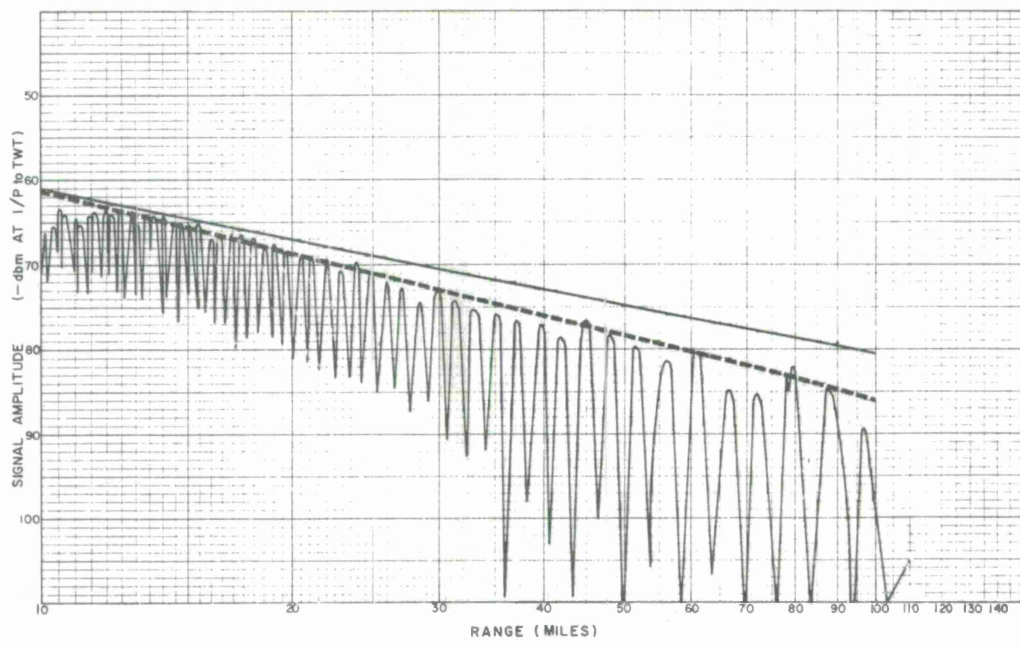
Legs 5, 6

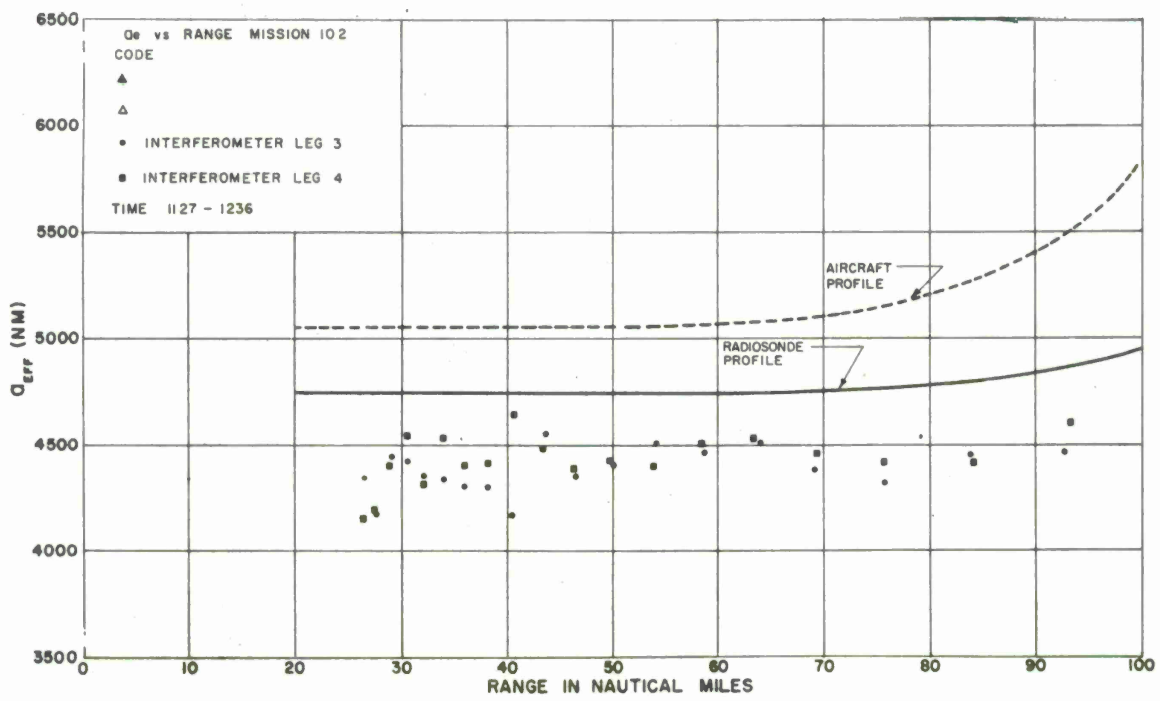
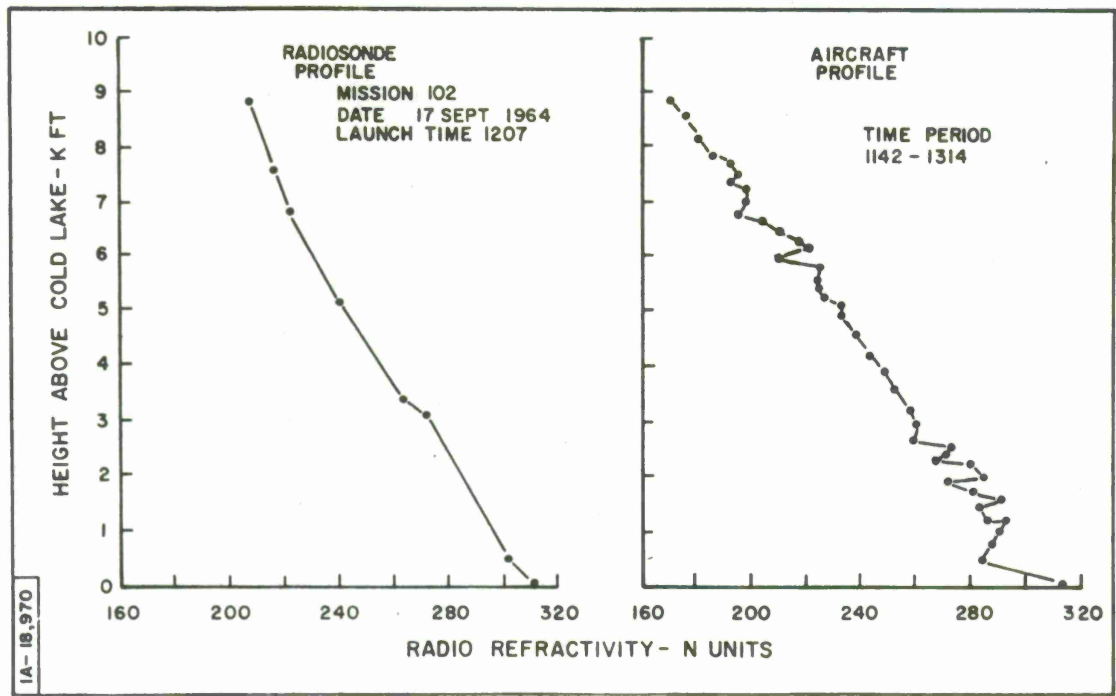
The comparison of  $A_e$  data shows that the radiosonde and aircraft data is very close to the interferometer data. The large surface gradient frequently observed with the aircraft measurements was not present at this time. The interferometer data shows a departure between legs. Leg 5 indicates that the overall bending is decreasing with range, whereas leg 6 shows that the bending is increasing with range, and these differences represent from 0.15 to about 0.7 milliradians in the elevation angle error. With reference to the interferometer data obtained previously on legs 3 and 4, there appears to be a significant temporal variation occurring during the period 1327 to 1435.

SIGNAL AMPLITUDE V/S RANGE  
 MISSION 102 LEG 3 DATE 17 SEP 64 TIME 1127-1157  
 BAND S FREQUENCY 3336 Mc/s POLARIZATION HORIZ  $\lambda$  2947 ft  $h_1$  58.94 ft  $h_2$  8600 ft

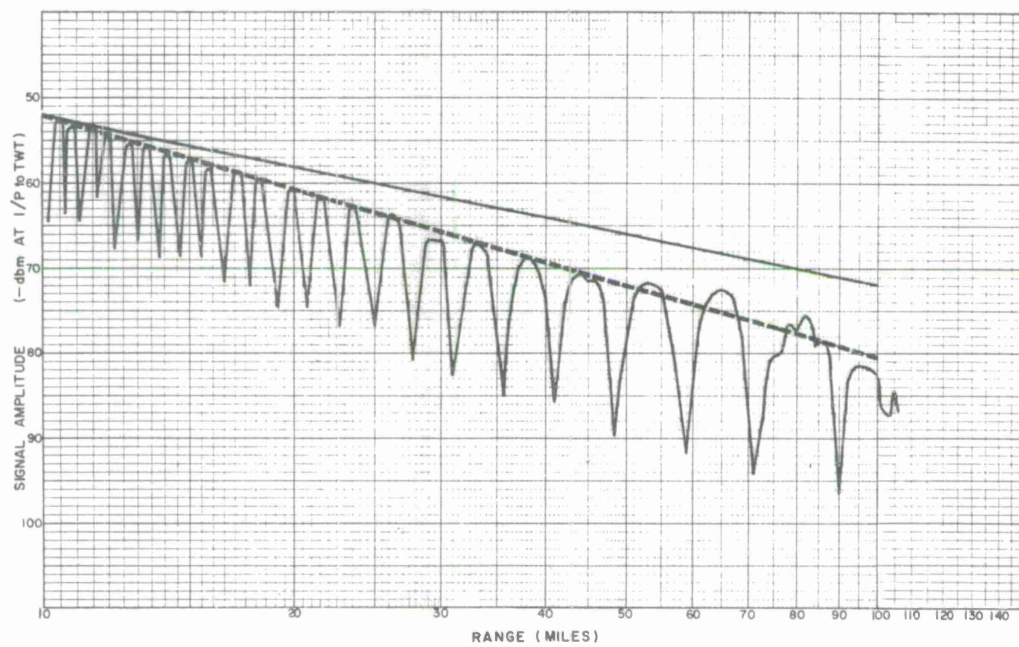


SIGNAL AMPLITUDE V/S RANGE  
 MISSION 102 LEG 4 DATE 17 SEP 64 TIME 1157-1236  
 BAND S FREQUENCY 3336 Mc/s POLARIZATION HORIZ  $\lambda$  2947 ft  $h_1$  58.94 ft  $h_2$  8600 ft

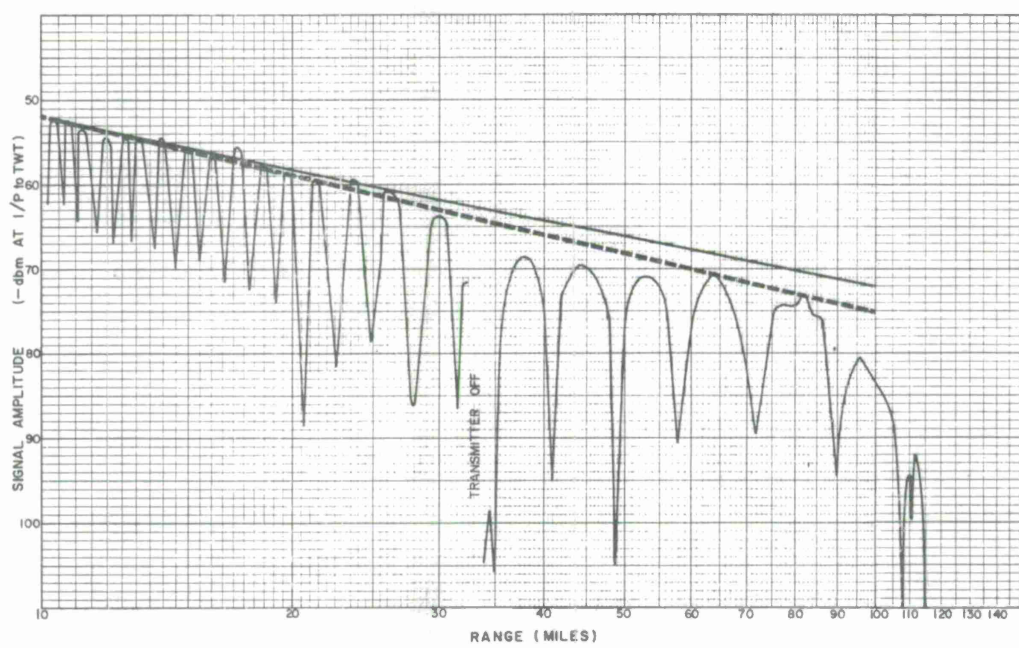


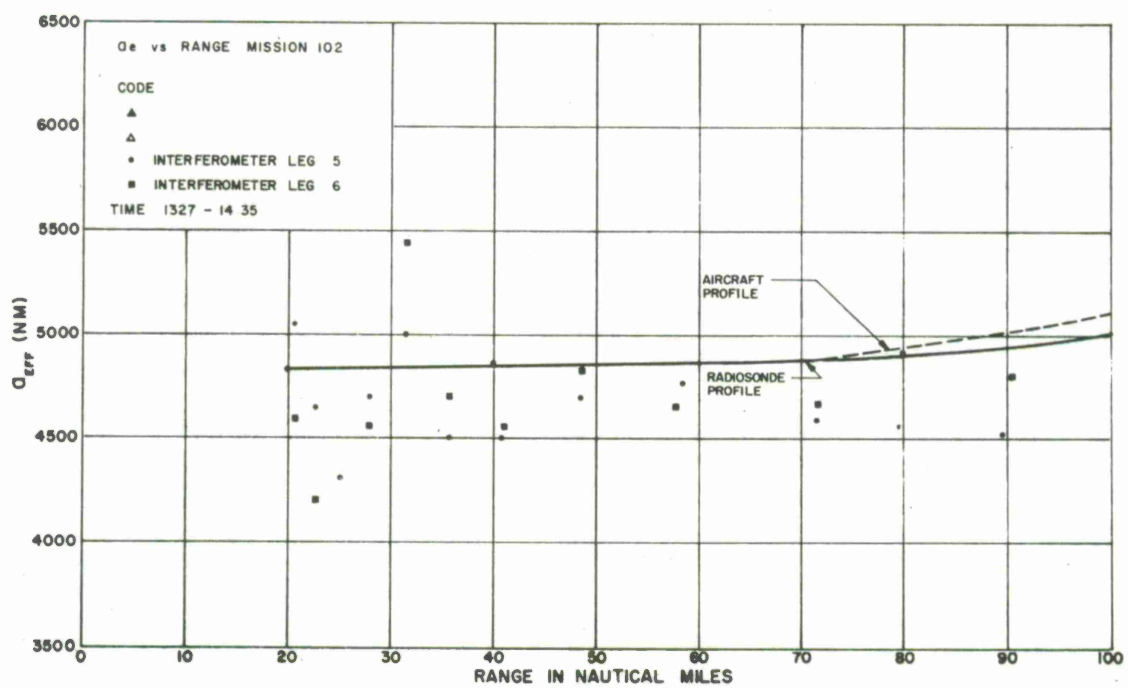
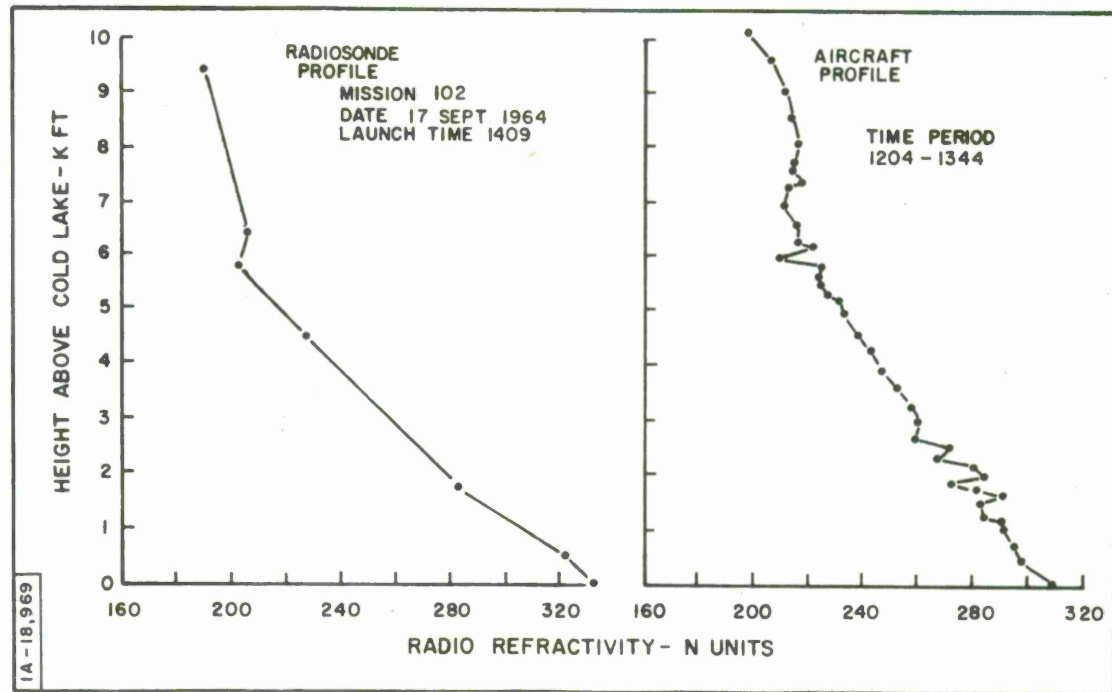


SIGNAL AMPLITUDE V/S RANGE  
 MISSION 102 LEG 5 DATE 17 SEP 64 TIME 1327-1400  
 BAND L FREQUENCY 1400 Mc/s POLARIZATION HORIZ  $\lambda$  7023 ft  $h_1$  59.36 ft  $h_2$  8600 ft



SIGNAL AMPLITUDE V/S RANGE  
 MISSION 102 LEG 6 DATE 17 SEP 64 TIME 1356-1435  
 BAND L FREQUENCY 1400 Mc/s POLARIZATION HORIZ  $\lambda$  7023 ft  $h_1$  59.36 ft  $h_2$  8600 ft





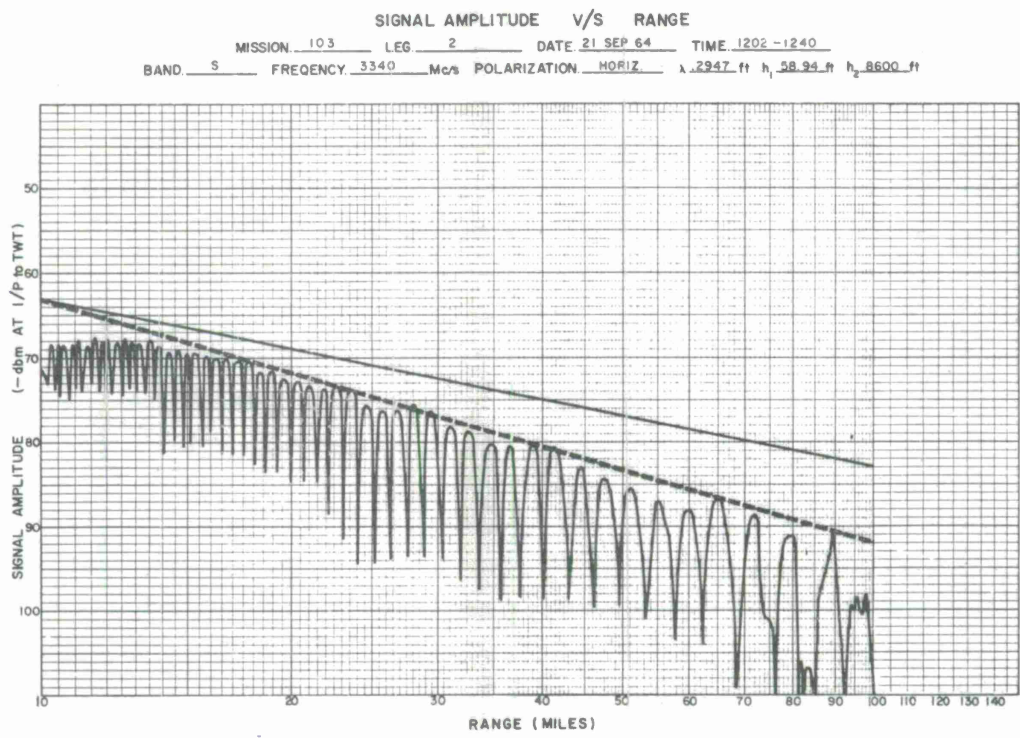
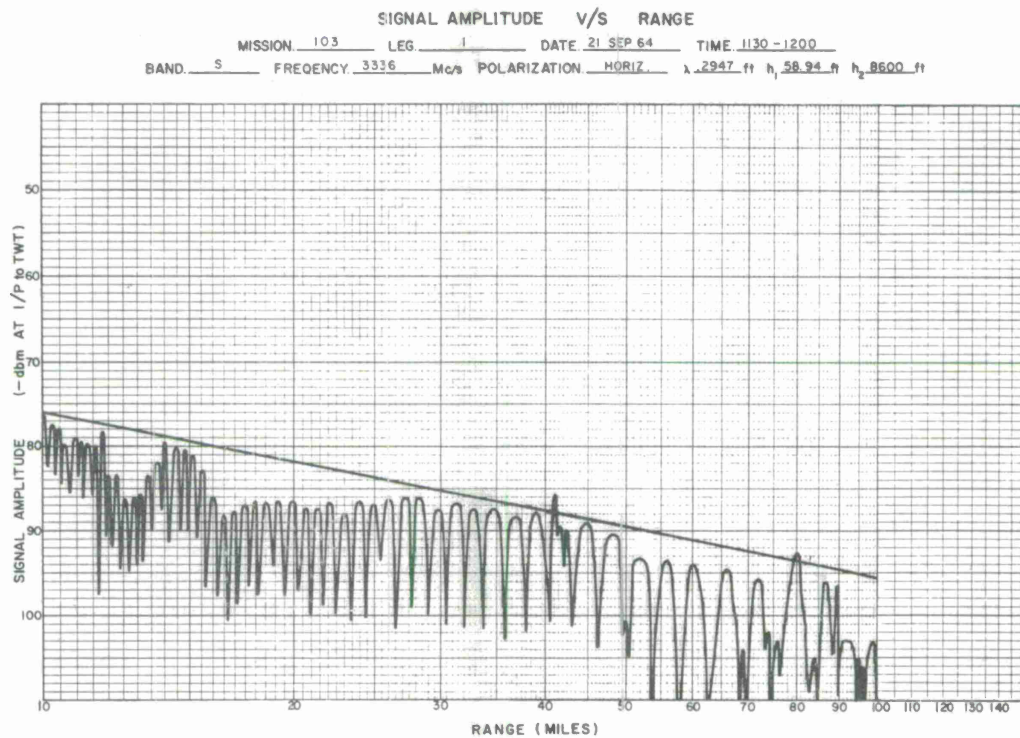
### General Summary of Mission 102

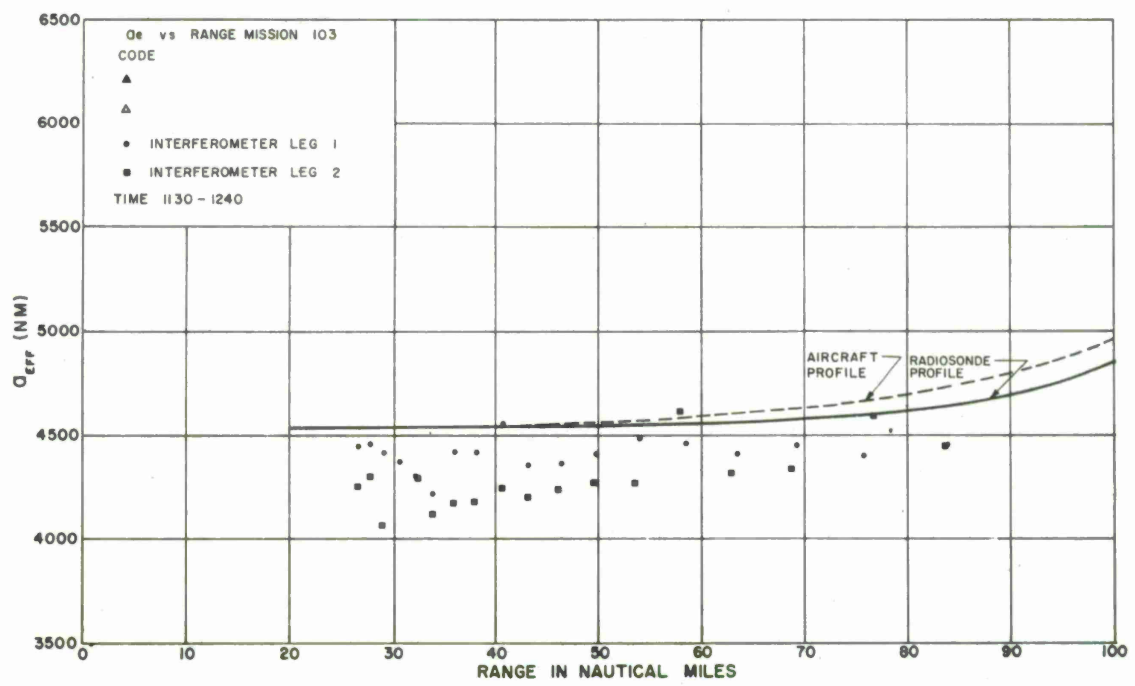
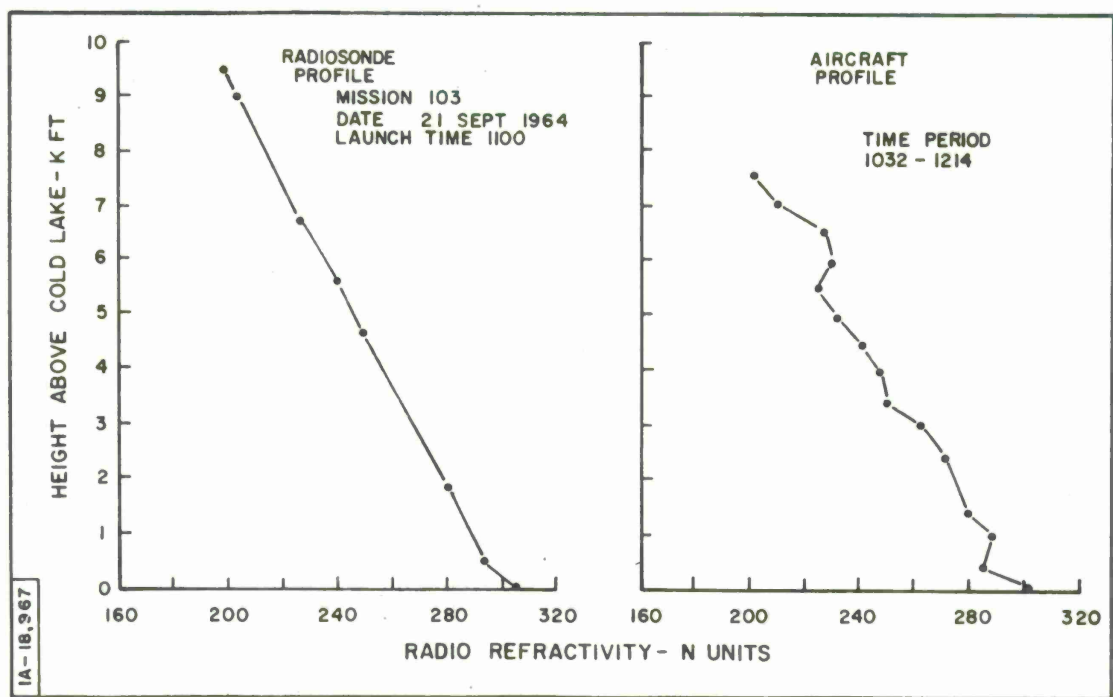
In general the interferometer  $A_e$  values tend to follow those values obtained using the radiosonde data.

The disagreement between absolute  $A_e$  values obtained from the two techniques is much larger at long ranges, which indicates the difficulty in trying to establish an extremely accurate measurement of the propagation conditions over the lake surface and in trying to offset spatial and temporal variations which are occurring in the propagation medium.

MISSION 103 - Early Afternoon  
Time: 1130-1240, 21 September 1964  
Legs 1, 2

A comparison of the radiosonde and aircraft profiles again shows a tendency for the aircraft measurements to depict a larger surface gradient than appears to be the case. This situation is reflected in the  $A_e$  plots where the aircraft values are slightly larger than either the radiosonde or interferometer data. Both the radiosonde and interferometer values indicate that the ray-path bending is gradually increasing at the lower elevation angles. The average difference between these values represents approximately 0.25 to 0.4 milliradians difference in the elevation angle error at ranges between 50 and 75 n.m. The difference between interferometer  $A_e$  values obtained in legs 1 and 2 is about the same order of magnitude. This again indicates that temporal variations were occurring.





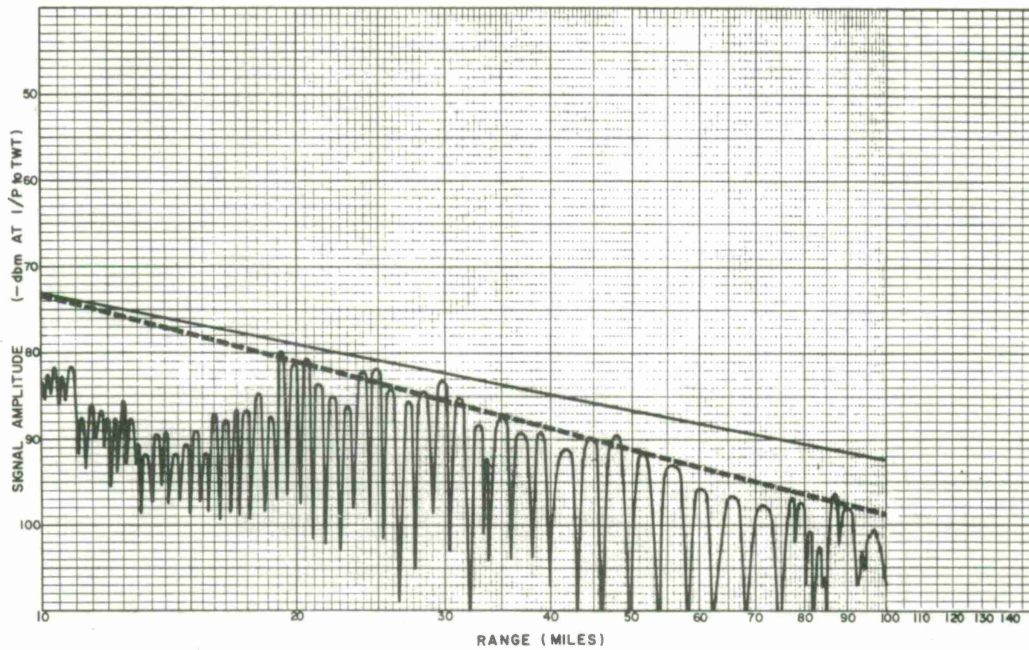
Mission 103 (Continued)

Time: 1252-1403, 21 September 1964

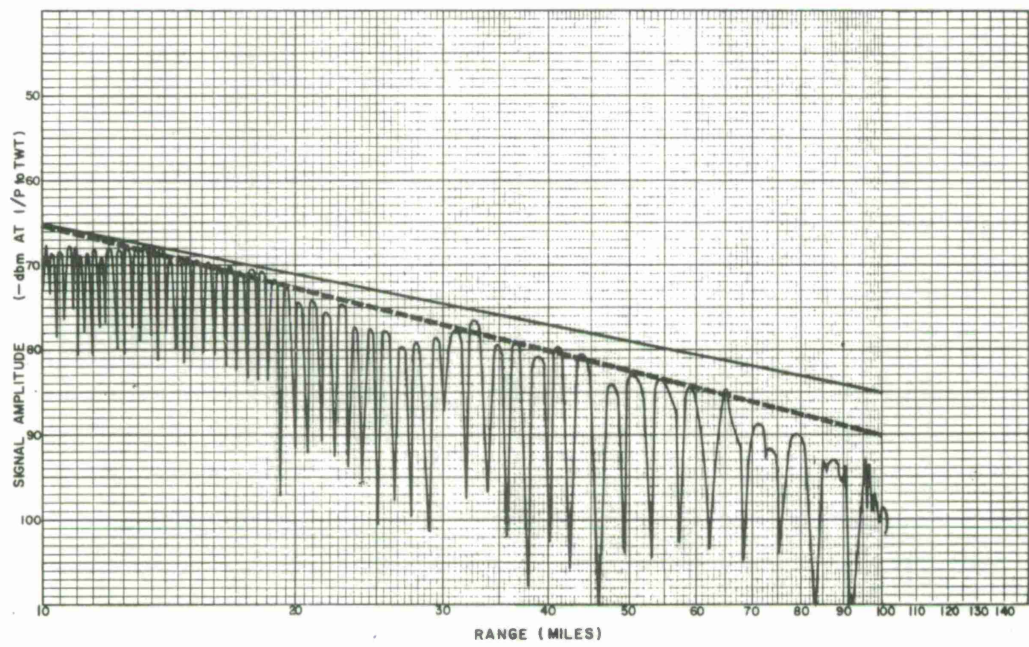
Legs 3, 4

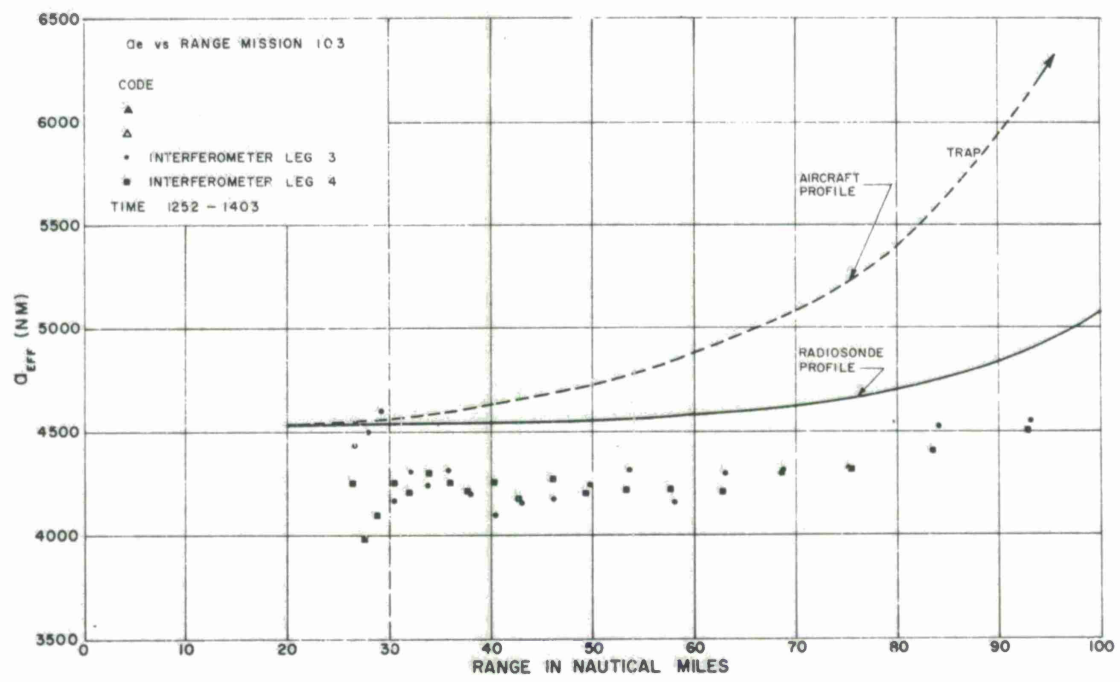
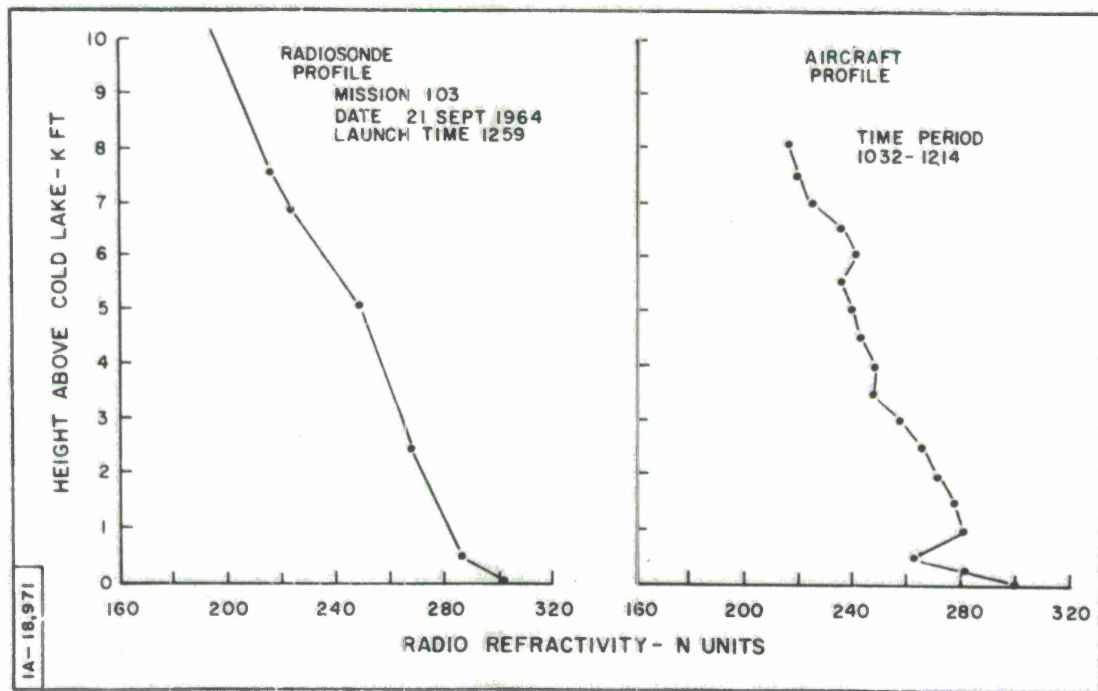
As previously discussed, the low-level aircraft data seems to be out of context with the propagation conditions illustrated by the radiosonde and interferometer data. The radiosonde and interferometer  $A_e$  plots show extremely good agreement in illustrating how the bending is increasing as the elevation angle decreases. However, the difference between the  $A_e$  magnitudes is consistently large and represents on the average about 0.9 milliradians difference in the elevation angle error. The good agreement between the two legs of interferometer data indicates that there was essentially no temporal variation over this test period. Therefore, the lack of agreement of the radiosonde ray-tracing calculations with the interferometer results is difficult to explain.

SIGNAL AMPLITUDE V/S RANGE  
 MISSION. 103 LEG. 3 DATE. 21 SEP 64 TIME. 1252-1322  
 BAND. S FREQUENCY. 3340 Mc/s POLARIZATION. HORIZ.  $\lambda$  2947 ft h 58.94 ft  $h_2$  8600 ft



SIGNAL AMPLITUDE V/S RANGE  
 MISSION. 103 LEG. 4 DATE. 21 SEP 64 TIME. 1326-1403  
 BAND. S FREQUENCY. 3340 Mc/s POLARIZATION. HORIZ.  $\lambda$  2947 ft h 58.94 ft  $h_2$  8600 ft





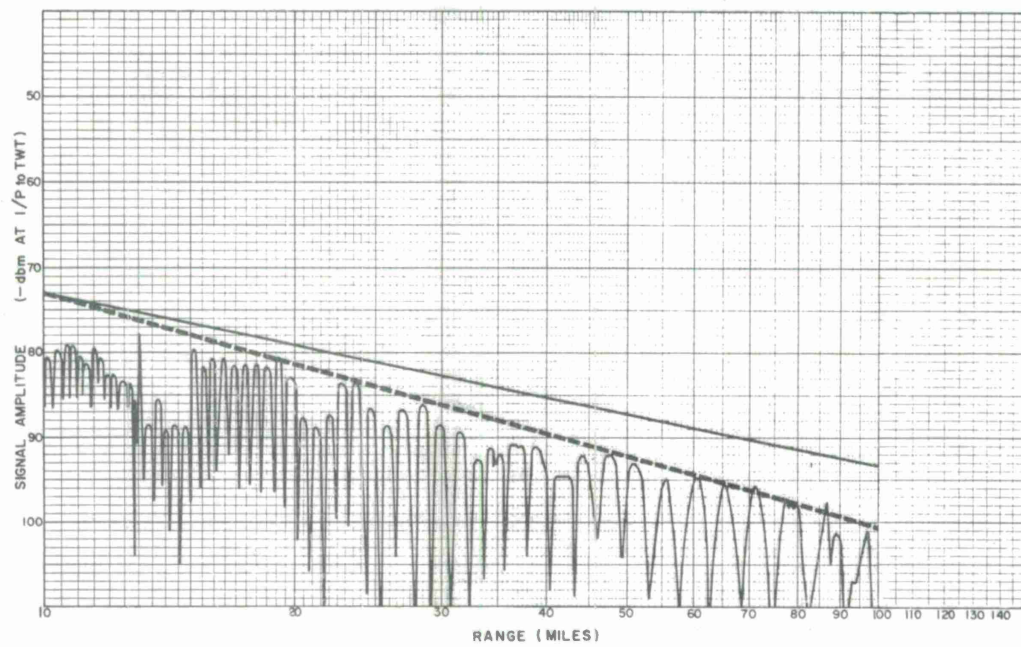
Mission 103 (Continued)

Time: 1412-1521, 21 September 1964

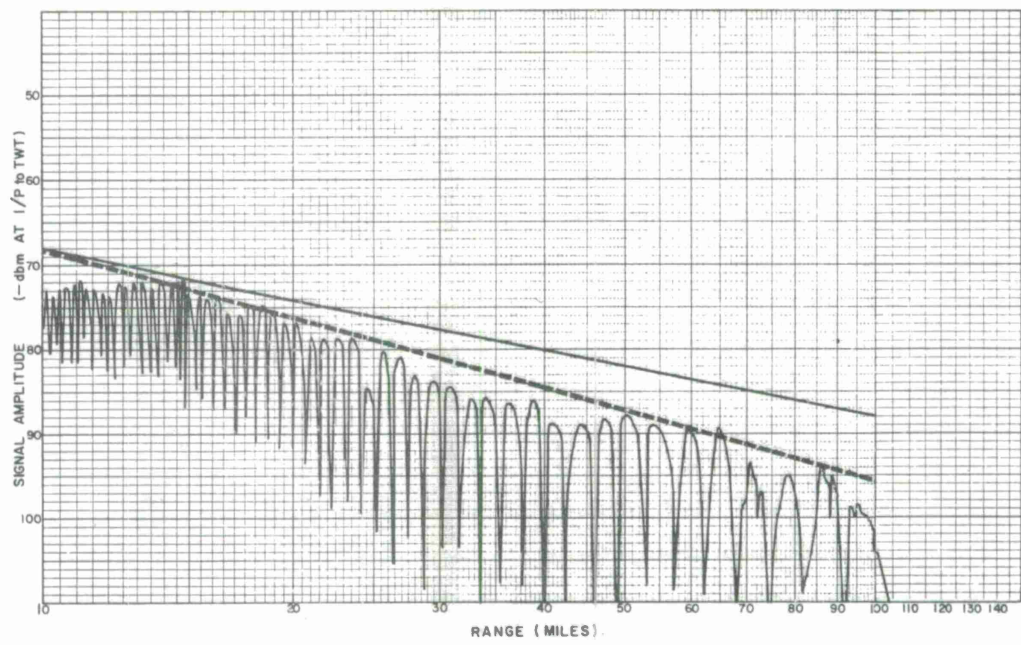
Legs 5, 6

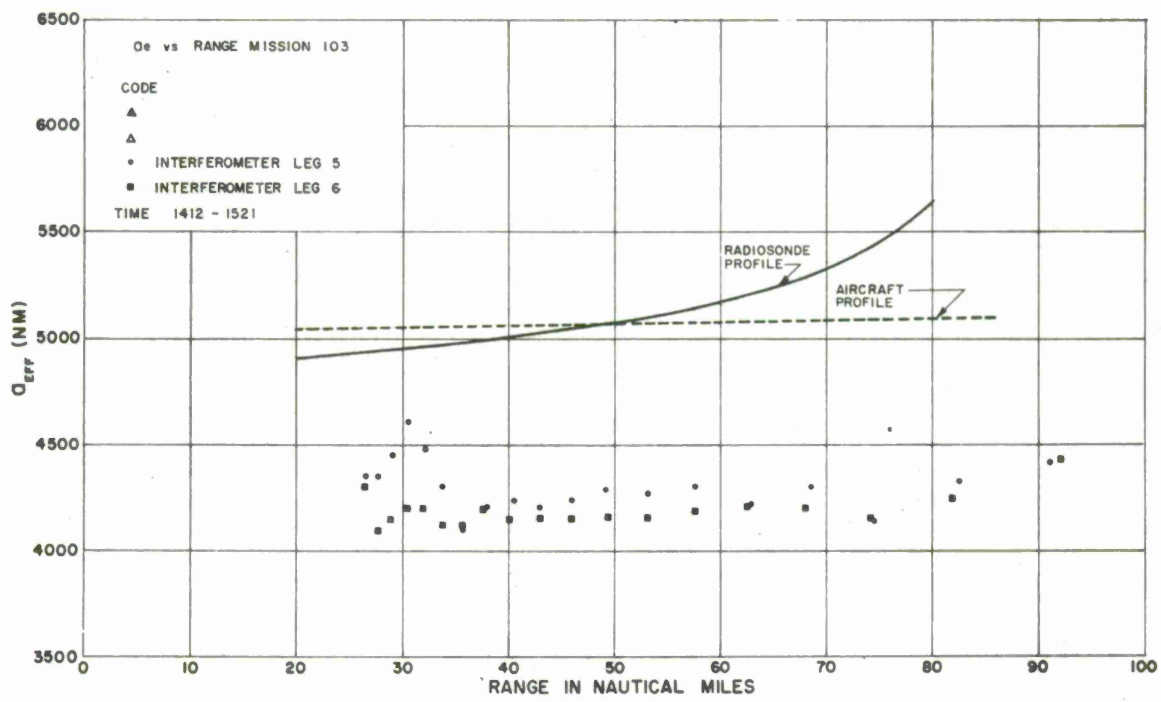
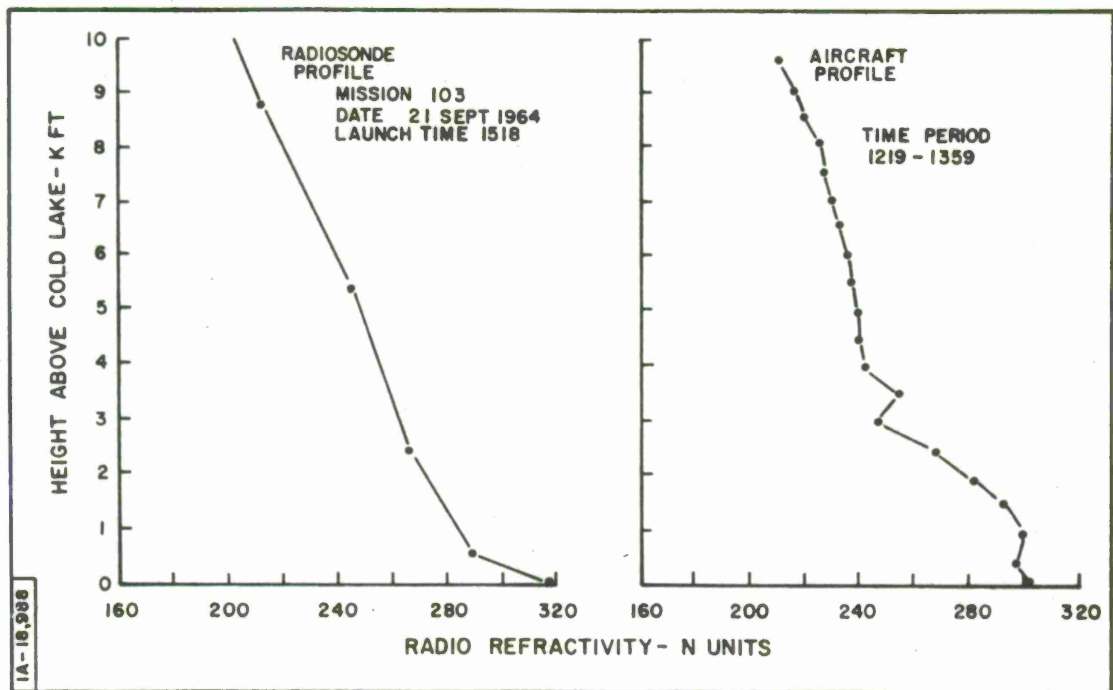
The interferometer and radiosonde values of  $A_e$  again indicate that the amount of bending was gradually increasing at the lower elevation angles. From the difference between interferometer results alone, there appears to be little temporal variation in the propagation conditions. The aircraft data indicates that there is no variation in bending with elevation angle and does not appear to agree with the true situation. The lack of agreement between radiosonde and interferometer data must again be attributed to the fact that there are significant spatial variations in the propagation conditions.

SIGNAL AMPLITUDE V/S RANGE  
 MISSION 103 LEG 5 DATE 21 SEP 64 TIME 1412-1441  
 BAND S FREQUENCY 3340 Mc/s POLARIZATION HORIZ  $\lambda$  2947 ft  $h_1$  58.94 ft  $h_2$  8600 ft



SIGNAL AMPLITUDE V/S RANGE  
 MISSION 103 LEG 6 DATE 21 SEP 64 TIME 1445-1521  
 BAND S FREQUENCY 3340 Mc/s POLARIZATION HORIZ  $\lambda$  2947 ft  $h_1$  58.94 ft  $h_2$  8600 ft





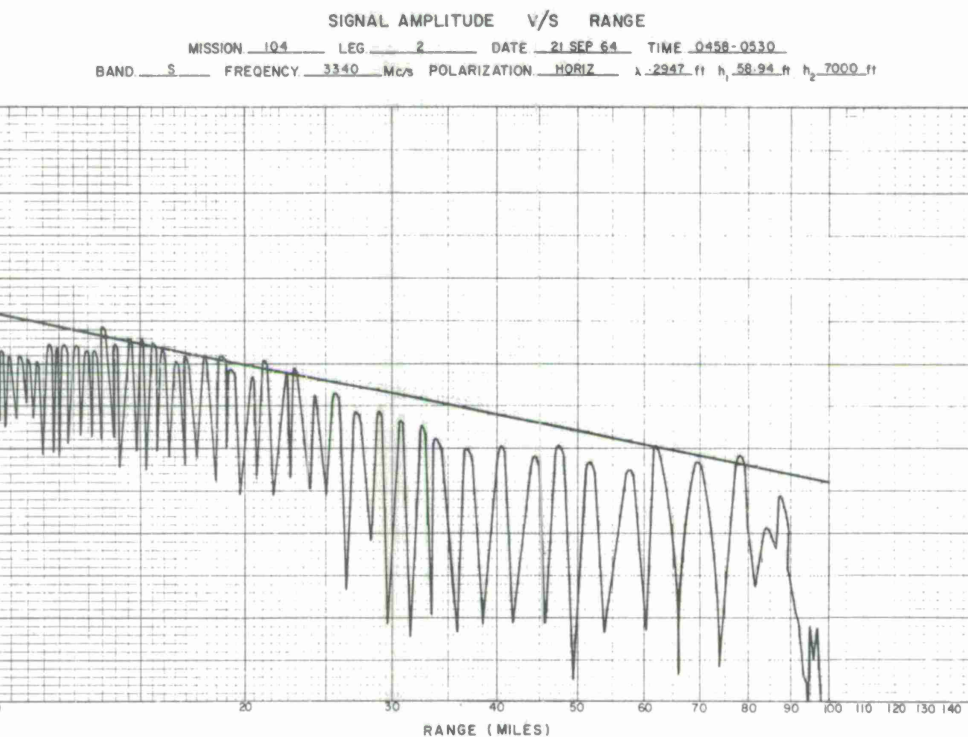
### General Comments on Mission 103

In spite of the lack of good agreement between radiosonde and interferometer values of  $A_e$ , it is significant to note that for the earlier legs the rate of change of  $A_e$  values as a function of range is in good agreement with the interferometer data. In the case of the last two legs, this agreement is poor as is the comparison of the actual values of  $A_e$ . As mentioned previously the effect of large scale spatial variability during the test period (1412-1521 hrs.) could account for this lack of agreement.

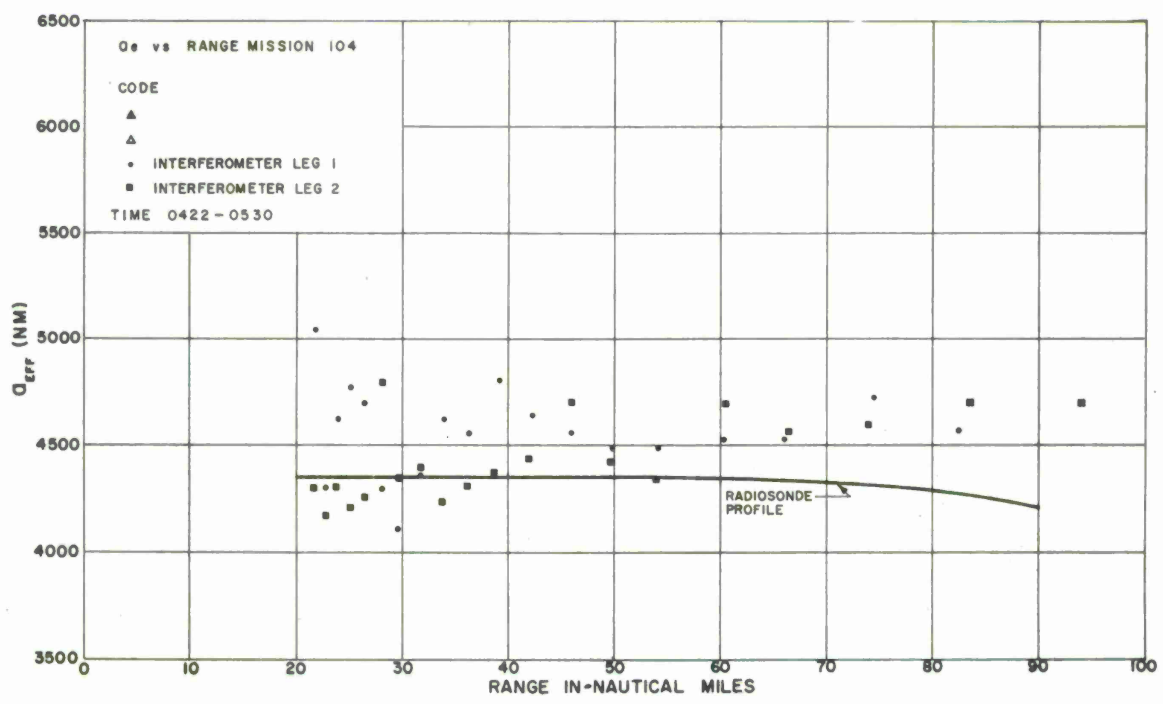
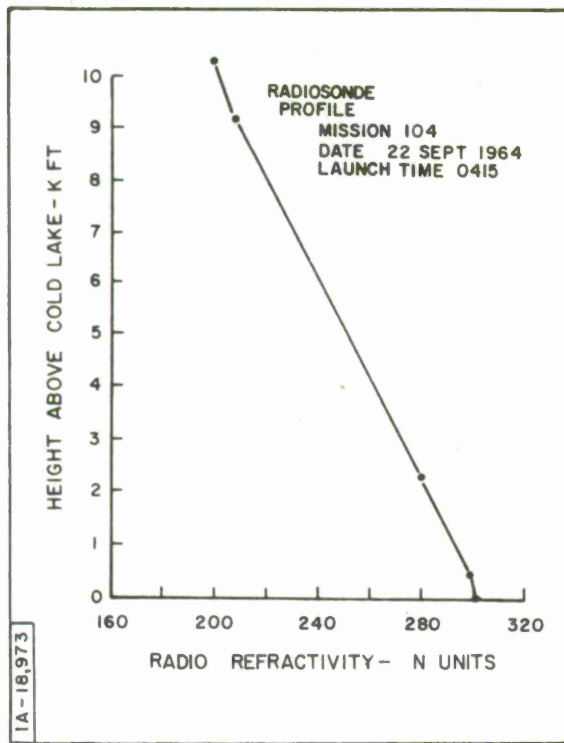
MISSION 104 - Early Morning  
Time: 0422-0530, 22 September 1964  
Legs 1, 2

Neither surface nor aircraft meteorological measurements were available during this mission. The extrapolation of radiosonde data to the surface of Cold Lake was based on estimates of the Cold Lake surface refractivity obtained from psychometric measurements at the receiving site. Therefore, the validity of the ray-tracing results at the low elevation angles is somewhat questionable.

A comparison of  $A_e$  data does indicate, however, that both the interferometer and radiosonde calculations show that the amount of bending was almost constant up to ranges in the order of 60 n.m. At longer ranges, the radiosonde data indicates that the amount of bending decreases slightly. On the other hand, the interferometer data indicates a tendency towards increased bending at the longer ranges, but the effect is very small. The difference between the radiosonde and the average of the interferometer data represents 0.25 and 1.0 mr. in the elevation angle error between 50 to 90 n.m.



No data for leg 1



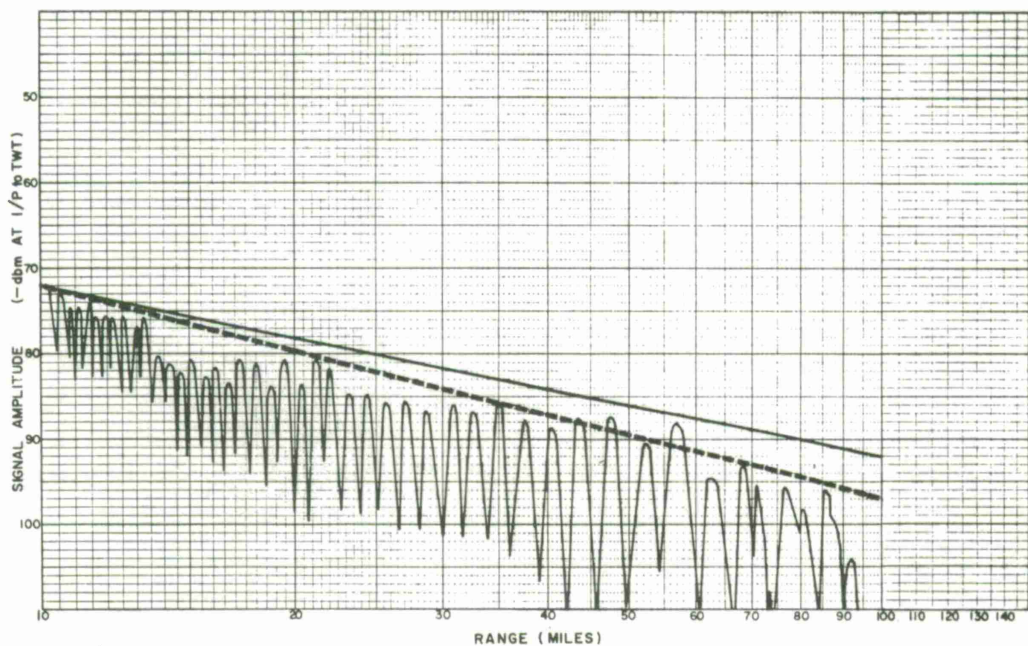
Mission 104 (Continued)

Time: 0537-0649, 22 September 1964

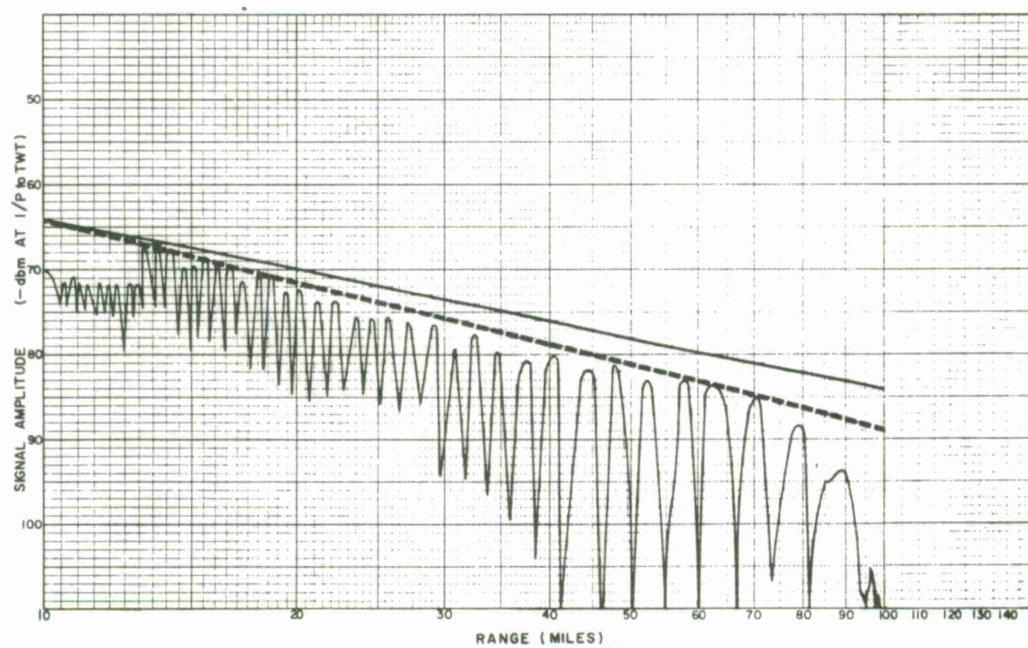
Legs 3, 4

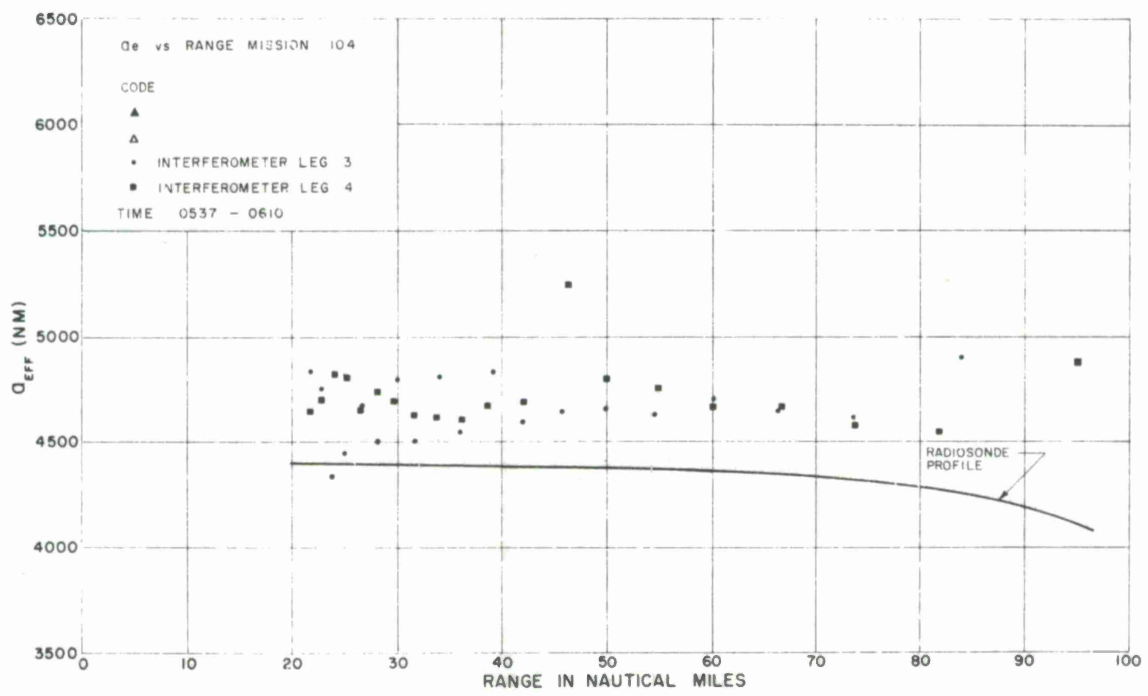
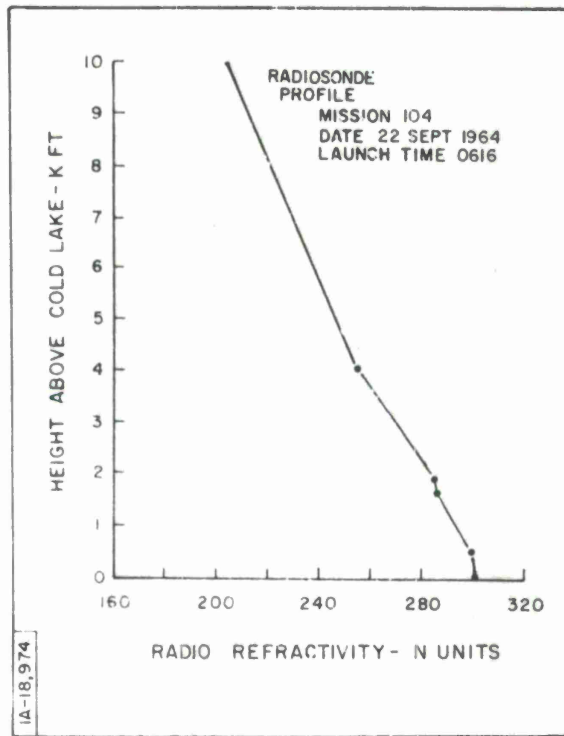
A comparison between interferometer and radiosonde data shows that the rate of change of bending with distance agrees very well up to about 75 n. m. Thereafter there are fluctuations in the interferometer data for leg 3. With reference to the signal amplitude plot for leg 3, it can be seen that there are large perturbations on the normally well behaved fade pattern. This indicates that somewhat anomalous propagation conditions are influencing the characteristics of the received radio signal at these low elevation angles. Although such propagation conditions are not evident in the signal amplitude plot for leg 4, the interferometer values show an abrupt increase in the amount of bending at extremely low elevation angles. It is significant that this sudden increase in bending at long ranges, for both legs, is representative of a super-normal surface refractivity gradient which could be approaching the condition for a surface trap.

SIGNAL AMPLITUDE V/S RANGE  
 MISSION. 104 LEG. 3 DATE. 21 SEP 64 TIME. 0536-0610  
 BAND. S FREQUENCY. 3340 Mc/s POLARIZATION. HORIZ  $\lambda$  2947 ft  $h_1$  58.94 ft  $h_2$  7000 ft



SIGNAL AMPLITUDE V/S RANGE  
 MISSION. 104 LEG. 4 DATE. 21 SEP 64 TIME. 0617-0649  
 BAND. S FREQUENCY. 3340 Mc/s POLARIZATION. HORIZ  $\lambda$  2947 ft  $h_1$  58.94 ft  $h_2$  7000 ft



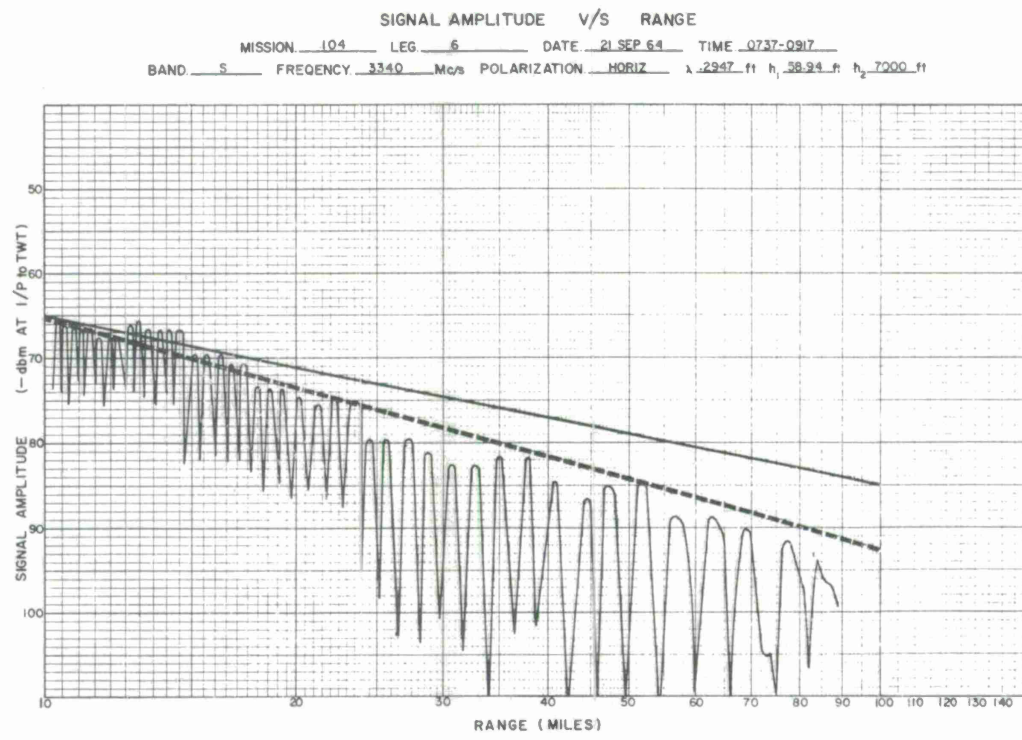
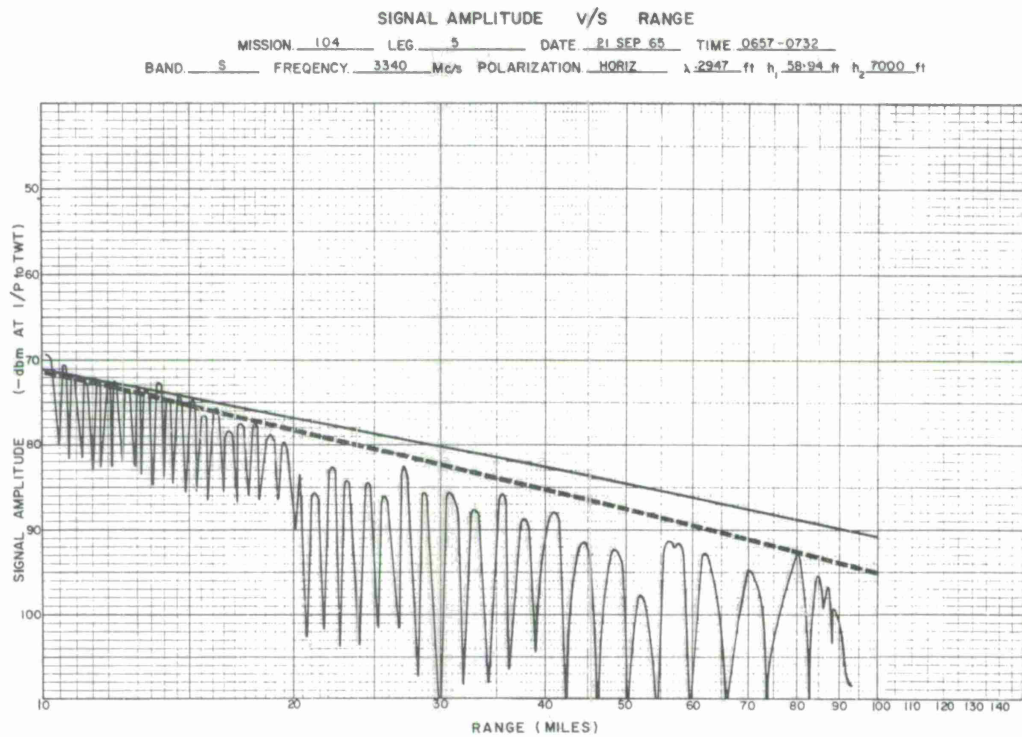


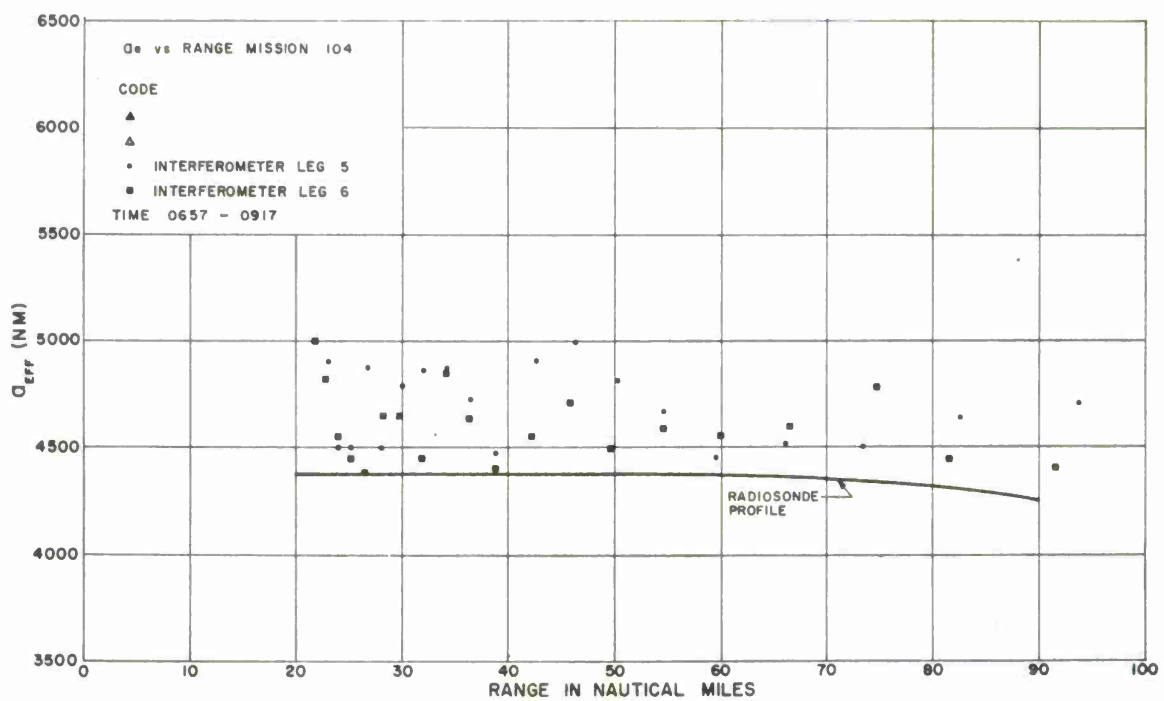
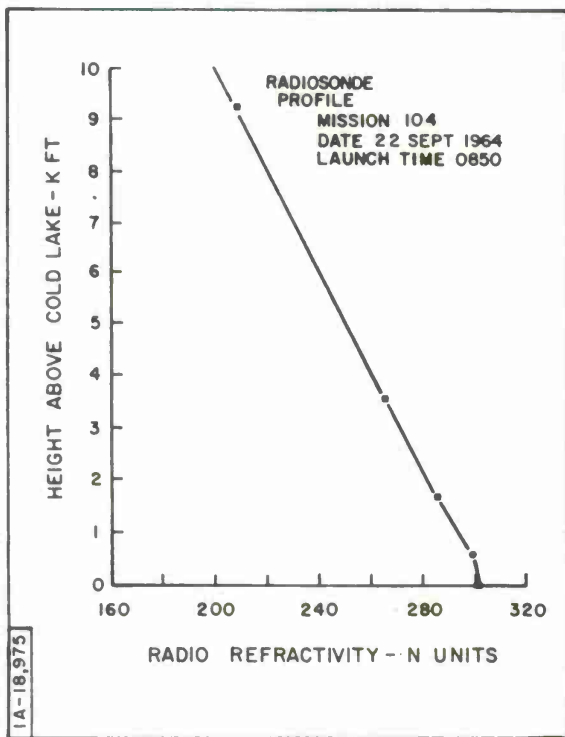
Mission 104 (Continued)

Time: 0657-0917, 22 September 1964

Legs 5, 6

As in the previous case the amount of bending tends to remain somewhat constant as the range increases. The interferometer plots for legs 5 and 6 differ significantly beyond 70 n. m., the latter showing a tendency towards decreased bending. The signal amplitude plots also show some perturbations at long ranges. As discussed previously this may indicate that the conditions were nonstandard near the surface.





### General Summary of Mission 104

The lack of meteorological surface data does not permit an accurate evaluation of the two methods at the long ranges. At shorter ranges where the loss of surface data is less significant, the interferometer and radiosonde measurements indicate that the amount of bending is essentially constant. This observation might have been derived directly by noting that the radiosonde profile is essentially linear, and, as discussed above (see equation 3), this constant refractivity gradient gives a single constant value for  $A_e$ .

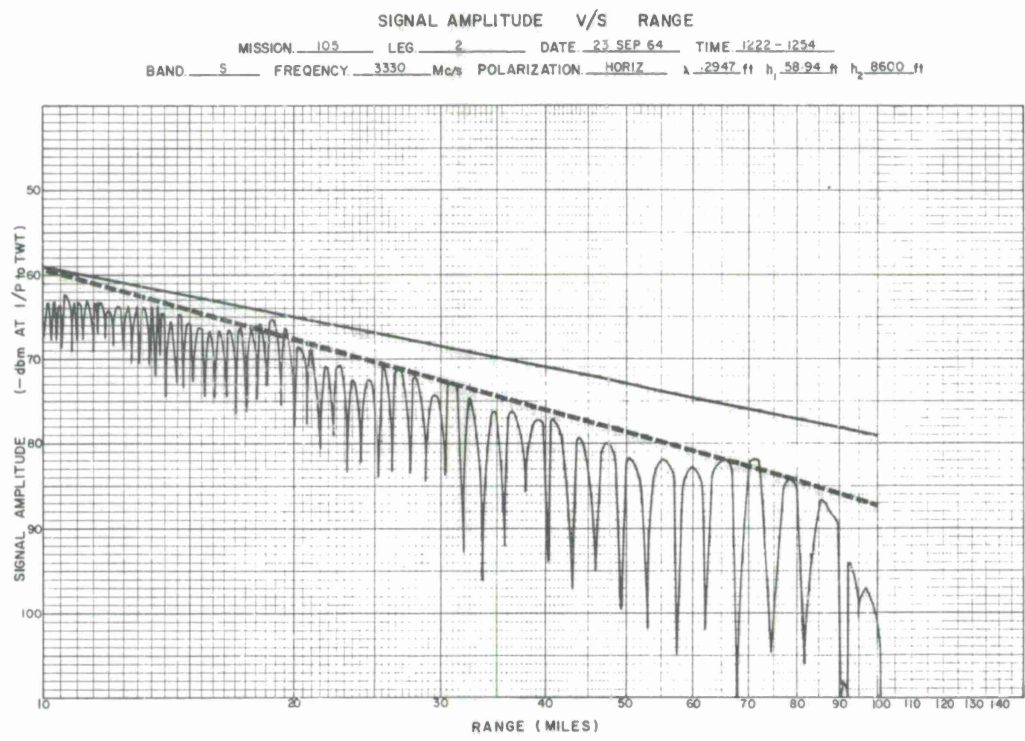
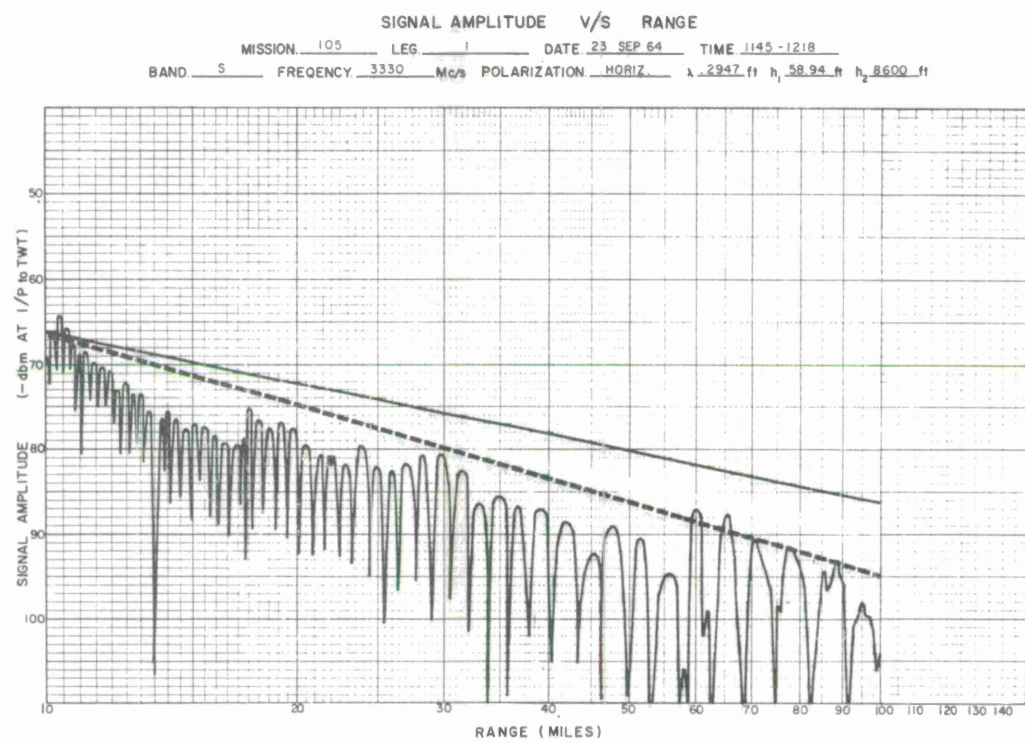
MISSION 105 - Early Afternoon

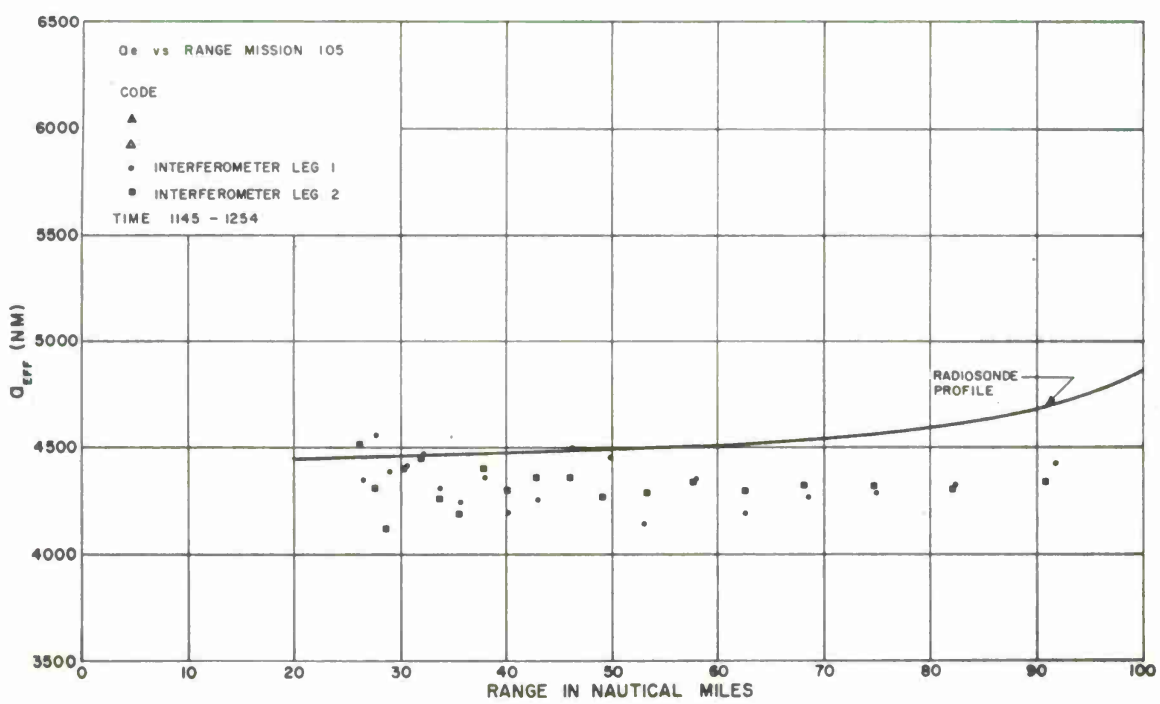
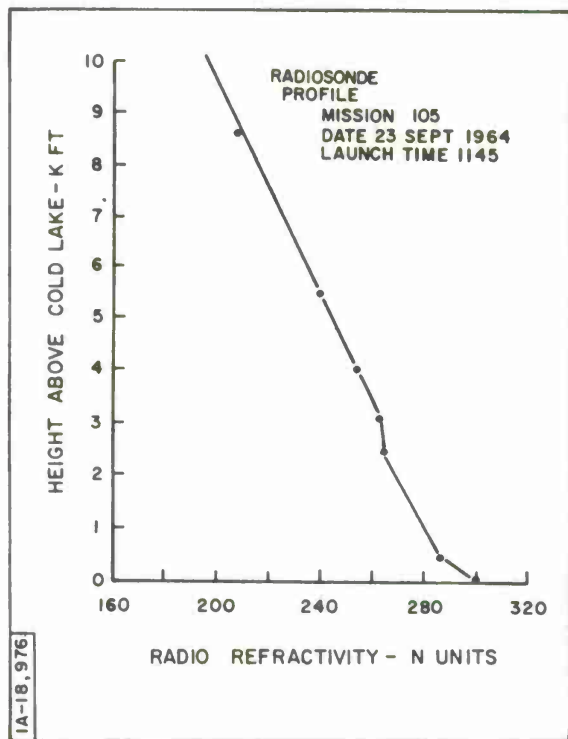
Time: 1145-1413, 23 September 1964

Legs 1, 2, 3, 4

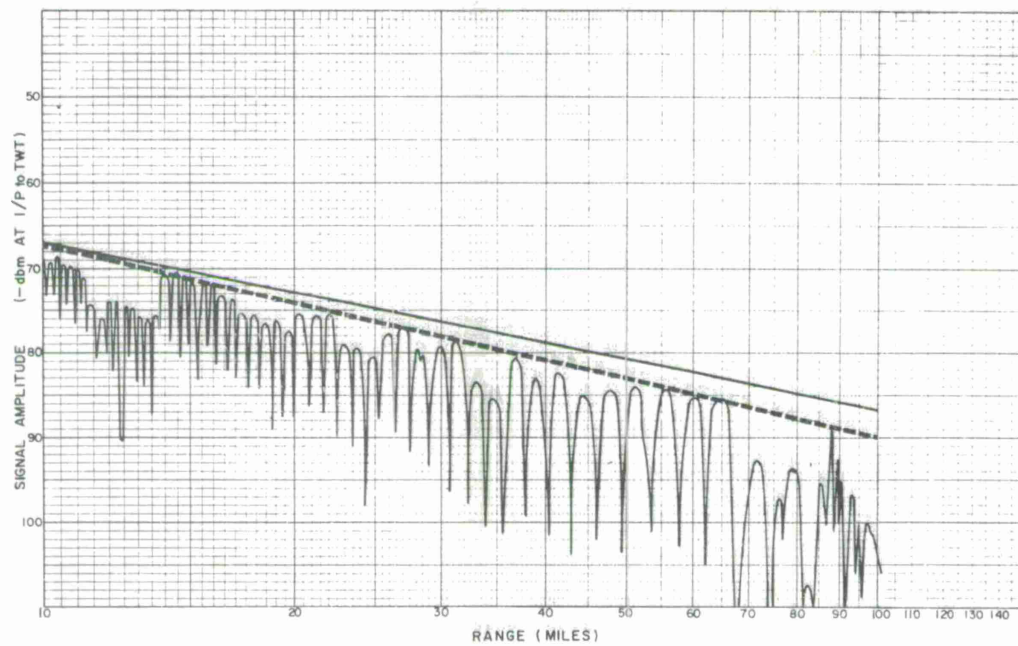
Due to a continuation of aircraft unserviceability, airborne meteorological data was not available and surface data was estimated. Only two radiosonde launches could be obtained, and the 1145 launch is used to depict the propagation conditions over the period from 1145 to 1413. The interferometer results for legs 1 through 4 are almost identical, and, since the same radiosonde data is applied to these results, this discussion will cover these four legs.

The radiosonde and interferometer calculations show that the amount of bending was essentially constant up to 70 n. m. Thereafter the tendency is for the  $A_e$  values to increase, which implies a tendency for the bending to increase. From the radiosonde profile, this result is to be expected with the exception that the surface conditions were estimated, and therefore the  $A_e$  calculations using the radiosonde could be in error at long ranges.

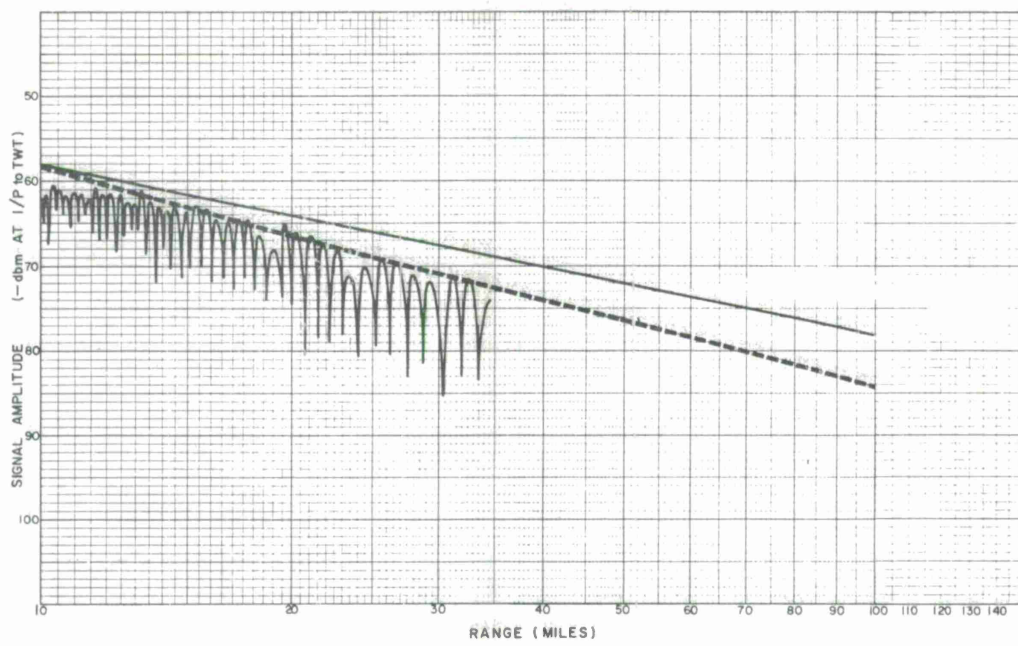


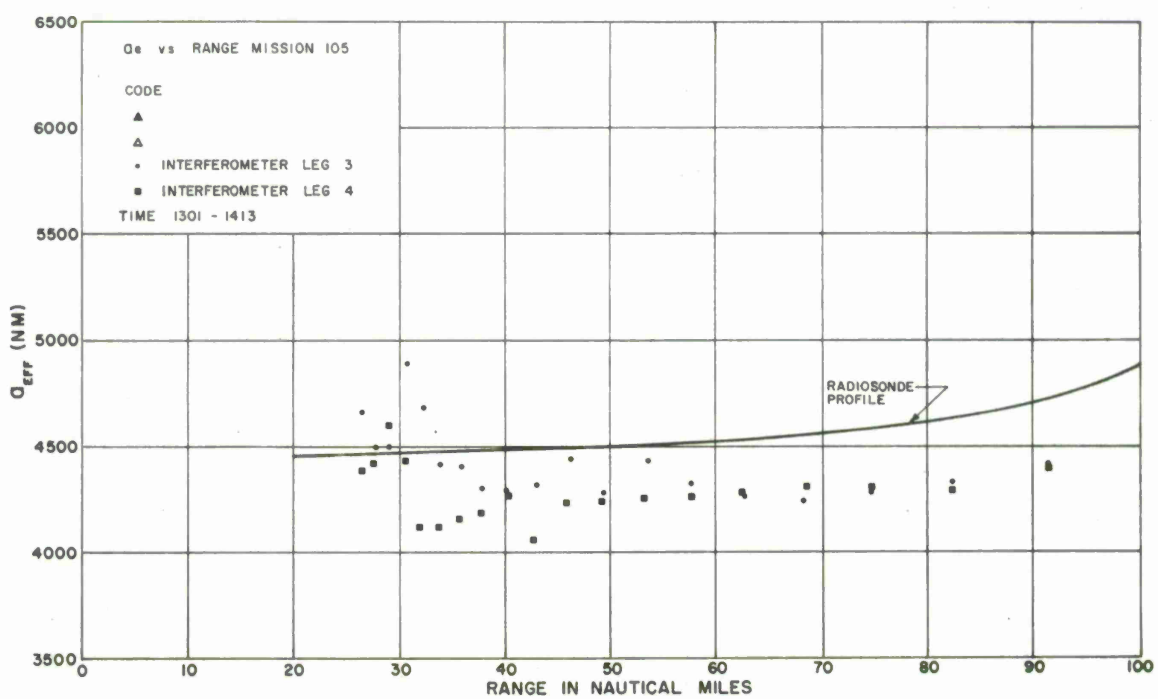
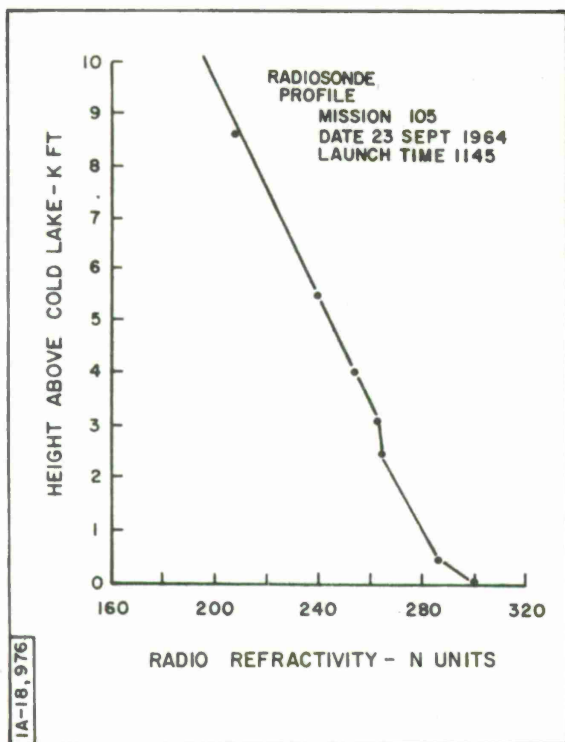


SIGNAL AMPLITUDE V/S RANGE  
 MISSION. 105 LEG. 3 DATE 23 SEP 64 TIME 1301-1335  
 BAND. S FREQUENCY. 3330 Mc/s POLARIZATION HORIZ.  $\lambda$  2947 ft  $h_1$  58.94 ft  $h_2$  8600 ft



SIGNAL AMPLITUDE V/S RANGE  
 MISSION. 105 LEG. 4 DATE 23 SEP 64 TIME 1402-1413  
 BAND. S FREQUENCY. 3330 Mc/s POLARIZATION HORIZ.  $\lambda$  2947 ft  $h_1$  58.94 ft  $h_2$  8600 ft





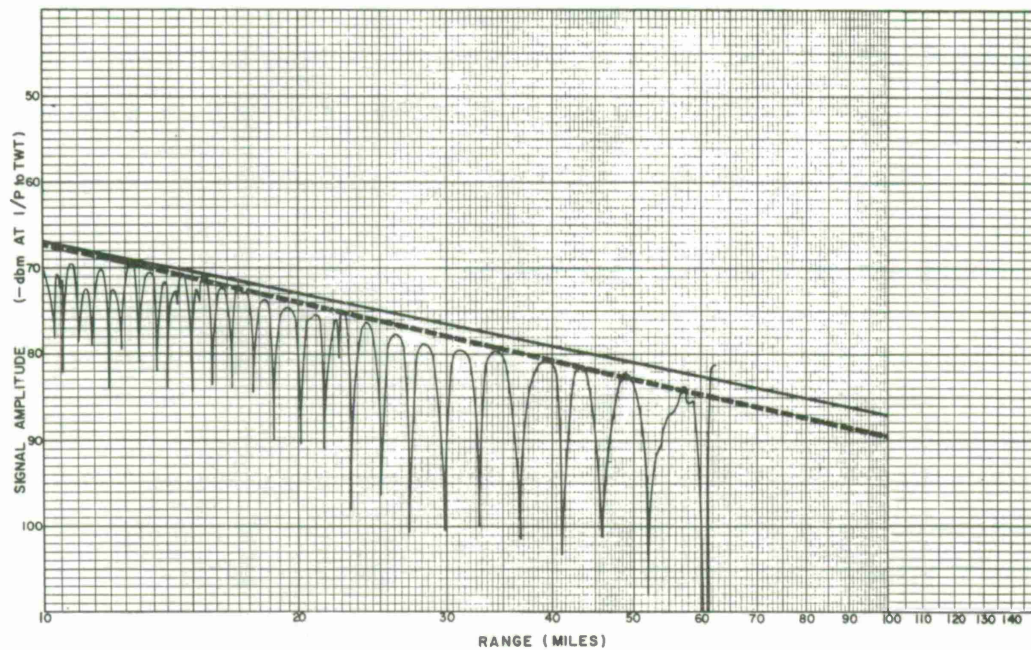
Mission 105 (Continued)

Time: 1423-1506, 23 September 1964

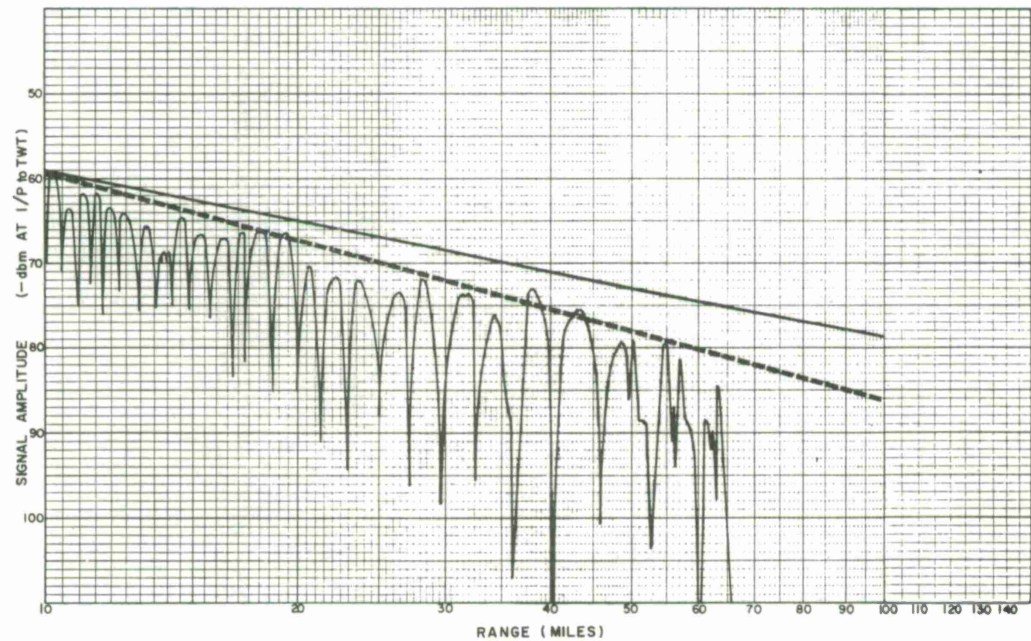
Legs 5, 6

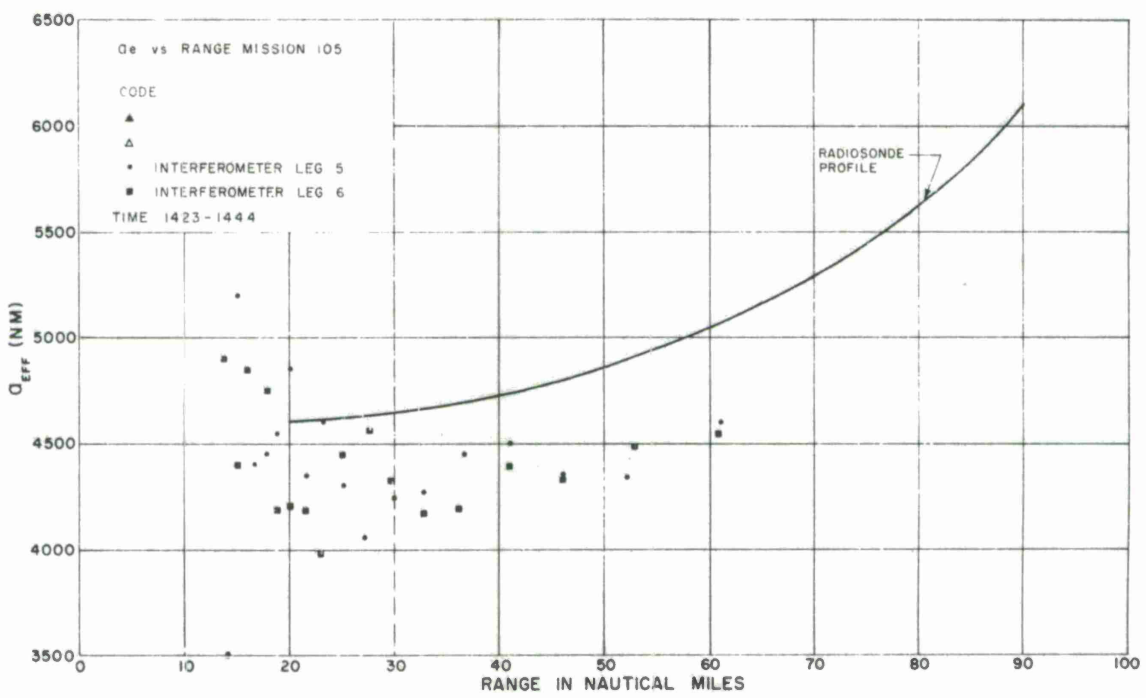
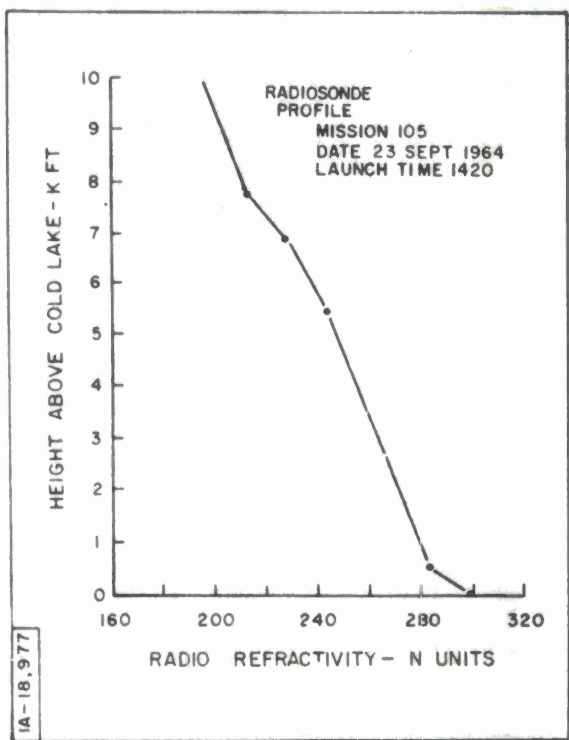
From the radiosonde profile, it is apparent that the propagation conditions are changing not only at the higher levels but most noticeably near the surface. Since the signal source aircraft was now at about half the altitude of the previous four legs, the radio horizon is sharply reduced and the data points stop at about 60 n.m. A comparison of radiosonde and interferometer  $A_e$  calculations both show a strong upward increase in the values as the radio horizon is approached. The lack of surface data does not permit a meaningful evaluation of the agreement between the two methods.

SIGNAL AMPLITUDE V/S RANGE  
 MISSION. 105 LEG. 5 DATE 23 SEPT 64 TIME 1423 - 1444  
 BAND. S FREQUENCY. 3330 Mc/s POLARIZATION. HORIZ  $\lambda$  2947 ft  $h_1$  58.94 ft  $h_2$  4300 ft



SIGNAL AMPLITUDE V/S RANGE  
 MISSION. 105 LEG. 6 DATE 23 SEP 64 TIME 1444-1506  
 BAND. S FREQUENCY. 3330 Mc/s POLARIZATION. HORIZ  $\lambda$  2947 ft  $h_1$  58.94 ft  $h_2$  4300 ft





### General Comments on Mission 105

It is significant that the way in which the  $A_e$  values vary with range provides qualitative information about the propagation conditions and particularly in how the refractivity might vary in height. For example, as the estimated surface gradient increases (1420 launch time), the rate of increase of  $A_e$  values obtained from the interferometer technique also show a marked increase at the low elevation angles (i. e., near the radio horizon). Similarly as the refractivity profile becomes more linear (launch time 1145), the interferometer  $A_e$  values become more constant. Discussion on subsequent missions will demonstrate this point more emphatically.

MISSION 106 - Noon Period

Time: 0927-1015, 24 September 1964

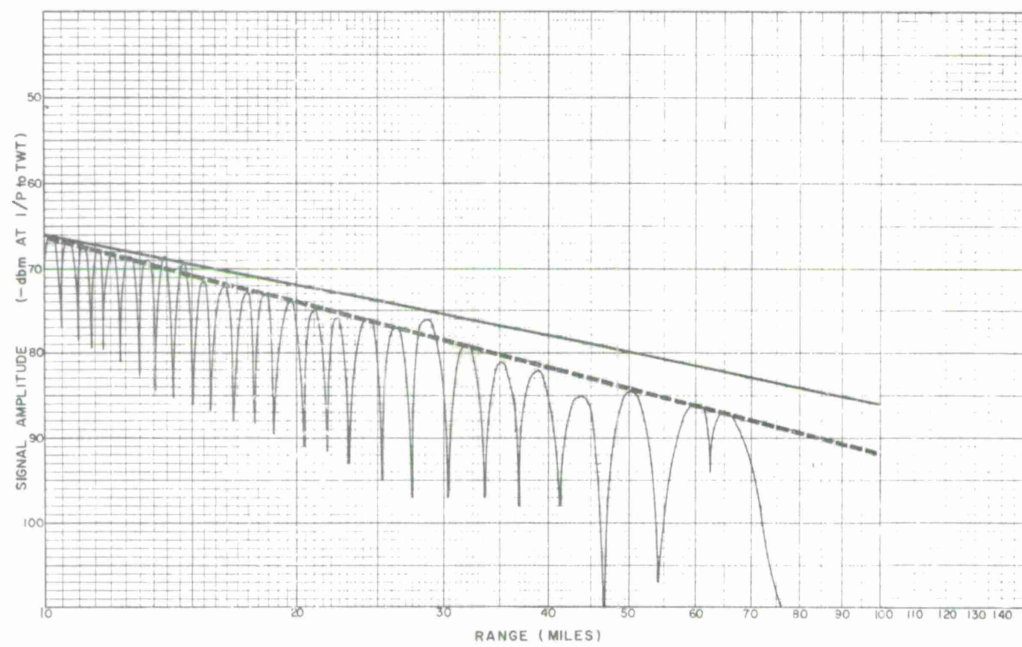
Legs 1, 2

The met aircraft measurements again exhibit large errors near the lake surface. Therefore, the analysis will concentrate on using radiosonde data together with surface measurements which were available during this mission. A comparison of radiosonde and interferometer calculations of  $A_e$  both show a tendency for the magnitudes of these data to increase with range. Beyond 40 n. m., the apparent increase in bending consistently presented by both legs is significantly larger than the radiosonde profile would have suggested. The lack of a strong surface refractivity gradient must necessarily indicate that this was not a true representation of the overall propagation conditions. This brings out an important point, because, the consistency displayed by the interferometer results would suggest that their  $A_e$  variations with range do, in fact, show a strong surface gradient was present. For less than 40 n. m. there is a distinct separation between the interferometer data of legs 1 and 2. With the transmitter height at only 4300 feet, a small height error will give a large  $A_e$  error as was previously discussed in the report. The split suggests that the height-error correction, when applied to leg 1, placed the aircraft below its true height and, when applied to leg 2, placed the aircraft above its

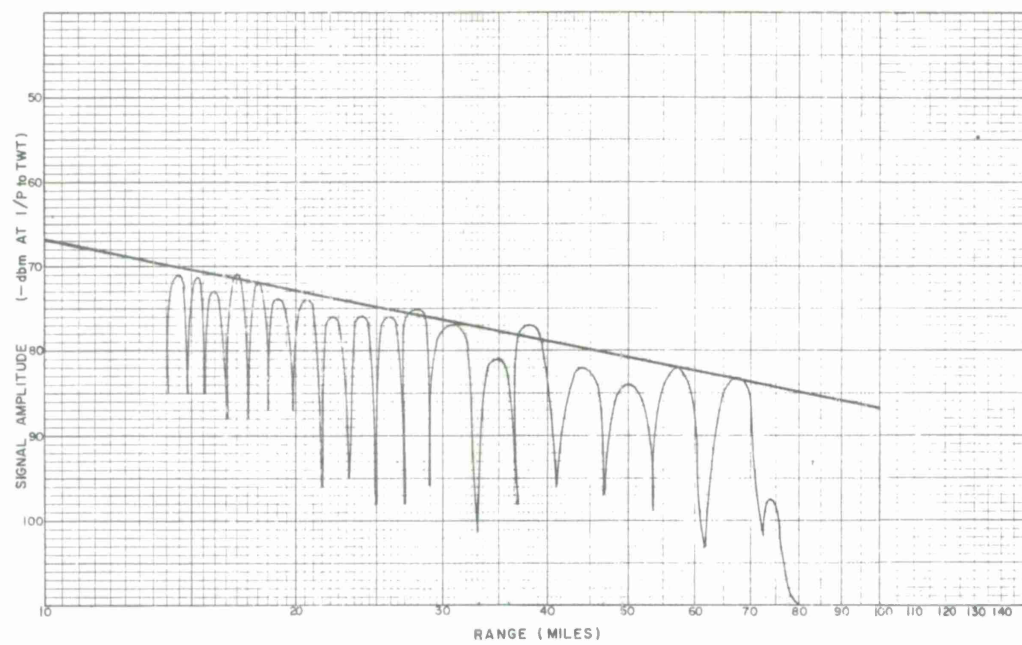
true height. Therefore, purely by chance, the data points for legs 1 and 2 diverge at the shorter ranges. This highly improbable situation occurs only on one other time, on mission 112, legs 5 and 6.

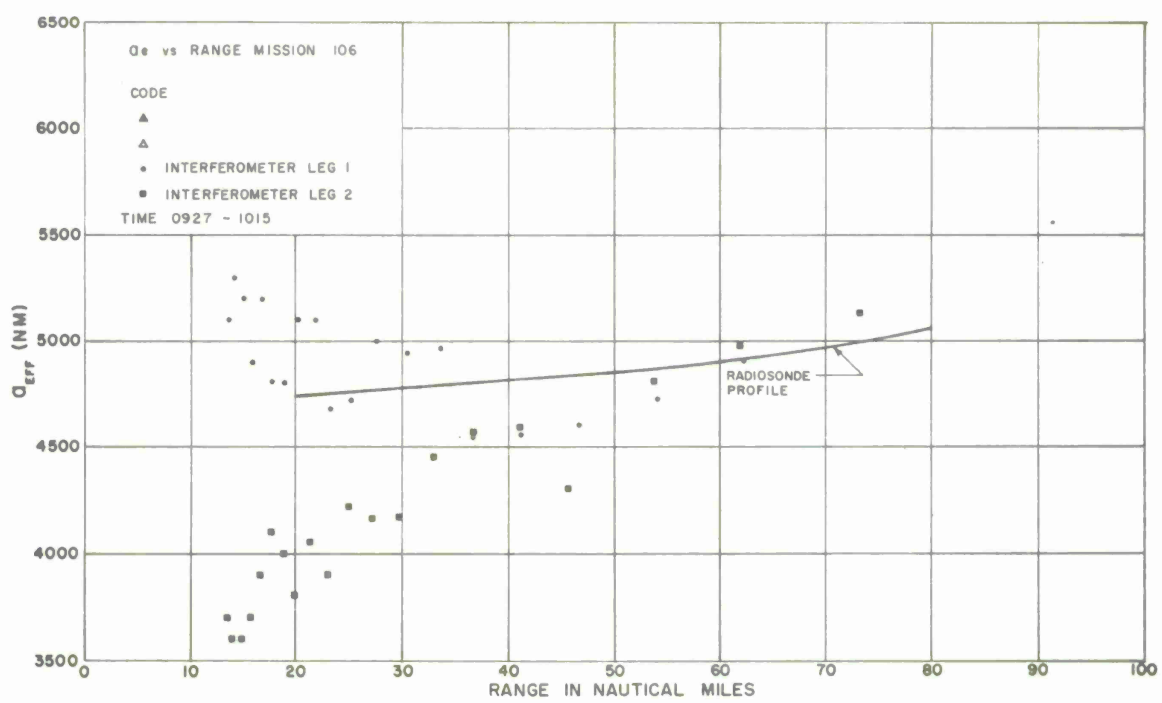
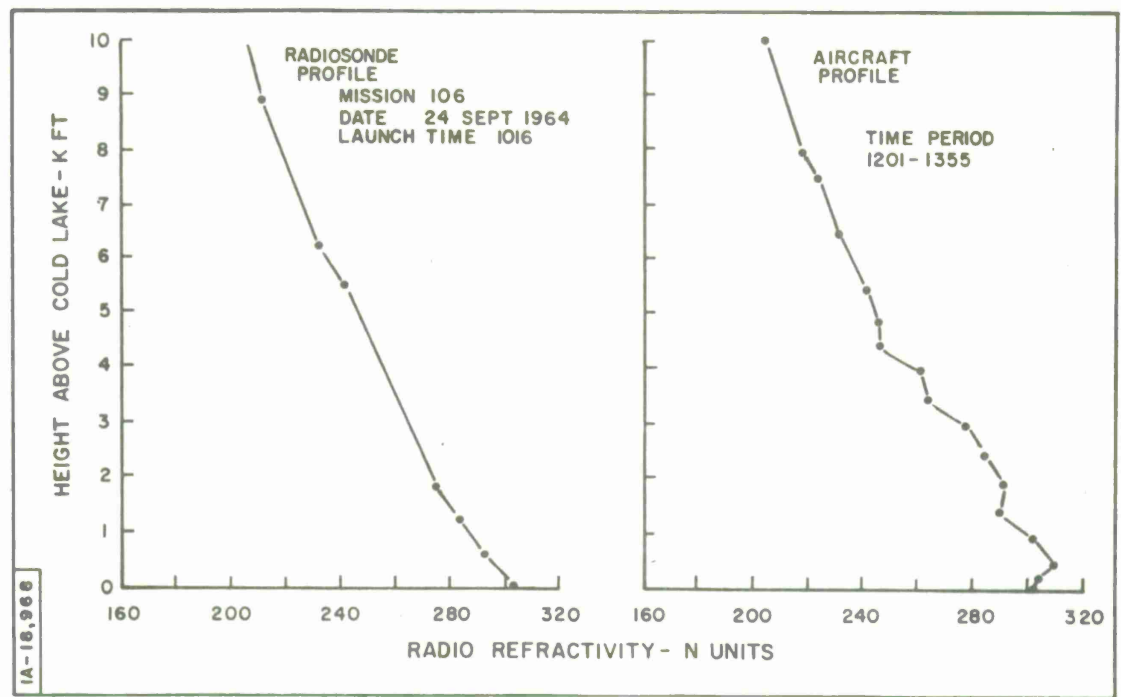
From 55 to 73 n. m. the difference between the radiosonde and interferometer data represents about 0.15 to 0.2 mr. difference in the elevation angle error. Within shorter ranges of useful data (37-55 n. m.) the interferometer results show significantly less ray-path bending than could be observed using the radiosonde profile.

SIGNAL AMPLITUDE V/S RANGE  
 MISSION 106 LEG 1 DATE 24 SEP 64 TIME 0927-0945  
 BAND S FREQUENCY 3336 Mc/s POLARIZATION HORIZ  $\lambda$  2948 ft  $h_1$  5894 ft  $h_2$  4300 ft



SIGNAL AMPLITUDE V/S RANGE  
 MISSION 106 LEG 2 DATE 24 SEP 64 TIME 0945-1015  
 BAND S FREQUENCY 3336 Mc/s POLARIZATION HORIZ  $\lambda$  2948 ft  $h_1$  5894 ft  $h_2$  4300 ft





Mission 106 (Continued)

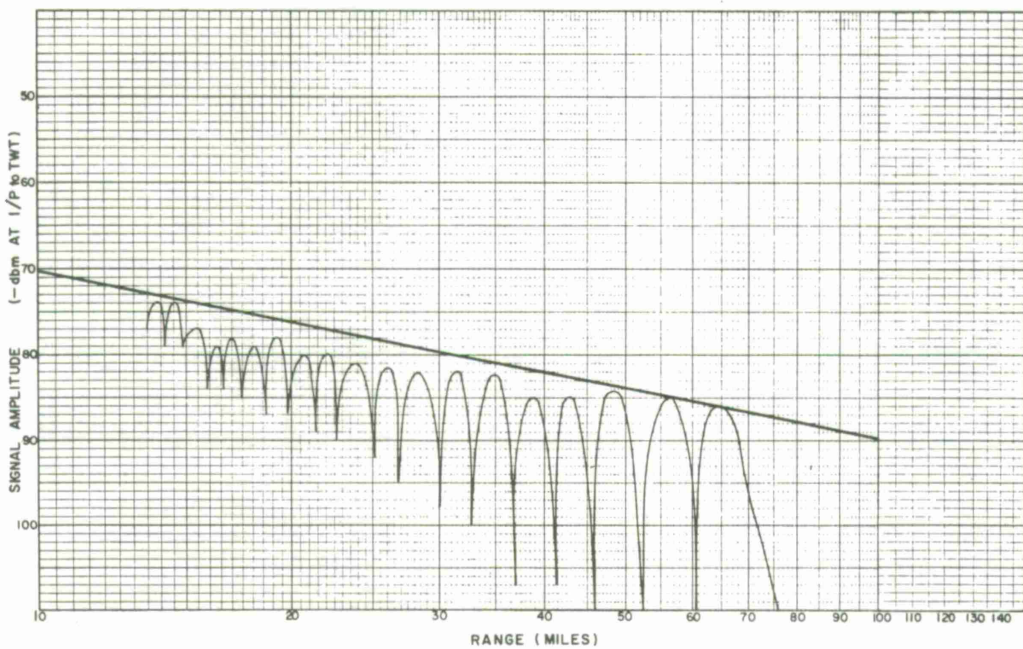
Time: 1029-1117, 24 September 1964

Legs 3, 4

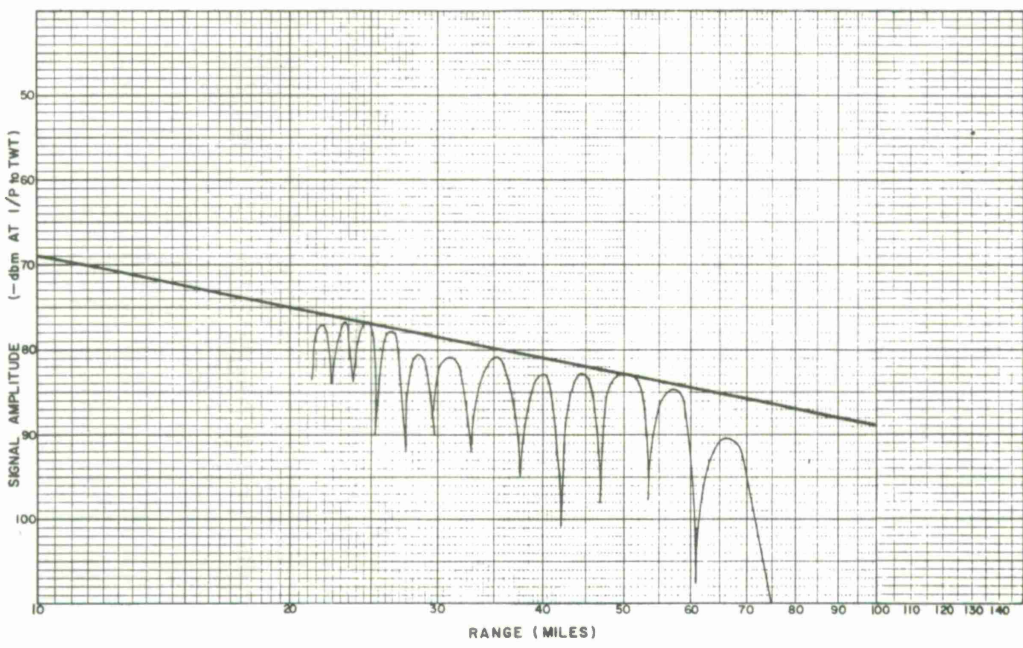
Legs 3 and 4 were flown using vertical polarization. As the aircraft range decreases, the angle of incidence of the reflected ray with the lake surface increases and approaches the Brewster angle. Therefore, the amplitude of the reflected signal received with the vertically polarized antenna would decrease, and the depth of fade decrease. [3]

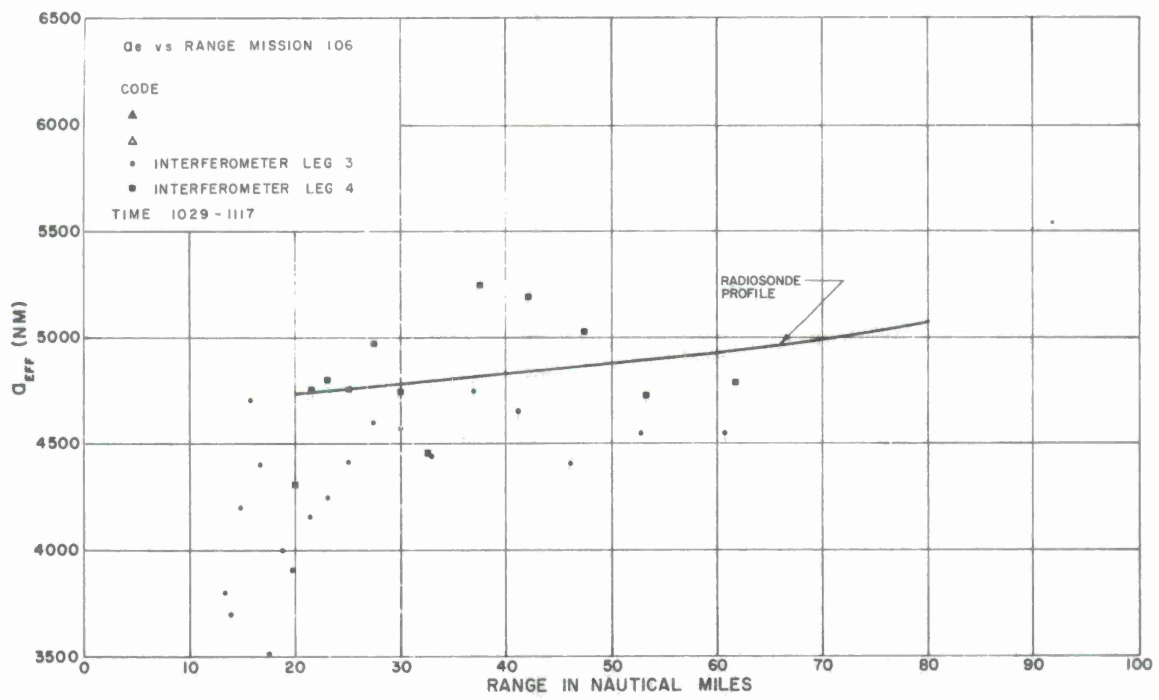
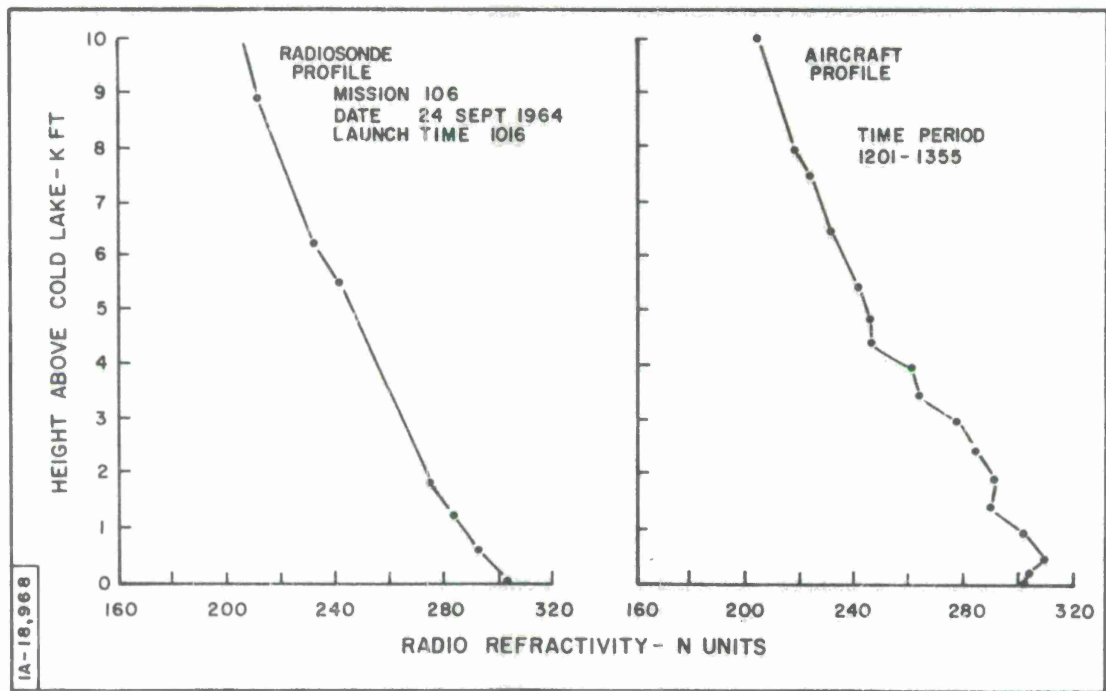
The  $A_e$  values obtained with the interferometer indicate that the ray-path bending is maximum for the transmitter at 38 n.m. The amount of bending decreases rapidly thereafter and then becomes essentially constant as the radio horizon is reached. The fact that this behavior is consistent for both legs indicates that the interferometer is observing large variations, due to the refractivity structure, which were not observed by the radiosonde. The aircraft refractivity profile does however indicate two substandard conditions at 400- and 1700-foot altitudes. Due to the apparent lack of meaningful refractivity data, neither the radiosonde nor aircraft calculations can be sensibly compared with the interferometer data.

SIGNAL AMPLITUDE V/S RANGE  
 MISSION 106 LEG 3 DATE 24 SEP 64 TIME 1029-1045  
 BAND S FREQUENCY 3336 Mc/s POLARIZATION VERT  $\lambda$  2948 ft  $h_1$  5890 ft  $h_2$  4300 ft



SIGNAL AMPLITUDE V/S RANGE  
 MISSION 106 LEG 4 DATE 24 SEPT 64 TIME 1100-1117  
 BAND S FREQUENCY 3336 Mc/s POLARIZATION VERT  $\lambda$  2948 ft  $h_1$  5890 ft  $h_2$  4300 ft





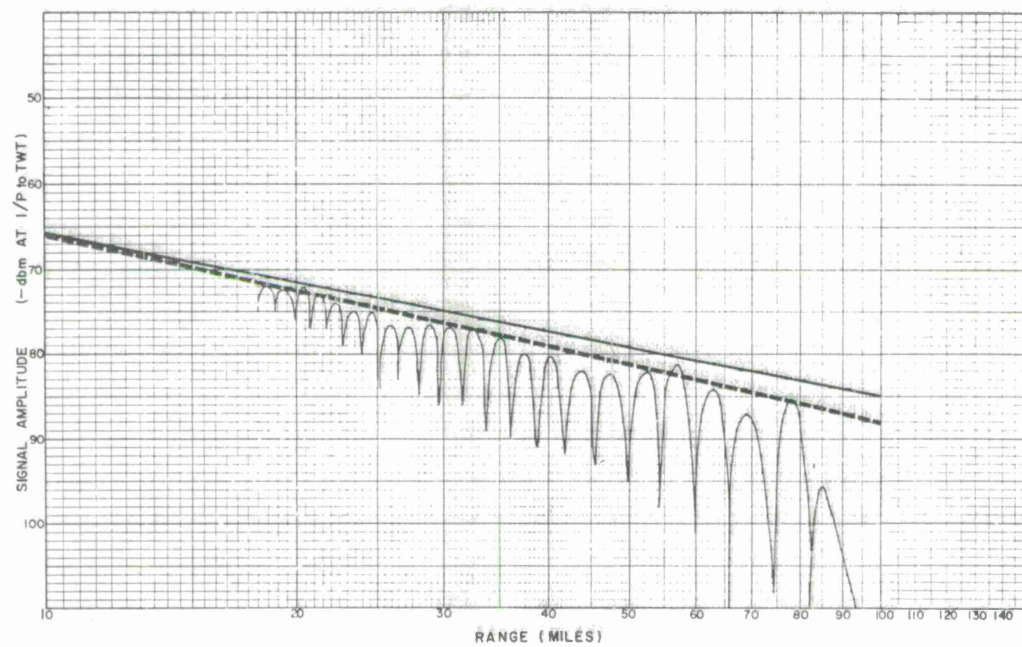
Mission 106 (Continued)

Time: 1143-1203, 24 September 1964

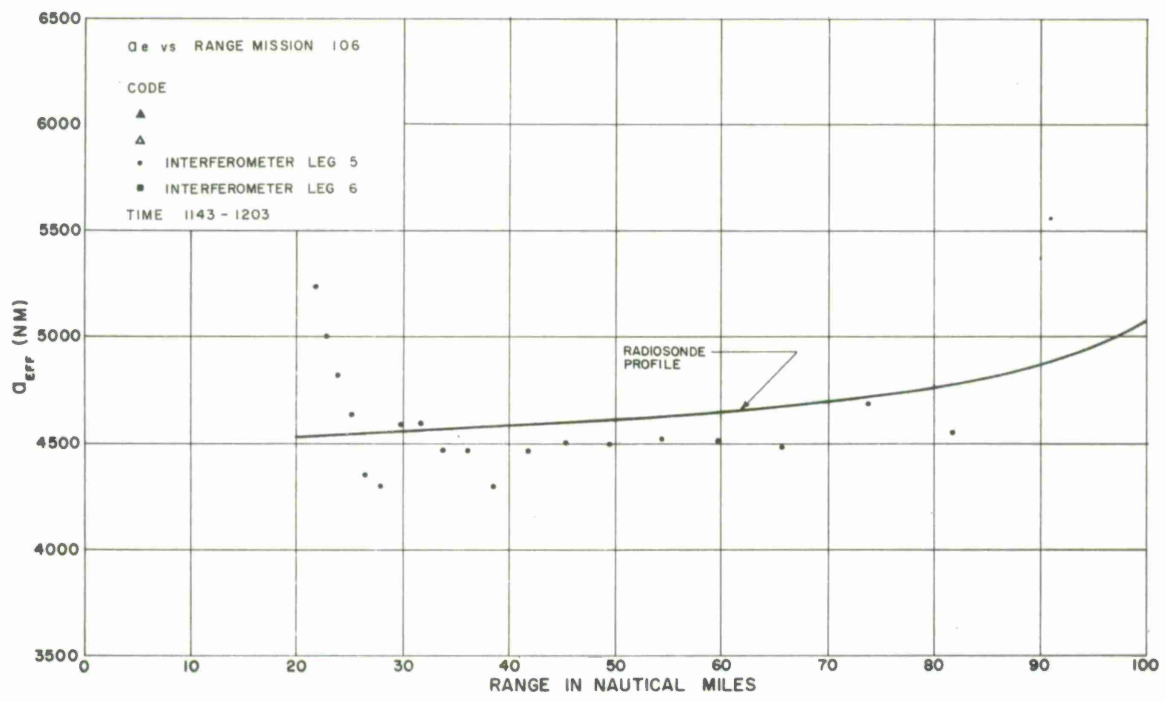
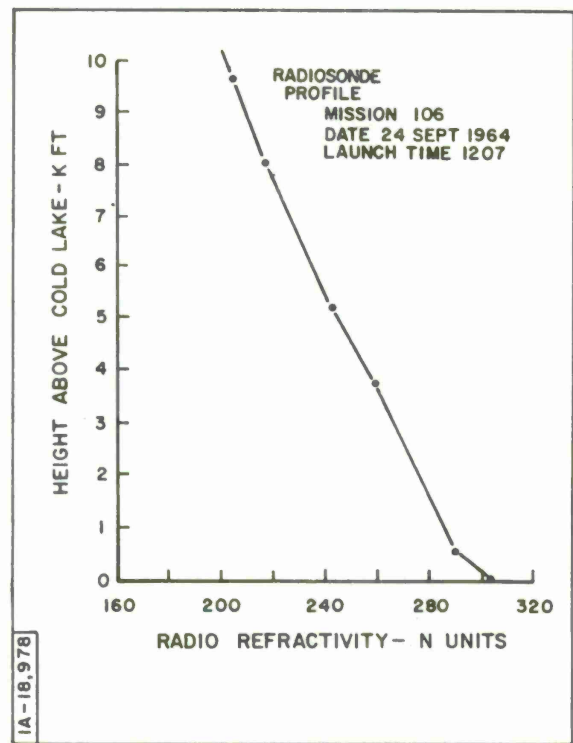
Leg 5

For legs 5 and 6, the transmitter height was increased to 7000 feet. This has the advantage of reducing the effect of an experimental height error on the interferometer results and also permits more of the signal propagation to occur at higher levels in the atmosphere. In the latter case, this makes the results less dependent on surface conditions. The interferometer results for leg 5 indicate that the amount of ray-path bending was essentially constant out to ranges of about 70 n. m. and, thereafter, slightly increasing with range. As indicated by the radiosonde calculations, and what might have been obvious from the radiosonde profile, the bending is essentially independent of range except for the final low-angle or long-range conditions. The agreement between data represents from 0.075 to 0.4 mr. difference in the elevation angle error between the ranges of 30 to 80 n. m.

SIGNAL AMPLITUDE V/S RANGE  
MISSION 106 LEG 5 DATE 24 SEPT 64 TIME 1143-1205  
BAND S FREQUENCY 3336 Mc/s POLARIZATION VERT  $\lambda$  2948 ft  $N_1$  58.90  $N_2$  7000 ft



No data for leg 6



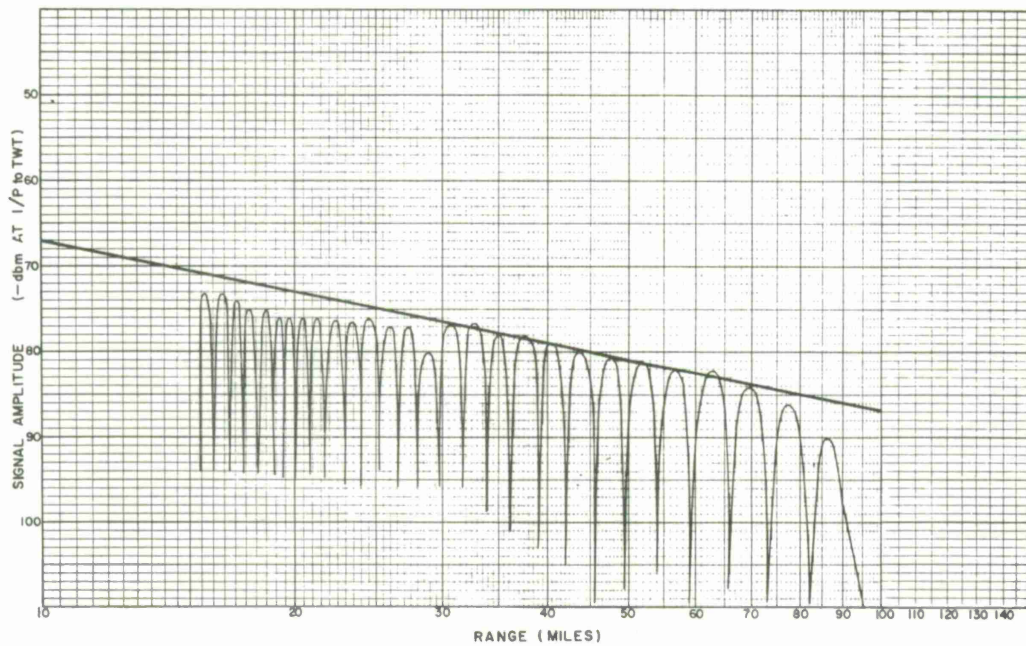
Mission 106 (Continued)

Time: 1303-1402, 24 September 1964

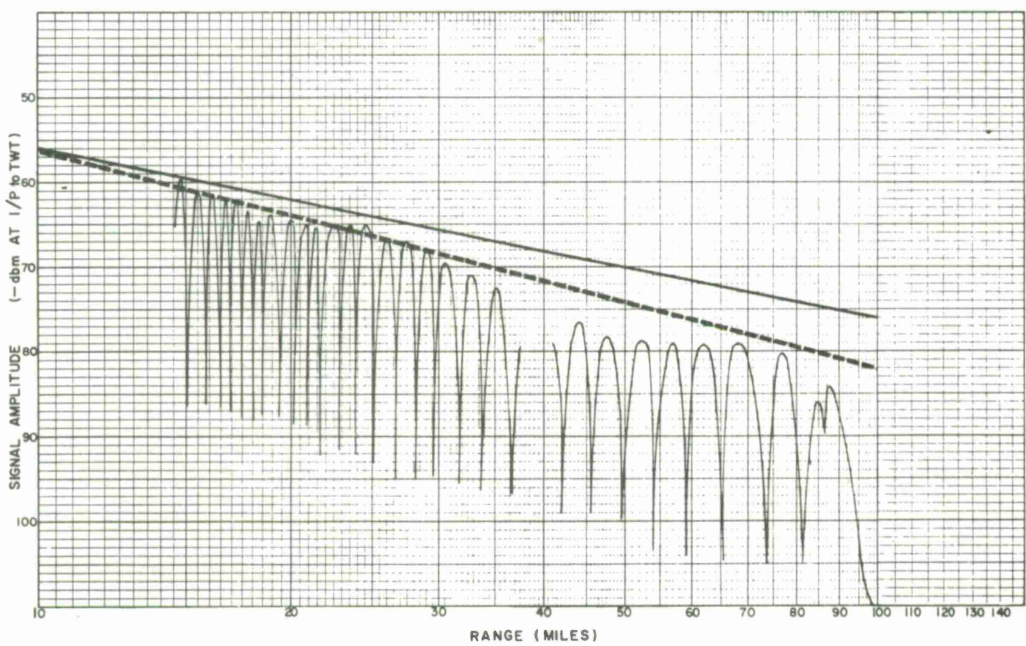
Legs 7, 8

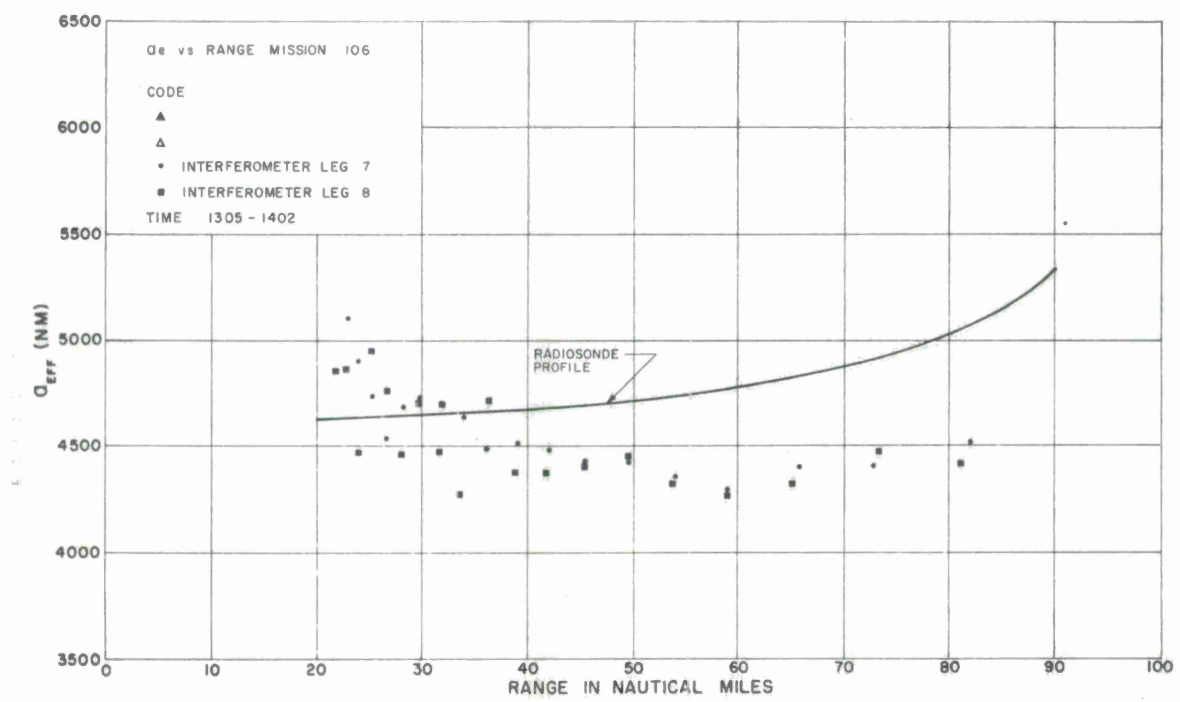
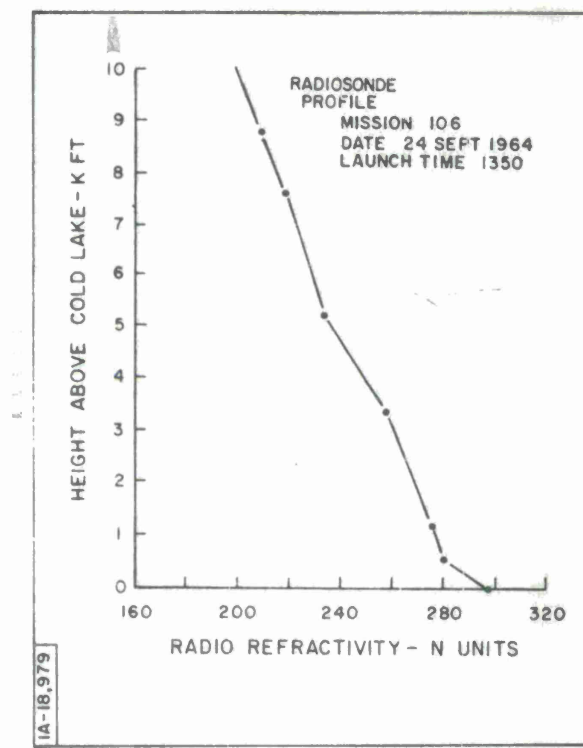
The interferometer data shows very good agreement between legs 7 and 8, which indicates there was very little temporal variation and also that the technique is describing the true propagation conditions. The somewhat constant  $A_e$  values between 40 to 80 n.m. suggests a near-linear refractivity profile. The decrease in refractivity gradient at 4000 feet might account for the reduction in  $A_e$  values observed between 50 to 67 n.m. Also, the tendency for the  $A_e$  values to increase beyond 60 n.m. might be anticipated due to the strong surface gradient of refractivity. Although the ray-tracing results show a general increase with range, due to a surface gradient, the magnitudes of the calculated bending are not close to the interferometer data. Here again, an important point is raised in that the radiosonde profile indicates how the  $A_e$  values might vary with range even though the profile may not provide an exact quantitative model of the propagation conditions.

SIGNAL AMPLITUDE V/S RANGE  
 MISSION 106 LEG 7 DATE 24 SEPT 64 TIME 1303-1330  
 BAND S FREQUENCY 3336 Mc/s POLARIZATION HORIZ  $\lambda$  2948 ft  $h_1$  58.94 ft  $h_2$  7000 ft



SIGNAL AMPLITUDE V/S RANGE  
 MISSION 106 LEG 8 DATE 24 SEPT 64 TIME 1340-1402  
 BAND S FREQUENCY 3336 Mc/s POLARIZATION HORIZ  $\lambda$  2948 ft  $h_1$  58.94 ft  $h_2$  7000 ft





### General Comments on Mission 106

In general the interferometer results are much better behaved for the higher transmitter heights. This is largely due to the fact that the experimental height error becomes less significant as the transmitter height is increased. The use of horizontal polarization is recommended because of the sharp and deep fades which are produced. Although the comparison of interferometer and ray-tracing data shows disappointingly large errors, this is somewhat offset by the consistent operation of the interferometer. In fact, as has been previously suggested, the interferometer technique may have its greatest potential in defining various propagation conditions which cannot be obtained directly from radiosonde or aircraft observations.

MISSION 107 - Sunset

Time: 1602-2002, 28 September 1964

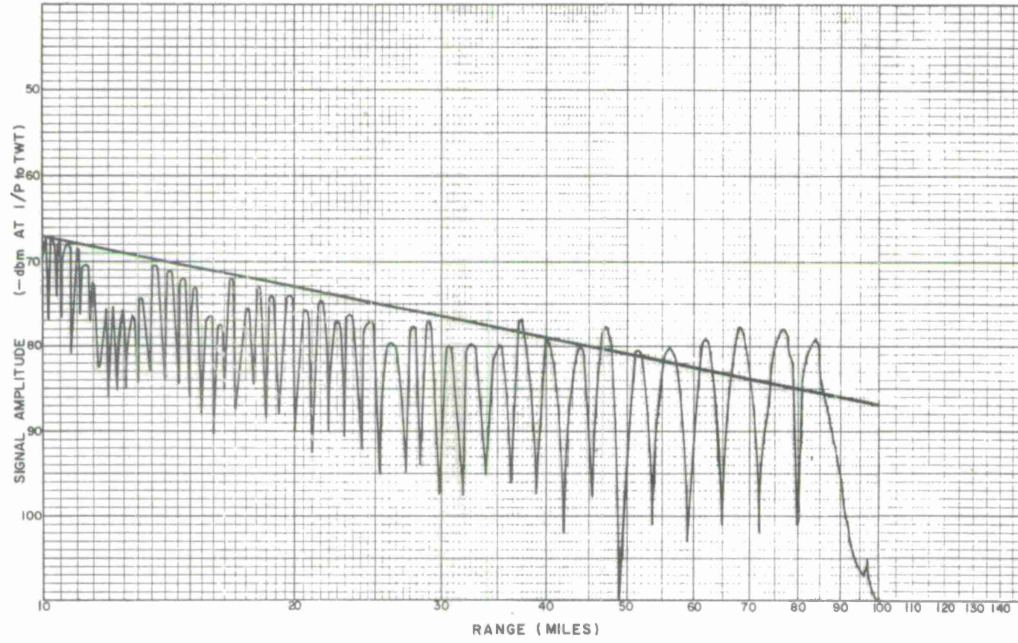
Legs 1, 2, 3, 4, 5, 6

The radiosonde soundings from 1613 through until 1934 indicate that there was great stability in the atmospheric conditions. Aircraft measurements made over this same period also show this situation was prevalent over the whole range area. However, the aircraft measurements at low levels over Cold Lake indicate a substandard refractivity condition which does not appear to fit the true situation. The stable conditions are evident from the interferometer  $A_e$  plots for legs 1 through 6. It should be observed that there is some perturbation in the interferometer data for legs 5 and 6. The radiosonde launch at 1934 indicates that the refractivity gradient is beginning to increase just above the launch height of 539 feet. This beginning of temporal instability is apparently reflected in the variations which are observed in the interferometer results for this period.

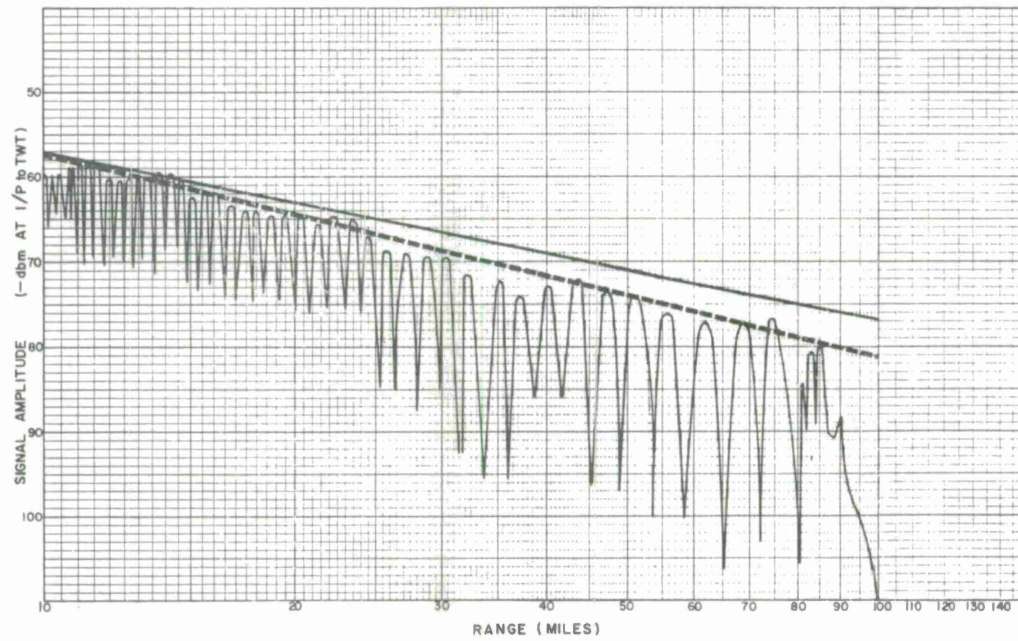
The general agreement between ray-tracing results using the radiosonde data and the interferometer calculations is extremely good. At 40 n. m. the error represents about 0.2 mr. difference in the elevation angle error and at 80 n. m. about 0.3 mr. The good agreement obtained during this mission can be attributed to the stability of the atmosphere, the fact that the refractivity profile is essentially

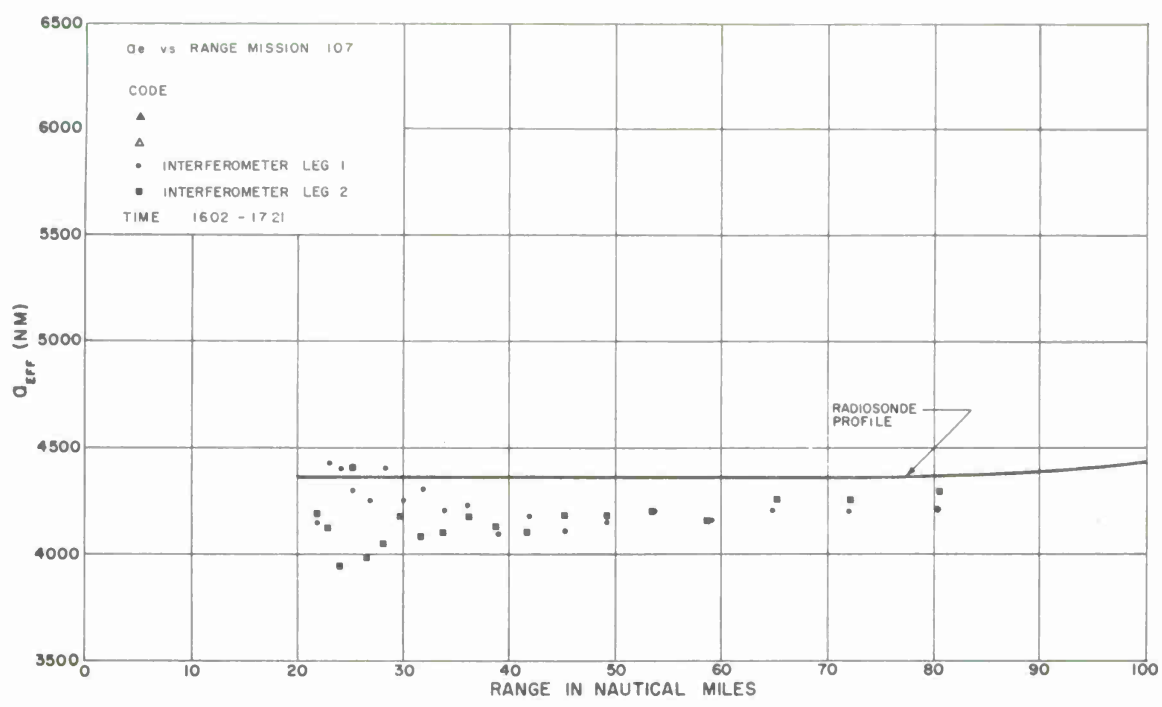
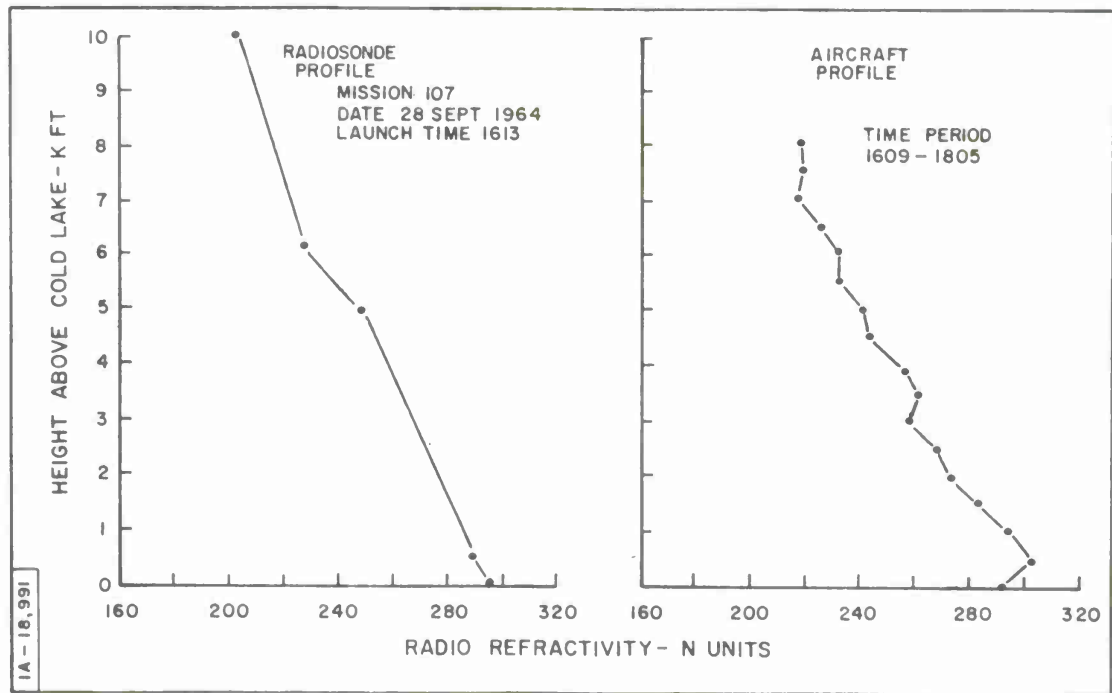
linear, that there is no strong surface gradient, and that the transmitter height was relatively high. The determination of  $A_e$  values to represent ray-path bending, of course, assumes that the index profile is linear with height.

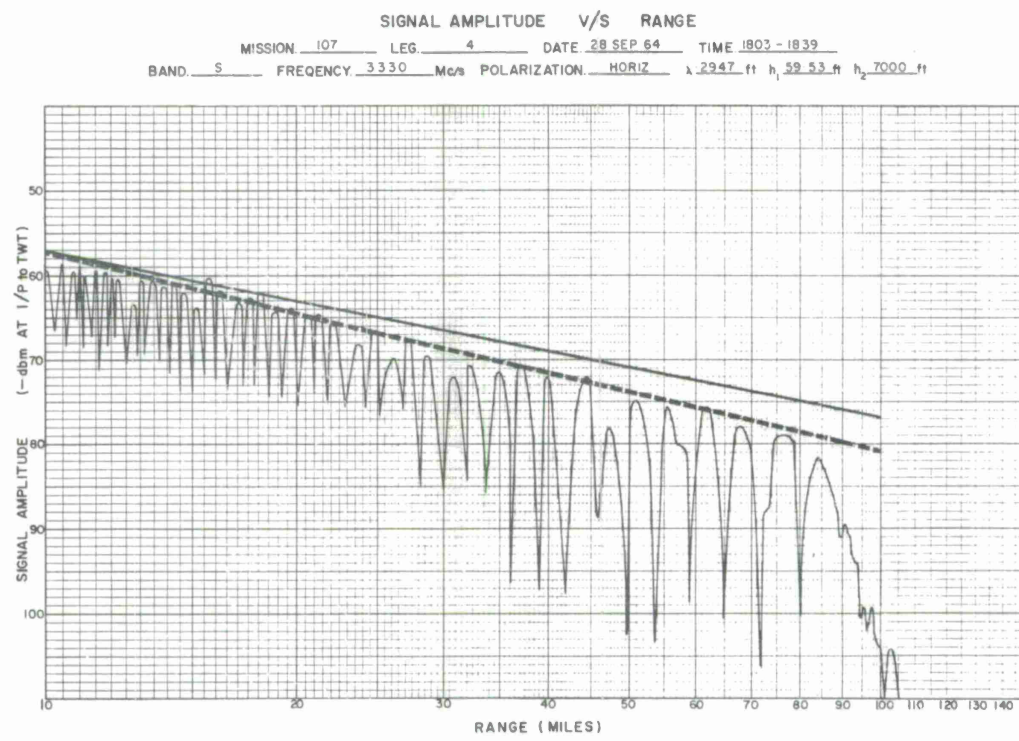
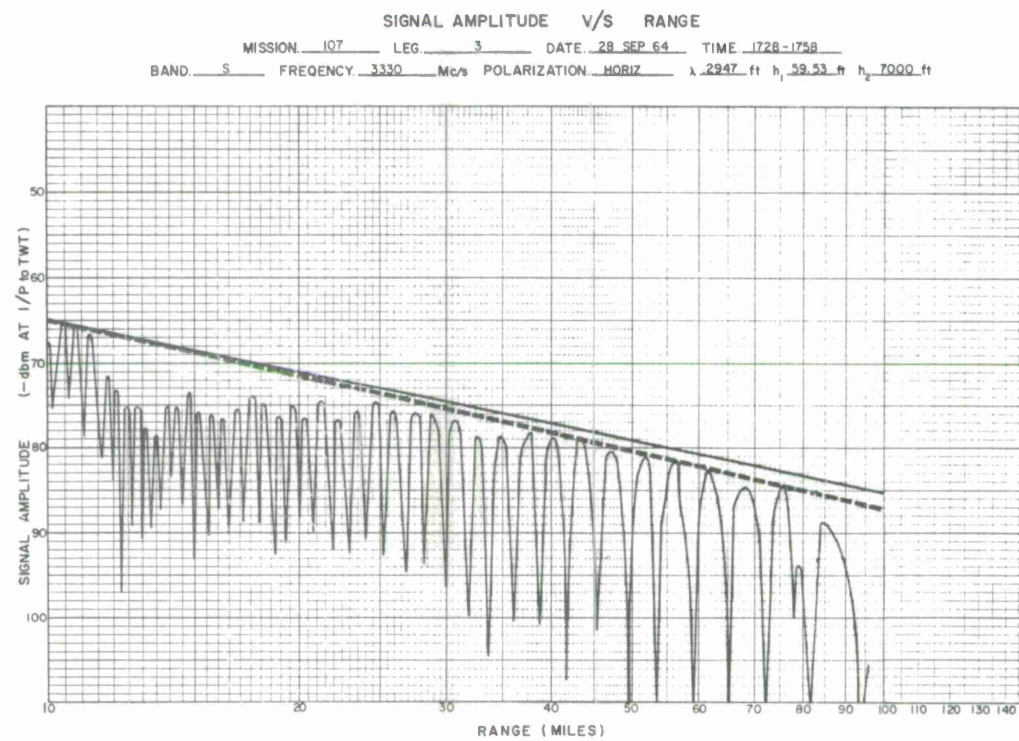
SIGNAL AMPLITUDE V/S RANGE  
 MISSION 107 LEG 1 DATE 28 SEP 64 TIME 1602-1642  
 BAND S FREQUENCY 3330 Mc/s POLARIZATION HORIZ  $\lambda$  2947 ft  $h_1$  59.53 ft  $h_2$  7000 ft

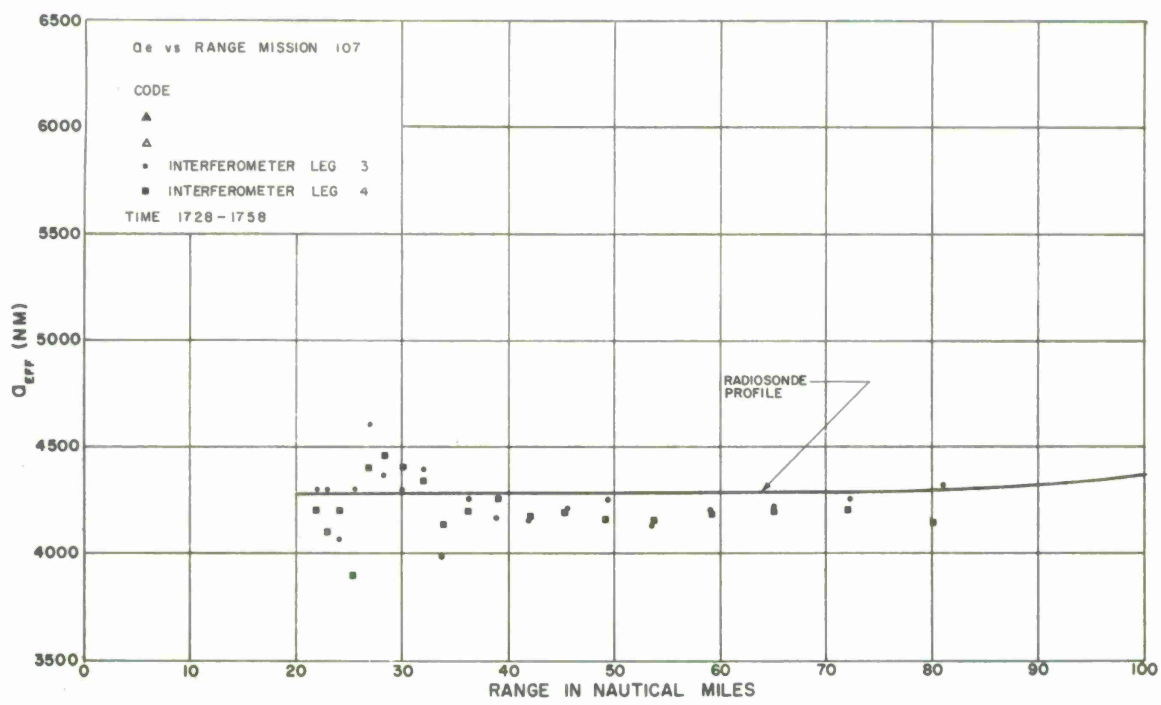
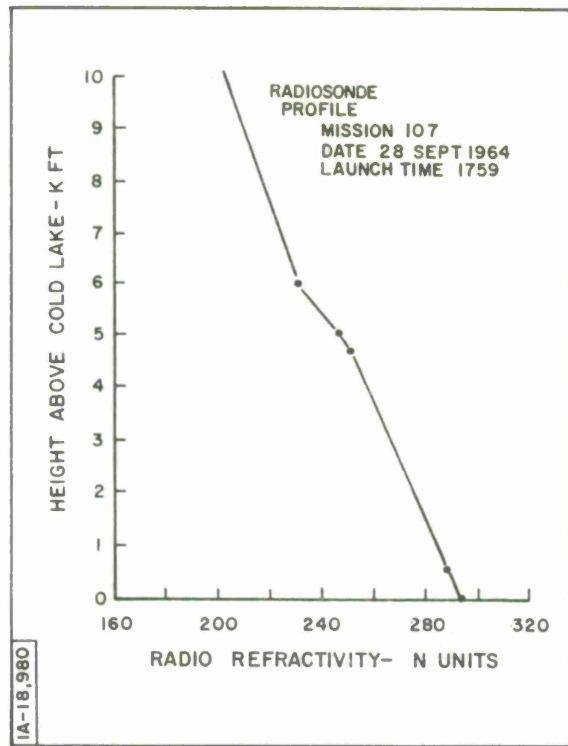


SIGNAL AMPLITUDE V/S RANGE  
 MISSION 107 LEG 2 DATE 28 SEP 64 TIME 1647-1721  
 BAND S FREQUENCY 3330 Mc/s POLARIZATION HORIZ  $\lambda$  2947 ft  $h_1$  59.53 ft  $h_2$  7000 ft

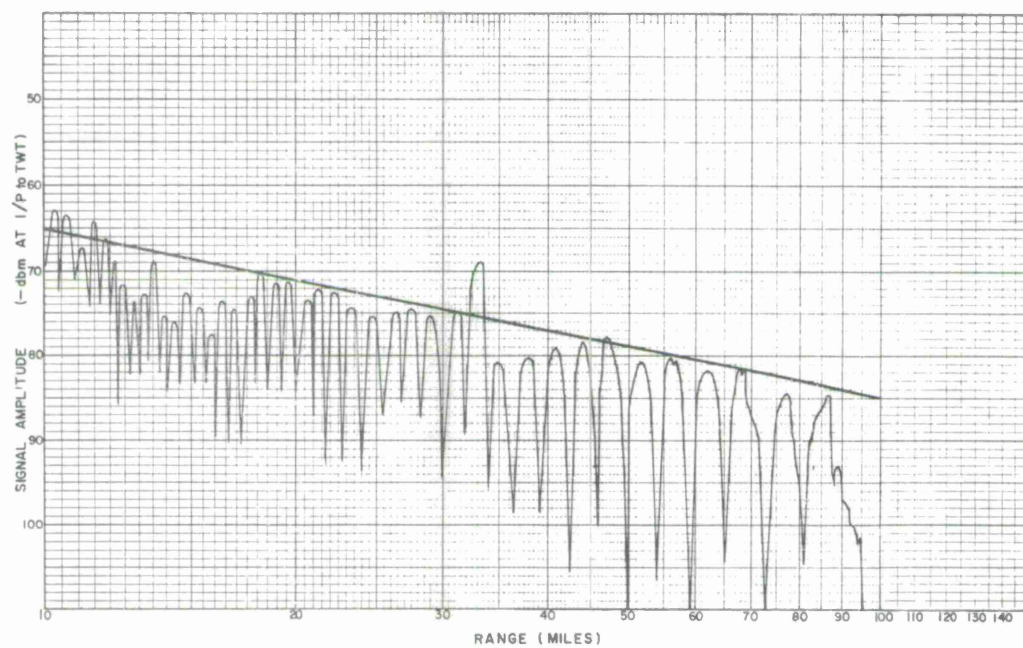




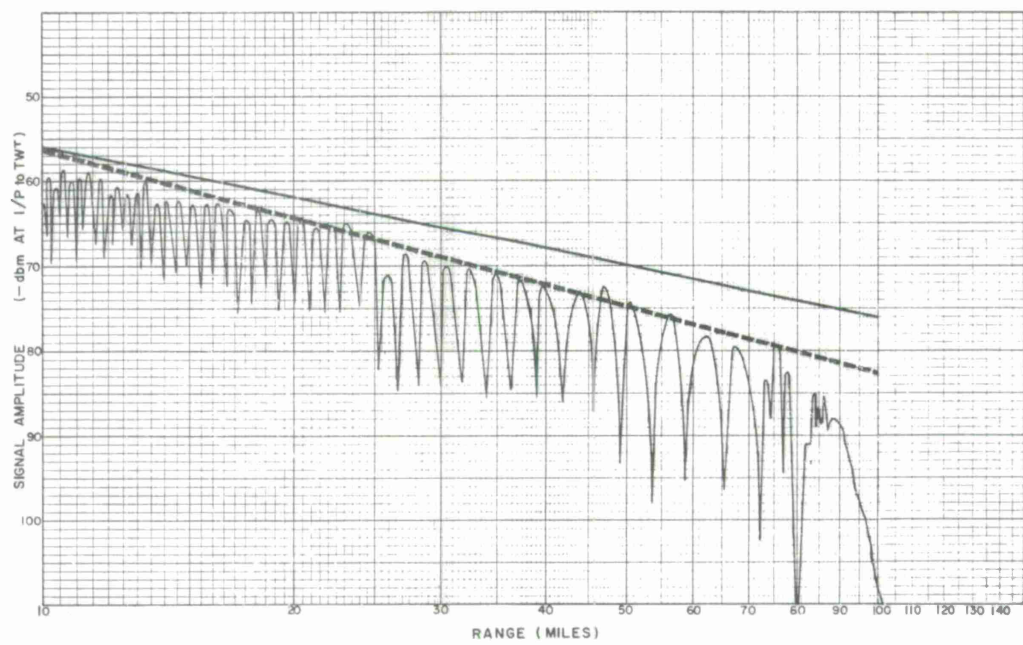


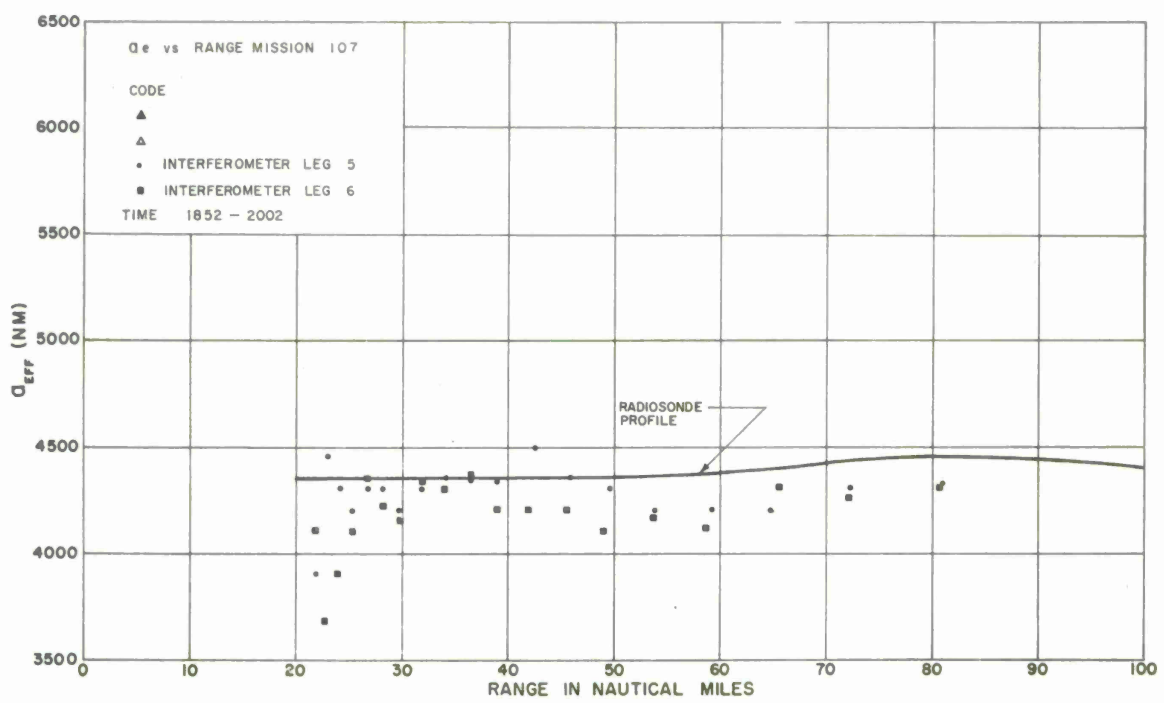
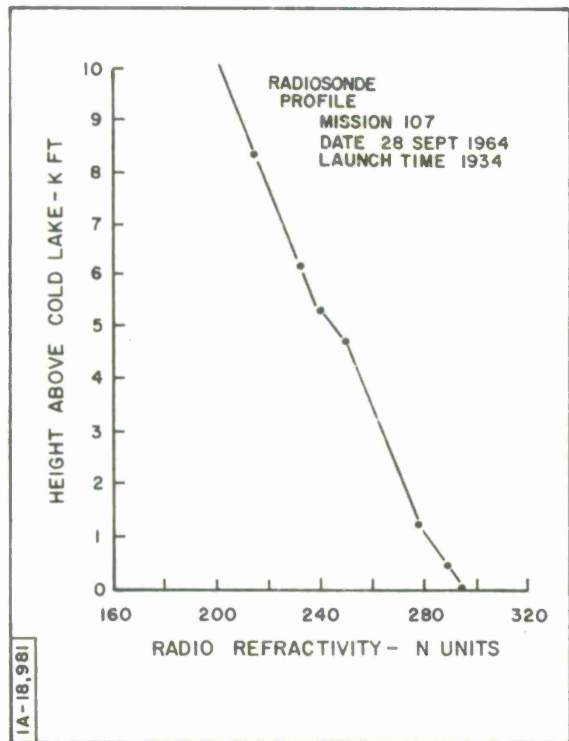


SIGNAL AMPLITUDE V/S RANGE  
 MISSION 107 LEG 5 DATE 28 SEP 64 TIME 1952 - 1921  
 BAND S FREQUENCY 3330 Mc/s POLARIZATION HORIZ  $\lambda$  2947 ft  $h_1$  5953 ft  $h_2$  7000 ft



SIGNAL AMPLITUDE V/S RANGE  
 MISSION 107 LEG 6 DATE 28 SEP 64 TIME 1924 - 2002  
 BAND S FREQUENCY 3330 Mc/s POLARIZATION HORIZ  $\lambda$  2947 ft  $h_1$  5953 ft  $h_2$  7000 ft





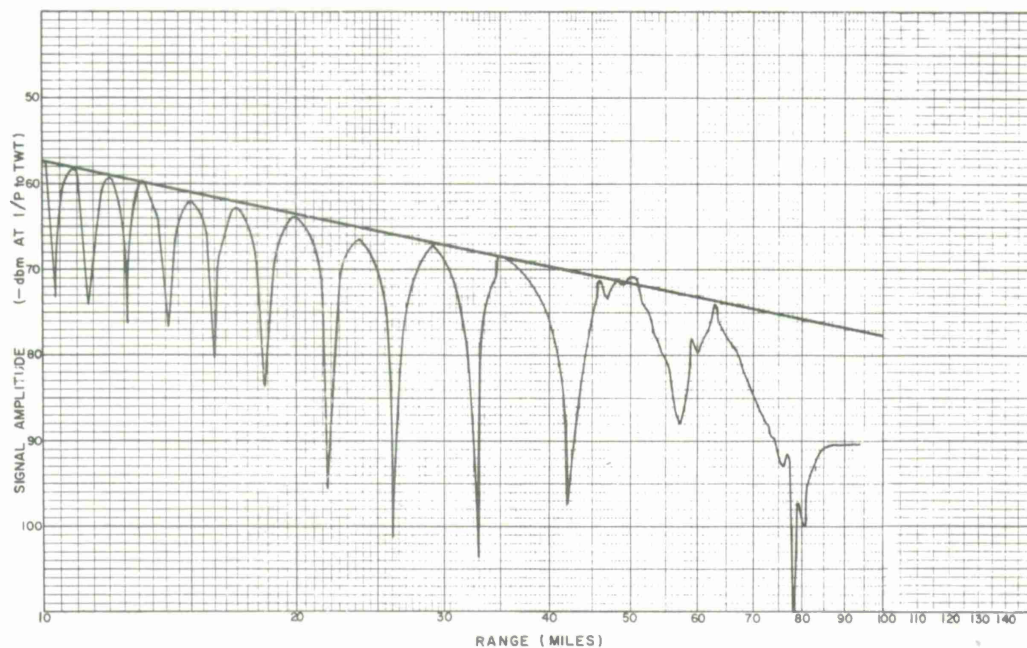
MISSION 108 - Afternoon

Time: 1254-1400 , 30 September 1964

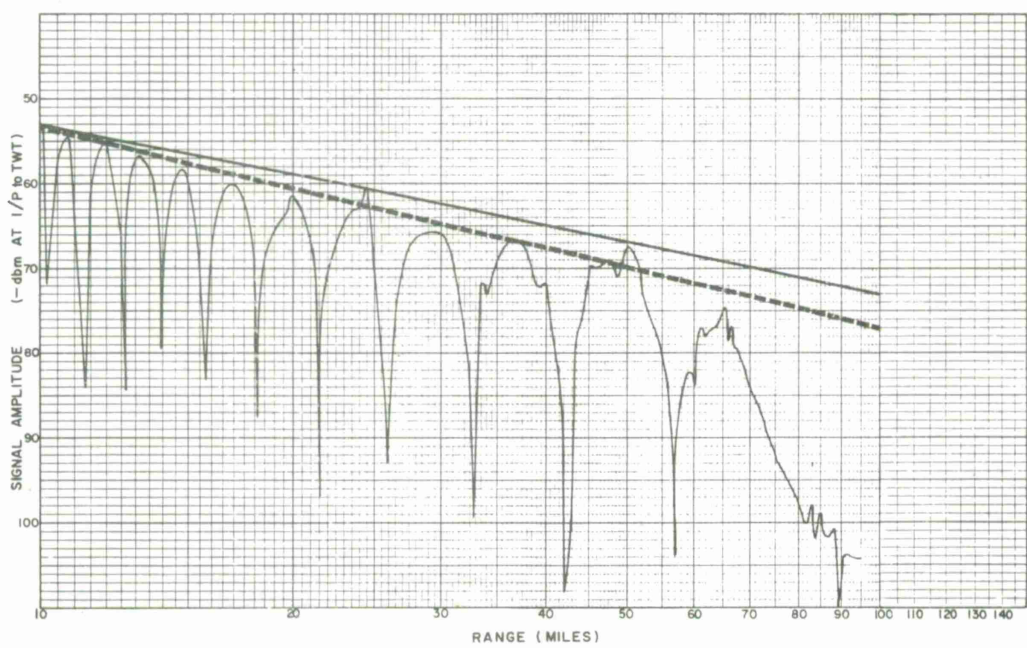
Legs 1, 2

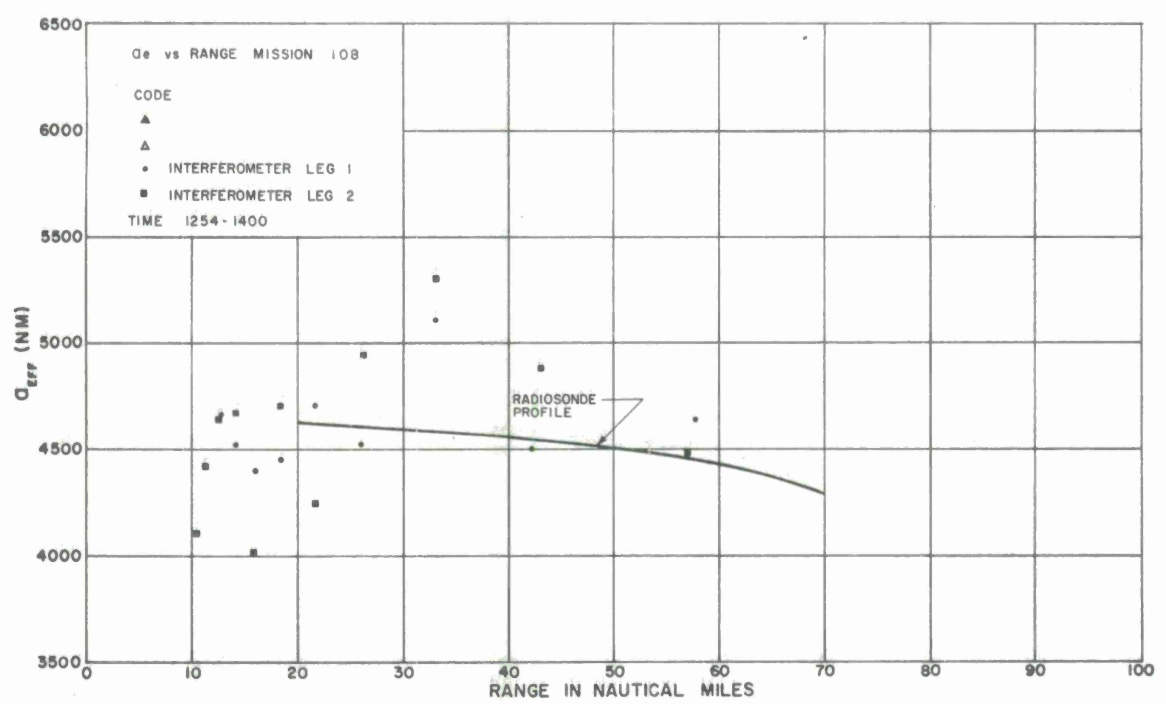
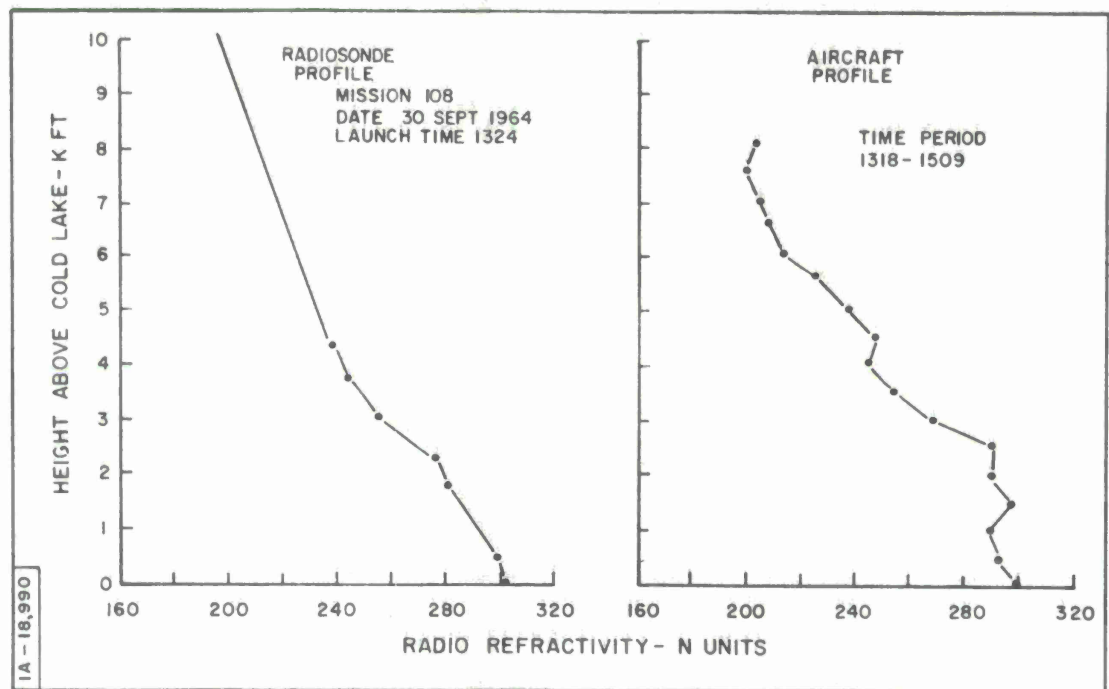
The aircraft refractivity profile shows a much stronger surface gradient than was observed with the radiosonde or could be implied from the interferometer results. Legs 1 and 2 of the interferometer data show large variations; however, this portion of the test was carried out with the transmitter at only 4300 feet, and, for reasons discussed previously, this can compromise the experimental accuracy. However, from 30 n. m. (the minimum useful range) to the radio horizon, the apparent path bending is decreasing very rapidly on the average. The ray-tracing results using the radiosonde profile also indicate that the bending is decreasing. This effect is seen directly from the radiosonde profile where the refractivity gradient below the transmitter height (4300 feet) decreases towards the surface. The experimental accuracy using the interferometer technique at ranges below 30 n. m. might account for the lack of agreement at these short ranges. Between 40 to 60 n. m. the maximum error between interferometer and ray-tracing results represents about 0.4 mr. , and at 58 n. m. about 0.3 mr. difference in the elevation angle error.

SIGNAL AMPLITUDE V/S RANGE  
 MISSION 108 LEG 1 DATE 5 SEP 64 TIME 1254-1320  
 BAND L FREQUENCY 1280 Mc/s POLARIZATION HORIZ  $\lambda$  7125 ft  $h_1$  59.95 ft  $h_2$  4300 ft



SIGNAL AMPLITUDE V/S RANGE  
 MISSION 108 LEG 2 DATE 5 SEP 64 TIME 1322-1400  
 BAND L FREQUENCY 1280 Mc/s POLARIZATION HORIZ  $\lambda$  7125 ft  $h_1$  59.95 ft  $h_2$  4300 ft





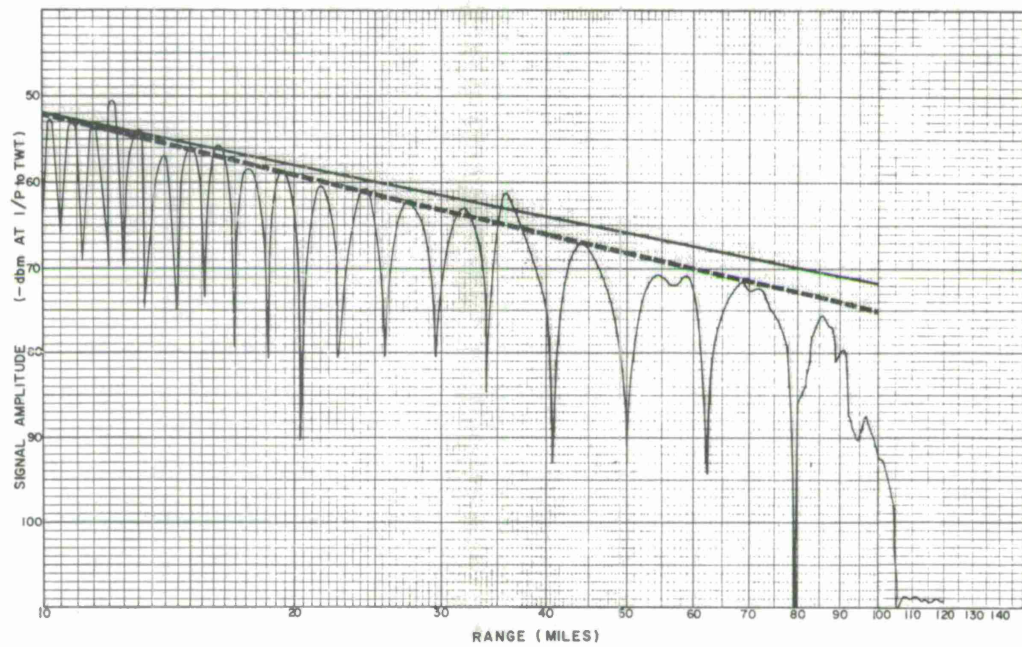
Mission 108 (Continued)

Time: 1422-1653, 30 September 1964

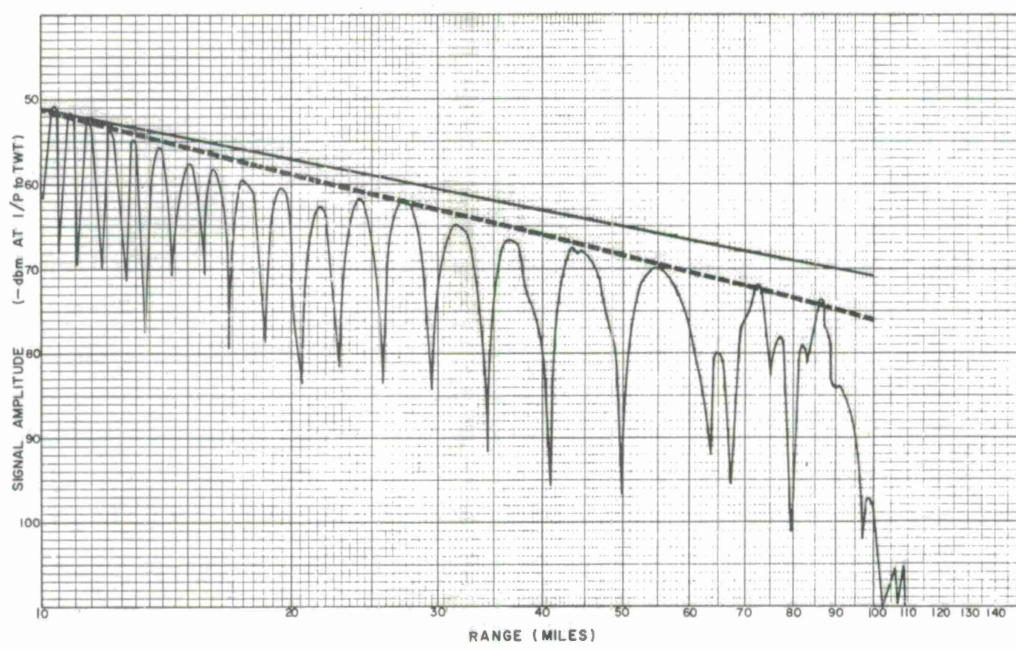
Legs 3, 4, 5, 6

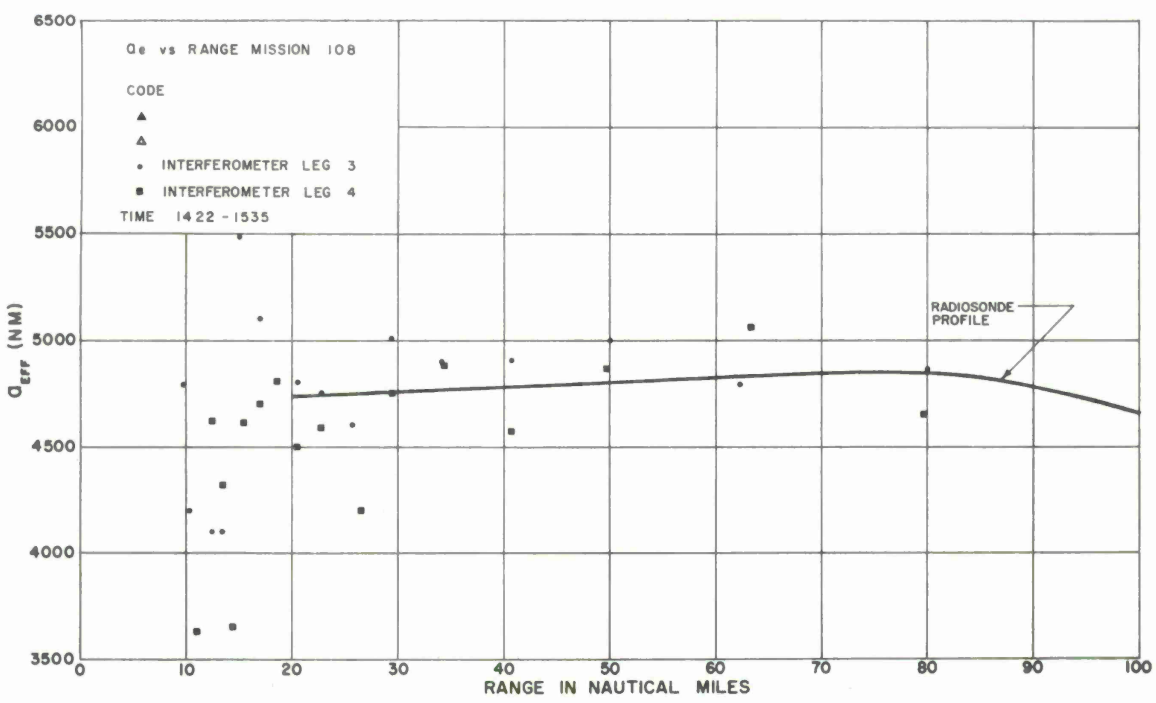
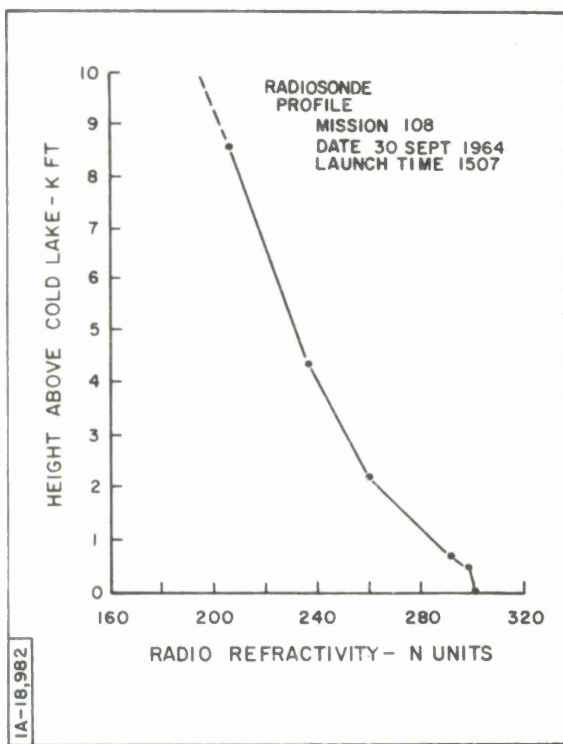
For legs 3 through 6, the transmitter height was increased to 7000 feet. Only one radiosonde profile was available during this period; however, from the interferometer calculations it appears that the stability of the atmosphere was reasonably good. From the radiosonde profile it may be deduced that the amount of bending should generally increase with range until the rays are propagated at very low elevation angles, in which case, the bending should decrease due to the decrease in the refractivity gradient near the surface. Beyond 40 n. m. range the interferometer data generally follows this pattern with an initial increase in bending to be followed eventually by a decrease as the radio horizon is approached. The ray-tracing results using the radiosonde profile also follow this pattern, although the break point is very close to the radio horizon. At 40 n. m. range the maximum error between interferometer and radiosonde results is about 0.2 mr., and at 80 n. m. is about 0.4 mr. difference in the elevation angle error.

SIGNAL AMPLITUDE V/S RANGE  
 MISSION. 108 LEG. 3 DATE. 5 SEP 64 TIME 1422 - 1453  
 BAND. L FREQUENCY. 1280 Mc/s POLARIZATION. HORIZ  $\lambda$  7125 ft  $h_1$  59.95 ft  $h_2$  7000 ft

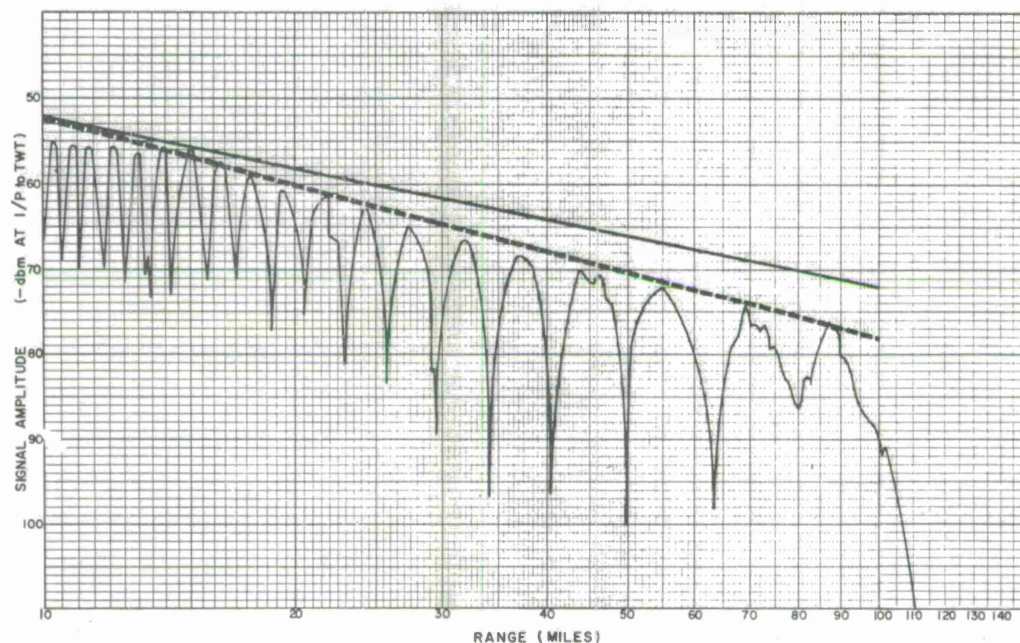


SIGNAL AMPLITUDE V/S RANGE  
 MISSION. 108 LEG. 4 DATE. 5 SEP 64 TIME 1458 - 1535  
 BAND. L FREQUENCY. 1280 Mc/s POLARIZATION. HORIZ  $\lambda$  7125 ft  $h_1$  59.95 ft  $h_2$  7000 ft

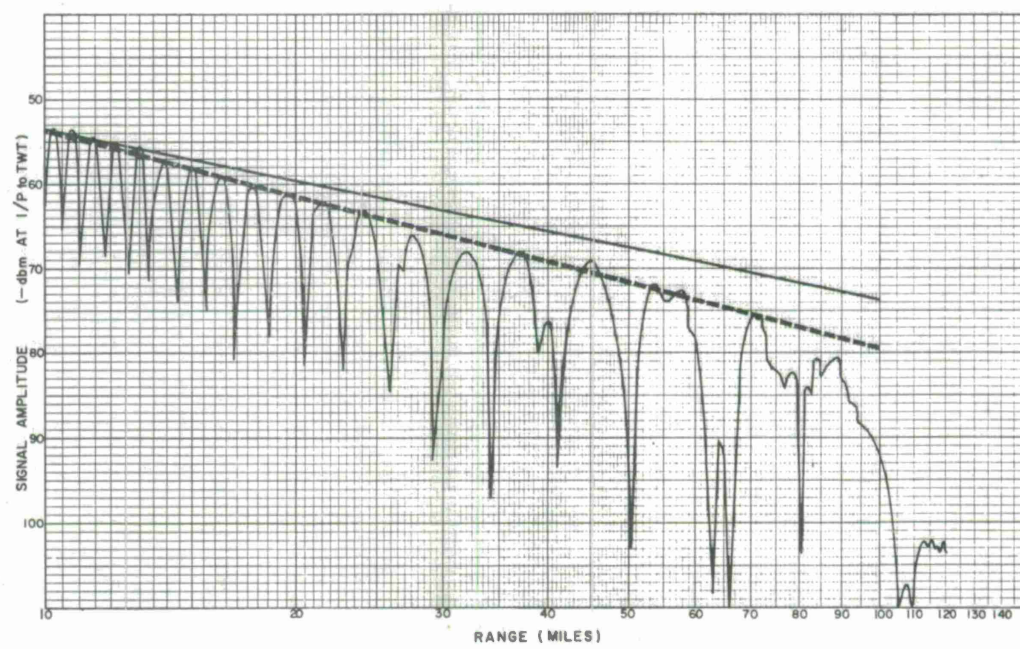


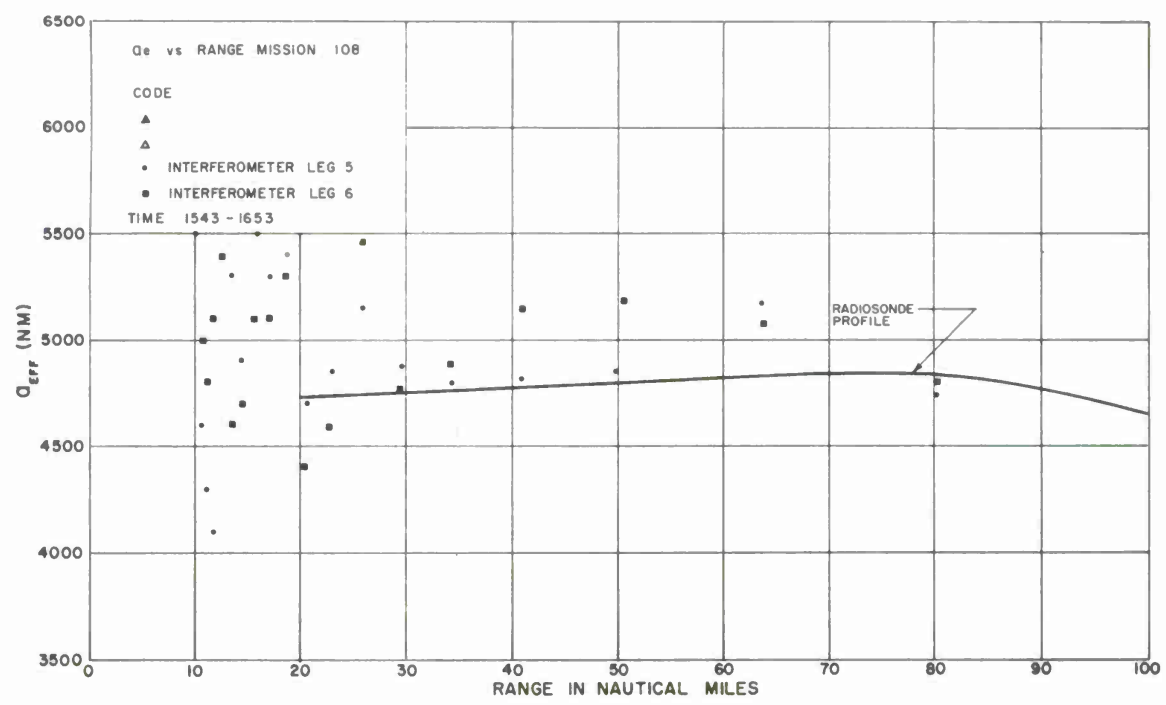
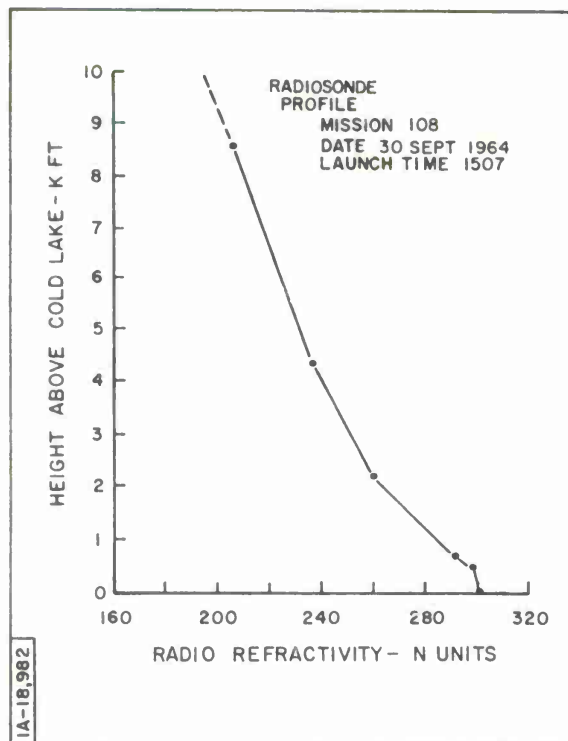


SIGNAL AMPLITUDE V/S RANGE  
MISSION 108 LEG 5 DATE 5 SEP 64 TIME 1543-1615  
BAND 1 FREQUENCY 1380 Mc/s POLARIZATION HORIZ  $\lambda$  7125 ft  $h_1$  59.95 ft  $h_2$  7000 ft



SIGNAL AMPLITUDE V/S RANGE  
MISSION 108 LEG 6 DATE 5 SEP 64 TIME 1618-1653  
BAND 1 FREQUENCY 1280 Mc/s POLARIZATION HORIZ  $\lambda$  7125 ft  $h_1$  59.95 ft  $h_2$  7000 ft





### Summary of Mission 108

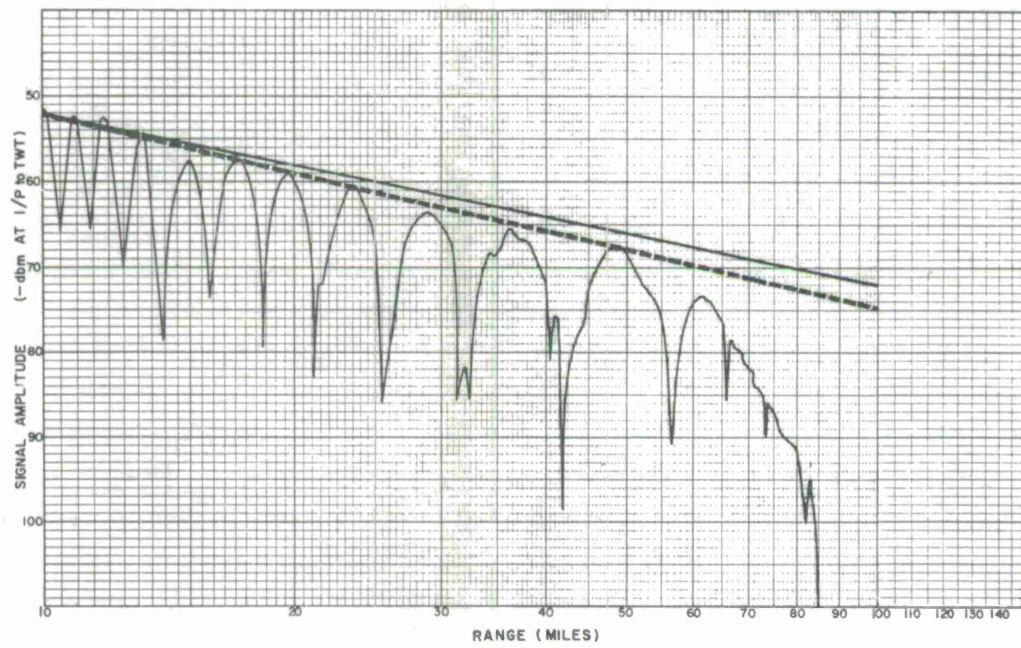
As previously observed, the correlation of results is much better when the transmitter is positioned at the higher altitudes. Also in comparison with previous missions, atmospheric conditions are much more stable during the late afternoon and evening test period.

MISSION 109 - Late Afternoon  
Time: 1606-1941, 1 October 1964  
Legs 1, 2, 3, 4, 5, 6

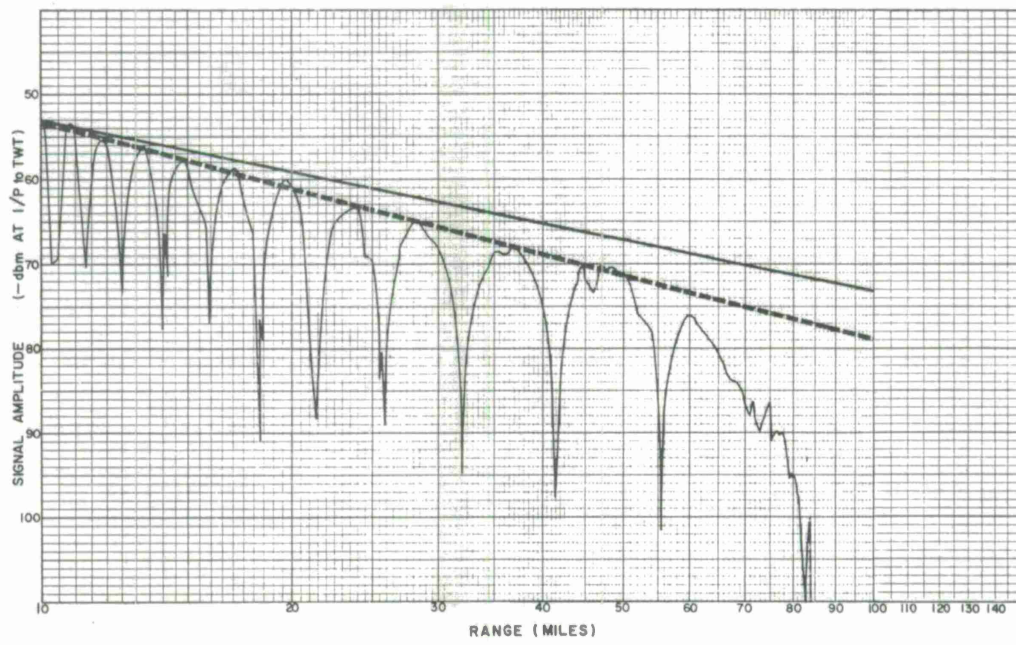
The radiosonde profiles for all legs flown during this mission are essentially linear. The aircraft measurements, however, indicate deviations and surface conditions which were not observed on any of the interferometer results during the mission. The interferometer data obtained for legs 1 and 2 are more scattered due to the lower transmitter height. However, an examination of the data for all six legs indicates that  $A_e$  values calculated both by ray-tracing and interferometer techniques show an essentially constant  $A_e$  with range, in good agreement with the radiosonde profile. In the latter four legs, a very slight increase in the surface gradient causes the ray tracing results to increase with range; however, this increase is very slight.

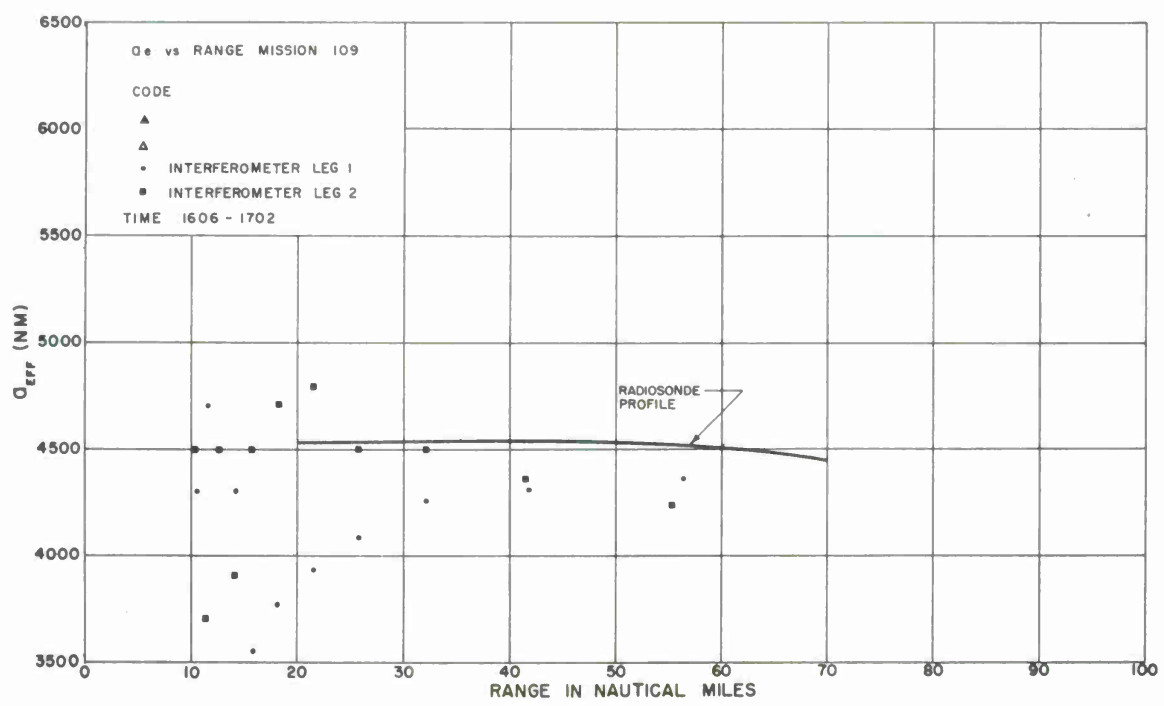
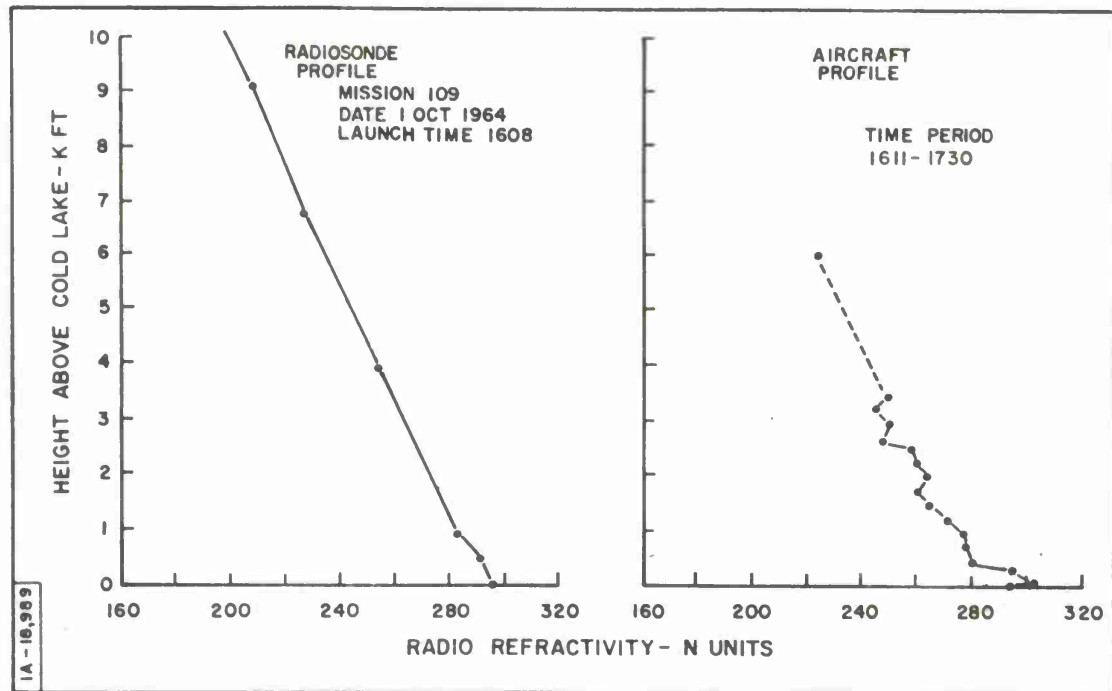
At 40 n. m., the maximum error between interferometer and ray-tracing results represents about 0.2 mr., and at 60 n. m., about 0.3 mr. difference in the elevation angle error.

SIGNAL AMPLITUDE V/S RANGE  
 MISSION. 109 LEG. 1 DATE. 1 OCT 64 TIME. 1606-1632  
 BAND. L FREQUENCY. 1380 Mc/s POLARIZATION. HORIZ  $\lambda$  7125 ft  $h_1$  59.95 ft  $h_2$  4300 ft

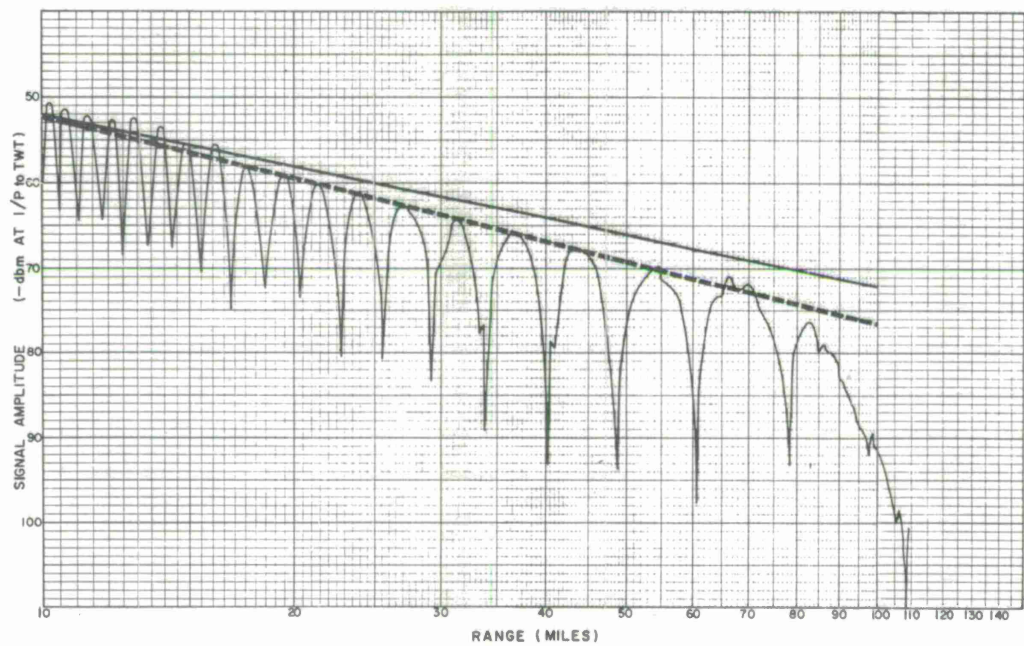


SIGNAL AMPLITUDE V/S RANGE  
 MISSION. 109 LEG. 2 DATE. 1 OCT 64 TIME. 1634 - 1702  
 BAND. L FREQUENCY. 1380 Mc/s POLARIZATION. HORIZ  $\lambda$  7125 ft  $h_1$  59.95 ft  $h_2$  4300 ft

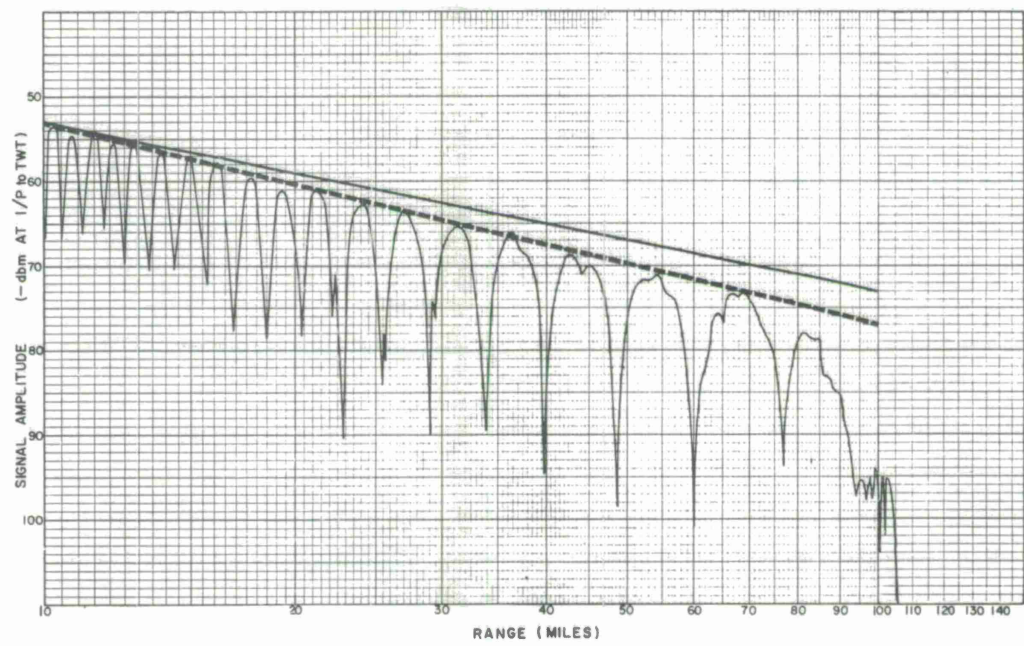


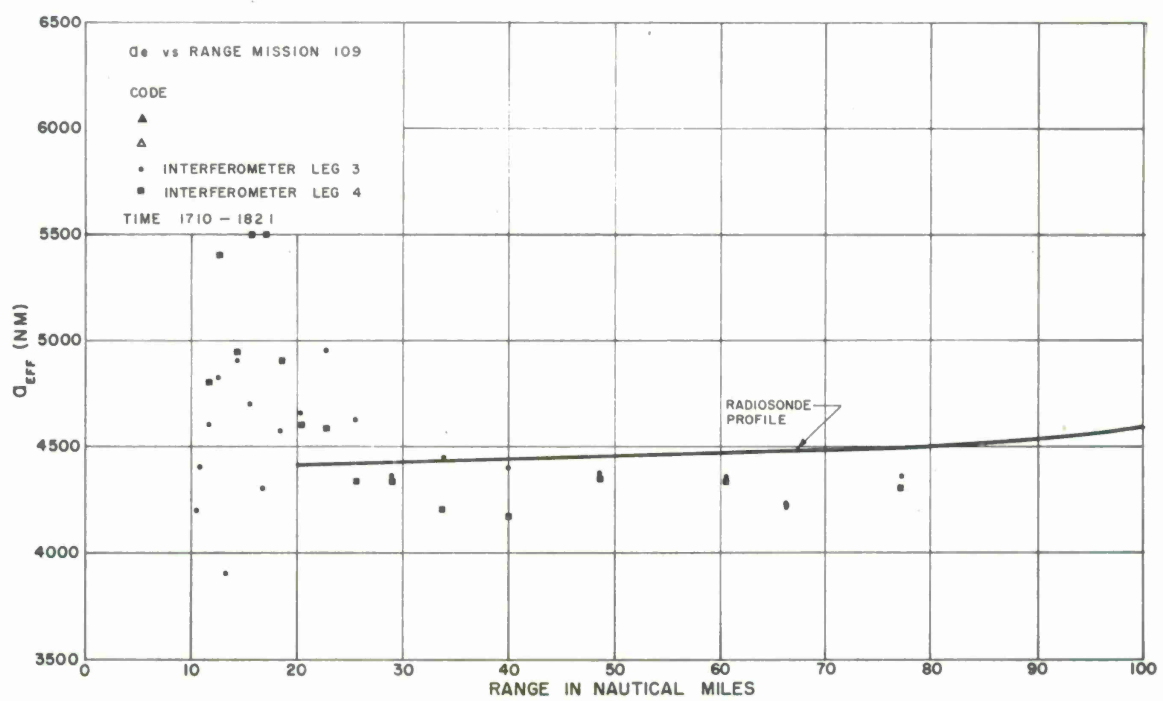
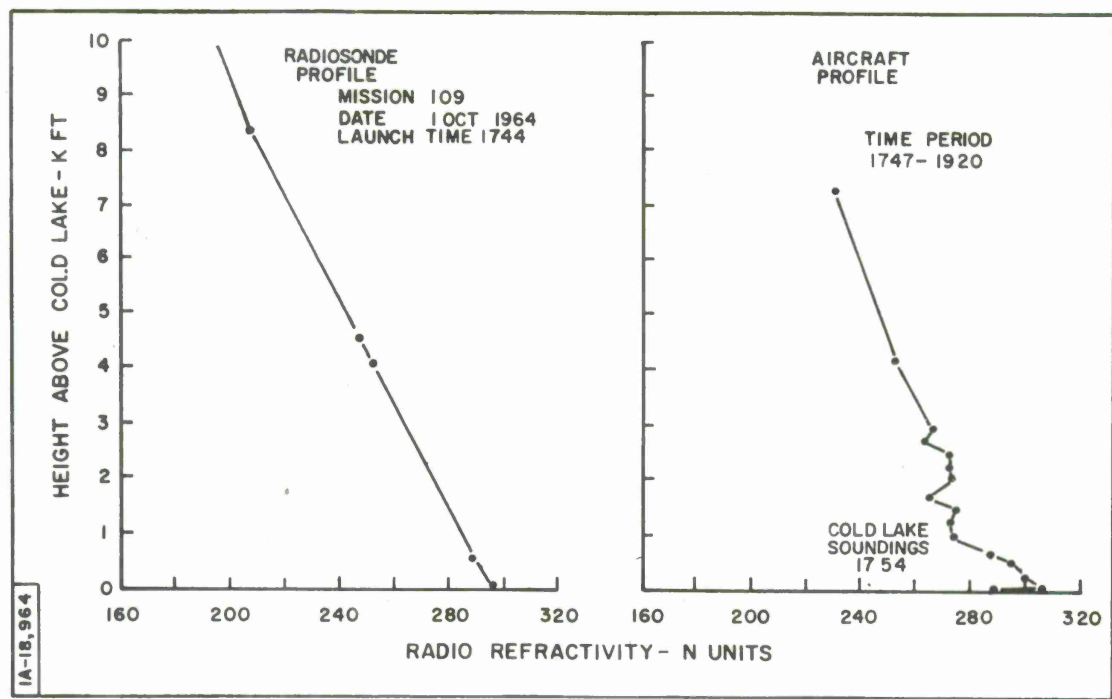


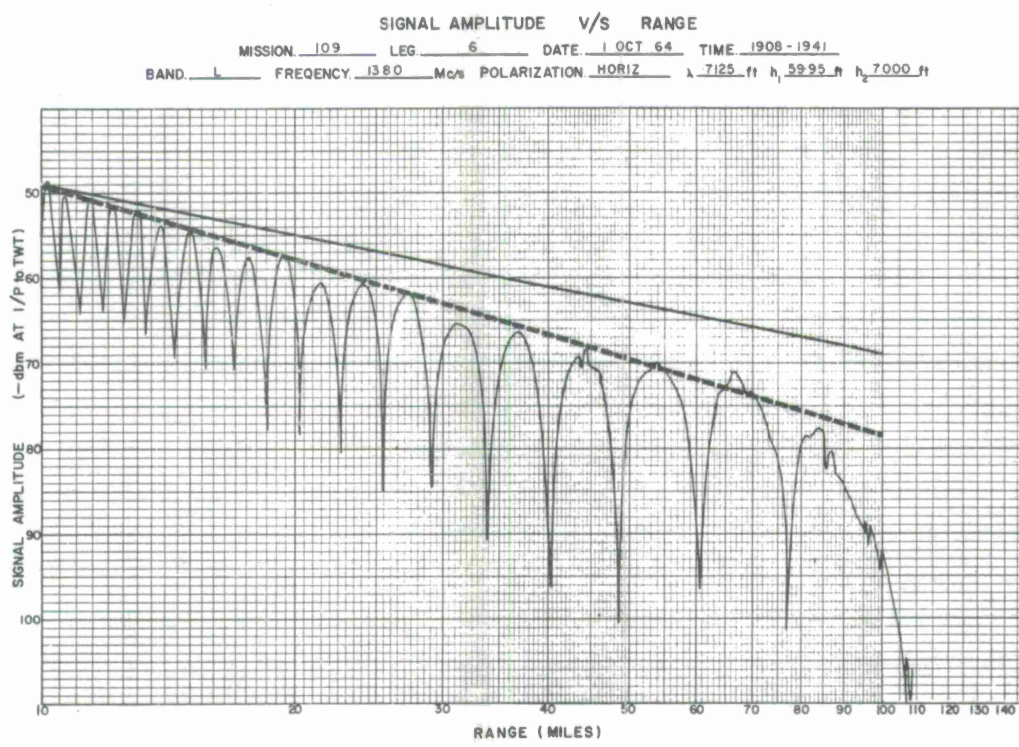
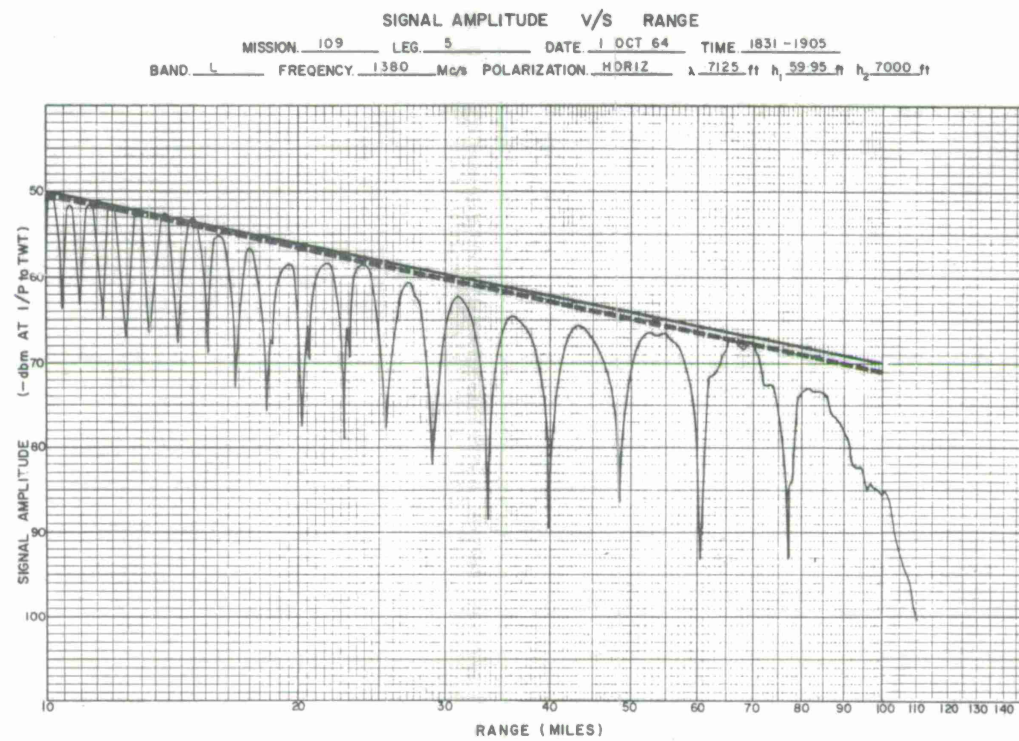
SIGNAL AMPLITUDE V/S RANGE  
 MISSION. 109 LEG. 3 DATE. 1 OCT 64 TIME. 1710 - 1744  
 BAND. L FREQUENCY. 1380 Mcs POLARIZATION. HORIZ  $\lambda$ . 7125 ft  $h_1$ . 59.95 ft  $h_2$ . 7000 ft

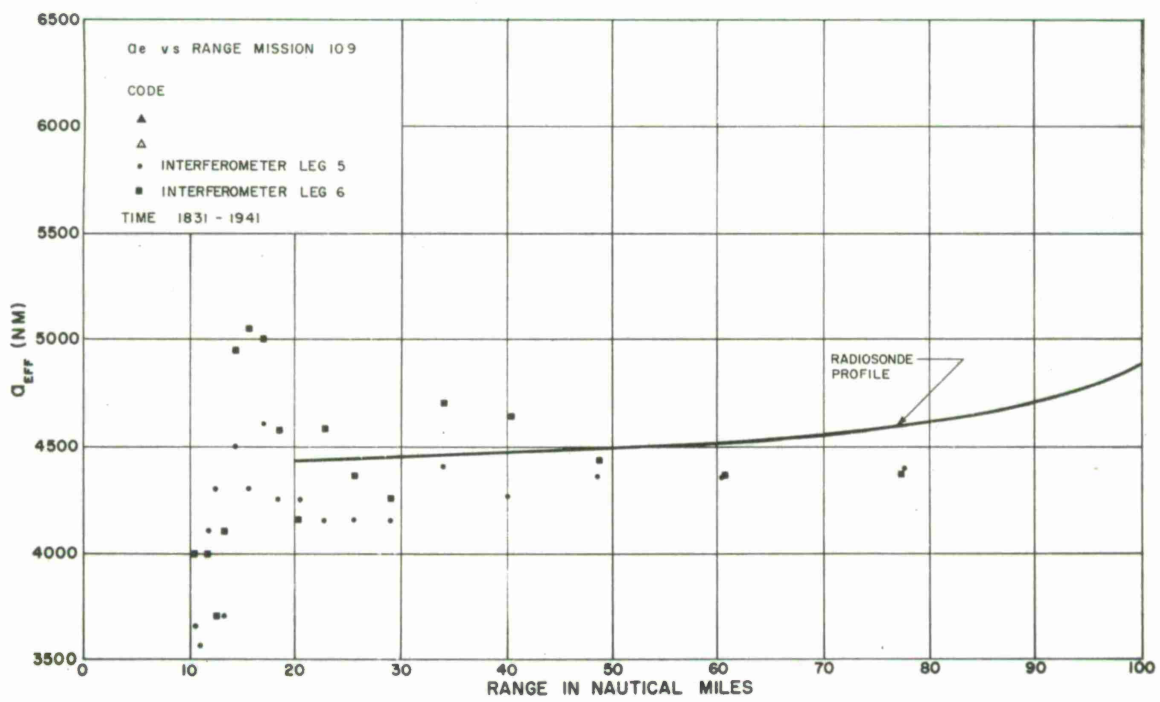
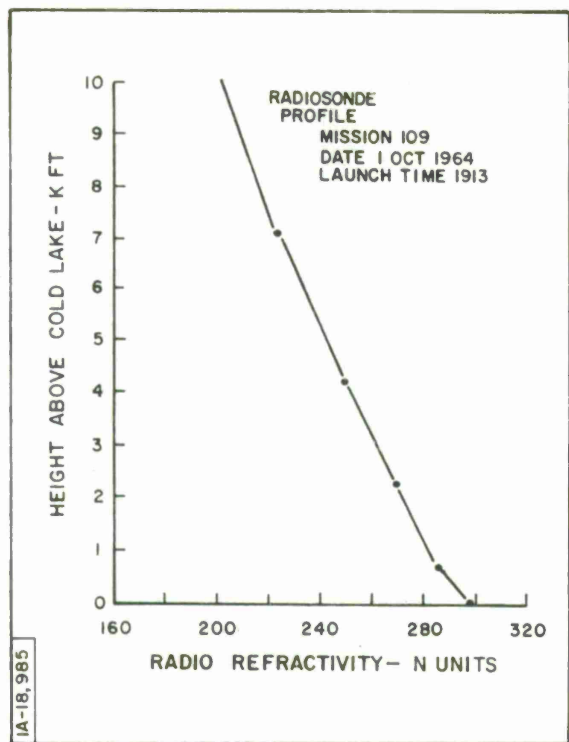


SIGNAL AMPLITUDE V/S RANGE  
 MISSION. 109 LEG. 4 DATE. 1 OCT 64 TIME. 1746 - 1821  
 BAND. L FREQUENCY. 1380 Mcs POLARIZATION. HORIZ  $\lambda$ . 7125 ft  $h_1$ . 59.95 ft  $h_2$ . 7000 ft









MISSION 110 - Dawn

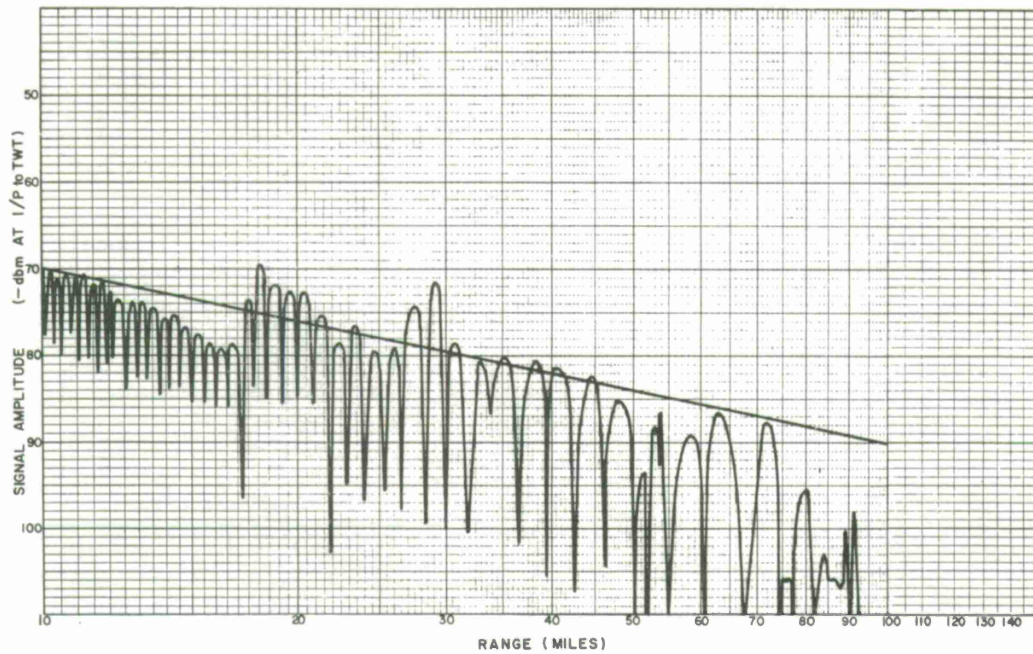
Time: 0402-0511, 5 October 1964

Legs 1, 2

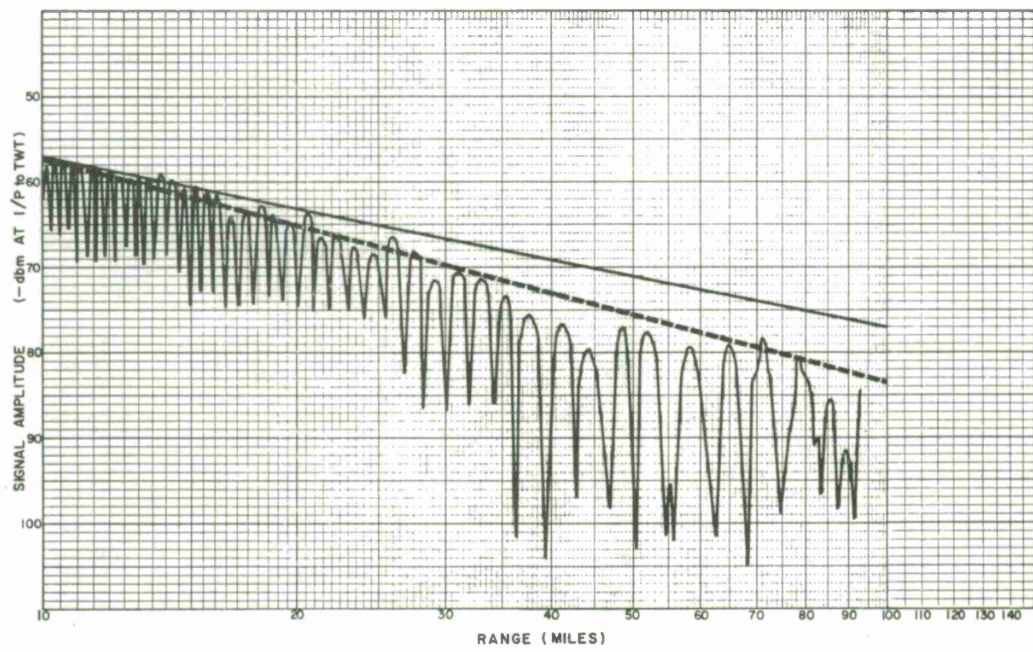
No aircraft or surface refractivity data were available during this mission; therefore, the refractivity structure was obtained solely from radiosonde launches together with estimates of surface conditions.

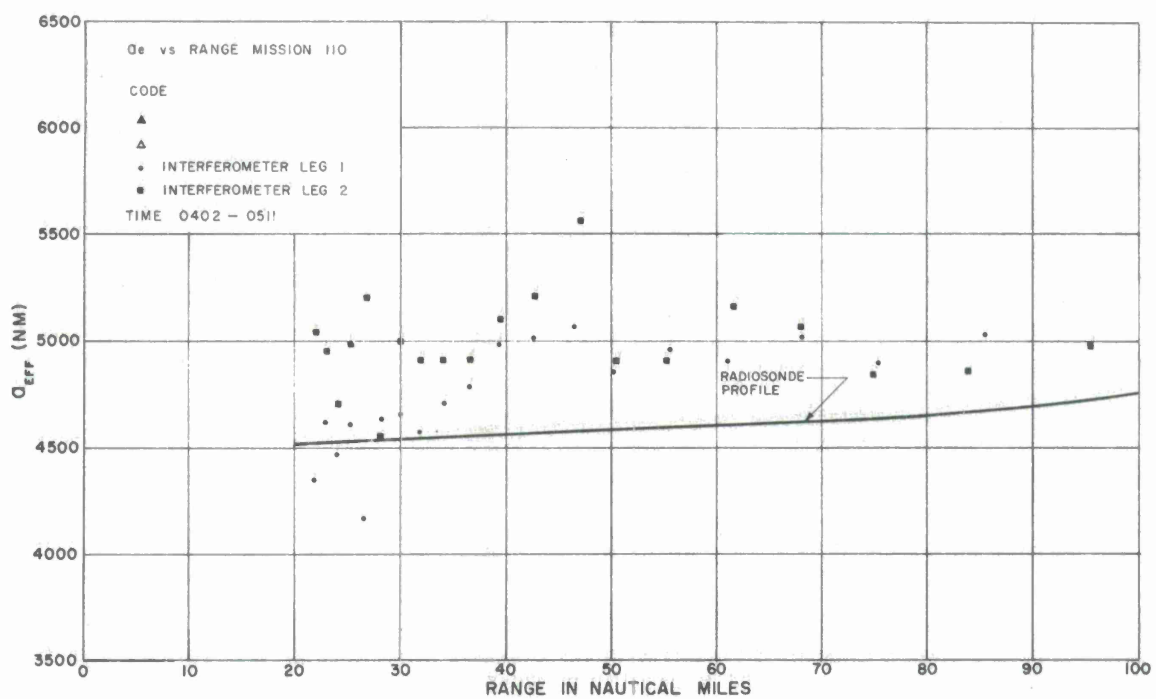
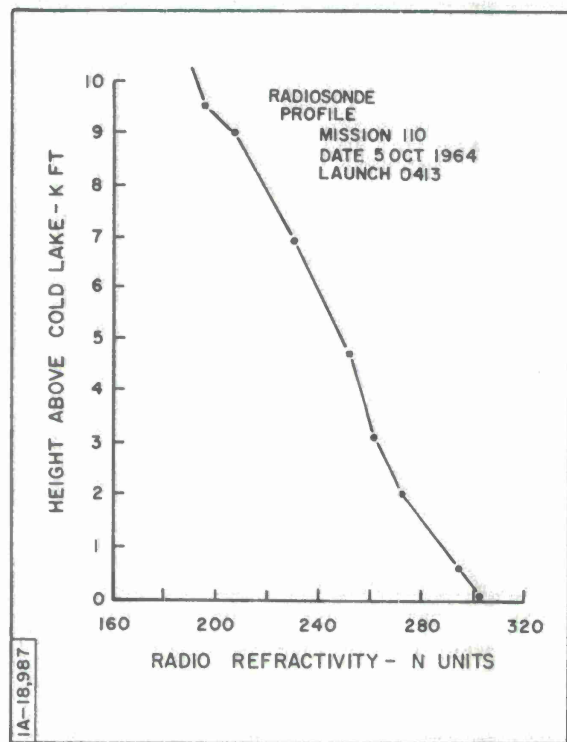
The interferometer data shows almost constant  $A_e$  values of 5000 n. m. for transmitter ranges beyond 50 n. m. With the exception of a perturbation of the data obtained during leg 2 between 40 to 50 n. m. , the interferometer results seem to depict propagation conditions representative of a linear refractivity profile. The difference between interferometer and ray-tracing results is partly due to the lack of accurate surface information; however, again the question arises as to the validity of the radiosonde data where temporal and spatial variations may be taking place in the early morning hours.

SIGNAL AMPLITUDE V/S RANGE  
 MISSION 110 LEG 1 DATE 5 OCT 64 TIME 0402 - 0434  
 BAND S FREQUENCY 3330 Mc/s POLARIZATION HORIZ  $\lambda$  .2947 ft  $h_1$  59.53 ft  $h_2$  7000 ft



SIGNAL AMPLITUDE V/S RANGE  
 MISSION 110 LEG 2 DATE 5 OCT 64 TIME 0439 - 0511  
 BAND S FREQUENCY 3336 Mc/s POLARIZATION HORIZ  $\lambda$  .2947 ft  $h_1$  59.53 ft  $h_2$  7000 ft





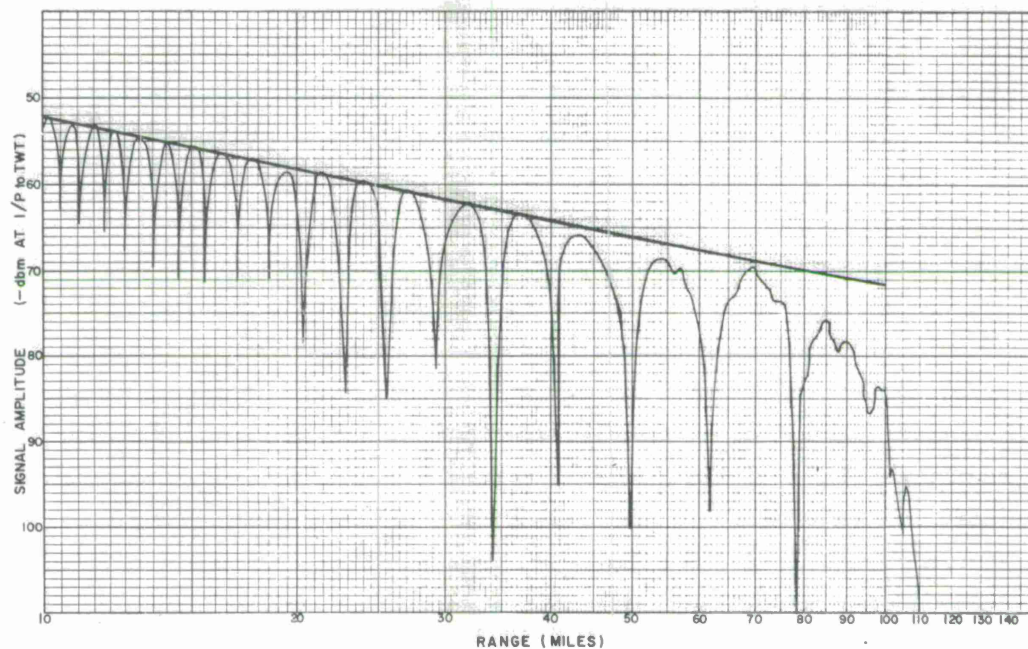
Mission 110 (Continued)

Time: 0524-0634, 5 October 1964

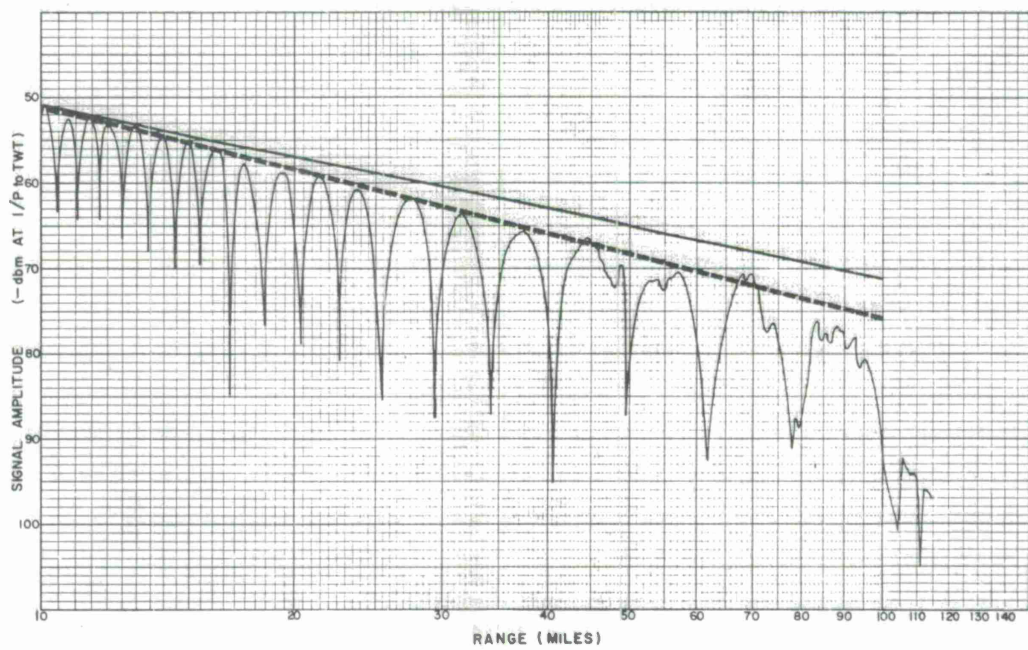
Legs 3, 4

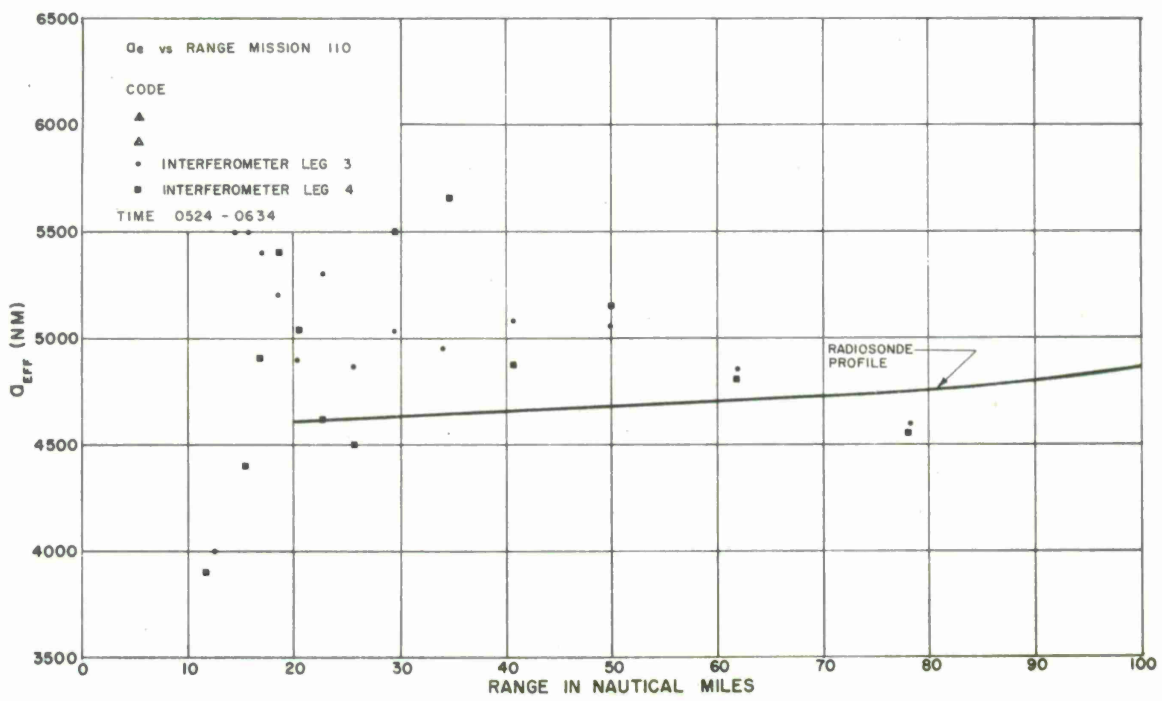
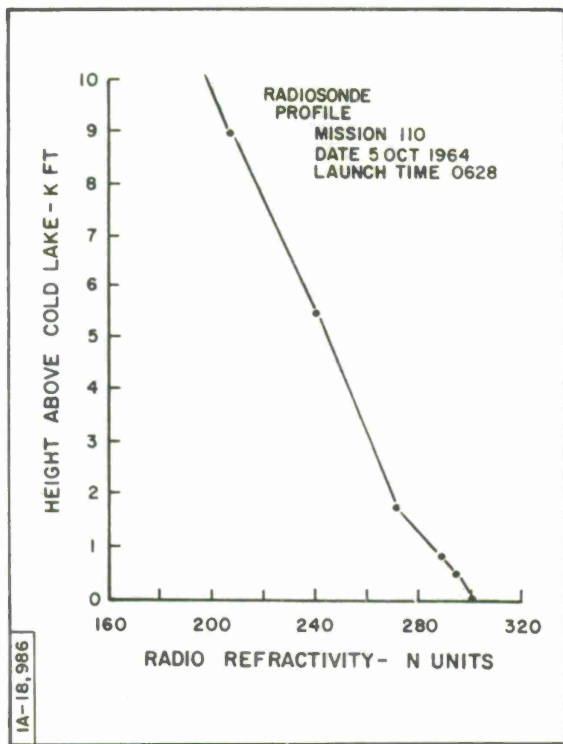
The radiosonde indicates that the refractivity profile is increasing slightly below 1300 feet; however, the interferometer data, although it does indicate some increase in bending at medium ranges, presents a significantly different picture. The rapid reduction in  $A_e$  magnitudes with range beyond 50 n. m. certainly indicates substandard refractivity conditions near the surface. It should be noted that this test period is at sunrise, and the fog layer normally present over the lake surface begins to dissipate and also ascend as the surface heating increases. This effect would tend to reduce the surface gradient and might very well be the reason for the reduced bending at longer ranges. A comparison of ray-tracing and interferometer results is somewhat meaningless, since there were no direct surface measurements, and since the radiosonde launch site is located over land. The consistent agreement between interferometer results at the low elevation angles is again further reason to believe that this technique was in fact observing the substandard conditions suggested above.

SIGNAL AMPLITUDE V/S RANGE  
 MISSION 110 LEG 3 DATE 5 OCT 64 TIME 0524-0559  
 BAND L FREQUENCY 1280 Mc/s POLARIZATION HORIZ  $\lambda$  7125 ft  $h_1$  59.95 ft  $h_2$  7000 ft



SIGNAL AMPLITUDE V/S RANGE  
 MISSION 110 LEG 4 DATE 5 NOV 64 TIME 0603-0634  
 BAND L FREQUENCY 1280 Mc/s POLARIZATION HORIZ  $\lambda$  7125 ft  $h_1$  59.95 ft  $h_2$  7000 ft





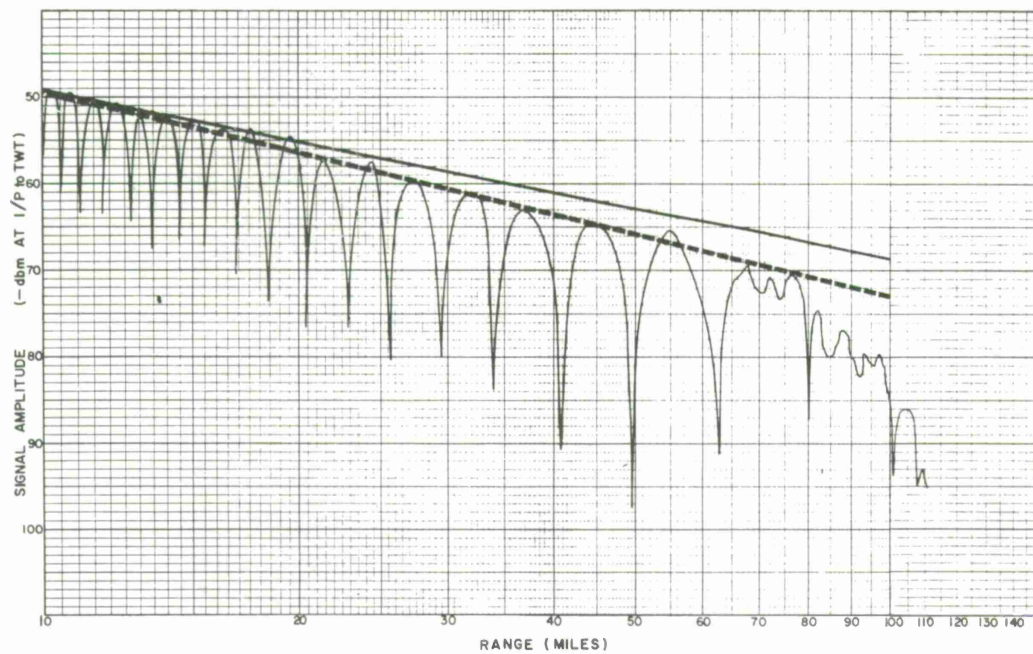
MISSION 110 (Continued)

Time: 0642-0753, 5 October 1964

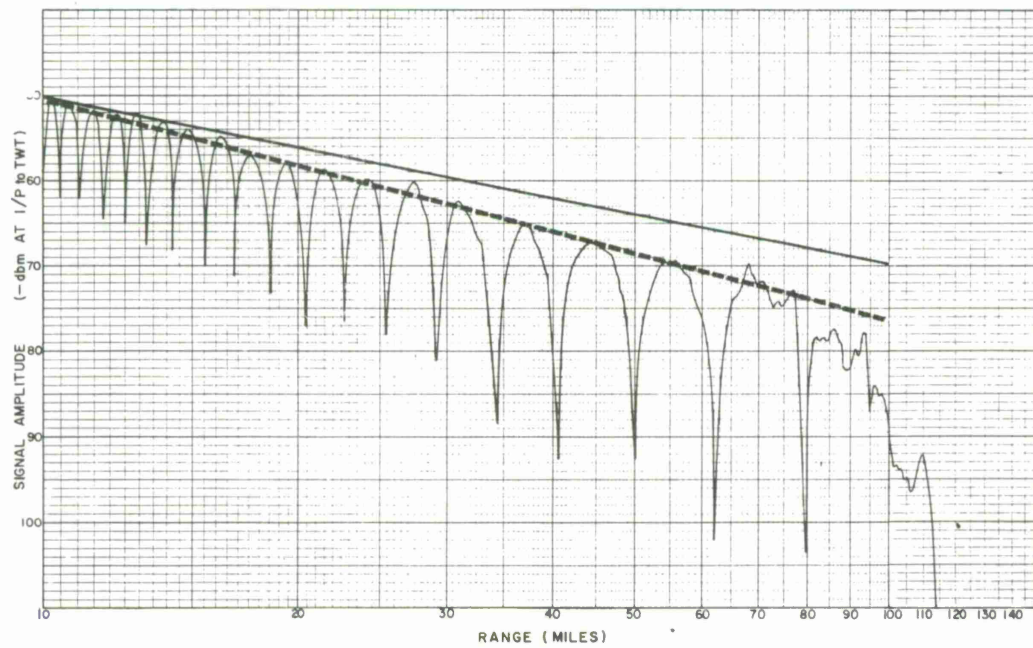
Legs 5, 6

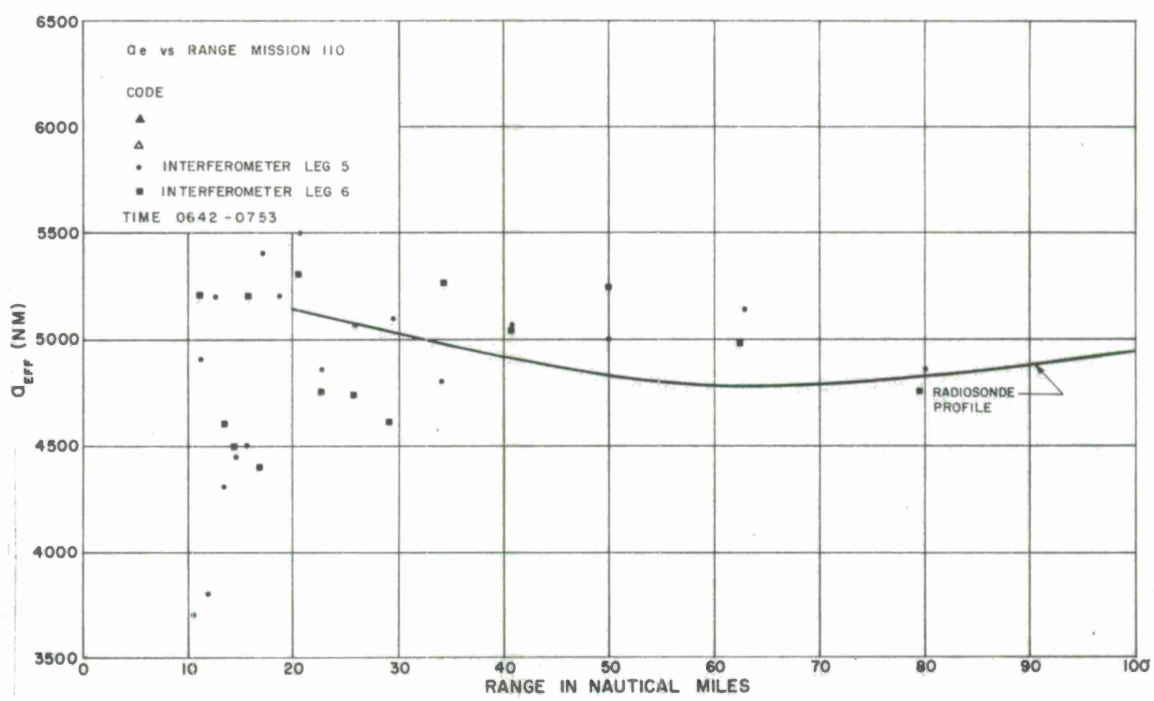
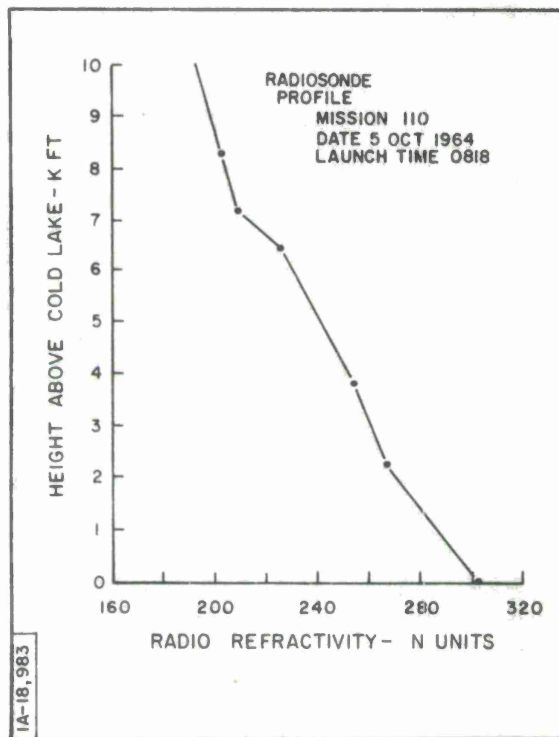
As previously discussed, the substandard conditions still appear to be present. The ray-tracing results are of little significance at the long ranges due to the overland position of the radiosonde launch site and the lack of surface measurements on Cold Lake.

SIGNAL AMPLITUDE V/S RANGE  
 MISSION 110 LEG 5 DATE 5 NOV 64 TIME 0642-0718  
 BAND L FREQUENCY 1280 Mc/s POLARIZATION HORIZ  $\lambda$  7125 ft  $h_1$  59.95 ft  $h_2$  7000 ft



SIGNAL AMPLITUDE V/S RANGE  
 MISSION 110 LEG 6 DATE 5 NOV 64 TIME 0720 - 0753  
 BAND L FREQUENCY 1380 Mc/s POLARIZATION HORIZ  $\lambda$  7125 ft  $h_1$  59.95 ft  $h_2$  7000 ft





### General Comments on Mission 110

This mission is particularly interesting because it spans the period of sunrise. Immediately following sunrise and under low wind conditions the surface becomes warmed, thereby increasing the amount of vertical air motion. This can have the combined effect of dissipating the mist but also increasing its overall thickness due to the upward ascent of air near the surface. This situation would produce substandard conditions near the surface, providing the surface wind speed was very low. During the mission, as distinct from other dawn missions which will be subsequently described, the wind velocity measured at the radiosonde launch site was very low. Therefore, the interferometer data, which tends to support those occurrences again brings up the apparent usefulness of this technique to investigate both propagation and meteorological conditions.

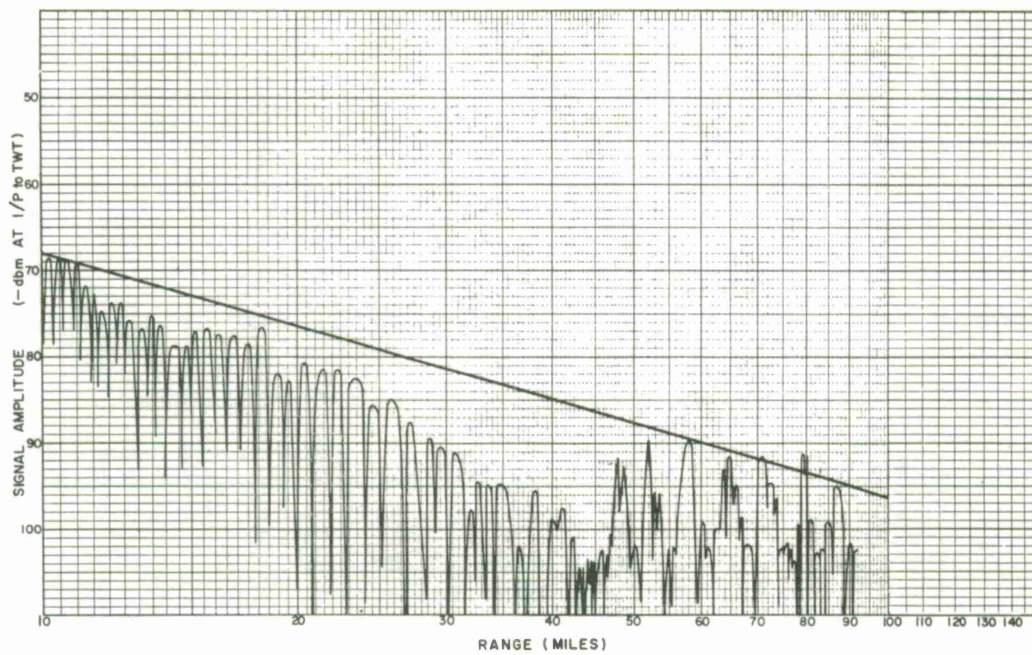
MISSION 111 - Dawn

Time: 0403-0514, 6 October 1964

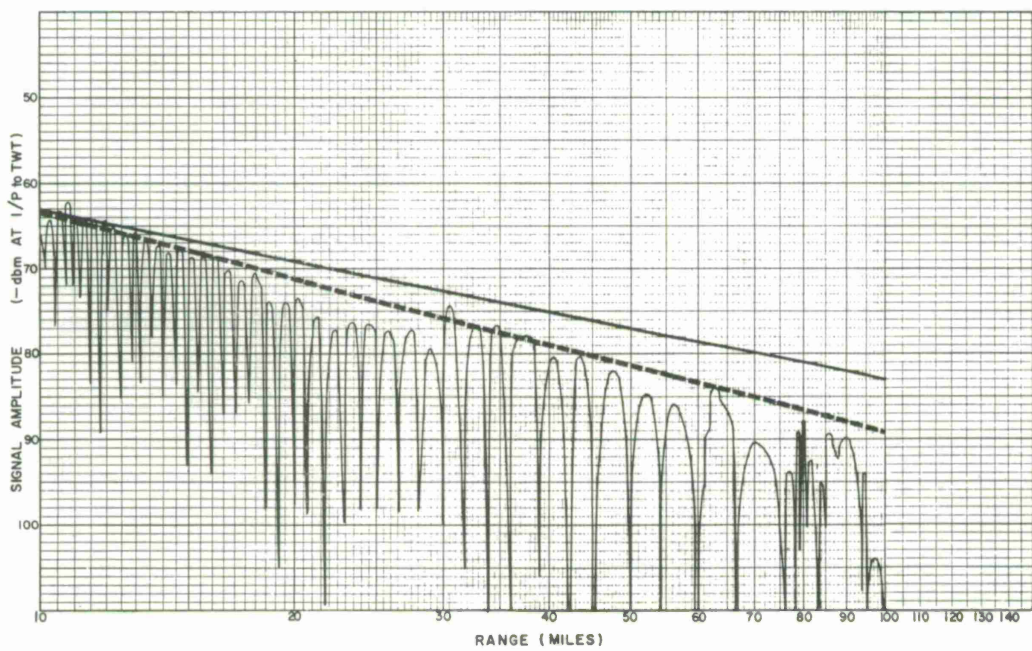
Legs 1, 2

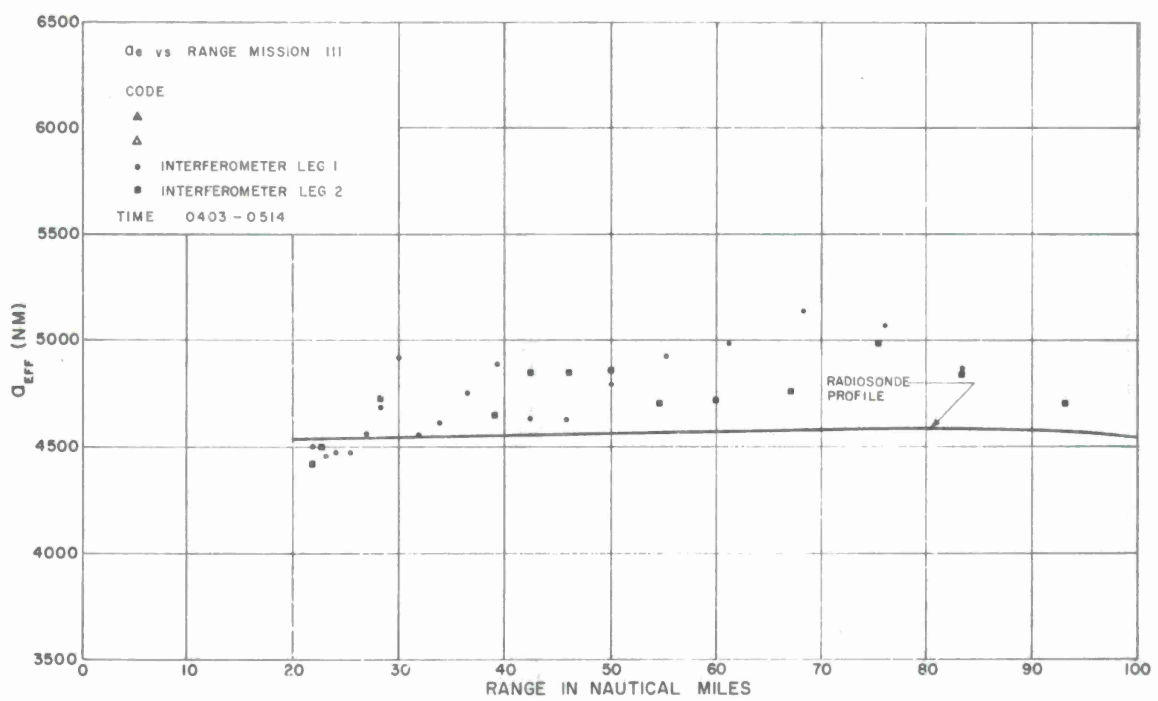
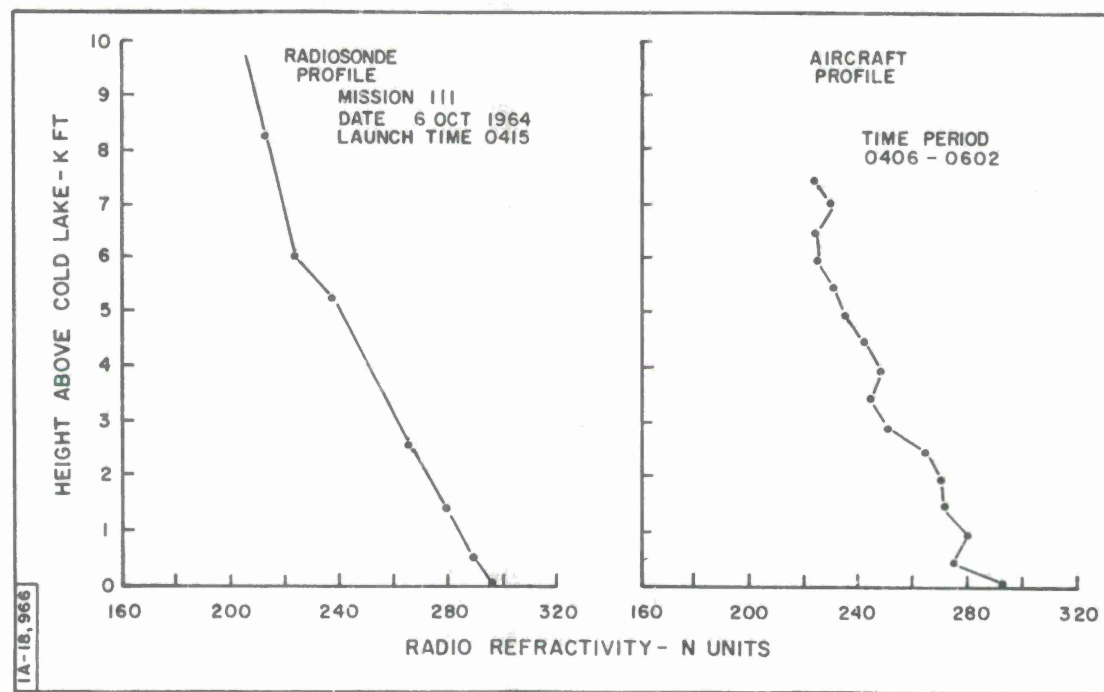
As in most previous cases, the aircraft meteorological measurements are of little value at the lower levels. From the linearity of the radiosonde profile the  $A_e$  values obtained by ray tracings would be expected to remain essentially constant, and in fact the results show this value to be about 4600 n.m. On the other hand, the interferometer results tend to show a subnormal condition near the surface. On the average, the  $A_e$  values are greater than the ray-tracing data, indicating that the overall refractivity gradient should be larger than that depicted by the radiosonde. With reference to the signal amplitude plot for leg 1, there appears to be some erratic behavior in the transmitter starting at 40 n.m. range and continuing through to the radio horizon. On the inbound leg 2 this difficulty is apparently cleared by the time the transmitter reaches 76 n.m. Because of this difficulty, the interferometer data points for leg 1 could be in error beyond 40 n.m. Therefore, comparing the differences between leg 2 interferometer data only and the radiosonde calculations gives a maximum error of 0.4 mr. at 40 and 60 n.m. and about 0.8 mr. at 80 n.m. in terms of the elevation angle error.

SIGNAL AMPLITUDE V/S RANGE  
 MISSION. III LEG. 1 DATE 6 OCT 64 TIME 0403-0432  
 BAND. S FREQUENCY 3336 Mc/s POLARIZATION HORIZ  $\lambda$  2947 ft  $h_1$  59.53 ft  $h_2$  7000 ft



SIGNAL AMPLITUDE V/S RANGE  
 MISSION. III LEG 2 DATE 6 OCT 64 TIME 0437-0514  
 BAND. S FREQUENCY 3336 Mc/s POLARIZATION HORIZ  $\lambda$  2947 ft  $h_1$  59.53 ft  $h_2$  7000 ft





Mission 111 (Continued)

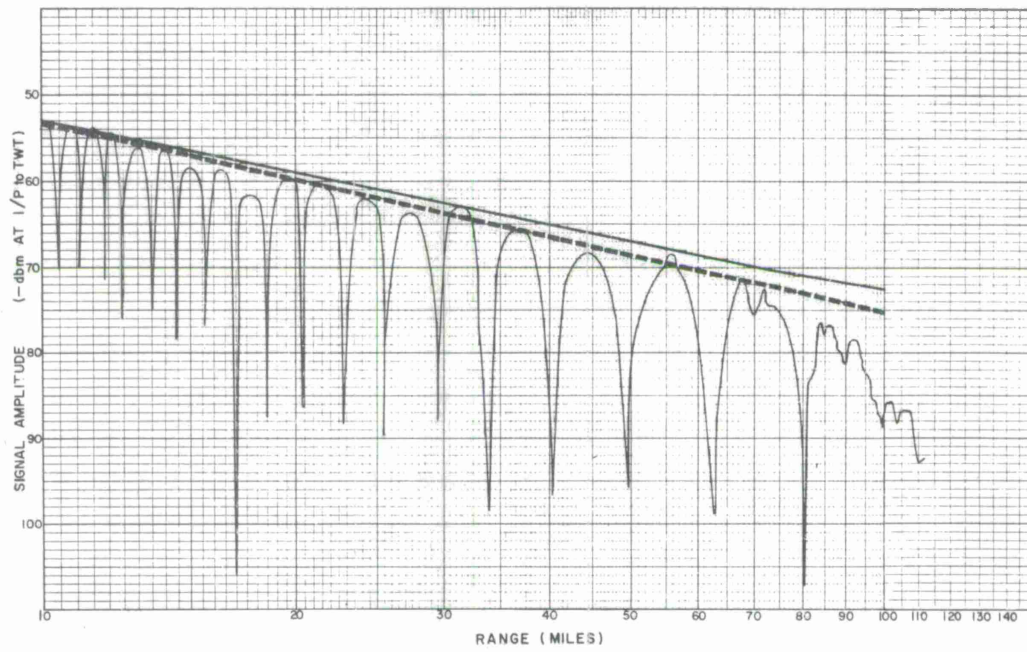
Time: 0531-0644, 6 October 1964

Legs 3, 4

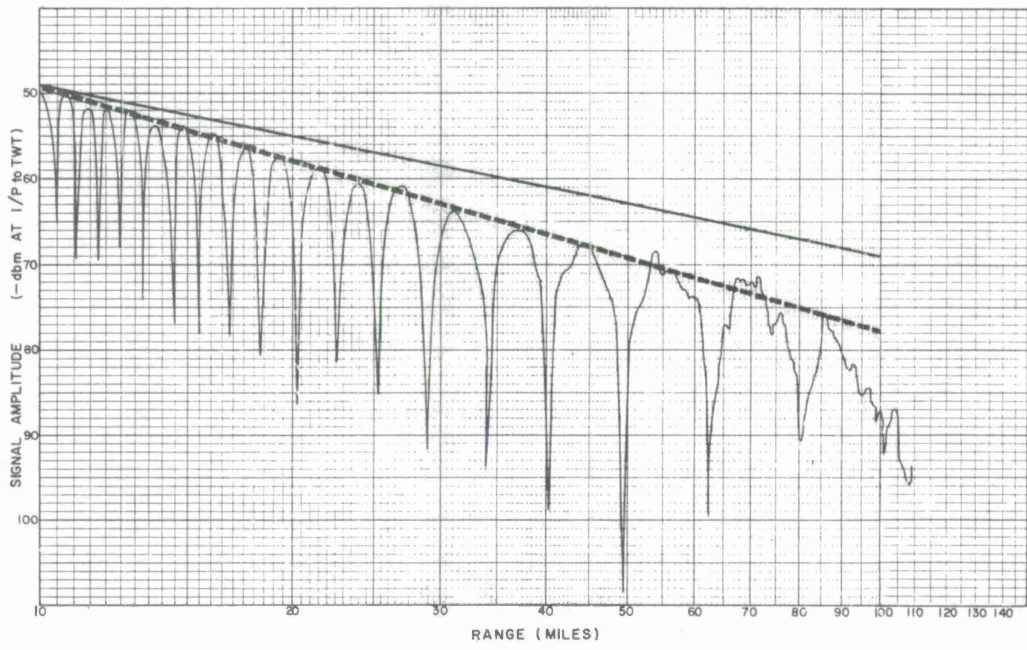
The aircraft refractivity profile again shows an abnormally large surface gradient, which is not in context with either the radiosonde or interferometer results. The interferometer data plots indicate that the bending was increasing with range, which suggests that the effect of a surface gradient is slightly larger than depicted by the radiosonde profile.

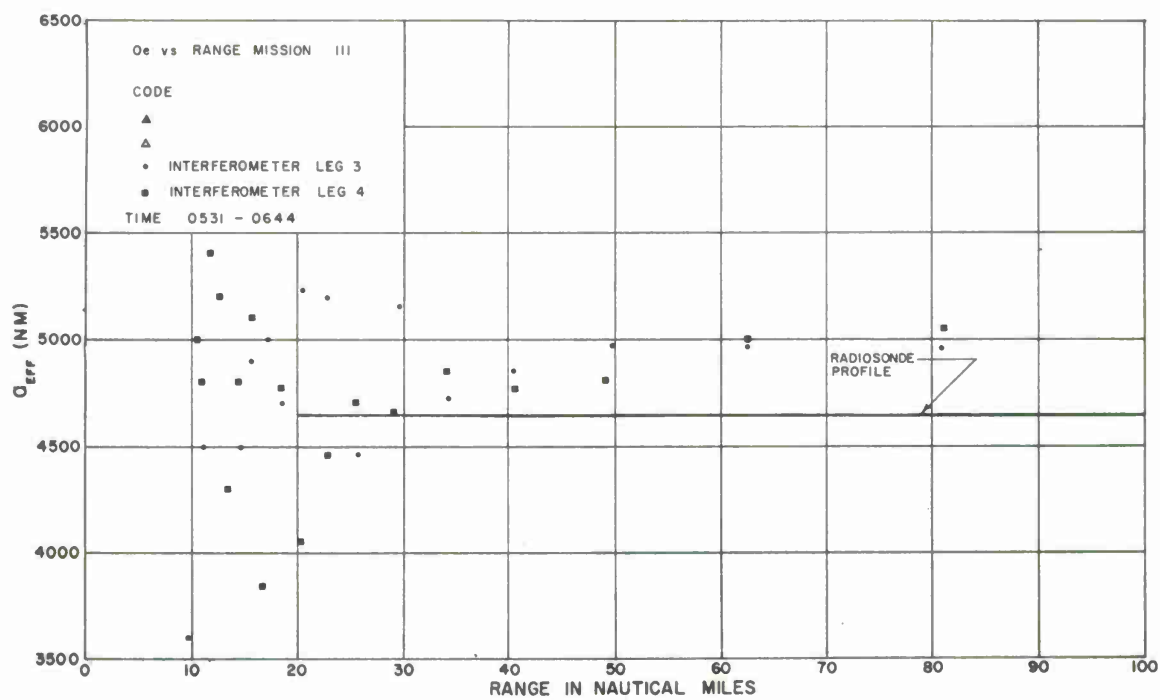
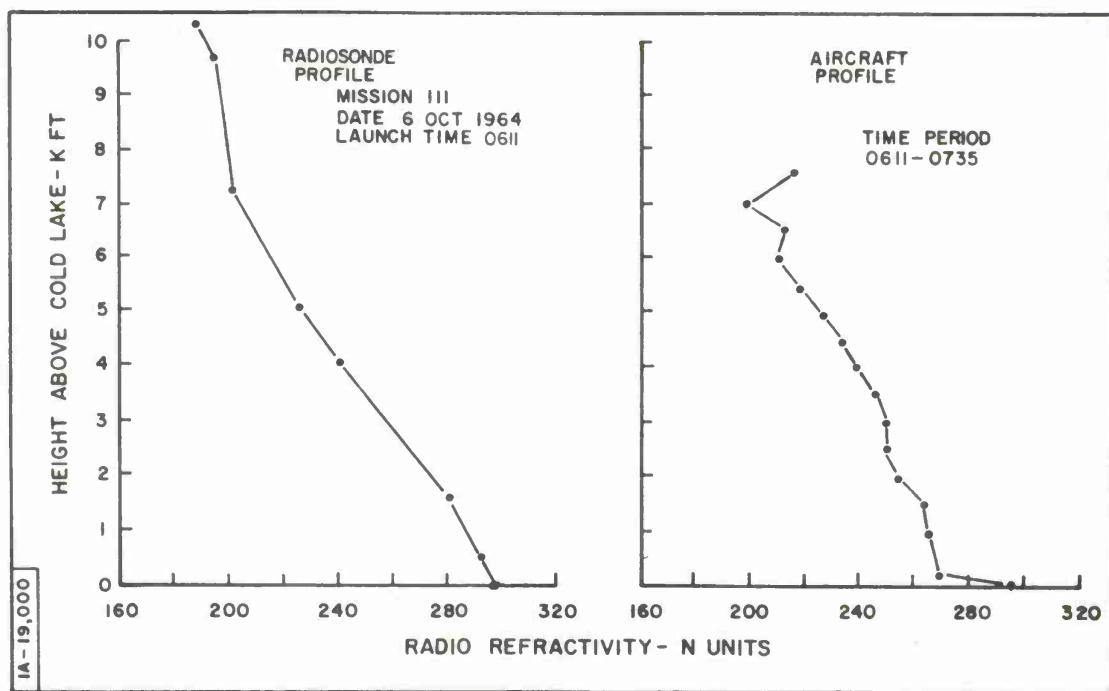
The maximum errors between interferometer and ray-tracing data represents 0.2 mr. at 30 n.m. and 0.8 mr. at 80 n.m. in terms of the initial elevation angle error.

SIGNAL AMPLITUDE V/S RANGE  
 MISSION III LEG 3 DATE 6 OCT 64 TIME 0531 - 0606  
 BAND L FREQUENCY 1380 Mc/s POLARIZATION HORIZ  $\lambda$  .7125 ft  $h_1$  .59.95 ft  $h_2$  2000 ft



SIGNAL AMPLITUDE V/S RANGE  
 MISSION III LEG 4 DATE 6 OCT 64 TIME 0609 - 0644  
 BAND L FREQUENCY 1380 Mc/s POLARIZATION HORIZ  $\lambda$  .7125 ft  $h_1$  .59.95 ft  $h_2$  2000 ft





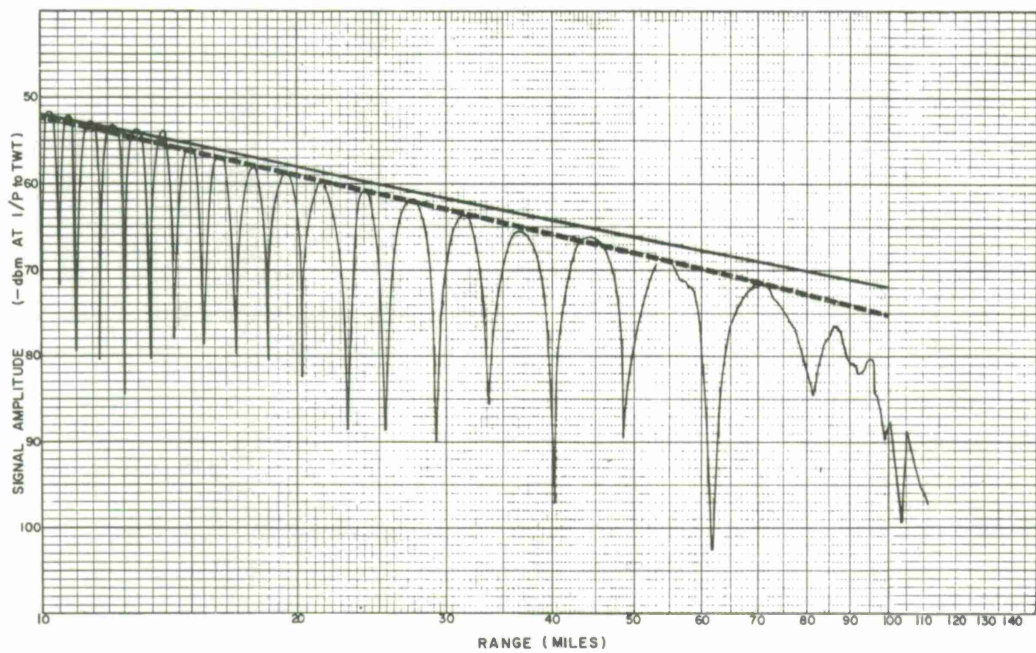
Mission 111 (Continued)

Time: 0652-0805, 6 October 1964

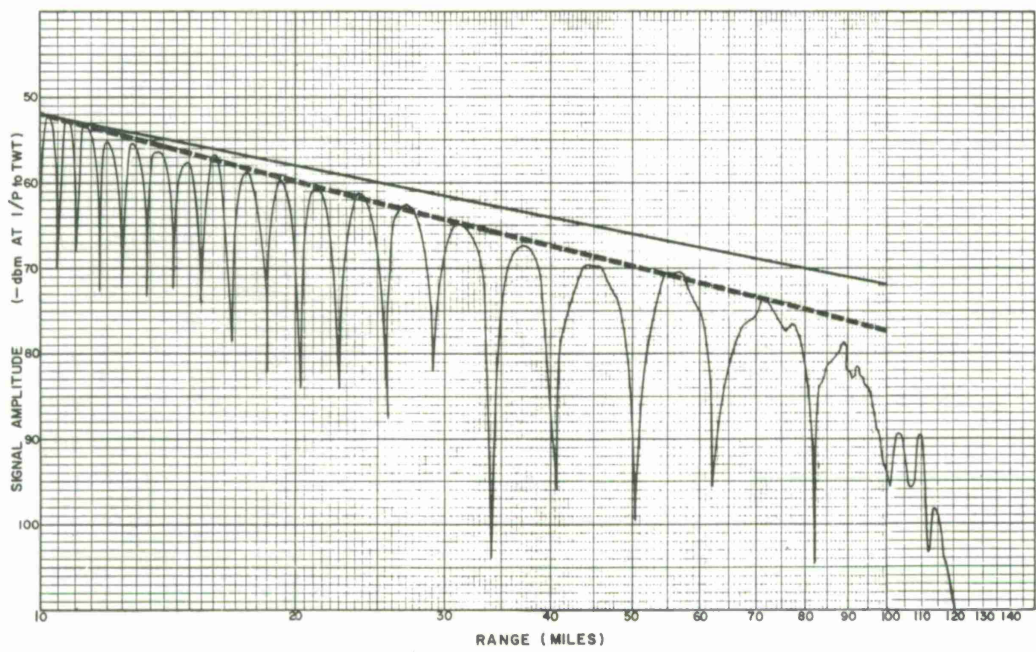
Legs 5, 6

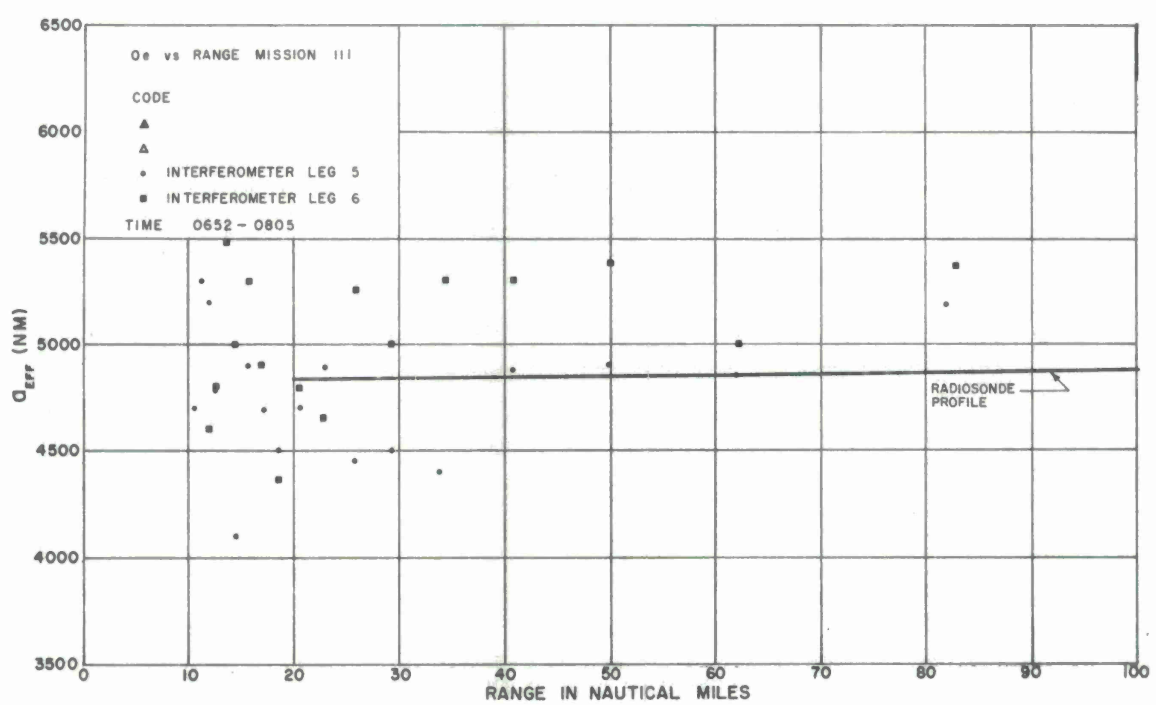
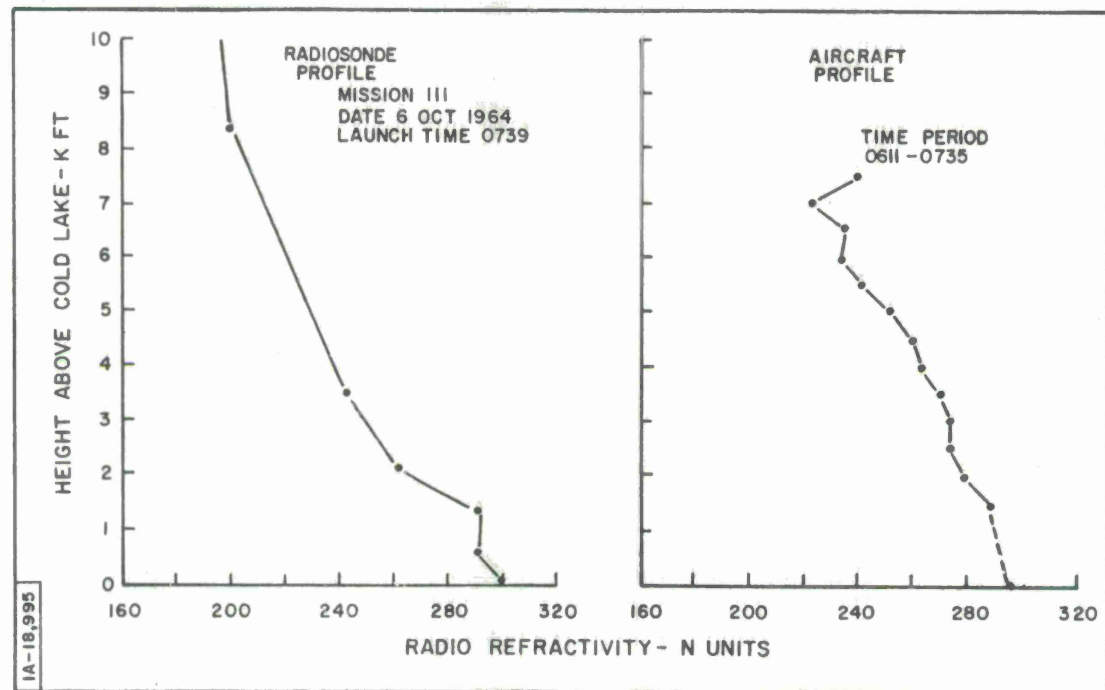
The radiosonde profile is significantly different than for the previous launch in that two increased gradients are observed, one at the surface and the other around 1700 feet. Although the ray-tracing data does not show the effect of these gradients, the interferometer data, particularly for leg 6, shows a large increase in bending at the low elevation angles in the region of 70 n.m. The characteristics of the interferometer data appear to be well related to the bending which would be suggested from the radiosonde profile. The errors between interferometer data for leg 6 and the ray-tracing results represents 0.4 mr. at 40 n.m., 0.3 mr. at 60 n.m., and 1.0 mr. at 82 n.m. in terms of the initial elevation angle error. The data for leg 5 is well within these limits.

SIGNAL AMPLITUDE V/S RANGE  
 MISSION III LEG 5 DATE 6 OCT 64 TIME 0652-0728  
 BAND L FREQUENCY 1380 Mc/s POLARIZATION HORIZ  $\lambda$  7125 ft  $h_1$  59.95 ft  $h_2$  7000 ft



SIGNAL AMPLITUDE V/S RANGE  
 MISSION III LEG 6 DATE 6 OCT 64 TIME 0730-0805  
 BAND L FREQUENCY 1380 Mc/s POLARIZATION HORIZ  $\lambda$  7125 ft  $h_1$  59.95 ft  $h_2$  7000 ft





### General Summary of Mission 111

In general the interferometer results describe a propagation environment which was not entirely observed from the radiosonde information. Although the differences between interferometer and ray-tracing data are generally large, the somewhat consistent behavior of the interferometer data for any two pairs of legs suggests that the propagation conditions may be more accurately depicted by the interferometer data.

In comparison with the previous mission, the interferometer data indicates that the substandard refractivity condition did not persist after sunrise. With reference to Vol. II, Appendix II, the surface air temperature did not increase after sunrise. The degree of vertical air motion and the saturated water vapor condition would therefore tend to remain within a layer very close to the surface. Although this effect could explain why the substandard effect did not intensify after sunrise, there is not yet an explanation for the apparent formation of superstandard conditions. These observations will be discussed in greater detail in Vol. II.

MISSION 112 - Dawn

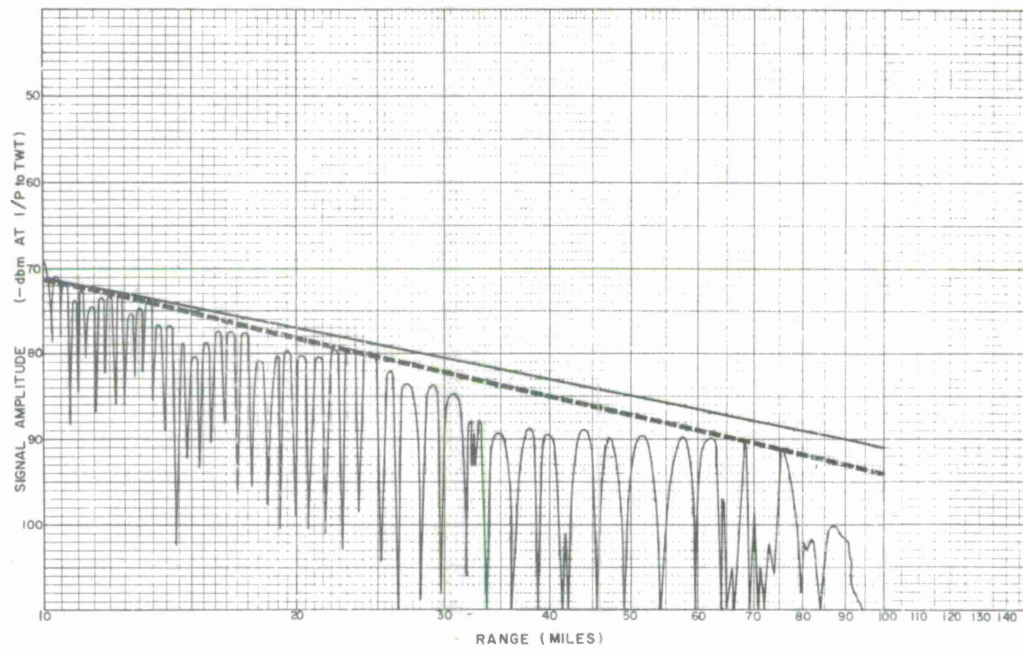
Time: 0402-0813, 7 October 1964

Legs 1, 2, 3, 4, 5, 6

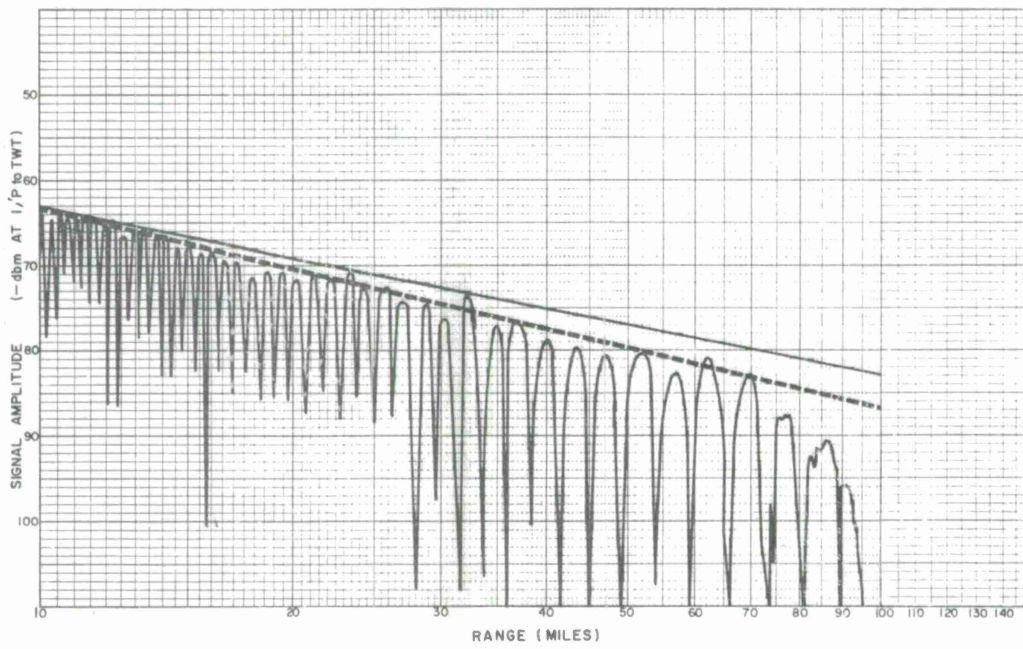
During this mission, both L- and S-band frequencies were used, as well as two different transmitter heights. All six legs are discussed together in order to compare the effect of a continuous increase in the surface refractivity gradient (shown by radiosondes) on the interferometer results. Again disregarding the aircraft refractivity profiles, it may be seen from the ray-tracing results, that the amount of bending is gradually increasing at long ranges due to this temporal increase in surface gradient. From the interferometer results, however, the amount of bending is decreasing with time at the long ranges. Although the comparison of data is extremely good in terms of  $A_e$  magnitudes for legs 3 through 6, the reversed tendencies in the bending characteristics of the two sets of data is of greater general interest. We have previously observed that the radiosonde profile does not always represent the effective propagation conditions. Since we are extrapolating refractivity from an overland launch site down to an overwater boat site, it would be reasonable to suspect that the radiosonde profiles do not always present accurate information about the effective radio propagation conditions near the surface. This observation is further substantiated by the consistently good behavior of the interferometer data. In mission

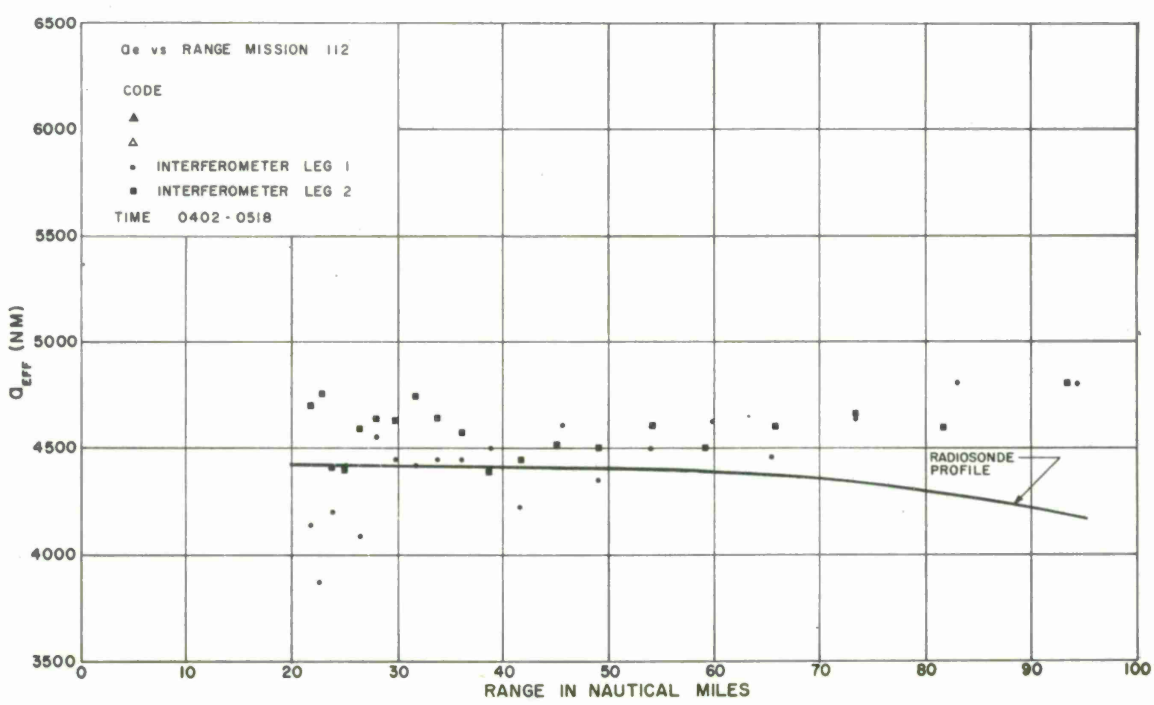
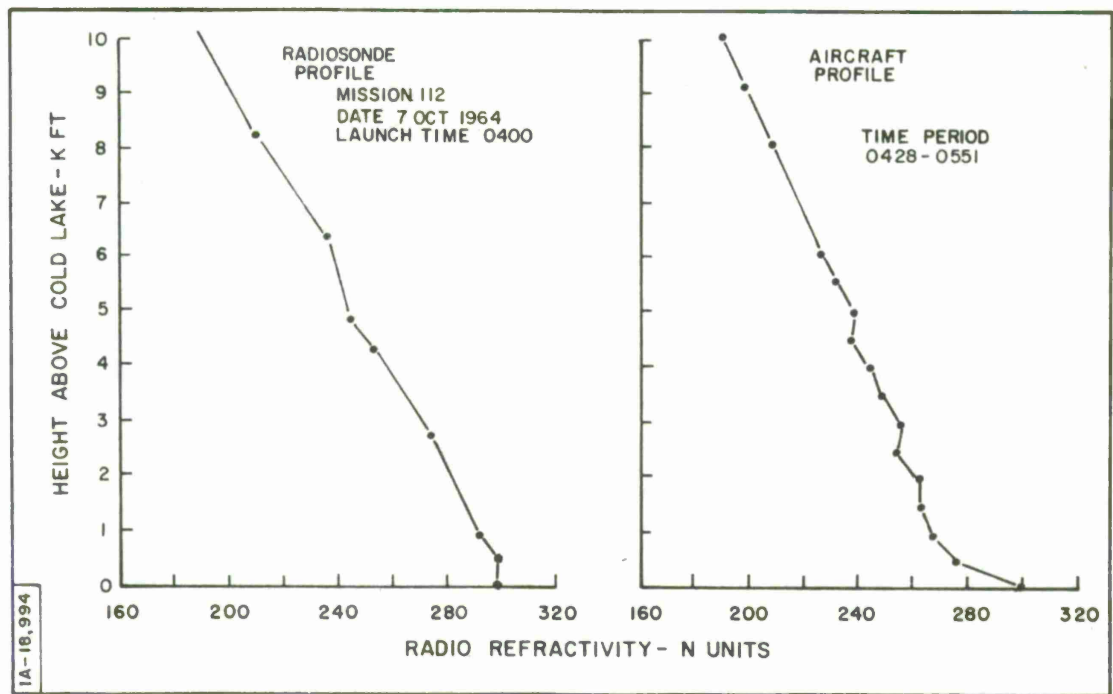
110 we have observed a tendency for the surface refractivity to become substandard after sunrise and the same effect is observed in this mission. Although there was no increase in surface heating during this mission, the wind speeds similar to mission 110 were much lower than in mission 111. Also, the wind direction for missions 110 and 112 was from the northwest, whereas it came from the south for mission 111. As is discussed in Vol. II, a south wind invariably increases the surface gradient because it causes dry air to be advected over the moist surface condition.

SIGNAL AMPLITUDE V/S RANGE  
 MISSION 112 LEG 1 DATE 7 OCT 64 TIME 0402 - 0439  
 BAND S FREQUENCY 333.6 Mc/s POLARIZATION HORIZ  $\lambda$  2947 ft  $h_1$  59.53 ft  $h_2$  7000 ft

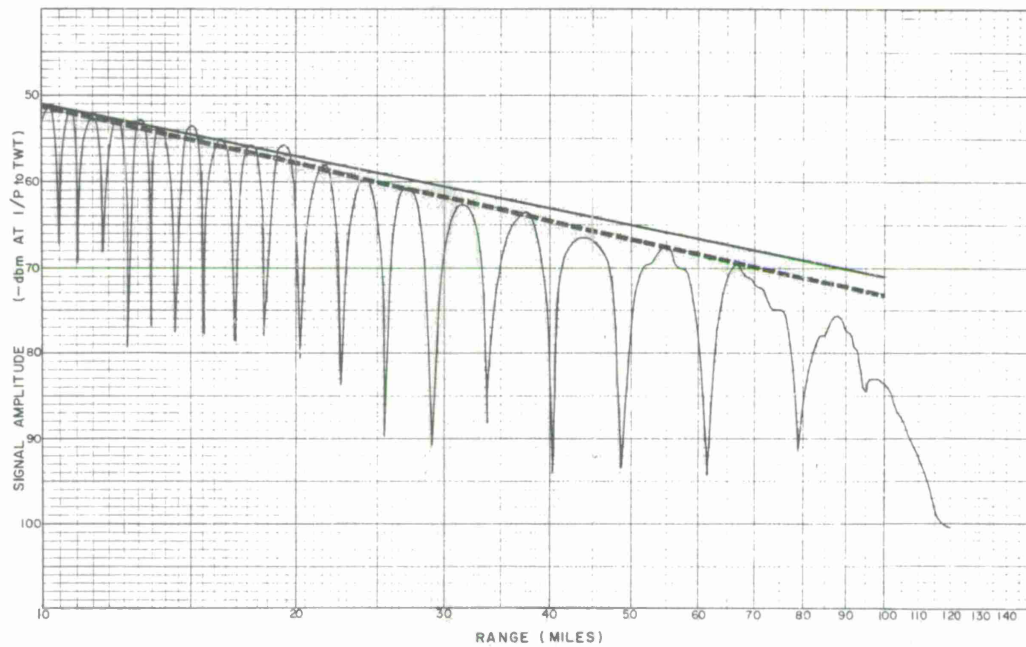


SIGNAL AMPLITUDE V/S RANGE  
 MISSION 112 LEG 2 DATE 7 OCT 64 TIME 0445 - 0518  
 BAND S FREQUENCY 333.6 Mc/s POLARIZATION HORIZ  $\lambda$  2947 ft  $h_1$  59.53 ft  $h_2$  7000 ft

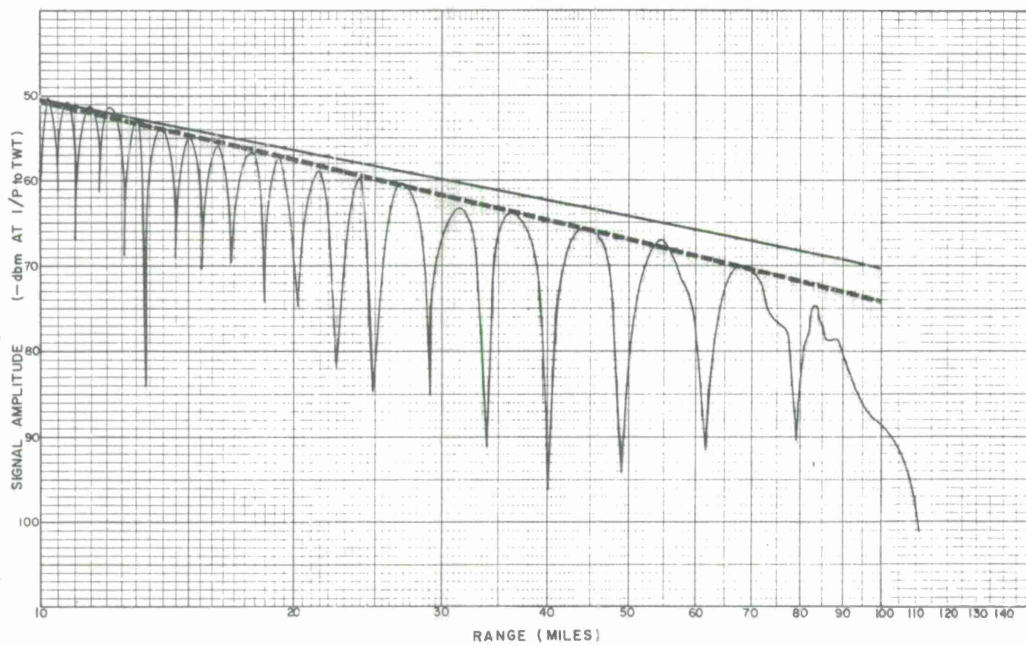


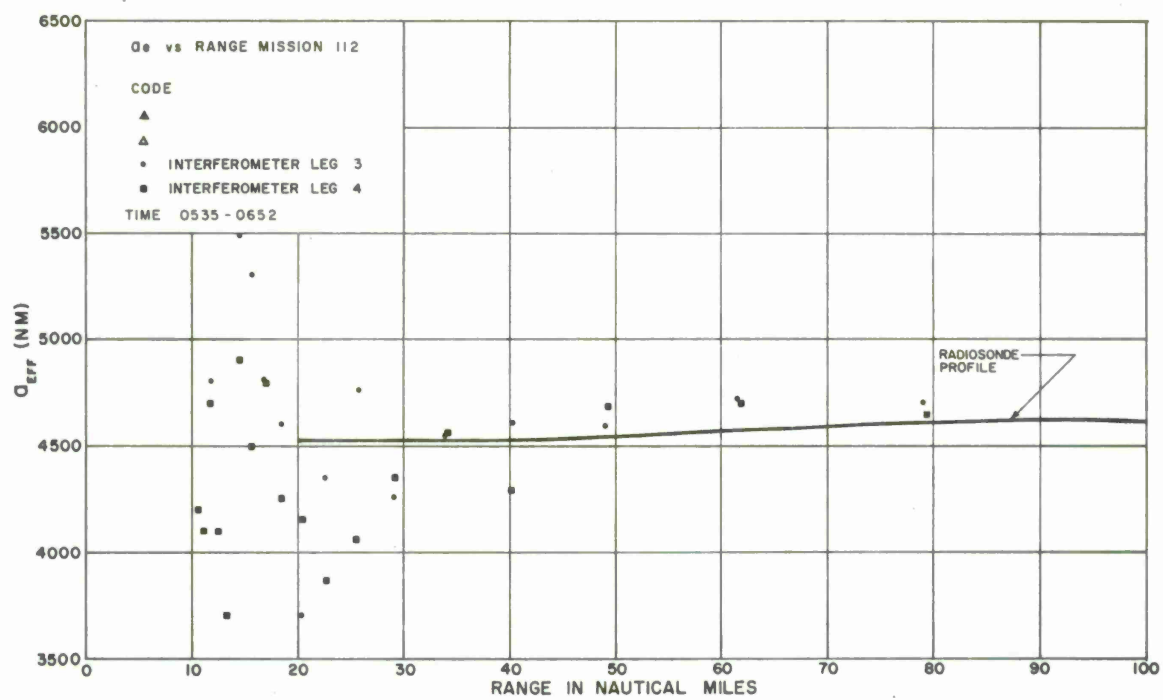
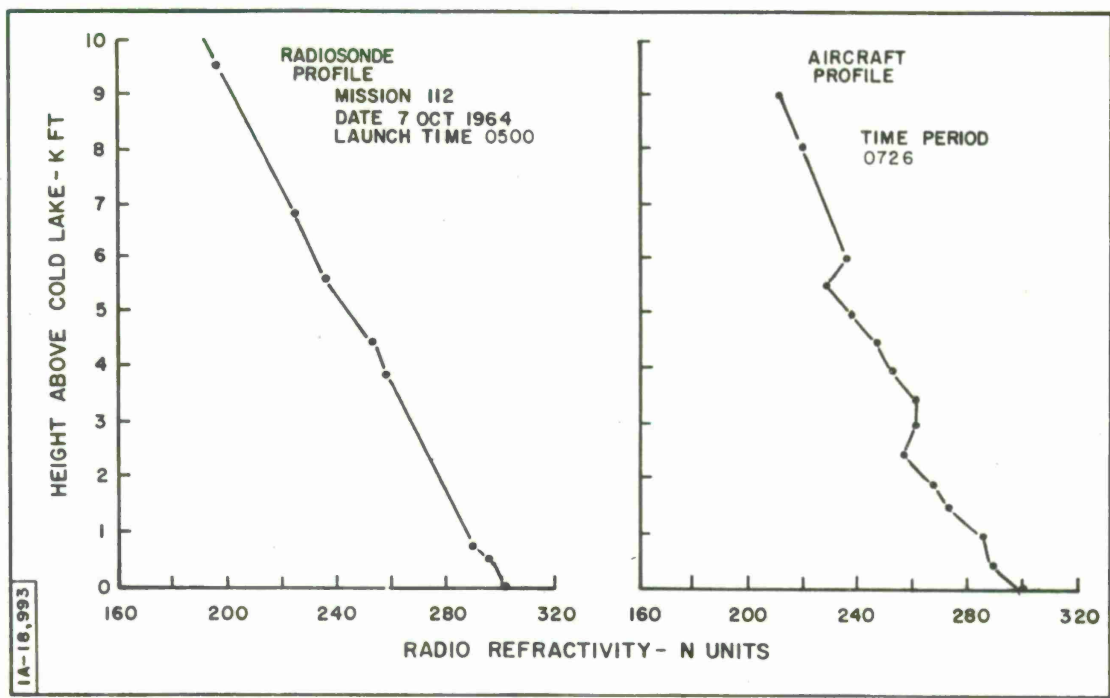


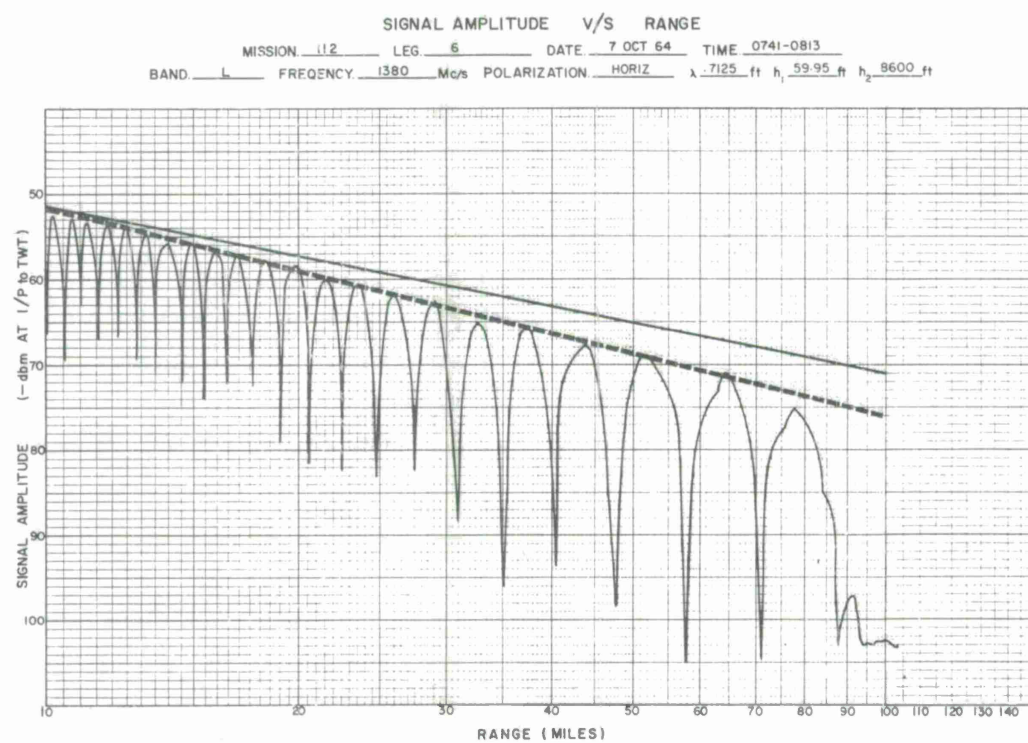
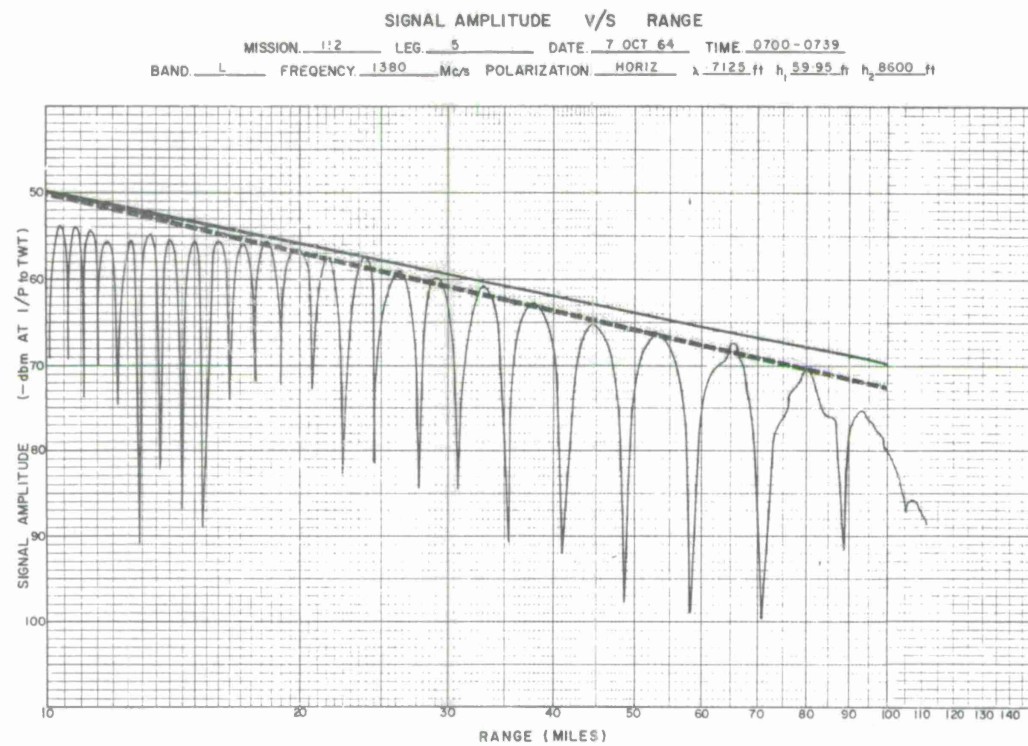
SIGNAL AMPLITUDE V/S RANGE  
MISSION 112 LEG 3 DATE 7 OCT 64 TIME 0536-0616  
BAND L FREQUENCY 1380 Mc/s POLARIZATION HORIZ  $\lambda$  7125 ft  $h_1$  59.95 ft  $h_2$  7000 ft

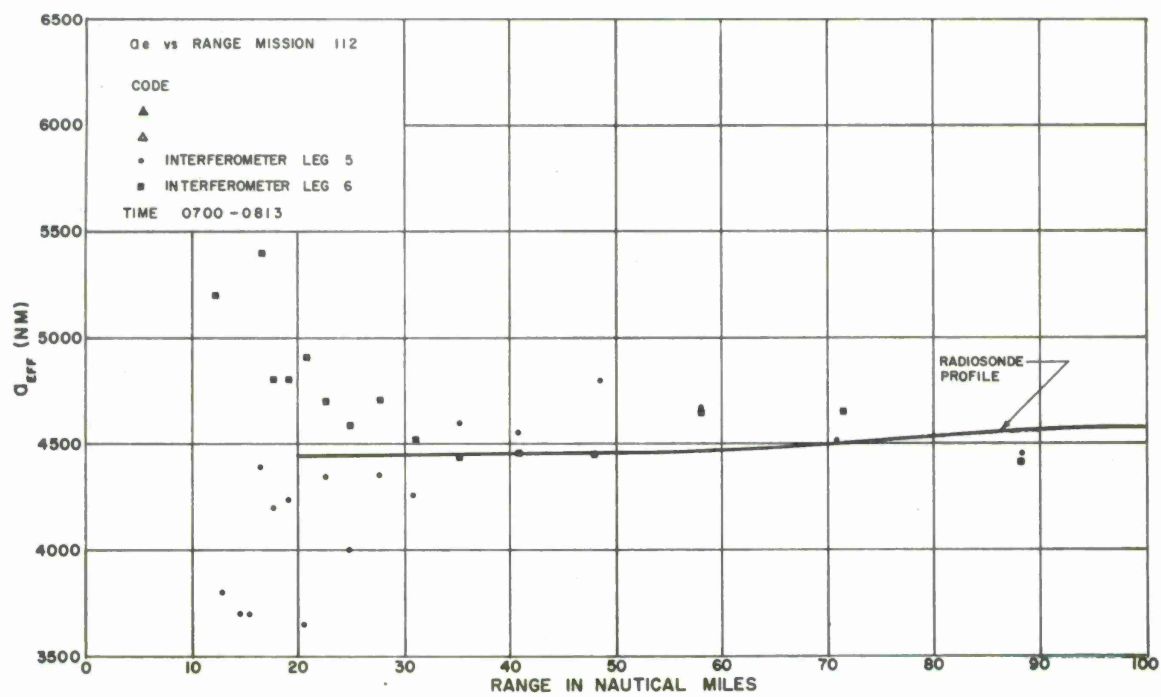
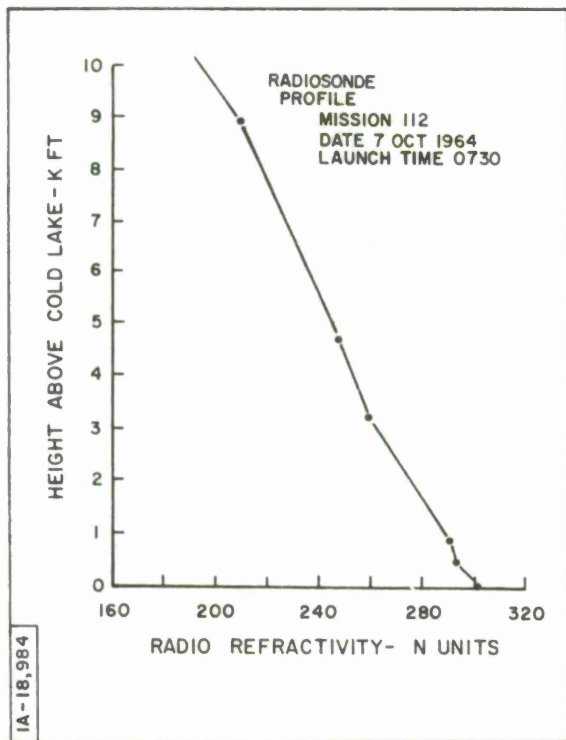


SIGNAL AMPLITUDE V/S RANGE  
MISSION 112 LEG 4 DATE 7 OCT 64 TIME 0619-0652  
BAND L FREQUENCY 1380 Mc/s POLARIZATION HORIZ  $\lambda$  7125 ft  $h_1$  59.95 ft  $h_2$  7000 ft







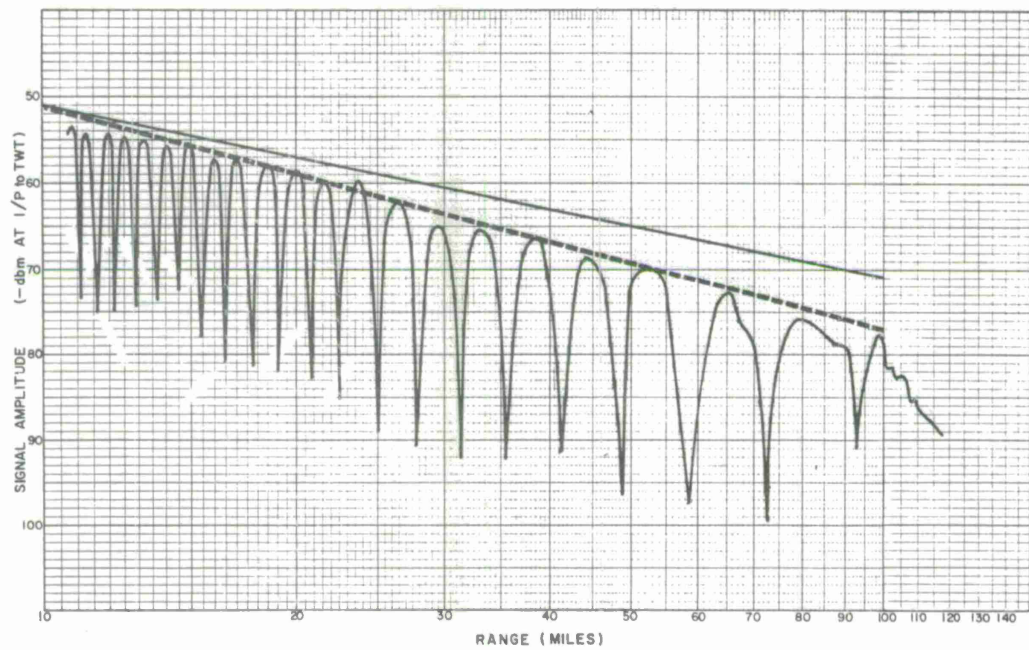


MISSION 113 - Spanning Sunrise  
Time: 0400-0800, 8 October 1964  
Legs 1, 2, 3, 4, 5, 6

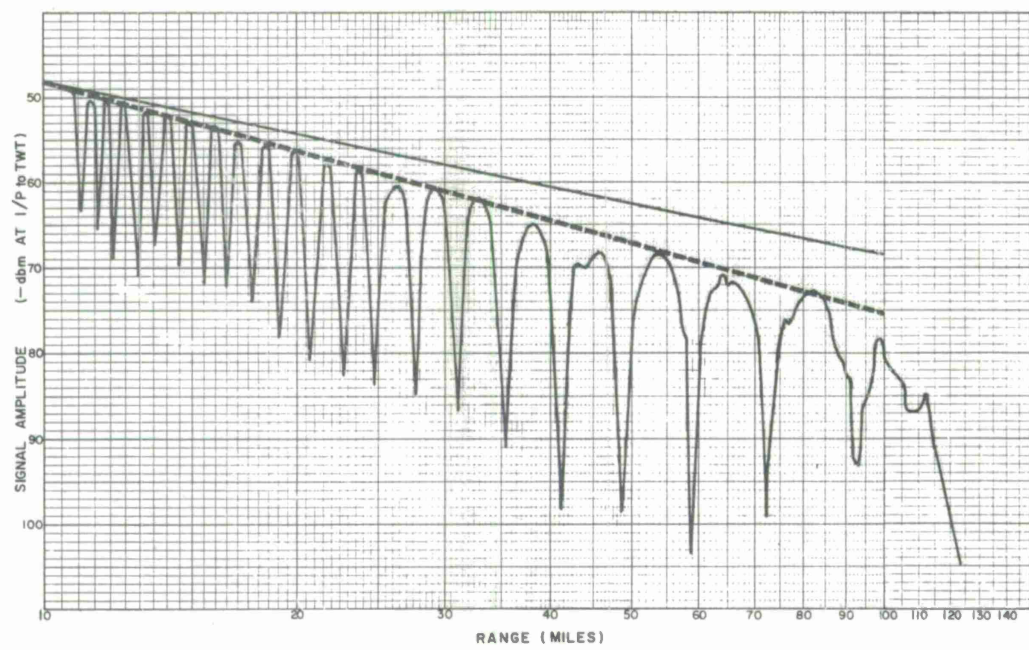
The aircraft refractivity profiles again present surface gradients which are larger than was observed with either the radiosonde or interferometer data. Using profile 0720-0728, the ray-tracing analysis indicates that trapping occurred near the surface which was not observed by the interferometer. The signal amplitude plots all show well behaved propagation out to the radio horizon. The radiosonde results indicate that the surface gradient was essentially constant up to about 600 feet for the entire mission; however, after sunrise the gradient between 600 to 1500 feet increases significantly. The measurements made at the radiosonde launch site show that the relative humidity was decreasing and that the winds were from the south. As discussed in Vol II, the influx of air from the south is generally dry and would therefore tend to cause the gradient to increase above the lake surface. The ray-tracing results correspondingly show an increase in the overall bending as this apparent elevated gradient is formed. The interferometer results indicate that at ranges in the order of 60 n.m., a point of maximum bending occurs (legs 5 and 6) corresponding to an increase in the refractivity gradient affecting medium elevation angles. Again referring to legs 5 and 6 and the corresponding radiosonde profile, the

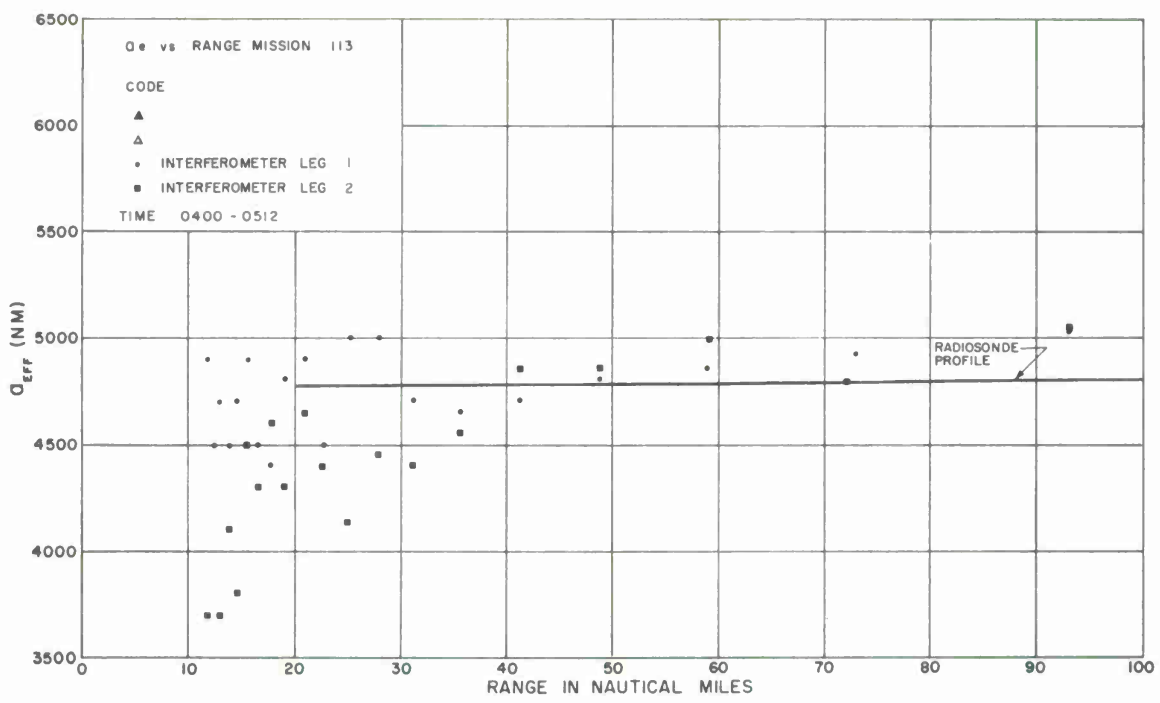
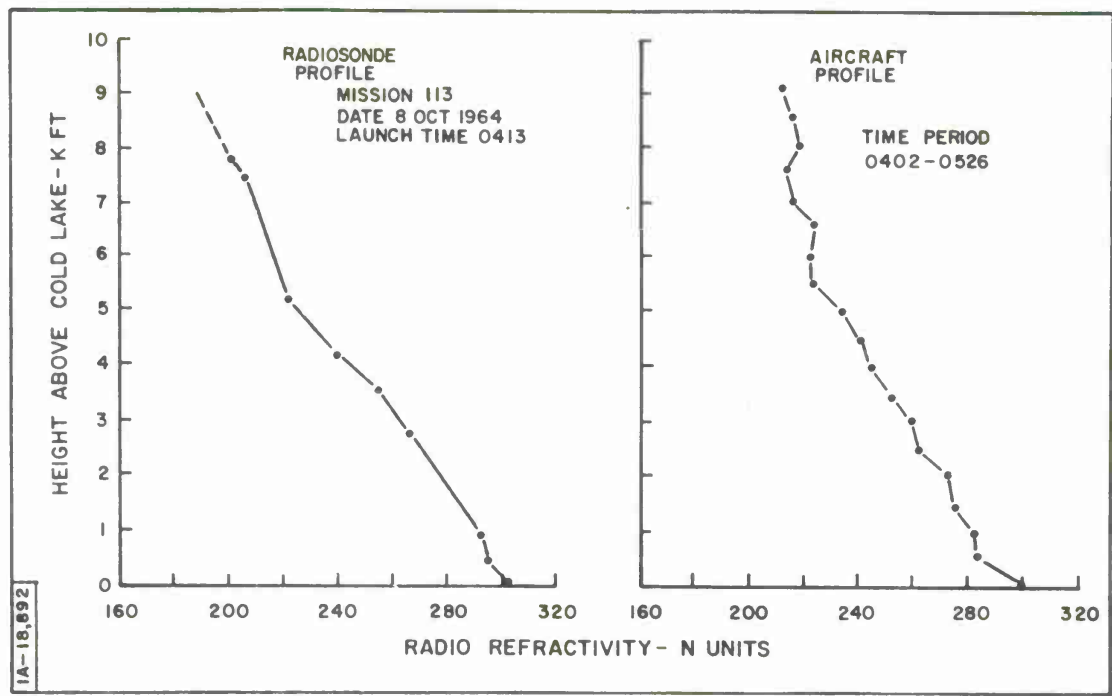
amount of bending should decrease for higher and lower elevation angles, since the gradient also decreases at the higher altitudes and at the surface. For legs 1 to 4, the interferometer data and the ray-tracing results are in good agreement except near the radio horizon. The maximum error represents about 0.1 mr. at 40 n.m., 0.3 mr. at 60 n.m., and 0.75 mr. at 90 n.m. in terms of the elevation angle error. The increased bending near the horizon, shown by the interferometer results, suggests in all cases that the surface refractivity gradient was larger than shown by the radiosonde profile. Once again, an interesting point is raised as to whether or not the radiosonde profile, which does not include horizontal stratification effects, is truly representative of the radio propagation conditions. In contrast, the interferometer observes the integrated effect of these conditions over many miles. Time permitting, it would be extremely interesting to construct a refractivity profile which when used in the ray-tracing analysis would present results similar to that observed with the interferometer. One might then attempt to justify this profile by including the effects of temporal and spatial refractivity variations.

SIGNAL AMPLITUDE V/S RANGE  
 MISSION 113 LEG 1 DATE 8 OCT 64 TIME 0400-0435  
 BAND L FREQUENCY 1380 Mc/s POLARIZATION HORIZ.  $\lambda$  7125 ft  $h_1$  59.95 ft  $h_2$  8600 ft

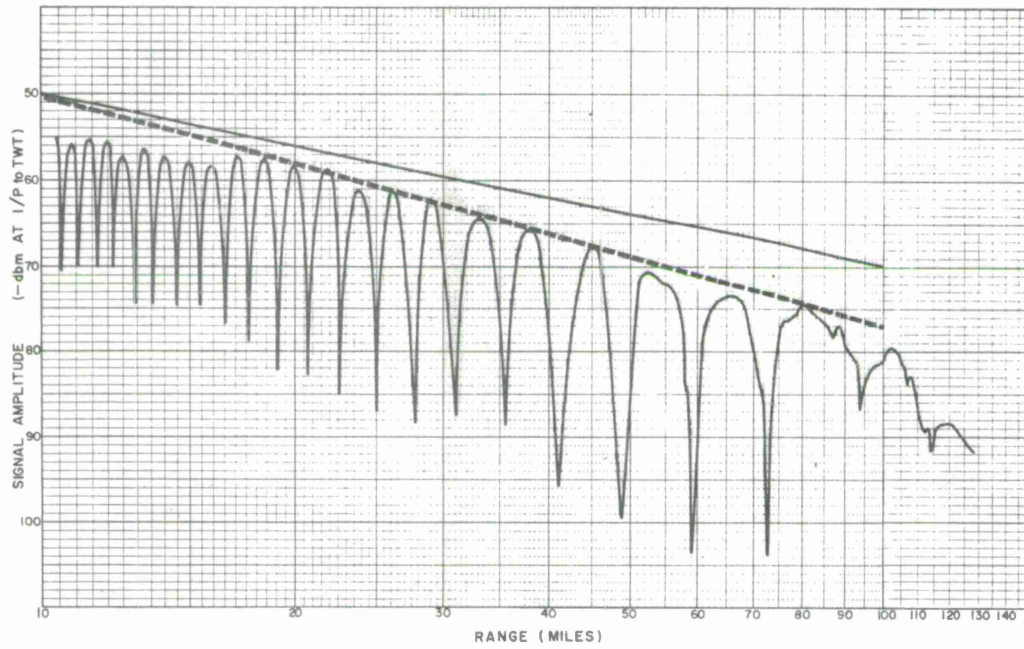


SIGNAL AMPLITUDE V/S RANGE  
 MISSION 113 LEG 2 DATE 8 OCT 64 TIME 0437-0512  
 BAND L FREQUENCY 1380 Mc/s POLARIZATION HORIZ.  $\lambda$  7125 ft  $h_1$  59.95 ft  $h_2$  8600 ft

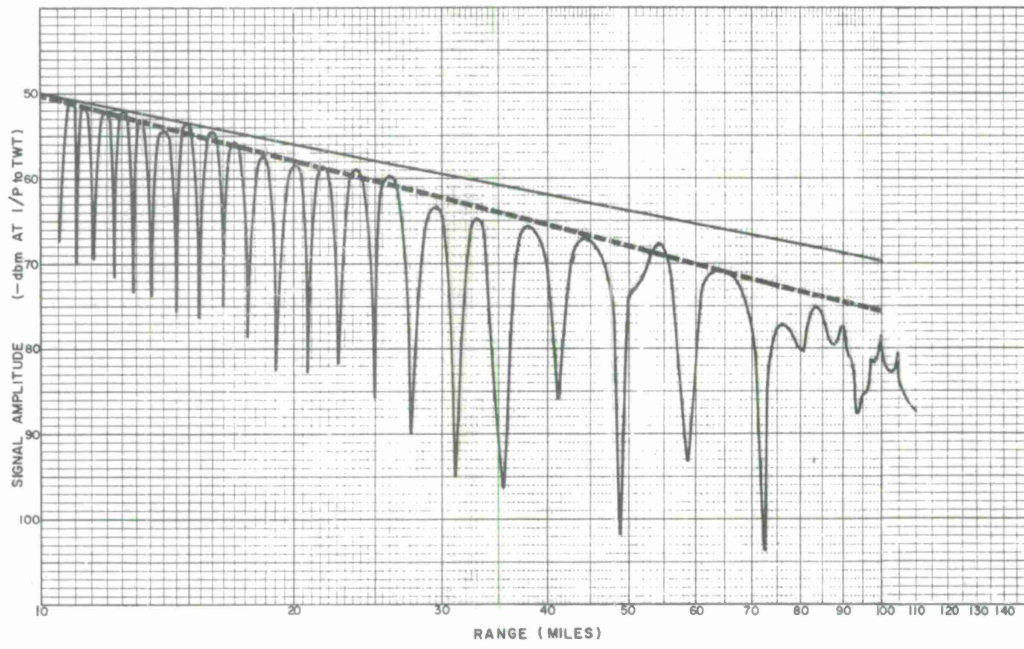


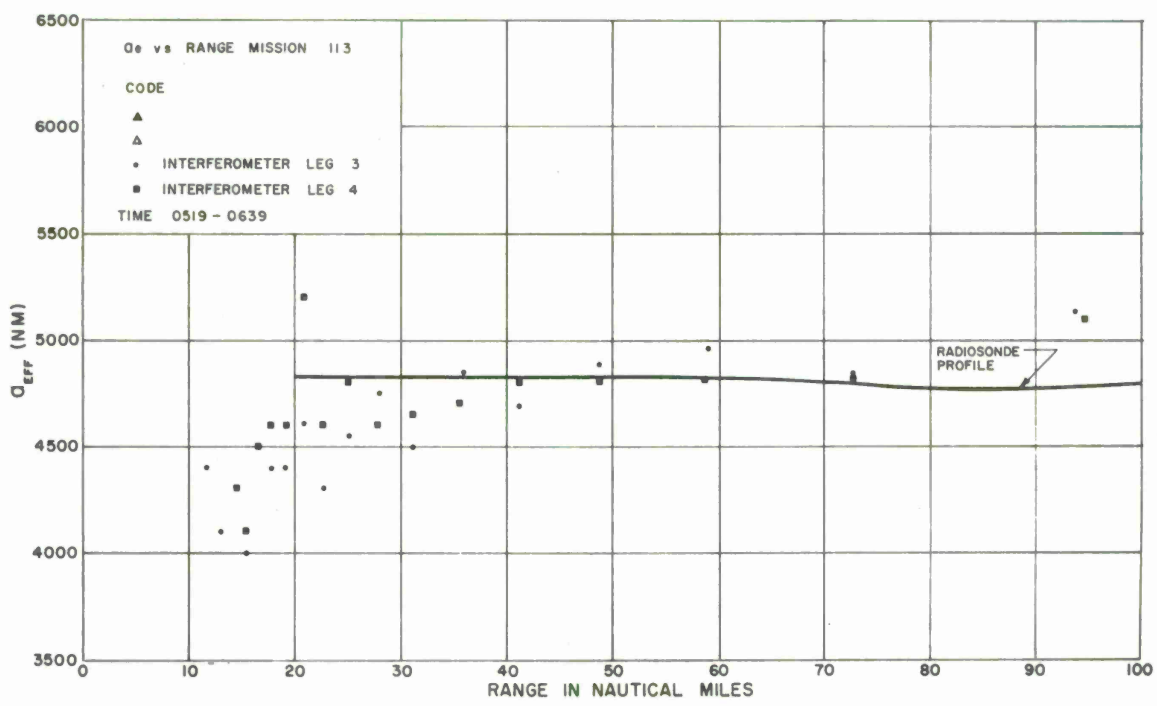
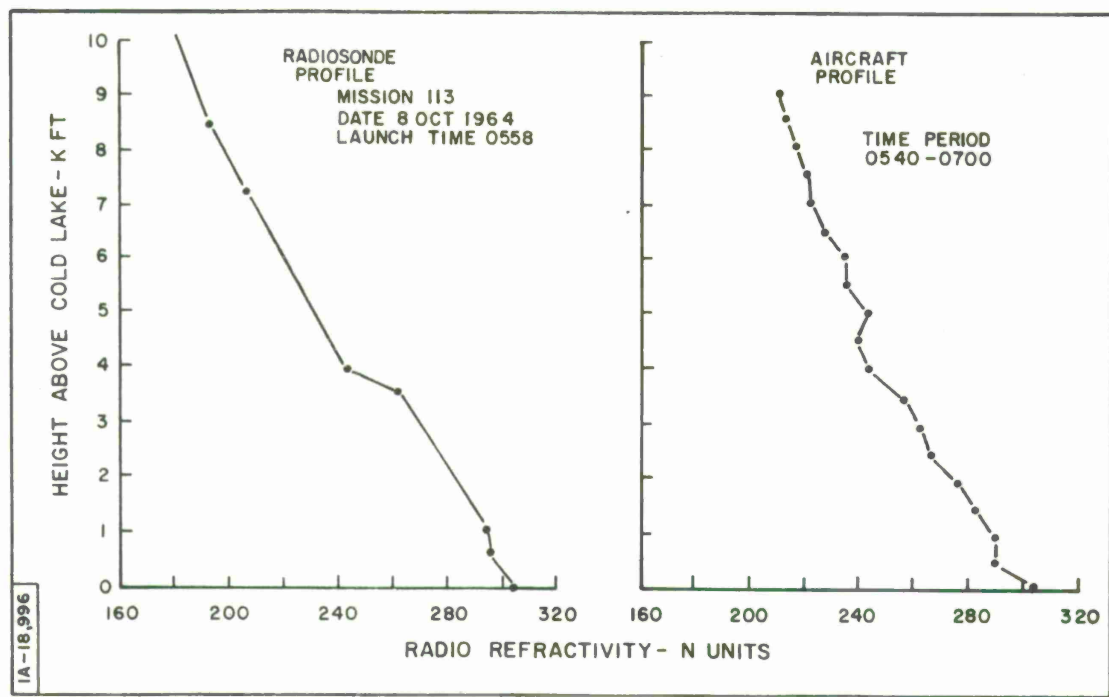


SIGNAL AMPLITUDE V/S RANGE  
 MISSION. 113 LEG. 3 DATE 8 OCT 64 TIME 0519-0558  
 BAND. L FREQUENCY. 1380 Mc/s POLARIZATION. HORIZ.  $\lambda$  7125 ft  $h_1$  59.95 ft  $h_2$  8600 ft

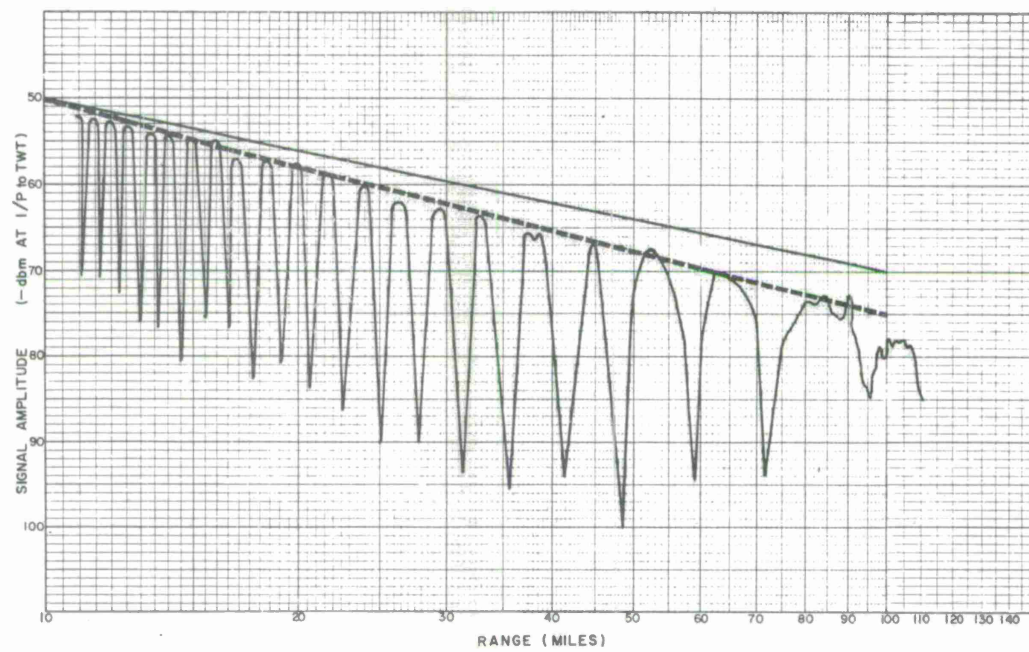


SIGNAL AMPLITUDE V/S RANGE  
 MISSION. 113 LEG. 4 DATE 8 OCT 64 TIME 0559-0639  
 BAND. L FREQUENCY. 1380 Mc/s POLARIZATION. HORIZ.  $\lambda$  7125 ft  $h_1$  59.95 ft  $h_2$  8600 ft

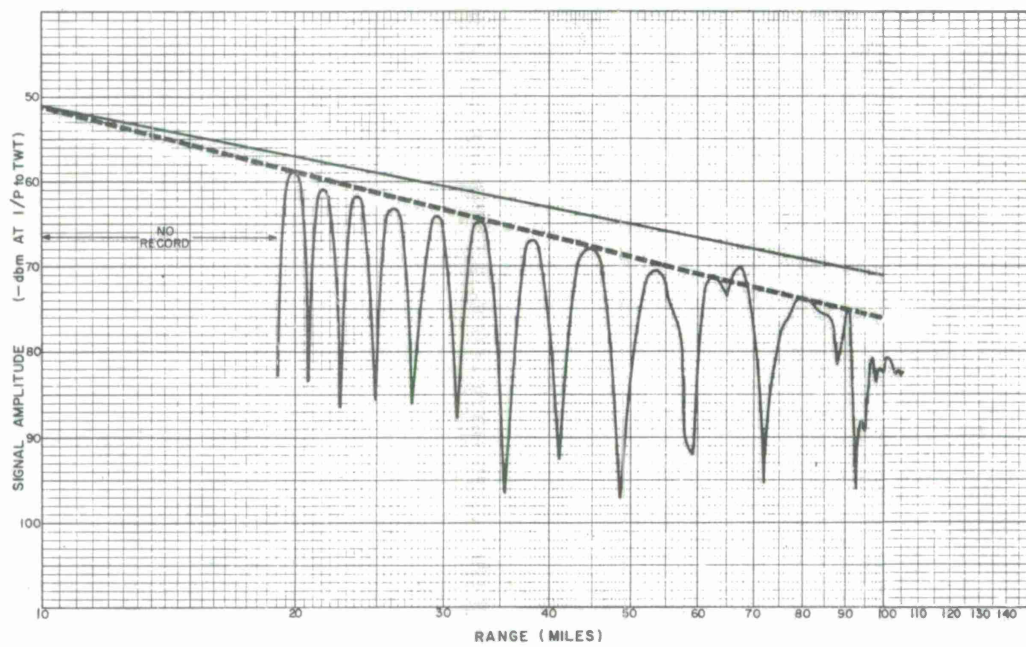


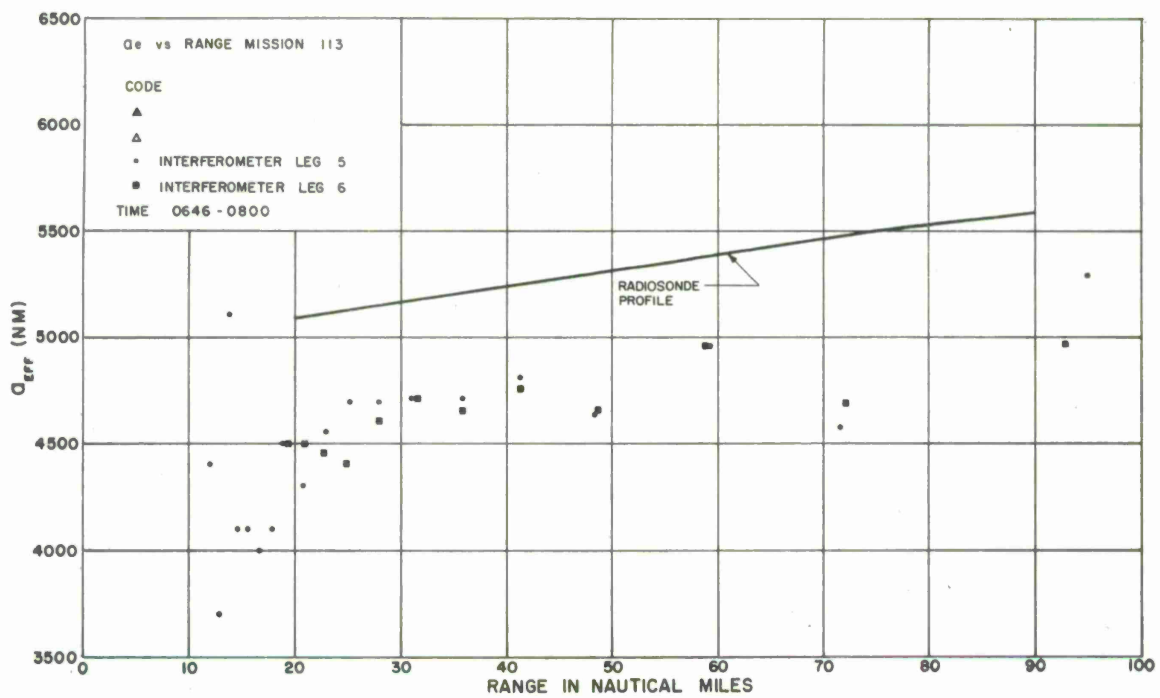
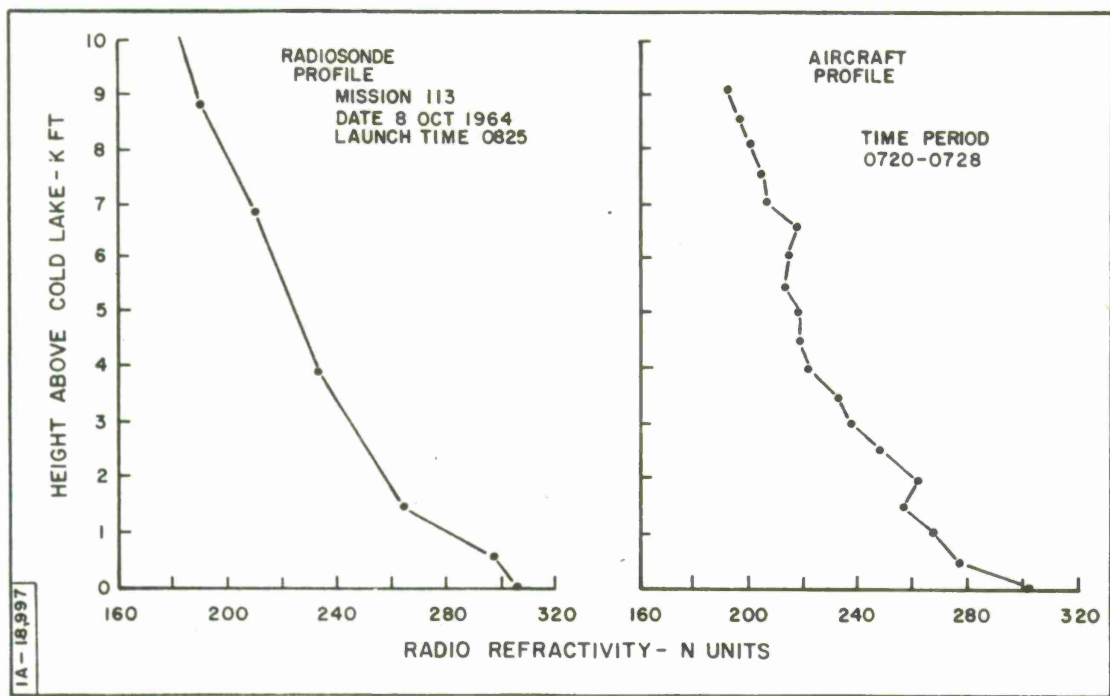


SIGNAL AMPLITUDE V/S RANGE  
 MISSION 113 LEG 5 DATE 8 OCT 64 TIME 0646 - 0722  
 BAND L FREQUENCY 1380 Mc/s POLARIZATION HORIZ.  $\lambda$  7125 ft  $h_1$  59.95 ft  $h_2$  8600 ft



SIGNAL AMPLITUDE V/S RANGE  
 MISSION 113 LEG 6 DATE 8 OCT 64 TIME 0724 - 0800  
 BAND L FREQUENCY 1380 Mc/s POLARIZATION HORIZ.  $\lambda$  7125 ft  $h_1$  59.95 ft  $h_2$  8600 ft





MISSION 114 - Dusk

Time: 1556-1952, 8 October 1964

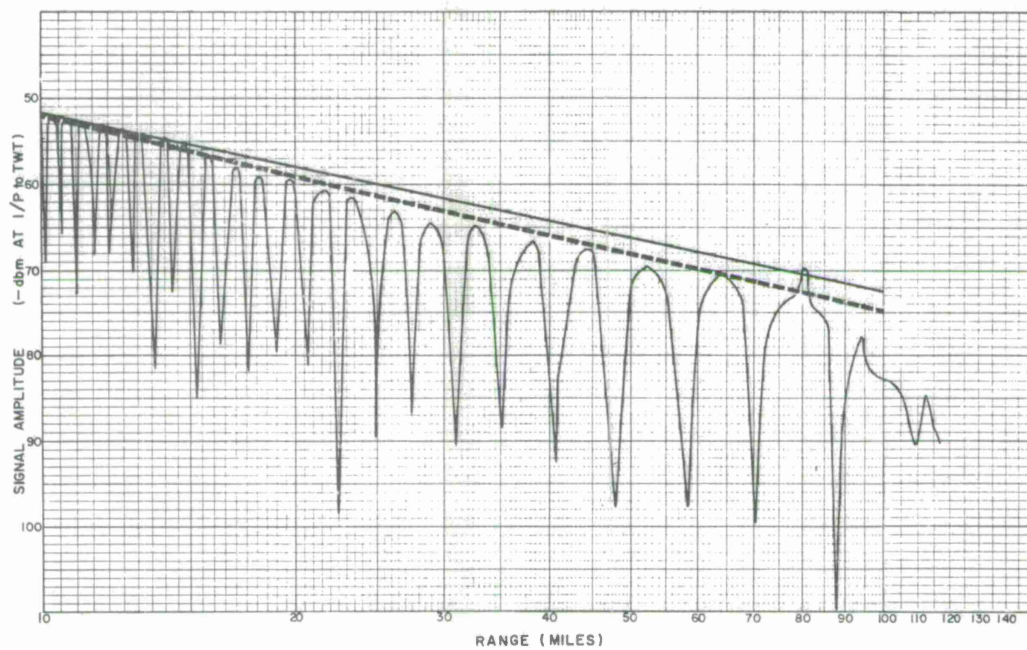
Legs 1, 2, 3, 4, 5, 6

Although the aircraft refractivity profiles are in somewhat better agreement with the radiosonde data, for the sake of consistency we will continue to consider only the radiosonde analysis. In all cases, the surface gradient would tend to make the calculated bending increase near the radio horizon. This behavior is generally shown to be the case for both ray-tracing and interferometer results. Beyond 50 n. m. the interferometer data is very consistent and indicates that the amount of bending is less than depicted from the radiosonde information. There is a tendency during legs 1 through 4, referring to the interferometer data, to have an increase in bending near 60 n. m. range, that is, at medium elevation angles. As discussed previously, this would suggest that the refractivity gradient within some height interval well above the surface is larger than the gradient either above or below this level. This effect diminishes and is observed to decrease in range with time.

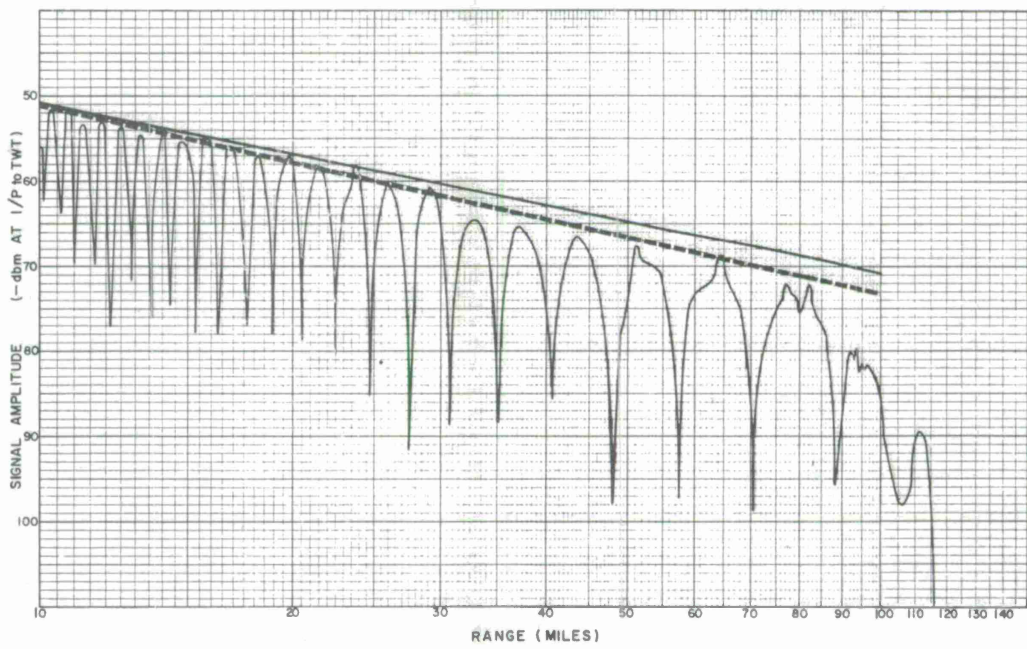
A comparison of radiosonde and interferometer results gives a maximum error of 0.4 mr. at 40 n. m., 0.45 mr. at 60 n. m., and about 1.0 mr. at the radio horizon in terms of the elevation error angle. Although the agreement is not very satisfying, the consistent pattern of behavior of the interferometer is possibly of greater importance. The interferometer results again show its potential as an

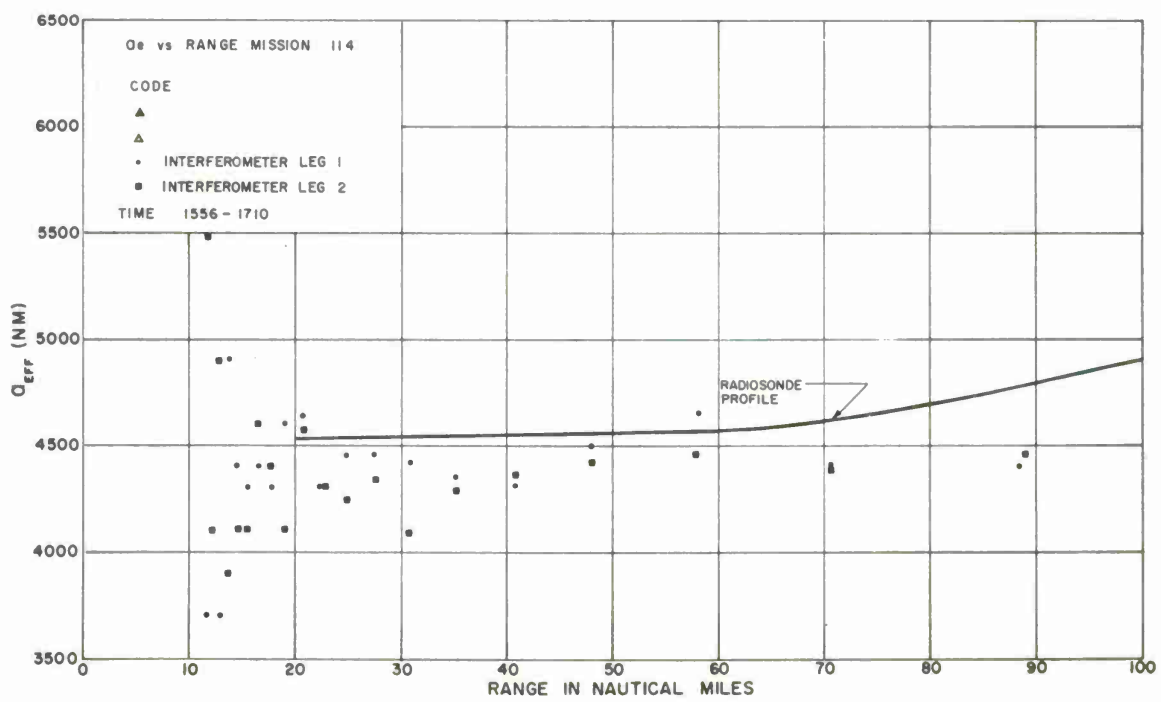
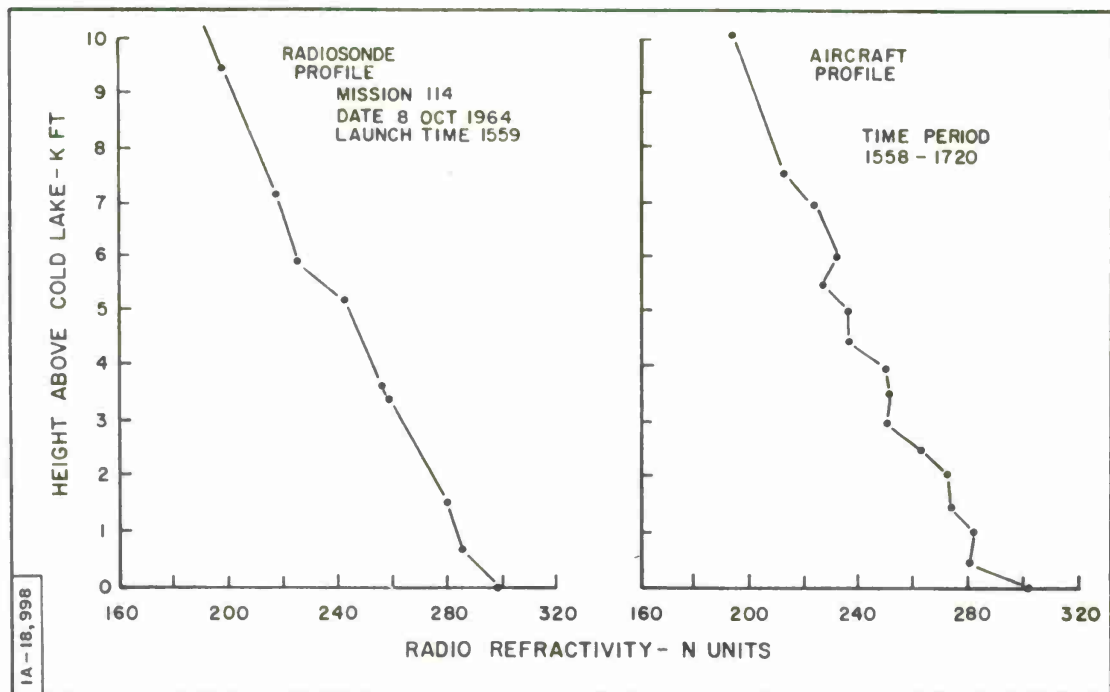
instrument to probe the behavior of propagation conditions using the direct effect of radio signal transmissions in the medium. This would be a more direct method than attempting to infer the conditions along the whole propagation path from aircraft or radiosonde measurements taken at one point or on a portion of the path.

SIGNAL AMPLITUDE V/S RANGE  
 MISSION 114 LEG 1 DATE 8 OCT 64 TIME 1556-1632  
 BAND L FREQUENCY 1380 Mc/s POLARIZATION HORIZ  $\lambda$  7125 ft  $h_1$  59.95 ft  $h_2$  8600 ft

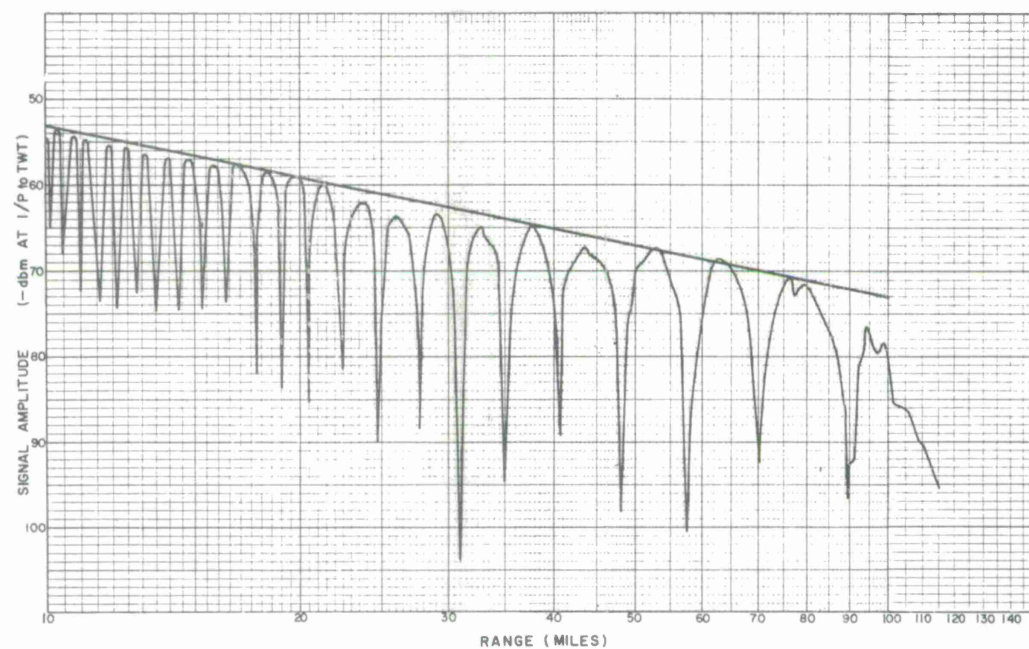


SIGNAL AMPLITUDE V/S RANGE  
 MISSION 114 LEG 2 DATE 8 OCT 64 TIME 1634-1710  
 BAND L FREQUENCY 1380 Mc/s POLARIZATION HORIZ  $\lambda$  7125 ft  $h_1$  59.95 ft  $h_2$  8600 ft

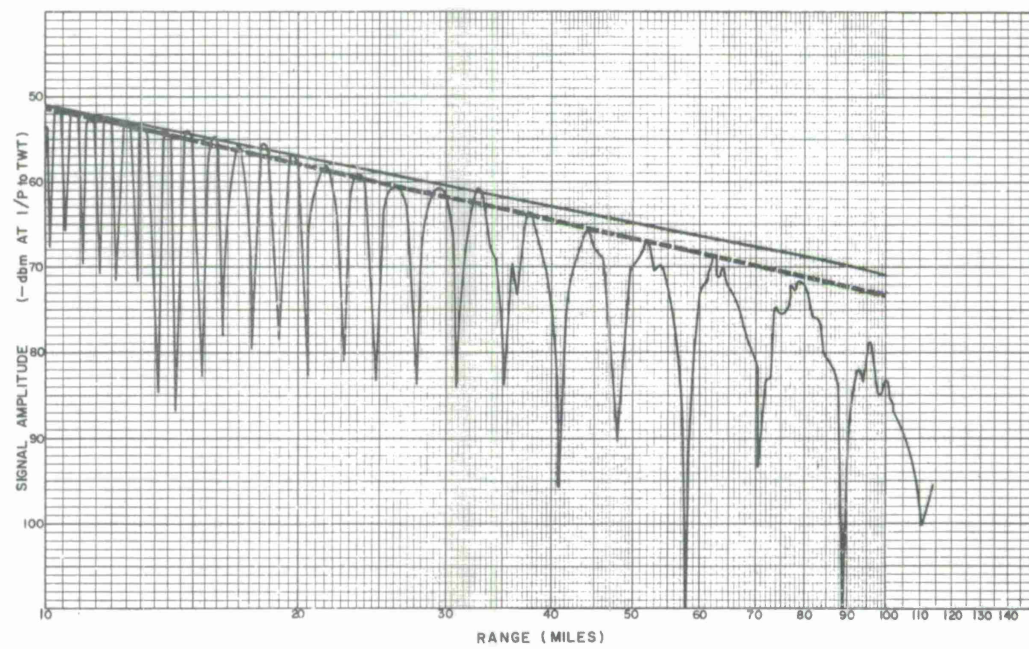


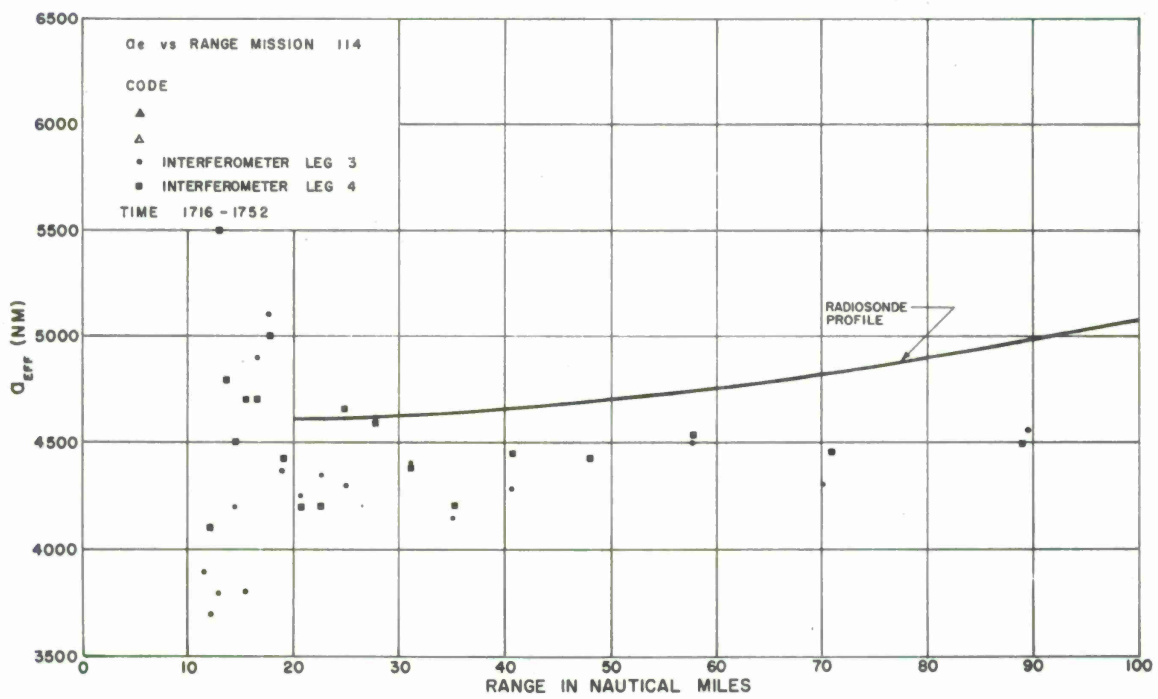
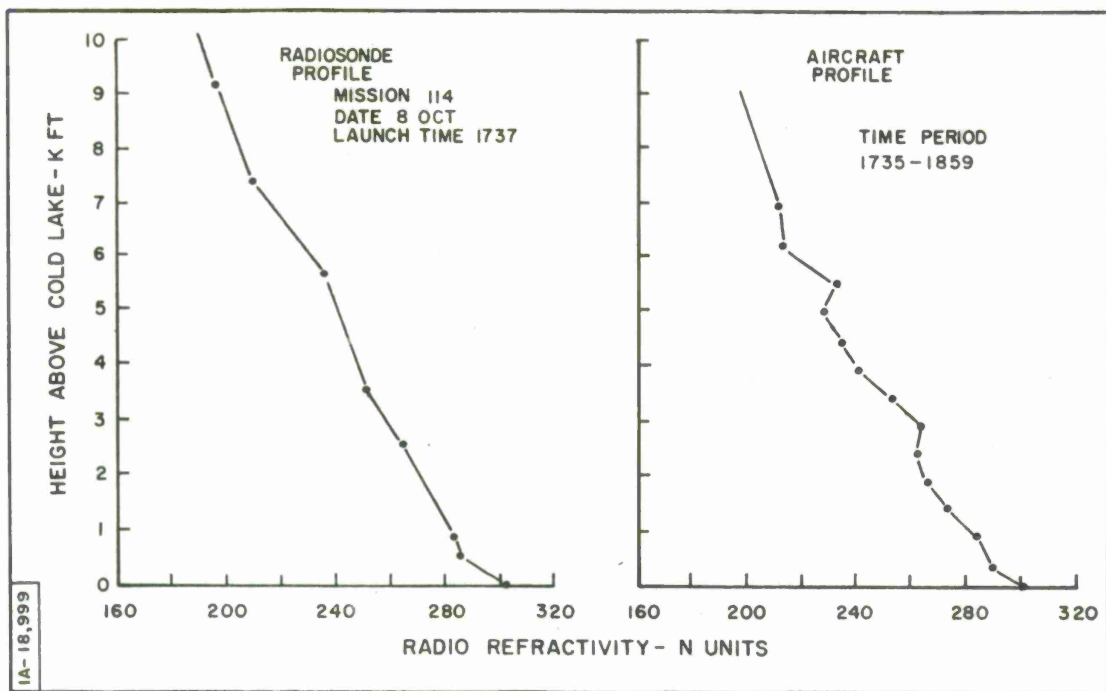


SIGNAL AMPLITUDE V/S RANGE  
 MISSION 114 LEG 3 DATE 8 OCT 64 TIME 1716-1752  
 BAND L FREQUENCY 1380 Mc/s POLARIZATION HORIZ  $\lambda$  7125 ft  $h_1$  59.95 ft  $h_2$  8600 ft

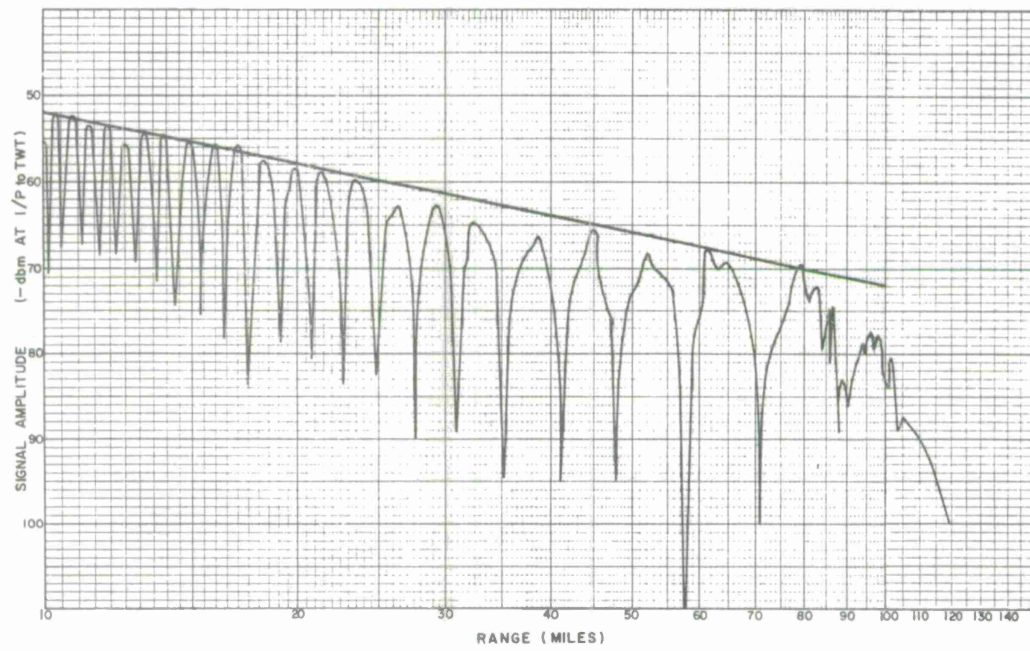


SIGNAL AMPLITUDE V/S RANGE  
 MISSION 114 LEG 4 DATE 8 OCT 64 TIME 1753-1831  
 BAND L FREQUENCY 1380 Mc/s POLARIZATION HORIZ  $\lambda$  7125 ft  $h_1$  59.95 ft  $h_2$  8600 ft

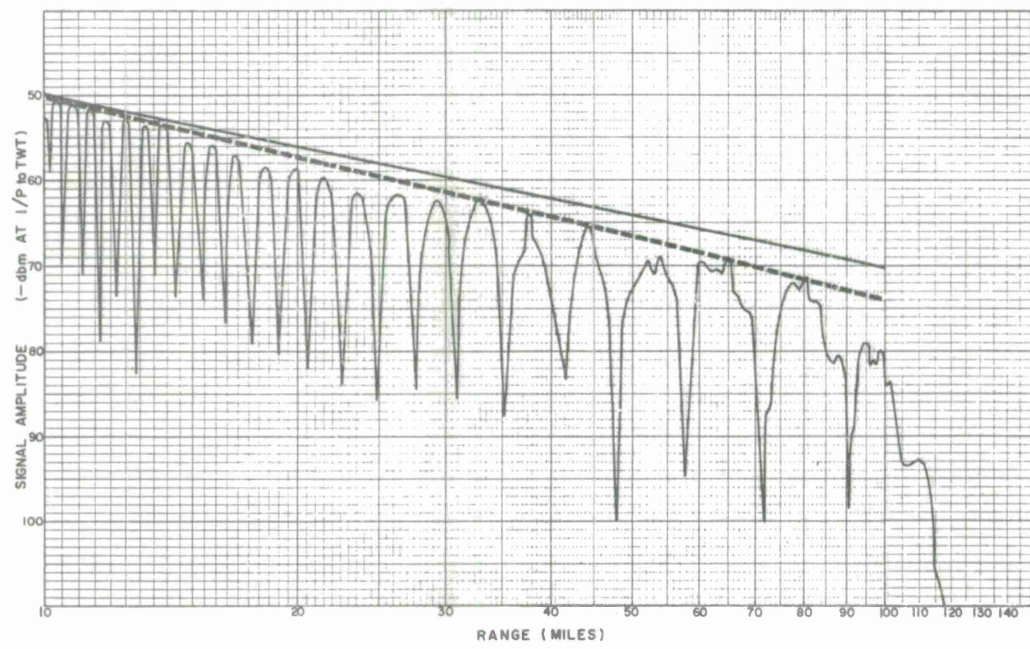


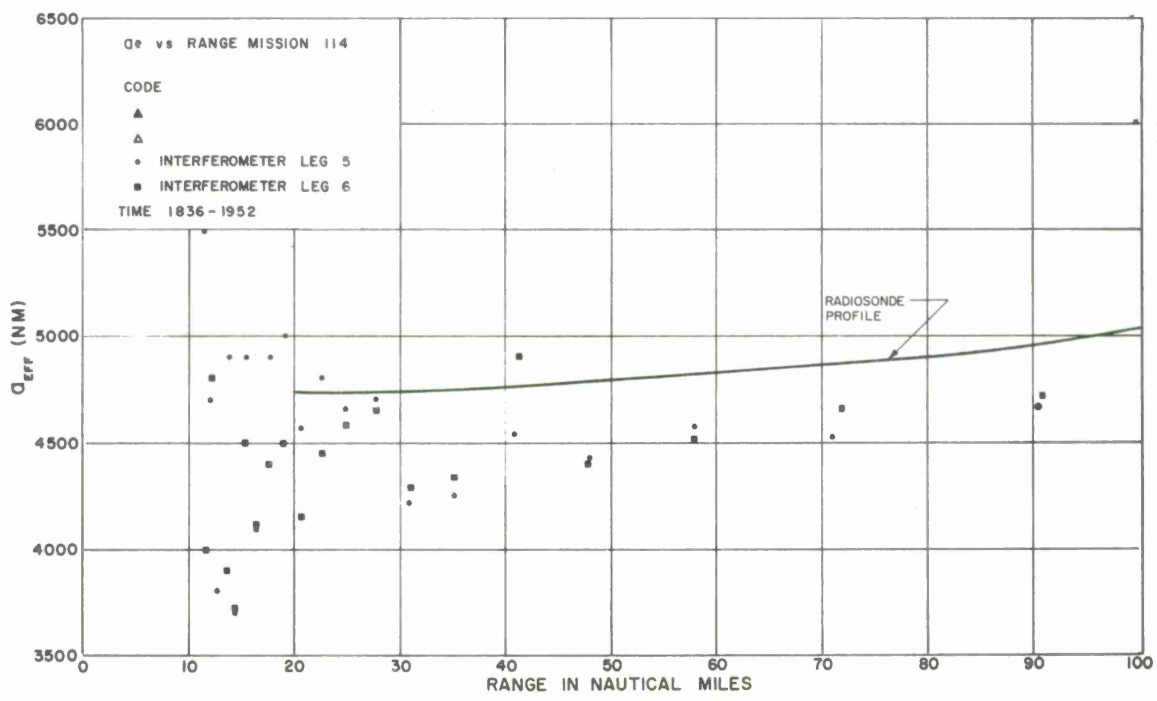
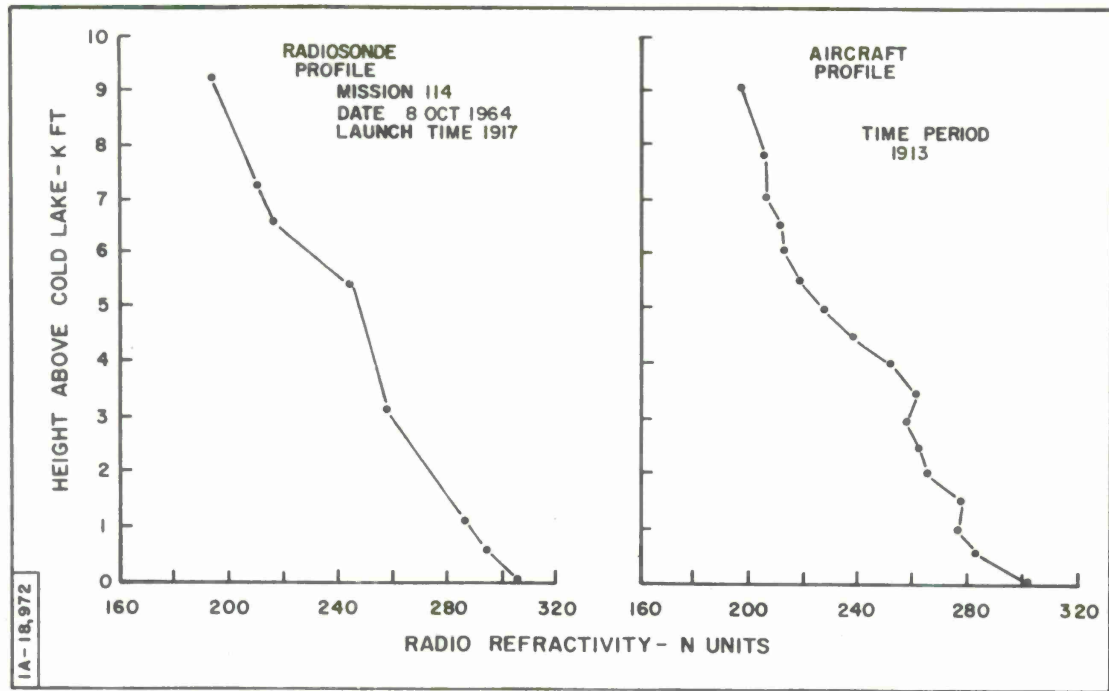


SIGNAL AMPLITUDE V/S RANGE  
 MISSION 114 LEG 5 DATE 8 OCT 64 TIME 1836-1912  
 BAND L FREQUENCY 1380 Mc/s POLARIZATION HORIZ  $\lambda$  7125 ft  $h_1$  59.95 ft  $h_2$  8600 ft



SIGNAL AMPLITUDE V/S RANGE  
 MISSION 114 LEG 6 DATE 8 OCT 64 TIME 1915-1952  
 BAND L FREQUENCY 1380 Mc/s POLARIZATION HORIZ  $\lambda$  7125 ft  $h_1$  59.95 ft  $h_2$  8600 ft





## SECTION V

### SUMMARY AND CONCLUSIONS

#### SIGNAL AMPLITUDE CHARACTERISTICS

The depth of fade increases at longer ranges, as expected, due to an increase in the amplitude of the reflected signal, or similarly due to an increase in the reflection coefficient. It should therefore be expected that the signal amplitudes for in-phase conditions would, if anything, fall off less rapidly in range than the inverse square relationship for free-space propagation. However, in general, the decrease in signal amplitude with range exceeded the free-space conditions. Also in most cases the fall-off was irregular, presenting a staircase pattern. Table VII summarizes the signal characteristics. As shown, the loss beyond free-space propagation at 100 n. m. range is seen to vary from 0 to 9 decibels. No firm conclusion was reached concerning the origin of this loss. However, the following mechanisms might have contributed:

- (a) the spherical earth divergence factor,
- (b) increased divergence of radio rays when penetrating strongly refracting layers (this might also explain the staircasing effect if such layers produced more than the normal two paths to the receiver),

Table VII  
Summary of Signal Amplitude Characteristics

Mission	Leg	Band / Pol.	TX Height (ft)	Time	Ampli- tude		Loss at 100 nm (db)	Remarks
					@ 10nm (-dbm)	at 100 nm (db)		
102	1	S/V	8600	AM				Cross-polarized to 50 nm
	2	S/V	8600	AM				Amplitude plot not available
	3	S/H	8600	AM	70	?		Pronounced stircasing
	4	S/H	8600	Noon	61	5.5		Slight stircasing
	5	L/H	8600	PM	52	8		Slight stircasing after 50 nm
	6	L/H	8600	PM	52	3		TX off at 33 nm
103	1	S/H	8600	AM	76			Amplitude low, strong stircasing
	2	S/H	8600	Noon	63	9		
	3	S/H	8600	PM	73	6.5		Amp. irregular, strong stircasing
	4	S/H	8600	PM	65	5		Strong stircasing
	5	S/H	8600	PM	73	7.5		Strong stircasing
	6	S/H	8600	PM	68	7.5		Strong stircasing
104	1	S/H	7000	Night				Amplitude plot not available
	2	S/H	7000	Night	64	0		Strong stircasing
	3	S/H	7000	Sunrise	72	5		Strong stircasing
	4	S/H	7000	AM	64	5		Slight stircasing
	5	S/H	7000	AM	71	4		Strong stircasing
	6	S/H	7000	AM	65	7.5		Strong stircasing
105	1	S/H	8600	Noon	66	9		Irregular, very strong stircasing
	2	S/H	8600	PM	59	8		Strong stircasing
	3	S/H	8600	PM	67	3.5		Strong stircasing
	4	S/H	8600	PM	58	6		TX off after 35 nm
	5	S/H	4300	PM	67	3		Slight stircasing
	6	S/H	4300	PM	59	7		Strong stircasing

Table VII (Cont.)

Mission	Leg	Band / Pol.	TX Height (ft)	Time	Ampli-	Loss	Remarks
					tude @ 10 nm	at 100 nm (-dbm) (db)	
106	1	S/H	4300	AM	66	6	Very little stircasing
	2	S/H	4300	AM	67	0	Strong stircasing
	3	S/V	4300	AM	70	0	Strong sc, Brewster angle evident
	4	S/V	4300	AM	69	0	Strong stircasing
	5	S/V	7000	AM	66	3	Slight stircasing
	6	S/V	7000	Noon			Amplitude plot not available
	7	S/H	7000	PM	67	0	Very slight stircasing
	8	S/H	7000	PM	56	6	Amplitude increased by 10 db
107	1	S/H	7000	PM	67		Very pronounced stircasing
	2	S/H	7000	PM	57	4	Strong stircasing
	3	S/H	7000	Sunset	65	2	Flat from 15-30 nm
	4	S/H	7000	Sunset	57	3.5	Slight stircasing
	5	S/H	7000	Night	65	?	Pronounced stircasing
	6	S/H	7000	Night	56	6	Slight stircasing
108	1	L/H	4300	PM	57	0	Amplitude is 5 db below the average
	2	L/H	4300	PM	53	4	
	2	L/H	4300	PM	53	4	Slight stircasing
	3	L/H	7000	PM	52	4	Extra fade at 67 nm
	4	L/H	7000	PM	51	5	Slight stircasing
	5	L/H	7000	PM	52	6	Extra fade at 66 nm
	6	L/H	7000	PM	53	6	Pronounced stircasing
109	1	L/H	4300	PM	52	2.5	
	2	L/H	4300	PM	53	6	
	3	L/H	7000	Sunset	52	4	
	4	L/H	7000	Sunset	53	4	
	5	L/H	7000	Night	50	1	Pronounced stircasing
	6	L/H	7000	Night	49	9	Stircasing
110	1	S/H	7000	Night	70	?	Very irregular, low amplitude
	2	S/H	7000	Night	57	6	Pronounced stircasing, extra fades
	3	L/H	7000	Sunrise	52	0	
	4	L/H	7000	Sunrise	51	4.5	
	5	L/H	7000	AM	49	4.5	
	6	L/H	7000	AM	50	6	

Table VII (Cont.)

Mission	Leg	Band / Pol.	TX Height (ft)	Time	Ampli- tude @ 10 nm		Loss at 100 nm (db)	Remarks	
					(-dbm)	(db)			
111	1	S/H	7000	Night	68	?	Very irregular, many extra fades		
	2	S/H	7000	Night	63	6	Pronounced stircasing		
	3	L/H	7000	Sunrise	53	2	Stircasing		
	4	L/H	7000	Sunrise	49	9			
	5	L/H	7000	AM	52	3			
	6	L/H	7000	AM	52	5			
112	1	S/H	7000	Night	71	3	Very strong sc, flat from 35-80 nm		
	2	S/H	7000	Night	63	4	Stircasing		
	3	L/H	7000	Sunrise	51	2			
	4	L/H	7000	Sunrise	50	4			
	5	L/H	8600	AM	50	3			
	6	L/H	8600	AM	51	5			
113	1	L/H	8600	Night	51	6			
	2	L/H	8600	Night	48	6			
	3	L/H	8600	Sunrise	50	7			
	4	L/H	8600	AM	50	6			
	5	L/H	8600	AM	50	5			
	6	L/H	8600	AM	51	5			
114	1	L/H	8600	PM	52	3			
	2	L/H	8600	PM	51	2			
	3	L/H	8600	Sunset	53	0			
	4	L/H	8600	Night	51	2			
	5	L/H	8600	Night	52	0			
	6	L/H	8600	Night	51	5			

- (c) the variations in the reflection coefficient of the lake due to waves,
- (d) direct loss due to scattering caused by atmospheric discontinuities,
- (e) antenna pattern modulation.

#### REFRACTIVITY PROFILES

In general, the ray-tracing analysis depended upon radiosonde data to obtain reasonable agreement with the interferometer calculations. Aircraft measurements close to the lake surface were misleading in nearly all cases. It is suspected that the presence of liquid droplets in the boundary layer not only biased the refractivity values low (due to presence of physical material in the cavity), but also caused large variations about the average values measured.

To obtain useful refractivity data at low levels, the radiosonde data at 539 feet (launch height relative to Cold Lake) and the Cold Lake surface readings were used to define an average gradient over this lower interval. This method is subject to considerable error if there are large horizontal variations in the refractivity structure. The radiosonde launch point was overland and was about 15 miles from the position of the boat. However, fortunately almost all tests were carried out in clear air conditions (required for range safety) and without large-scale

frontal disturbances which would normally degrade horizontal stratification. An examination of aircraft measurements at the higher levels did not indicate that there were significant horizontal variations above 750 feet, relative to the level of Cold Lake (see Figure 8, flight plan). Certainly it is always easy in retrospect to see how the surface measurements should have been improved. Obviously the use of tethered balloons along the path would have provided much more meaningful measurements of the vertical and horizontal refractivity pattern over and beyond the lake surface. These resources were simply not available at the time, and all efforts were being made to at least ensure that adequate radiosonde soundings were available, and that surface observations were made at the launch site and of course on Cold Lake.

#### EFFECTIVE EARTH RADIUS CALCULATIONS

The total of all ray-tracing results using extrapolated radiosonde data and the reflection interferometer calculations are compared in several ways.

First, a direct comparison of the effective earth radii data is shown in Figure 18. The average difference, together with the standard deviation of results, is plotted against the transmitter range. It is apparent that the experimental results are very close to the overall objective for this test, namely, that the average error between effective earth radii

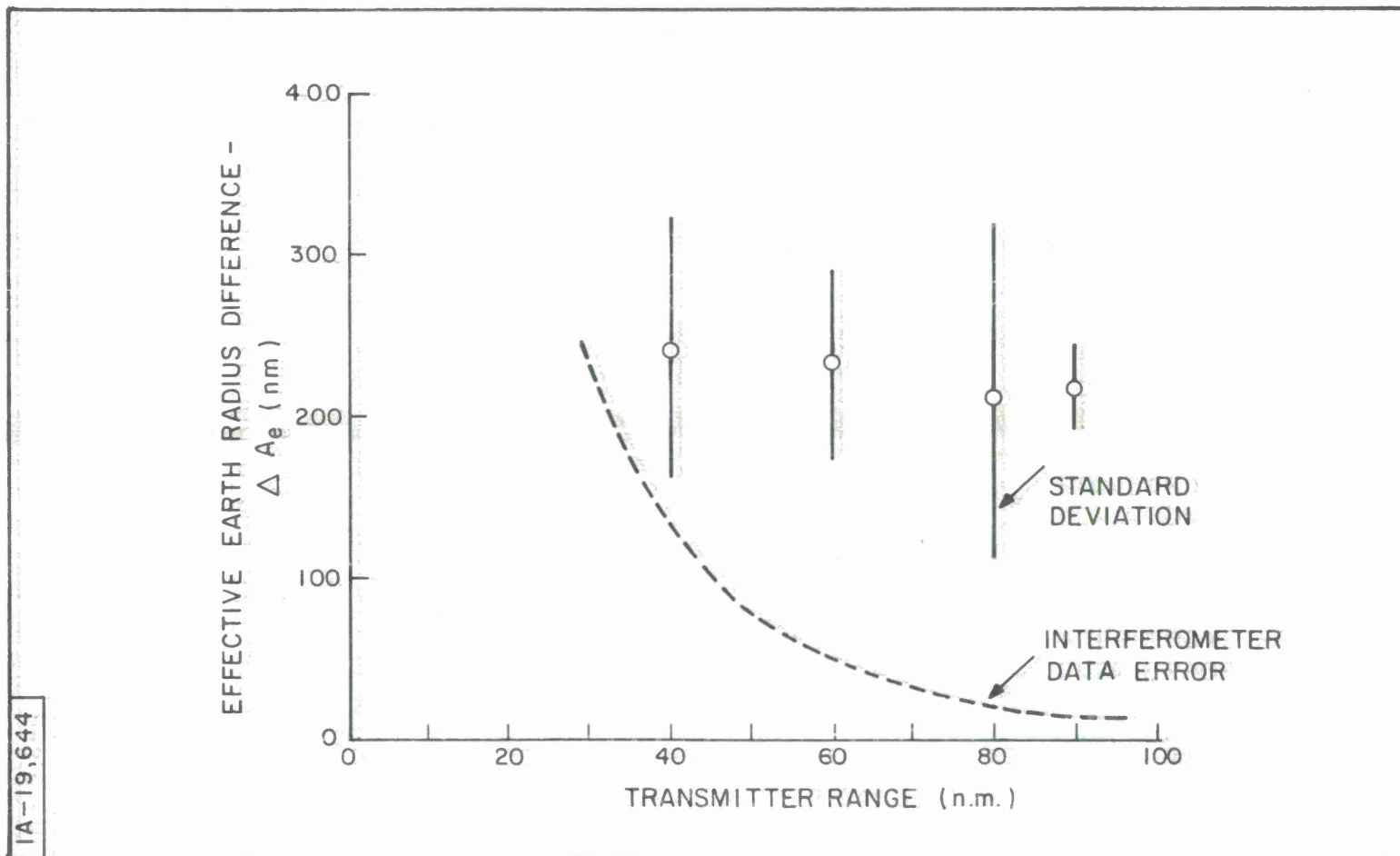


Figure 18. Effective Earth Radius Difference (n.m.) Between Ray-Tracing and Interferometer Results vs Range

calculations remain within 200 n. m. If radiosonde data from the surface of Cold Lake had been available, the accuracy of the ray-tracing results should have improved. The estimated error with the reflection interferometer, from Figure 17 (page 59), is shown superimposed on Figure 18. It is apparent that the error between the two methods at long ranges and low initial elevation angles is largely due to the ray-tracing results. As mentioned previously this error at low angles is directly related to the errors in defining an effective refractivity profile over the surface of Cold Lake.

From the ray-tracing results, such as shown in Table II (page 32), it is possible to relate the earth radius variation to an equivalent variation in the elevation angle error,  $\epsilon$ . Also, as the transmitter range and height changes, a corresponding initial elevation angle  $\theta_0$ , can be obtained. From a compilation of many such printouts an average magnitude of these relative variations was obtained. The relationship between elevation angle error variation,  $\Delta\epsilon$ , versus transmitter range is shown in Figure 19, where the earth radius was changed by 100 n.m. This relationship was checked for various transmitter heights and also for cases when the earth radius variation was several hundred nautical miles. The straight line relationship shown on Figure 19 was found to be generally applicable over a wide range of conditions.

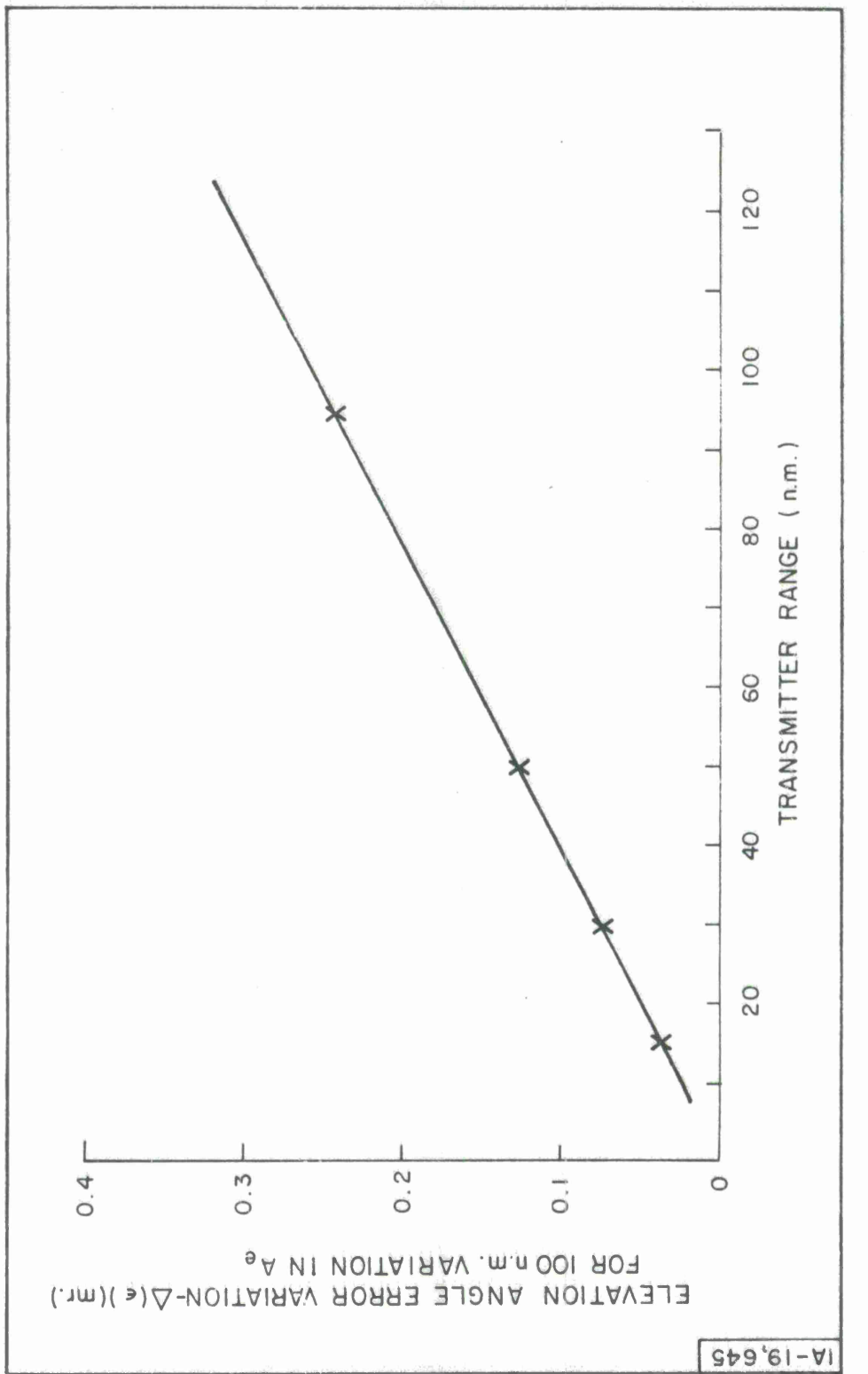


Figure 19. Variation in Elevation Angle Error  $\Delta\epsilon$  (mr) for 100 n.m.  
 Variation in  $\Delta\epsilon$  vs Transmitter Range

From the above curve, the effective earth radii errors were converted into elevation error angle differences,  $\Delta\epsilon$ , and plotted against transmitter range, as shown on the upper graph of Figure 20. Multiplying these angle errors by transmitter range immediately converts the plot into height errors. Selecting a representative linear refractivity profile (102-0949) the ranges corresponding to initial elevation angles are shown on the lower graph. It should be noted that within the useful range the experiment concentrated on low-angle propagation conditions, generally below two degrees initial elevation angle.

On the other hand, from Reference 15, residual radar height errors are generally about  $\pm 400$  feet after applying a model atmosphere correction, and for initial elevation angles of 10 mr., an aircraft height of 16,500 feet and an aircraft range of 124 n.m. Using both surface and initial gradient correction techniques, the uncorrected standard error can be reduced to about 260 feet, on the average. [18]

In spite of the difficulty in obtaining good surface refractivity data, it is apparent that the Cold Lake results compare very favorably with the most recent refraction correction techniques. In fact, had radiosonde data been available from the surface of Cold Lake, it is felt that the results would have been significantly improved.

Table VIII summarizes the mean and extreme values of effective earth radii calculated from the interferometer results. An

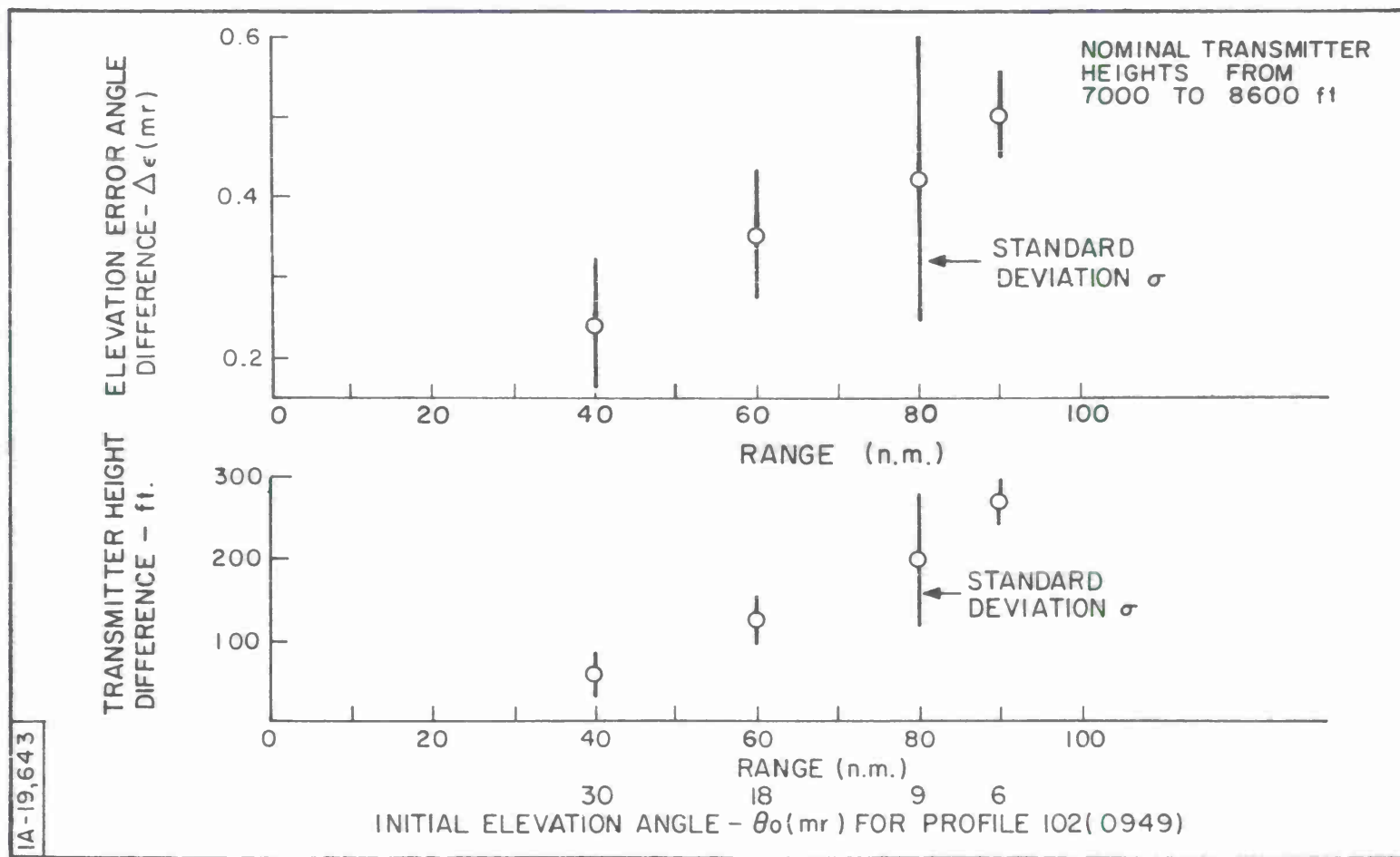


Figure 20. Elevation Error Angle Difference and Transmitter Height Difference Between Ray-Tracing and Interferometer Results vs Range

Table VIII  
Summary of Interferometer  $A_e$  Values

Mission	Leg	Band		Height (ft)	Time	$A_e$ (nm)			Comments
		/	Pol.			Min.	Max.	Av.	
102	1&2	S/V		8600	AM	4200	4700	4500	Fluctuating
	3&4	S/H		8600	AM	4400	4550	4450	Fluctuating
	5&6	L/H		8600	AM	4500	4750	4600	Slightly descending with range
103	1&2	S/H		8600	AM	4250	4550	4450	Fluctuating, slight ascending
	3&4	S/H		8600	Noon	4200	4500	4300	Ascending after 60 n.m.
	5&6	S/H		8600	PM	4200	4450	4250	Ascending after 75 n.m.
104	1&2	S/H		7000	Night	4400	4700	4550	Fluctuating
	3&4	S/H		7000	Sunup	4600	4800	4650	Slightly fluctuating
	5&6	S/H		7000	AM	4500	4800	4650	Fluctuating
105	1&2	S/H		8600	Noon	4250	4400	4300	Slightly ascending
	3&4	S/H		8600	PM	4260	4450	4300	Slightly ascending
	5&6	S/H		4300	PM	4250	4550	4400	Fluctuating and ascending
106	1&2	S/H		4300	AM	4500	5250		Ascending
	3&4	S/V		4300	AM			4600	Uncertain
	5	S/V		7000	Noon	4400	4650	4500	Slightly ascending
	7&8	S/H		7000	PM	4350	4500	4400	Depressed in mid ranges
107	1&2	S/H		7000	PM	4150	4300	4200	Slightly ascending
	3&4	S/H		7000	Sunset	4150	4300	4200	Slightly ascending
	5&6	S/H		7000	Night	4150	4300	4250	Depressed in mid ranges
108	1&2	L/H		4300	PM	4550	5200	4700	Convex up and descending
	3&4	L/H		7000	PM	4700	5000	4850	Convex up and descending
	5&6	L/H		7000	PM	4900	5450	5100	Convex up and descending

Table VIII (Cont.)

Mission	Leg	Band / Pol.	Height (ft)	A <sub>e</sub> (n.m.)			Comments
				Time	Min.	Max.	
109	1&2	L/H	4300	PM		4300	Flat
	3&4	L/H	7000	Sunset		4350	Flat
	5&6	L/H	7000	Night		4350	Flat
110	1&2	S/H	7000	Night	4850	5050	Fluctuating
	3&4	L/H	7000	Sunup	4550	5050	Descending after 50 n.m.
	5&6	L/H	7000	AM	5000	5250	Descending after 60 n.m.
111	1&2	S/H	7000	Night	4600	5200	Fluctuating
	3&4	L/H	7000	Sunup	4750	5050	Slightly ascending
	5&6	L/H	7000	AM	4400	5300	Ascending after 60 n.m.
112	1&2	S/H	7000	Night	4300	4800	Ascending after 70 n.m.
	3&4	L/H	7000	Sunup	4450	4700	Slightly fluctuating
	5&6	L/H	8600	AM	4450	4650	Slightly descending
113	1&2	L/H	8600	Night	4800	5050	Slightly ascending after 70 n.m.
	3&4	L/H	8600	Sunup	4700	5150	Slightly ascending after 70 n.m.
	5&6	L/H	8600	AM	4600	5250	Fluctuating
114	1&2	L/H	8600	PM	4300	4550	Slightly fluctuating
	3&4	L/H	8600	Sunset	4200	4550	Fluctuating and ascending after 70 n.m.
	5&6	L/H	8600	Night	4250	4650	Fluctuating below 50 n.m. then ascending

inspection of these results readily reveals that the average  $A_e$  values are generally greatest around sunrise. The mean value here is 4840 n.m., with a standard deviation of 160 n.m. It is interesting to note that the overall mean for all the measurements gives a value for  $A_e$  of about 4600 n.m., which corresponds to the standard atmosphere or  $4/3$  earth radius condition. Hence, in general, the radio propagation experiment was conducted in an area and during a period of the year when reasonably standard propagation conditions were prevalent.

## CONCLUSIONS

The close agreement between the effective earth radius values obtained from the meteorological measurements and the interferometer technique indicates that this type of radio interferometer can provide meaningful and surprisingly accurate information on the radio propagation conditions. It might, in fact, provide the best method to measure integrated radio-meteorological conditions when continuous monitoring is required and when the use of complex meteorological instrumentation would be impractical.

The results also indicate that the radiosonde data, if sufficient care is taken to calibrate it before launch, can give very satisfactory information about the radio propagation conditions. Aircraft refractometer measurements of course provide a great deal more fine structure

than the radiosonde. However, unless this data can be related to the horizontal and temporal variations prevalent, it may lead to a mis-understanding about the effective propagation conditions. At low levels, over large bodies of water, it was observed that the refractometer data was generally biased to indicate that much greater surface gradients were present than could be accounted for from the extrapolated radiosonde data or the interferometer results.

The interferometer technique has one very important advantage over the ray-tracing methods. In many instances, where strong refractivity gradients are present at or above the surface, the ray-tracing analysis will frequently indicate that trapping is prevalent. Unfortunately, in nearly all ray-tracing programs the effect of the radio signal wavelength,  $\lambda$ , cannot be taken into account. It is well known that for a given refractivity gradient as well as its vertical extent (layer thickness) a maximum wavelength can be found which will permit the radio signal to become trapped.<sup>[5]</sup> For greater wavelengths the layer will not support trapping. Therefore, even if accurate meteorological measurements of the radio refractivity can be obtained, the significance of this information in defining the radio propagation conditions is still subject to careful consideration. Certainly in this respect the radio interferometer has a most powerful advantage in that direct, real time observations of

the effective propagation conditions can be made, and for selected wavelengths. These observations are based on the actual effects of the medium on the radio signal as it propagates through the atmosphere, the most direct method imaginable.

## APPENDIX I

### THE "EFFECTIVE EARTH RADIUS" CONCEPT

Referring to Figure 21, a receiver, 'A', at height  $h_1'$  will receive signals along two paths from a transmitter, 'F', at height  $h_2'$ . The first is the direct path F to A, and assuming that the surface is highly reflective, the second path is FGA. As the transmitter moves in range, the signals combine at the receiver to produce minima and maxima amplitude variations. For a water surface and with small grazing angle,  $\beta$ , the phase of the reflected signal is changed by 180 degrees, i.e.,  $\pi$  radians. The first fade inside the radio horizon

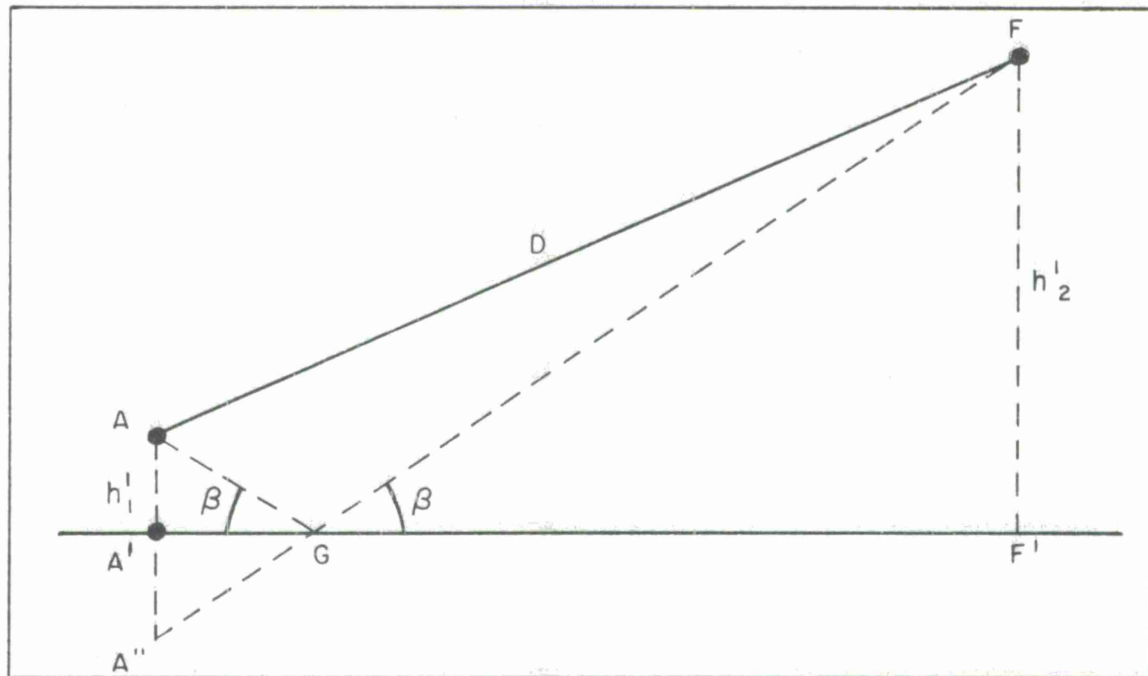


Figure 21. Flat Earth Reflection Geometry

is given the order  $n = 1$  and it occurs at a corresponding transmitter range  $D_1$ . As the transmitter moves towards the receiver, each fade condition (minimum received signal) occurs for ranges given by

$$D_n \simeq \frac{2h'_1 \cdot h'_2}{n\lambda} \quad (I-1)$$

where

$$n = 1, 2, 3, \dots \text{etc.}$$

$\lambda$  = the radio signal wavelength

In the real situation, of course, the reflector becomes the surface of a spherical earth. As shown in Figure 22, the true heights of the receiver and the transmitter over the spherical surface are  $AA'$  and  $BB'$  respectively. If a plane is passed through the reflection point  $C$ , Equation (I-1) can be used to determine the fade dependence upon range if  $h'_1$  and  $h'_2$  are expressed in terms of  $h_1$  and  $h_2$  respectively.

From triangle  $BCO$ ,

$$\sin \beta = \frac{(A + h_2)^2 - A^2 - r_2^2}{2Ar_2} \quad (I-2)$$

also from triangle  $BCB''$

$$h'_2 = r_2 \sin \beta \quad (I-3)$$

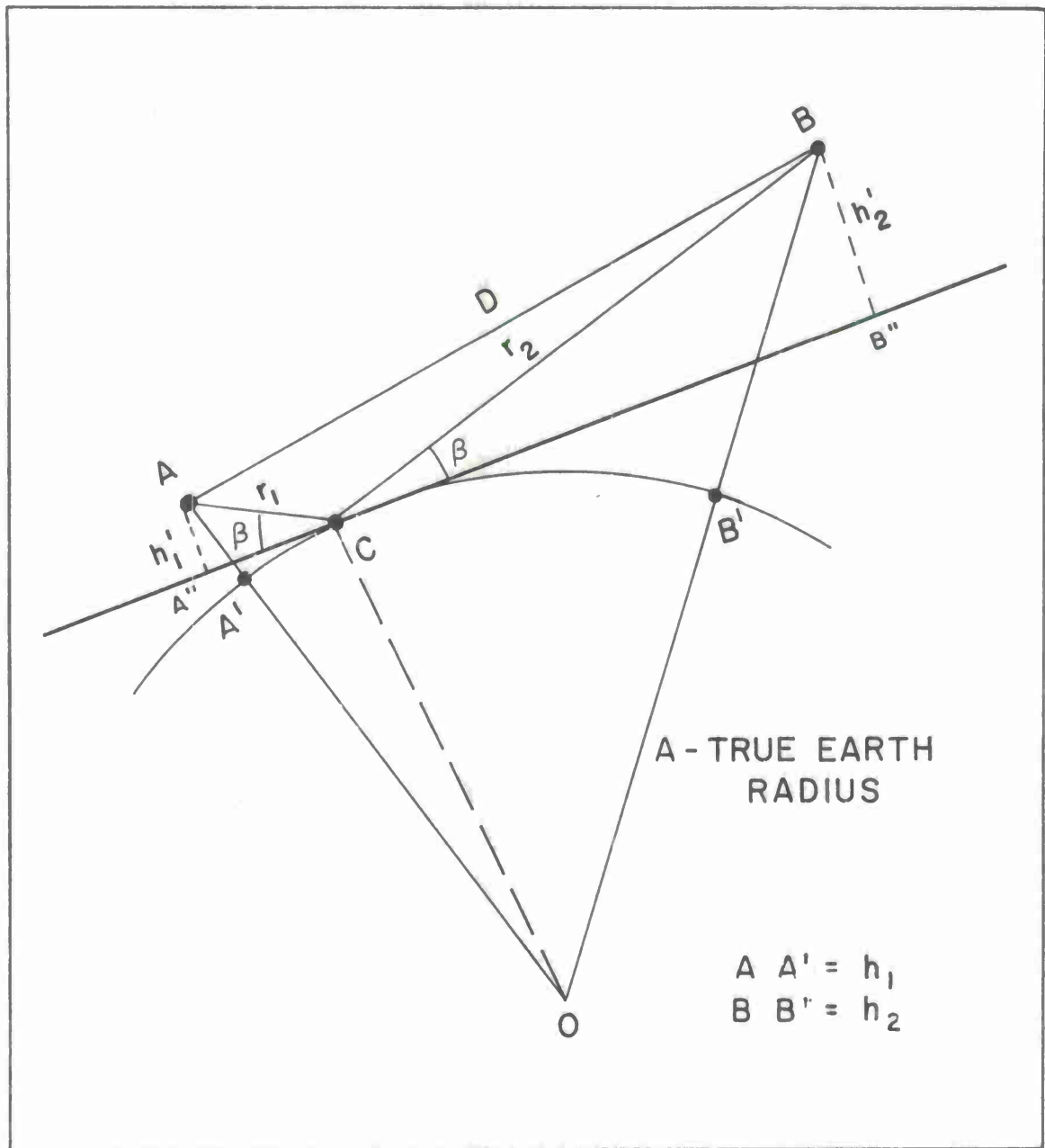


Figure 22 Geometry of Flat Earth Approximation

Substituting for  $\sin \beta$  into Equation (I-3) and simplifying gives

$$h'_2 = h_2 + \frac{h_2^2 - r_2^2}{2A} \quad (I-4)$$

Over the range of experimental interest  $r_2$  will be very much greater than  $h_2$ . Therefore

$$h'_2 \approx h_2 - \frac{r_2^2}{2A} \quad (I-5)$$

Similarly it can be shown that

$$h'_1 \approx h_1 - \frac{r_1^2}{2A} \quad (I-6)$$

Substituting these equations into Equation (I-1) gives

$$D_n \approx \frac{2 \left( h_1 - \frac{r_1^2}{2A} \right) \left( h_2 - \frac{r_2^2}{2A} \right)}{n \lambda} \quad (I-7)$$

Since the angles of incidence and reflection are equal, we have

$$\frac{r_1}{h_1 - \frac{r_1^2}{2A}} = \frac{r_2}{h_2 - \frac{r_2^2}{2A}} \quad (I-8)$$

However, at any particular fade, of order  $n$ , we have

$$(r_1 + r_2) - D_n = n\lambda \quad (I-9)$$

or

$$r_2 = D_n - r_1 + n\lambda \quad (I-10)$$

Over the range of experimental interest,  $n\lambda$  will be less than about 20 feet ( $n \leq 50$  for  $\lambda \sim 10$  cm and  $n \leq 20$  for  $\lambda \sim 30$  cm) and  $r_1$  will be greater than 10 miles. Therefore Equation (I-10) is approximately

$$r_2 \approx D_n - r_1 \quad (I-11)$$

Substituting into Equations (I-7) and (I-8) gives

$$D_n \approx \frac{2 \left( h_1 - \frac{r_1^2}{2A} \right) \left( h_2 - \frac{(D_n - r_1)^2}{2A} \right)}{n\lambda} \quad (I-12)$$

and

$$\frac{r_1}{h_1 - \frac{r_1^2}{2A}} = \frac{D_n - r_1}{h_2 - \frac{(D_n - r_1)^2}{2A}} \quad (I-13)$$

Finally from triangle AA''C and Equation (I-6),

$$\sin \beta \approx \frac{h_1 - \frac{r_1^2}{2A}}{r_1} \quad (I-14)$$

Under propagation conditions in the real atmosphere, of course, the range  $D_n$  to the transmitter is a curved path rather than a straight line. However, if a straight path range  $D_n$  is assumed, and the terminal heights  $h_1$  and  $h_2$  retained in magnitude, the geometry as shown in Figure 22 will simply give a value of the earth's radius  $A_e$  which is larger than the true earth radius  $A$ . The above equations are therefore quite general and by substituting  $A_e$  for  $A$ , they can be used to generate values of the effective earth's radii.<sup>[4]</sup> A 7094 computer program was used to solve the above equations for the particular, known input parameters  $\lambda$ ,  $n$ ,  $D_n$ ,  $h_1$  and  $h_2$  involved in this experiment. From the resulting tables the appropriate values for  $A_e$  can be selected, corresponding to the experimental conditions at any particular fade of order  $n$ . A typical table is shown on pages 54 and 55; the complete set of tables will be retained in storage at MITRE for future reference.

Of course, as previously described in the report,  $A_e$  can be related to an "effective" index gradient by

$$A_e \approx \frac{n_0 A}{n_0 + A \cdot \frac{dn}{dh}} \quad (I-15)$$

where  $n_0$  = a representative value of the surface refraction

$A$  = true earth radius

$dn/dh$  = index gradient.

Since  $dn/dh$  can vary in both the horizontal and vertical directions, the effective earth's radius  $A_e$ , derived from interferometer results, does not have any direct physical meaning. However, the  $A_e$  values calculated from the above equations may be used as an indicator of the refractive index structure. The effective radius,  $A_e$ , would be constant with any transmitter range or height if the refractive gradient remained essentially constant in both vertical and horizontal directions. In some instances during the experiment this condition did result, but in general the  $A_e$  values were dependent upon range.

## APPENDIX II

### INTERFEROMETER ERROR ANALYSIS

The error introduced in the  $A_e$  calculations can be determined based on the experimental accuracies of  $D_n$ ,  $\lambda$ ,  $h_1$  and  $h_2$ . To simplify this analysis, an approximate relationship between these parameters can be determined from the geometry of Figure 23. This geometry was not used for  $A_e$  calculations (Ref. Appendix I) because it is slightly less accurate and does not give all the parameters required in the overall analysis such as  $\beta$ ,  $r_1$  and  $r_2$ . Under the range of experimental conditions of interest it may be assumed that the reflection point is very near the receiving terminal and the earth is essentially flat within this confined area. Therefore the flat earth equation (I-1) can be applied. From Figure 23, it can be shown that

$$h_2' = h_2 - \frac{2A + h_2}{2(A + h_1)} - \frac{D_n^2}{2(A + h_1)} + \frac{h_1^2}{2(A + h_1)} \quad (II-1)$$

and for  $h_1 \ll A$  and  $h_2 \ll A$  Equation (II-1) becomes

$$h_2' \simeq h_2 - \frac{D_n^2}{2A} \quad (II-2)$$

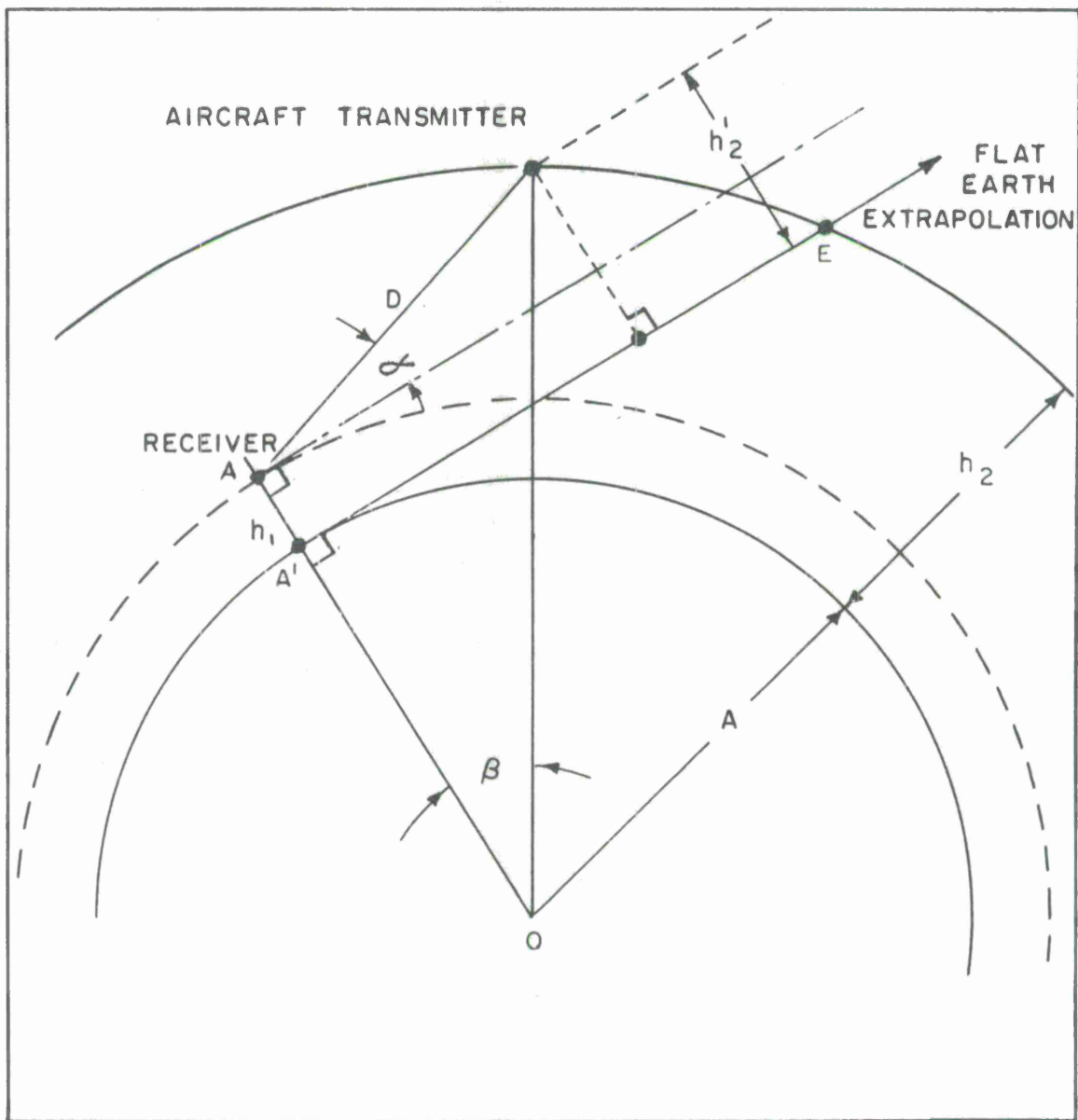


Figure 23 Geometry of Flat Earth Approximation (II)

Substituting this equation into (I-1), which becomes

$$D_n \simeq \frac{2h_1 h_2'}{n\lambda}$$

(since  $h_1' = h_1$ ), we find that

$$A \simeq \frac{D_n^2 h_1}{2 h_1 h_2 - n \lambda D_n} \quad (II-3)$$

Again, this equation is general and  $A$  can be replaced by  $A_e$  to obtain the dependence of  $A_e$  on the parameters measured and applied in the interferometer analysis. Then,

$$\log A_e = 2 \log D_n + \log h_1 - \log (2h_1 h_2 - n\lambda D_n) \quad (II-4)$$

The effect of errors in each of the separate parameters  $D_n$ ,  $h_1$ ,  $h_2$  and  $\lambda$  can be found by differentiating Equation (II-4) to give

$$\left( \frac{\delta A_e}{A_e} \right)_{D_n} = \left( \frac{2}{D_n} + \frac{n\lambda}{2h_1 h_2 - n\lambda D_n} \right) \delta D_n \quad (II-5)$$

$$\left( \frac{\delta A_e}{A_e} \right)_{h_1} = \left( \frac{1}{h_1} + \frac{2h_2}{2h_1 h_2 - n\lambda D_n} \right) \delta h_1 \quad (II-6)$$

$$\left( \frac{\delta A_e}{A_e} \right)_{h_2} = \left( \frac{2h_1}{2h_1 h_2 - n \lambda D_n} \right) \delta h_2 \quad (II-7)$$

$$\left( \frac{\delta A_e}{A_e} \right)_\lambda = \left( \frac{n D_n}{2h_1 h_2 - n \lambda D_n} \right) \delta \lambda \quad (II-8)$$

From Equation (II-3),

$$2h_1 h_2 - n \lambda D_n \simeq \frac{D_n^2 h_1}{A} \quad (II-9)$$

Substituting this equation into the above, gives

$$\left( \frac{\delta A_e}{A_e} \right)_{D_n} = \left( 2 + \frac{n \lambda A_e}{h_1 D_n} \right) \frac{\delta D_n}{D_n} \quad (II-10)$$

$$\left( \frac{\delta A_e}{A_e} \right)_{h_1} = \left( 1 - \frac{2h_2 A_e}{D_n^2} \right) \frac{\delta h_1}{h_1} \quad (II-11)$$

$$\left( \frac{\delta A_e}{A_e} \right)_{h_2} = \left( \frac{2h_2 A_e}{D_n^2} \right) \frac{\delta h_2}{h_2} \quad (II-12)$$

$$\left( \frac{\delta A_e}{A_e} \right)_{\lambda} = \left( \frac{n \lambda \ A_e}{h_1 \ D_n} \right) \ \frac{\delta \lambda}{\lambda} \quad (II-13)$$

Table II-1 shows the individual errors in  $\delta A_e/A_e$  for various test conditions and the total error equivalent to the sum of the individual errors. Finally, multiplying this total error by average earth radii conditions gives the estimated maximum errors in the  $A_e$  calculations. A graph of this error relationship to transmitter range is shown in Figure 17.

Table II-1

Interferometer Accuracy for  $A_e$  Determination

n	$D_n$	Freq. Band	TX Height	$\left(\frac{\delta A_e}{A_e}\right)_\lambda$ $\times 10^{-3}$	$\left(\frac{\delta A_e}{A_e}\right)_{D_n}$ $\times 10^{-3}$	$\left(\frac{\delta A_e}{A_e}\right)_{h_2}$ $\times 10^{-3}$	$\left(\frac{\delta A_e}{A_e}\right)_{h_1}$ $\times 10^{-3}$	Total Error $\times 10^{-3}$	Maximum Error in $A_e$ n. m.	
1	57.0	L	4300	1.26	0.84	10.89	1.22	11	47	
3	33.0	L	4300	6.51	3.31	32.45	6.43	33	142	
5	22.0	L	4300	16.28	10.18	73.09	16.23	74	318	
10	11.0	L	4300	65.13	72.49	292.4	69.11	300	1290	
<hr/>										
209	1	77.0	L	7000	0.30	0.57	5.97	0.94	6	26
	3	49.0	L	7000	4.39	1.72	14.73	4.38	15	65
	5	34.0	L	7000	10.53	4.60	30.60	10.61	31	133
	10	19.0	L	7000	37.70	25.03	98.01	37.07	100	430
<hr/>										
	1	88.0	L	8600	0.81	0.48	4.56	0.80	5	22
	3	58.0	L	8600	3.71	1.32	10.51	3.67	11	47
	5	41.0	L	8600	8.74	3.30	21.04	8.75	24.6	108
	10	23.0	L	8600	31.15	17.33	66.87	13.85	81.8	353

(Continued on page 210.)

Table II-1 (Cont. )

n	D <sub>n</sub>	Freq. Band	TX Height	$\left(\frac{\delta A_e}{A_e}\right)_\lambda$	$\left(\frac{\delta A_e}{A_e}\right)_{D_n}$	$\left(\frac{\delta A_e}{A_e}\right)_{h_2}$	$\left(\frac{\delta A_e}{A_e}\right)_{h_1}$	Total Error $\times 10^{-3}$	Maximum Error in A <sub>e</sub> n. m.
				$\times 10^{-3}$	$\times 10^{-3}$	$\times 10^{-3}$	$\times 10^{-3}$		
1	69.0	S	4300	1.04	0.55	7.43	0.94	7.7	32
5	41.0	S	4300	8.74	1.89	21.04	8.87	24.5	105
10	25.0	S	4300	28.66	6.88	56.60	29.61	70.3	302
15	18.0	S	4300	59.71	17.94	109.2	60.27	139.4	600
210	1	90.0	S	7000	0.79	0.41	4.37	0.75	4.5
	5	60.0	S	7000	5.97	1.03	9.83	5.94	13.0
	10	39.0	S	7000	18.37	3.13	23.26	18.69	35.2
	15	29.0	S	7000	37.06	7.54	42.07	36.53	67.3
1	102.0	S	8600	0.70	0.36	3.40	0.57	3.5	15
5	70.0	S	8600	5.12	0.83	7.22	5.03	10.2	44
10	47.0	S	8600	15.24	2.28	16.71	16.10	27.9	120
15	34.0	S	8600	31.61	5.48	30.60	32.29	54.8	236

## REFERENCES

1. B. J. Starkey and F/L G. A. Fatum, Experimental Results on Fading of Noise Type Jamming Signals in L and S Frequency Bands, Canadian Forces Headquarters, REF VF 64/4, November 1964.
2. L. G. Rowlandson, Radio Ray Bending in the Lower Troposphere Measured with a Reflection Interferometer, The MITRE Corporation, MTR-114, 1 June 1966.
3. M. Born and E. Wolf, Principles of Optics, Pergamon Press, 1959.
4. J. C. Schelleng, C. R. Burrows, and E. B. Ferrel, Ultra-shortwave Propagation, Proc. IRE 21, 427-463, March 1933.
5. D. E. Kerr, Propagation of Short Radio Waves, Vol. 13, Radiation Laboratory Series, McGraw-Hill Book Company, p. 53, 1951.
6. J. S. McPetrie, B. J. Starkey, H. Jarkowski, and L. Sicinski, Overseas Propagation on Wavelengths of 3 and 9 Centimeters, Proc. IRE 37, 243, 1949.
7. Report of Factual Data from the Canterbury Project (1951), Vols. I-III, Dept. Sci. Indus. Research, Wellington, New Zealand.
8. P. J. Rubenstein, I. Katz, L. J. Neelands, and R. M. Mitchell, Microwave Transmission Over Water and Land Under Various Meteorological Conditions, Radiation Laboratory, M.I.T., Cambridge, Report 547, July 13, 1944.
9. E. A. Bondurant, J. C. Katzin, M. Katzin, A. B. Washburn, and E. A. Wolff, Project Neptune - Investigation of the Communications Potentialities of the Trade Wind Inversion Duct, Electromagnetic Research Corporation, College Park, Maryland, Report ERC-7435-1, 1961.
10. N. W. Guinard, J. Ransone, D. Randall, C. Purves, and P. Watkins, Propagation Through an Elevated Duct: Tradewinds III, IEEE Trans. AP-12:479, July 1964.

#### REFERENCES (CONT.)

11. B.R. Bean and E.J. Dutton, Radio Meteorology, National Bureau of Standards Monograph 92, U.S. Government Printing Office, Washington, D.C., March 1, 1966.
12. Smythe Research Associates, San Diego, California, Atmospheric Refraction Effects on Precision Radar Tracking, U.S. Government Printing Office, Washington, D.C., Report AD 605140, February 1961.
13. J.R. Bauer, W.C. Mason, and F.A. Wilson, Radio Refraction in a Cool Exponential Atmosphere, Technical Report No. 186, Lincoln Laboratory, M.I.T., Cambridge, 27 August 1958.
14. D.L. Ringwalt, A Study of Meteorological Phenomena as Related to the Errors in Radio Interferometer Tracking Systems, Electromagnetic Research Corporation, College Park, Maryland, Prepared for Air Force Cambridge Research Labs, AFCRL-64-587 (Part I), 15 June 1964.
15. L.G. Rowlandson, The Ability to Predict Low-Angle Height Errors with the NBS Surface-Corrected Model Atmosphere, The MITRE Corporation, MTR-113, 8 February 1966.
16. C.M. Crain, Apparatus for Recording Fluctuations in the Refractive Index of the Atmosphere at 3.2 Centimeter Wavelength, Rev. Sci. Instr. 21, 456-457, May 1950.
17. C.M. Crain and A.P. Deam, Measurement of Tropospheric Index of Refraction Profiles with an Airplane-Carried Direct Reading Refractometer, Electrical Engineering Research Laboratory, University of Texas, August 1951.
18. W.B. Sweezy and B.R. Bean, Correction of Atmospheric Refraction Errors in Radio Height Finding, National Bureau of Standards, CRPL Report 7977, October 25, 1963.

## Unclassified

Security Classification

## DOCUMENT CONTROL DATA - R &amp; D

(Security classification of title, body of abstract and indexing annotation must be entered when the overall report is classified)

1. ORIGINATING ACTIVITY (Corporate author) The MITRE Corporation Bedford, Massachusetts		2a. REPORT SECURITY CLASSIFICATION Unclassified
		2b. GROUP
3. REPORT TITLE Cold Lake Radio Propagation and Meteorological Experiment (in 3 Vols.), Vol. I, Description of a Radio-Meteorological Experiment to Measure Ray-Path Bending in the Troposphere with a Vertical Interferometer		
4. DESCRIPTIVE NOTES (Type of report and inclusive dates) N/A		
5. AUTHOR(S) (First name, middle initial, last name) Starkey, B.J.; Rowlandson, Lyall G.; Fatum, Gordon A.		
6. REPORT DATE August 1967		7a. TOTAL NO. OF PAGES 220
8a. CONTRACT OR GRANT NO. AF 19(628)-5165		7b. NO. OF REFS 18
b. PROJECT NO. 7010		9a. ORIGINATOR'S REPORT NUMBER(S) ESD-TR-67-357, Vol. I
c.		9b. OTHER REPORT NO(S) (Any other numbers that may be assigned this report) MTR-118, Vol. I
d.		
10. DISTRIBUTION STATEMENT This document has been approved for public release and sale; its distribution is unlimited.		
11. SUPPLEMENTARY NOTES		12. SPONSORING MILITARY ACTIVITY Deputy for Surveillance & Control Systems, Aerospace Instr. Prog. Office; Electronic Systems Div., L. G. Hanscom Field, Bedford, Mass.
13. ABSTRACT The purpose of the experimental program described in this report was to determine the direct relationship between meteorological and radio-propagation measurements and then to evaluate the validity of radio-meteorological results for predicting the radio-propagation conditions. The meteorological information was derived from radiosonde measurements and airborne microwave refractometer data. The radio experiments were based on the vertical interferometer technique, in which a single airborne transmitter (S and L Band) was used to establish an interference pattern at the ground-based receiver, due to the combination of direct and lake-surface-reflected signals. Extreme accuracy in the measurements of the parameters involved, in particular in the interferometer experiment, was the keynote to success. The close agreement between the effective earth's radius value obtained from the meteorological measurements and the interferometer technique indicates that this type of radio interferometer can provide meaningful and surprisingly accurate information on the radio propagation conditions. The results also indicate that the radiosonde data, if sufficient care is taken to calibrate it before launch, can give very satisfactory information about radio propagation conditions.		

14 KEY WORDS	LINK A		LINK B		LINK C	
	ROLE	WT	ROLE	WT	ROLE	WT
REFRACTION						
PROPAGATION						
Multipath						
Microwave						
Radio						
ATMOSPHERIC PHYSICS						
RADIO - METEOROLOGY						

